Investigation of Approach Slab Construction and Evaluation of Modular Approach Slab Designs

Final Report

Larry A. Fahnestock, Ph.D., P.E.
Professor

James M. LaFave, Ph.D., P.E.
Professor

Gaoyu Liu
Graduate Research Assistant

Himanshu Joshi
Graduate Research Assistant

Marian Chee
Graduate Research Assistant

University of Illinois at Urbana-Champaign
Department of Civil and Environmental Engineering
January 2021

ABSTRACT

Integral abutment bridges (IABs) eliminate the joints between the bridge deck and abutments and hence have become more prevalent in the United States due to lower maintenance costs and longer service life. However, approach slab cracking, which requires maintenance, repair, and even premature replacement, has been a recurring issue for IABs that are owned and maintained by the Illinois State Toll Highway Authority. An agency survey conducted across the U.S. indicates that many states are experiencing similar approach slab cracking issues. Field inspections done on existing bridges in Illinois suggest that there are some shared crack patterns among the mainline interstate highway bridges and cross-road bridges. To further study the long-term behavior of IAB approach slabs, a four-lane cast-in-place approach slab and a three-lane precast approach slab were instrumented during construction.

Over several years, changes in concrete strain and temperature at different locations in plan and through the slab depth were measured, along with global longitudinal displacements of the slabs. The field results indicate that the deformations and stresses in the slabs have a strong correlation to temperature. Different from free expansion and contraction, the slabs have restraints at the bottom surfaces and at the ends, which may vary due to seasonal effects and other time-dependent conditions, such as the settlement of the embankment. The two instrumented slabs experience similar ambient environmental conditions and traffic loading. The temperature at the top reinforcement mat is more sensitive to ambient environmental changes. The load-related strains at the gage locations for the cast-in-place slab ranged from approximately 200 $\mu\varepsilon$ in compression to 200 $\mu\varepsilon$ in tension, while for the precast slab, the range was from approximately 200 $\mu\varepsilon$ in compression to 240 $\mu\varepsilon$ in tension. The field data suggest that there are several locations at the bottom of the slabs with a potential risk of cracking. However, only one very small crack was observed at the entrance side of the ramp for the cast-in-place slab. Voids were observed at the north and south (shoulder) boundaries of the slabs in 2019. Field measurements indicate that there is moderate in-plane clockwise rotations at the precast slab. Static truck testing was conducted to study live load effects and then compare them to thermally-induced effects. Corresponding numerical modeling was conducted, and the numerical results provided reasonable agreements to the field data. It is noted that the parapet of the approach slab at the shoulders affects the bending behavior of the slab as it provides additional stiffness to the slab. Short-term thermal behavior during the truck test days suggests that solar radiation has significant impact on the thermal stresses in the slab.

Numerical simulations and a parametric study were conducted for the approach slabs considering various geometric configurations, live load cases, thermal load cases, and boundary conditions. The principal stresses generally follow a decreasing trend when the bridge skew increases due to the two-way slab bending and the more direct load path to the supports for larger skew. The IL-120 truck, mild skews (10°), more loaded traffic lanes, and reduced support from the subbase together contribute to the critical principal stress in the approach slab (>550 psi). Thermal analysis suggests that overall temperature changes in the slab, temperature gradients through the slab thickness, differences in temperature distribution between the approach slab and supports (abutment and pile bent), and restraint of the supports can significantly affect the critical stresses in the approach slab. Hypothetical cases in the parametric study indicate that with an overall

change of -72°F in slab temperature, a +1.26°F/inch temperature gradient, no temperature change in the supports, and full restraint of translation at the slab support locations, the critical stresses can be greater than 2 ksi.

For the two monitored approach slabs, the current Tollway approach slab details (both cast-in-place and precast) appear to be performing well with almost no evidence of cracking. For future designs, longitudinal reinforcement for the bottom mat at the middle lanes could be increased for extra robustness against high truck load demands, especially for wide approach slabs. A well-compacted subbase is observed to help reduce the stress demand due to the truck loads for both cast-in-place and precast approach slabs. However, a well-compacted subbase is only realistic for partial-length approach slab support due to granular backfill behind the integral abutment. In addition, partially releasing lateral restraint between the approach slab and the integral abutment through modified details will allow the approach slab to expand and contract with less restriction. Analyses of approach slabs indicate that this increased flexibility in the transverse direction is expected to reduce the potential risk of cracking due to thermal effects.

ACKNOWLEDGEMENTS

Contents

Figures

11

14

Tables

1 Introduction

This chapter provides essential background on concepts closely related to the research: bridge abutments, integral abutment bridges (IABs), and approach slabs. Various types of abutments that are adopted in bridge design are covered in section 1.1. The advantages and challenges associated with IABs, a subset of jointless bridges, due to their structural characteristics and behavior are discussed in section 1.2. Section 1.3 provides an overview of bridge approach slabs. Lastly, section 1.4 describes the scope and primary tasks of this study.

1.1 Bridge Abutment Types

A bridge abutment transfers the structural loads from the superstructure to the bridge foundation. The abutment, as well as the wingwalls, if there are any, retains the embankment (Xanthakos 1994, Briaud et al. 1997). Xanthakos (1994) specified the primary loads that bridge abutments withstand:

1. Dead load from the weight of abutment and bridge superstructure.
2. Live load on the superstructure or on the approach slab, if any.
3. Transverse wind forces and longitudinal forces when bearings are fixed, and longitudinal forces due to friction or shear resistance at expansion bearings.
4. Centrifugal forces for curved bridges.
5. Earth pressures.

There are various ways to categorize bridge abutments (Briaud et al. 1997, IDOT 2012); however, certain abutment types are shared among them: closed, open, and vaulted.

The closed (high) abutment is a relatively old design solution and has a wall that extends down to the foundation, as shown in Figure 1.1. Such an abutment must be constructed before the embankment and is subjected to higher earth pressure than other types of the abutment. The embankment fill near the abutment is difficult to compact owing to the limited space (Briaud et al. 1997). Due to the high cost and construction challenges, closed abutments are rarely adopted in current practice. The Illinois State Toll Highway Authority – ISTHA, referred to herein as the Illinois Tollway (2019) – generally does not allow closed abutments to be used to support new or replacement structures unless specifically authorized if integral or semi-integral abutments are not feasible.
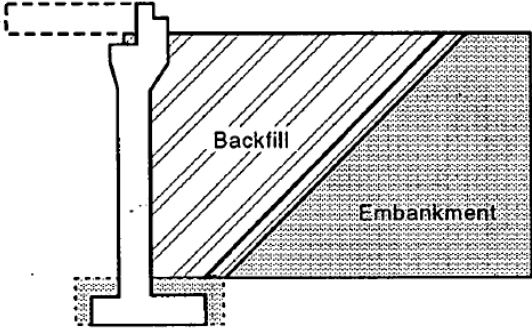
Figure 1.1 Typical closed abutment (Briaud et al. 1997).

Open abutments have also been referred to as pile bent or spill through abutments (IDOT 2012). Such abutments generally have less height of wall compared to closed abutments. If an open abutment is designed in an old fashion, supported on columns as seen in Figure 1.2, it must be constructed before the embankment. It is challenging to compact the embankment fill between the columns. However, if the abutments become so-called "stub type", they can be supported on shallow foundations or piles, which makes it possible to be constructed after the embankment is filled up to the height corresponding to the bottom of the abutment. As a result, the compaction of embankment fill is simplified (Briaud et al. 1997).
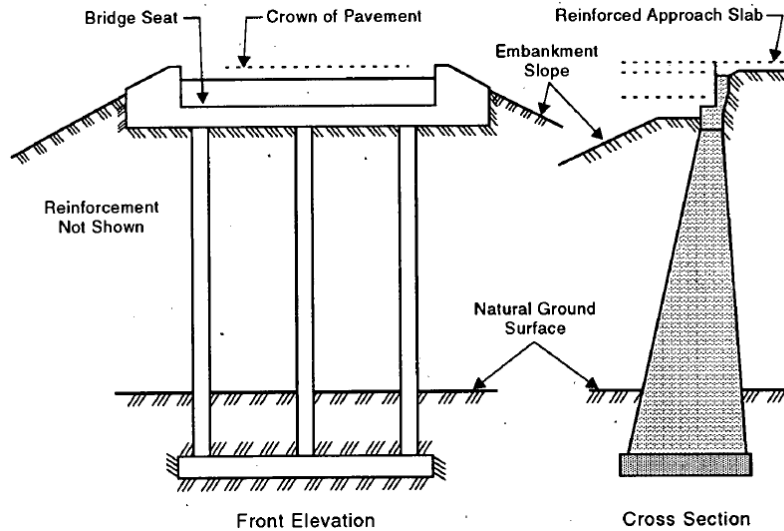
Figure 1.2 Typical spill-through abutment supported on columns (Briaud et al. 1997).

Vaulted abutments include filled and unfilled. The standard vaulted abutment in Illinois uses precast, prestressed beams to support the abutment span, as illustrated in Figure 1.3. This type of abutment is used when the abutment design span at right angles is larger than 6.4 m (21 ft). Similar to closed abutments, vaulted abutments are not allowed by the Illinois Tollway (2019) for new or replacement structures unless specifically authorized.
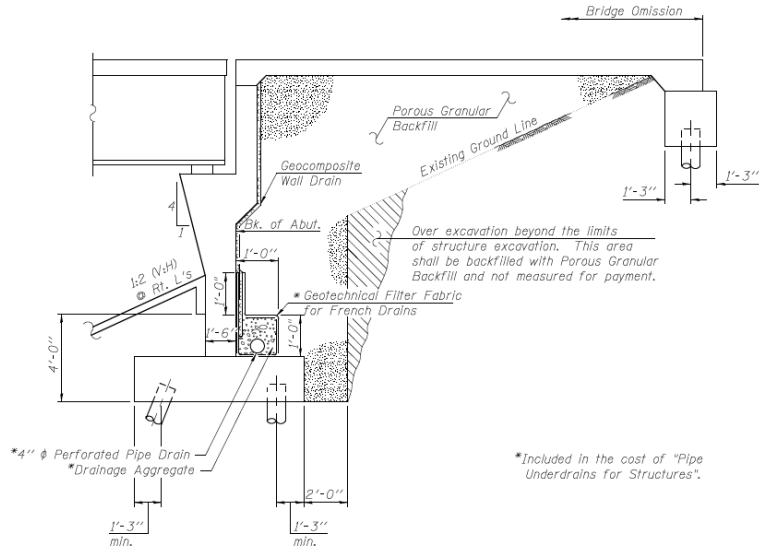
Figure 1.3 Typical section through filled vaulted abutment (IDOT 2012).

Per recent design practice, open abutments include integral, semi-integral, and stub abutments (IDOT 2012). The typical sections through integral and semi-integral abutments are shown in Figures 1.4 and 1.5, respectively (IDOT 2019). An integral abutment allows the structure to be connected rigidly to the abutment so that the bridge acts as a single structural unit. The key difference between a semi-integral abutment bridge and an IAB is that there is generally a joint with a flexible bearing surface in the semi-integral abutment allowing shear, but not moment, to be transferred from the upper part of the abutment to the pile cap. Thus, for a semi-integral abutment subjected to lateral cyclic loading due to the thermal deformation of the bridge, rotation may be allowed at its connection to the pile cap so as to reduce the lateral displacement of piles (Soltani and Kukreti 1992, Arsoy et al. 2004). There are expansion joints between the bridge abutments and superstructure for stub abutment bridges.
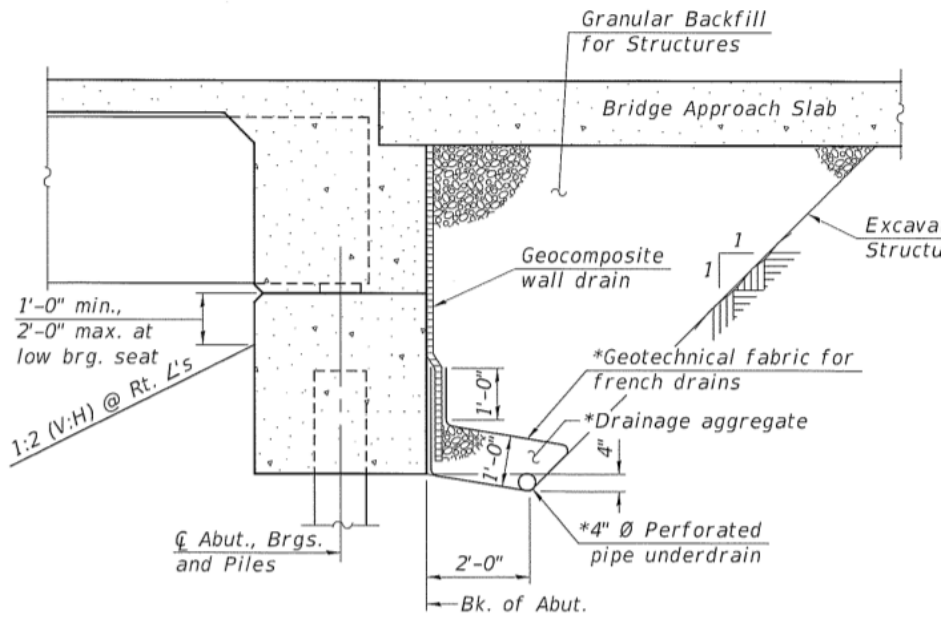
Figure 1.4 Typical section through integral abutment (IDOT 2019).
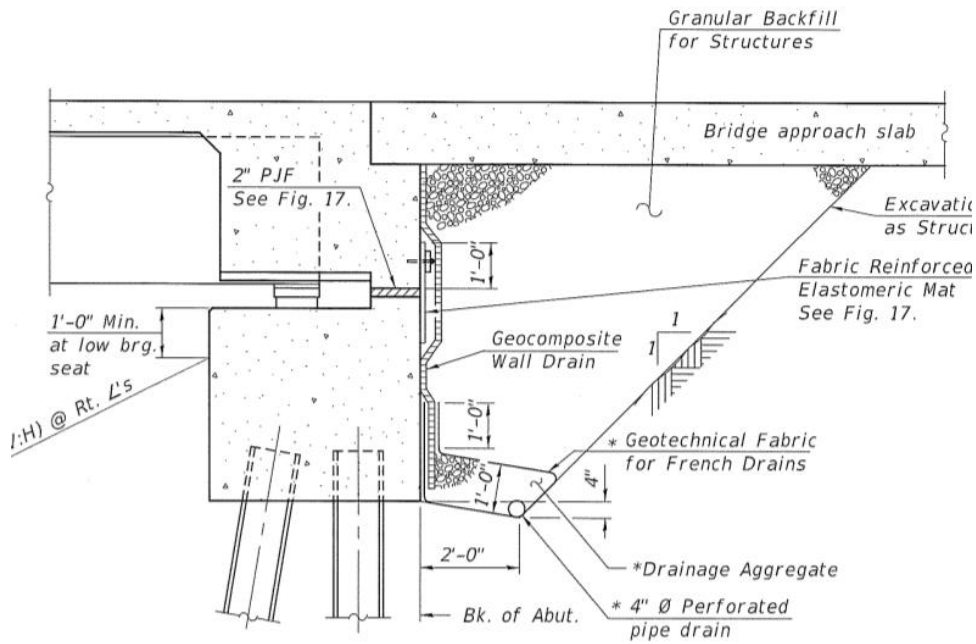
Figure 1.5 Typical section through semi-integral abutment (IDOT 2019).

In Illinois, integral abutments are preferred if: 1) the bridge skew is no more than 30°; 2) total bridge length for steel structures is less than or equal to 94.5 m (310 ft); 3) total bridge length for

concrete structures is no more than 125 m (410 ft); 4) the bridge girders are not curved; 5) the abutments and piers are parallel; and 6) a single row of certain permitted vertical H-piles or Metal Shell piles are used (IDOT 2012). The Illinois Tollway (2019) has also placed IABs at the top of their option list for new grade separation structures and stream and railroad crossings. The first five IDOT conditions (IDOT 2012) also apply to the use of semi-integral abutments in Illinois when the soil conditions require two or more rows of piles to support the loads (Illinois Tollway 2019). In addition, stub abutments with expansion joints shall be selected when the skew or bridge length cannot meet the requirements for integral and semi-integral abutments. Two or more rows of piles shall also be used with stub abutments (Illinois Tollway 2019).

1.2   Integral Abutment Bridges (IABs)

Bridges with expansion joints have long been used to accommodate the thermal movements of bridges as the temperature changes. Nonetheless, bridge engineers and state agencies found expansion joints and expansion bearings unfavorable for several important reasons (Greimann et al. 1987, Soltani and Kukreti 1992, Wasserman and Walker 1996, Lawver et al. 2000, Kunin and Alampalli 2000, Horvath 2000, Thippeswamy et al. 2002, Barker and Puckett 2013). Wasserman and Walker (1996) provided the following summary:

1. Joints are costly to buy, install, maintain, and repair. Sometimes repair can be as expensive as replacement. Joints intended to be waterproof can leak, allowing water to pour through the joint and thus accelerating deterioration to girders, bearings, abutments, and piers. Accumulated dirt, rocks, and trash filling elastomeric glands can lead to failure. Joint hardware can be damaged or loosened by snowplows as well as heavy traffic.
2. Bearings are expensive to purchase, install, and even replace. Steel bearings may tip over and/or seize up, whereas elastomeric bearings can split and rupture.
3. Joints and malfunctioning expansion bearings can lead to unexpected structural damage.

Since Hardy Cross introduced the moment distribution method in 1932 to simply analyze continuous beams and frames (Cross 1932), continuous bridges and bridges with more than one continuous unit, including jointless bridges, began to be adopted in design practice. Wolde-Tinsea and Klinger (1987) classified jointless bridges into four groups: flexible arch bridges, slip joint bridges, abutment-less bridges, and integral bridges.

Examples of components of a typical integral abutment bridge (IAB), a subset of jointless bridges, are shown in Figure 1.6 (Arsoy et al. 1999) for a single span and in Figure 1.7 (Kong et al. 2015) for multiple spans. Basically, an IAB consists of a bridge system and an approach system. In the bridge system, the superstructure of a bridge is the portion of the structure that acts as the span and directly supports the traffic loads. It consists of a deck and girders. Under the superstructure, there is the substructure that transfers the loads applied to the superstructure and the self-weight of the superstructure, as discussed in section 1.1. In an IAB, the superstructure is rigidly connected to the abutments, which are supported in part by the foundation (usually piles). The approach system, consisting of the backfill, approach fill, and soil foundation, provides a transition from the bridge abutment to the pavement. Approach slabs, if there are any, are placed between the bridge deck and roadway pavement, with one end supported by the abutment and the other end supported by a sleeper pad/slab or pile bent. These approach slabs are designed as structural elements to span

without support from the underlying soil. Transition slabs are pavement elements that connect the approach slabs (and therefore the whole bridge) to the standard roadway pavement.
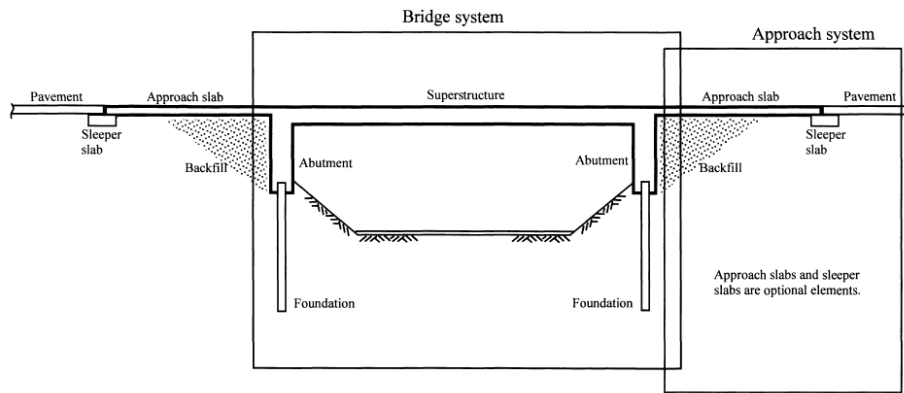
Figure 1.6 Simplified components of an IAB (Arsoy et al. 1999).
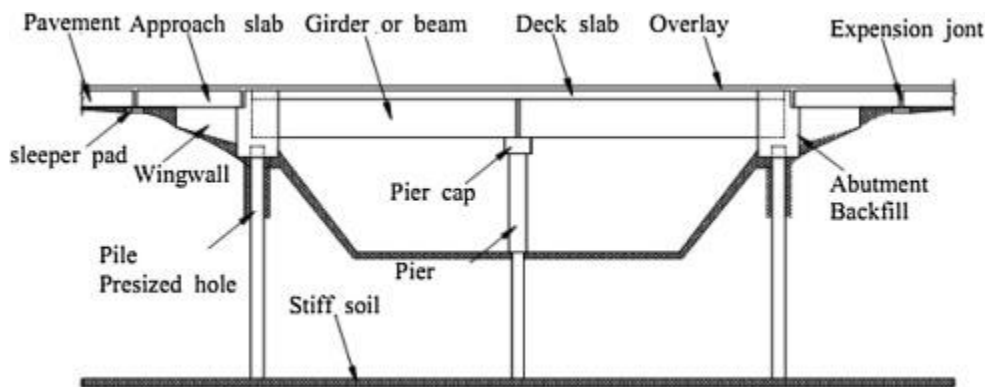
Figure 1.7 Typical IAB with two spans (Kong et al. 2015).

As the use of continuous structural components expanded in a general sense, the use of integral abutments also advanced. In the 1930s and 1940s, Ohio, South Dakota, and Oregon pioneered the use of jointless concrete bridges. California also started to adopt IABs in the mid-1950s. By the mid-1960s, Tennessee and five other states had chosen continuous bridges with integral abutments as standard construction (Wasserman and Walker 1996). The New York State Department of Transportation (NYS-DOT) started using IABs from the late 1970s (Kunin and Alampalli 2000). In addition, Kunin and Alampalli (2000) document the 31 states/provinces in the U.S. and Canada with the year of first use of IABs and number of IABs built up through 1996.

The popularity of IABs can be attributed to the following advantages:

1. Lower construction costs due to elimination of joints (Greimann et al. 1987, Soltani and Kukreti 1992, Wasserman and Walker 1996, Lawver et al. 2000, Kunin and Alampalli 2000, Horvath 2000, Burdette et al. 2004, Barker and Puckett 2013).

22

2. Lower maintenance costs because of no need of joint repair (Greimann et al. 1987, Soltani and Kukreti 1992, Hoppe and Gomez 1996, Oesterle et al. 1999, Lawver et al. 2000, Kunin and Alampalli 2000, Breña et al. 2007).
3. Reduced substructure costs (Kunin and Alampalli 2000).
4. Improved seismic performance thanks to the rigid connection between the bridge deck and abutment; increased redundancy for catastrophic events (Hoppe and Gomez 1996, Wasserman and Walker 1996, Oesterle et al. 1999, Kunin and Alampalli 2000).
5. Only one row of piles for the abutment; i.e., fewer piles are needed (Soltani and Kukreti 1992, Hoppe and Gomez 1996).
6. Simple and rapid construction (Wasserman and Walker 1996).
7. The bridge deck is more aesthetically pleasing, and the vehicular riding quality is improved (Soltani and Kukreti 1992, Oesterle et al. 1999, Kunin and Alampalli 2000, Breña et al. 2007, Barker and Puckett 2013).
8. Lower impact load and reduced snowplow damage (Oesterle et al. 1999, Kunin and Alampalli 2000).
9. Better design efficiency, as IABs can reduce the load distribution longitudinally and transversely;. the lateral and longitudinal loads applied to the superstructures of IABs are distributed to the abutment embankments (Burke 1993, Wasserman and Walker 1996).
10. Enhanced load distribution for girders at bridge ends thanks to the continuous and full-depth diaphragm at bridge ends (Wasserman and Walker 1996).
11. Improved protection for weathering girders (Wasserman and Walker 1996).
12. Greater end span ratio ranges due to the weight of abutment and uplift capacity of piling (Wasserman and Walker 1996).

However, there are also problems and uncertainties with IABs:

1. Settlement of approach fill caused by thermal displacement of the abutment leading to a void developed behind the abutment (Wolde-Tinsea and Klinger 1987, Hoppe and Gomez 1996). Settlement of approach fill can also be caused by traffic loads (Wolde-Tinsea and Klinger 1987). Thus, proper compaction of the embankment backfill is essential (Soltani and Kukreti 1992).
2. Secondary forces due to shrinkage, creep, settlement, temperature, and earth pressure can lead to cracks in concrete abutments (Wolde-Tinsea and Klinger 1987). The effect of elastic shortening after post-tensioning for prestressed concrete girders need to be considered carefully (Soltani and Kukreti 1992).
3. Skewed IABs tend to rotate due to the cyclic changes in earth pressure on the abutment backwall (Hoppe and Gomez 1996, Oesterle et al. 1999).
4. Limitations of use: weak embankments or subsoil is not favorable to integral abutments, and IABs can only be used for limited bridge lengths (Wasserman and Walker 1996).
5. Horvath (2000) argued that structural component damage caused by the abutment movements inflate the true life-cycle cost of IABs, making the maintenance costs of IABs comparable to jointed bridges. Hoppe and Gomez (1996) mentioned that some maintenance problems in IABs were shifted from the bridge structure to the embankments.

The temperature-related behavior of IABs not only includes expansion and contraction of the superstructure, which leads to abutment displacements but also contains the secondary bending moments due to temperature gradients through the depth of the bridge deck and girders. (The

relationship between the cyclic displacement of abutments, movements of embankment backfill, and associated problems with approach slabs will be discussed in section 2.1.) The cause of such secondary bending moment is that the centroid of the temperature distribution curve and the centroid of the (typically composite) cross-section of the girders may not coincide (Arsoy et al. 1999). Emerson (1977), Hoffman et al. (1983), Imbsen et al. (1985), and Potgieter and Gamble (1989) all studied the temperature distribution through bridge girders. Oesterle et al. (1999) conducted an experimental study for composite bridge sections in Illinois and monitored a heavily skewed steel IAB in Tennessee. The most critical factors identified in the study are the maximum temperature differential and the distribution of the differential through the depth of the section (Oesterle et al. 1999). It can be observed that the temperature differential changes more drastically in the bridge deck than through the depth of the bridge girders. Thippeswamy et al. (2002) stated that the temperature gradient is a major contributor to total stress in a bridge superstructure. Consequently, the distribution of temperature should be considered in a bridge's design. Details of the findings regarding the temperature gradients of bridge superstructure will be presented in section 2.1. Based on the reviewed studies, Arsoy et al. (1999) assessed that the moments caused by the thermal gradient are similar to those caused by creep and shrinkage.

Another potential effect that needs to be considered in the design of IABs is pavement growth. There is accumulated thermal expansion (growth) of the pavement due to friction between the pavement and subbase after repeated temperature cycles. Such pavement growth may need to be considered in bridge design in the form of longitudinal compression. Burke (1993) found that the pavement growth at the pressure relief/expansion joint can be rapid and incremental. James et al. (1991) observed cracking and dislocation of backwalls of reinforced concrete abutments. The distress is attributed to the longitudinal growth of the reinforced concrete pavement.

Soltani and Kukreti (1992) conducted a survey of all 50 states in the U.S. to primarily learn the maximum IAB length, design details, and problems associated with thermal movement. Wasserman and Walker (1996) documented that previous surveys among 28 states in the U.S. showed that 11 states limited the maximum length for IABs to 91.4 m (300 ft); 7 states limited it to 76.2 m (250 ft); and 3 states permitted bridge lengths up to 212.9 m (400 ft). Kunin and Alampalli (2000) also summarized the maximum allowable limits for IABs, such as thermal movements, bridge total length, skew, and abutment dimension among 28 states in the U.S. as of 1996. Most responding states, including Illinois, limited any skew to no more than 30°.

1.3 Overview of IAB Approach Slabs

Approach slabs are structural components used as a transitional span between the road pavement and a bridge superstructure. In the past few decades, the approach systems of bridges have oftern suffered from the "bump" problem at the end of the abutment due to settlement (Hopkins 1969, Hu et al. 1979, Allen 1985, Laguros et al. 1990, Wahls 1990, Kramer and Sajer 1991, Briaud et al. 1997, Long et al. 1998, Hoppe 1999, Seo et al. 2002, Bowders et al. 2003, White et al. 2005, White et al. 2007, Breña et al. 2007, Puppala et al. 2009, Martin and Kang 2013). This has especially been the case when approach slabs were not used. Hence, approach slabs as a solution to alleviate the differential settlement at the approach system were introduced. Figure 1.8 shows a typical elevation view of approach slabs used in Illinois. The approach slabs in Illinois are generally 9.1 m (30 ft) long and reinforced with both top and bottom rebar mats. One row of vertical anchor

rods is used to connect the abutment and the approach slab. On the other side of the approach slab, it is supported by a pile bent or a sleeper slab. An expansion gap is placed at the interface of the approach slab and the transition slab, which is typically 21.3 m (70 ft) long.
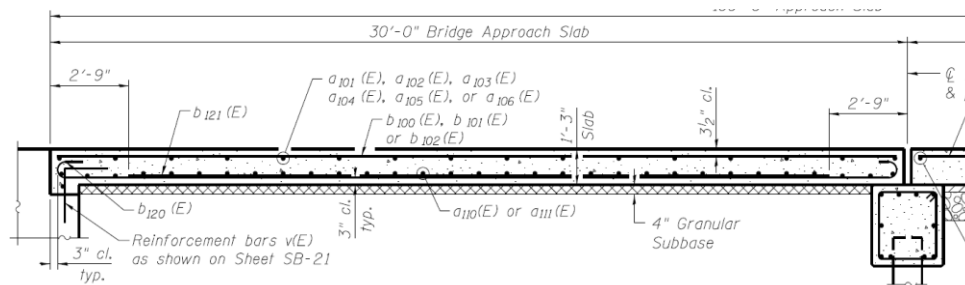
Figure 1.8 Elevation view of a typical IAB approach slab (Illinois Tollway 2015).

Briaud et al. (1997) summarized the primary functions of an approach slab:

1. To span the void that may develop below the slab.
2. To minimize slab deflection, which could result in settlement near the abutment.
3. To provide a ramp for the differential settlement between the embankment and the abutment; this function is affected by the length of the approach slab and the magnitude of differential settlement.
4. To provide a better seal against water percolation and erosion of the embankment.

Approach slabs have proven effective for minimizing the bump problem related to differential settlements in the approach system, and they have been used by almost every highway department in the U.S. (Kramer and Sajer 1991). However, the settlement problem still existed even when approach slabs were used, and distress of the approach slabs was reported. According to Kramer and Sajer (1991), sometimes, the use of approach slabs simply moves the bump problem from the abutment-approach interface to the approach slab-pavement interface. Kunin and Alampalli (2000) reported that all 50 IABs built in Arizona needed expensive repair of approach slabs. Kramer and Sajer (1991) also suggested that structural damage to approach slabs can be difficult and expensive to repair.

The Illinois Tollway observed significant cracking in IABs constructed in 2013 and 2014, and found cracking to be a concern for mainline interstate bridges in Illinois. Approach slabs with high skew angles were reported to have a large number of cracks, while slabs with low skew angles were generally observed to incur fewer cracks. The Illinois Tollway has used precast slabs to reduce cracking, but some cracks have been observed on the precast slabs as well.

Though many efforts have been made to study the behavior of approach slabs and improve their design, which will be discussed in detail in chapter 2, the design of approach slabs and IABs are still empirical to some extent, and there are still unresolved issues with approach slabs. Studies on the thermal behavior of IABs appear more extensive than those of approach slabs. Consequently,

25

it is necessary to further study the factors that affect IAB approach slab performance and the behavior of the approach slabs under primary and secondary loads.

1.4 Approach slab investigation

This research project was funded by the Illinois Tollway to investigate cracking that has been observed in bridge approach slabs, particularly at integral abutment bridges, with the goals of understanding the mechanism of approach slab cracking, improving performance, and reducing maintenance at bridge approach slabs on the Tollway. The results of this research project will contribute to improved ride quality, reduced approach slab repair/replacement costs, and efficient future approach slab construction. The primary tasks undertaken by the research team from the University of Illinois Urbana-Champaign were:

- Literature review;
- Agency survey;
- Review and synthesis of prior approach slab field inspections (crack surveys);
- New approach slab field inspections (crack surveys);
- Field instrumentation of two Tollway approach slabs,
- Long-term data collection and evaluation of traffic and thermal effects,
- Short-term static truck loading tests and evaluation of thermal effects,
- Numerical simulations, including parametric studies, of approach slab behavior under traffic and thermal effects.

2 Literature Review, Agency Survey, and Crack Survey

A summary of the reviewed literature pertaining to select studies of IABs is given in this chapter to provide context and background information for the present research in comparison with previous studies. The literature review covers topics related to design, performance issues and possible mitigation strategies, field monitoring of IAB approach slabs, and numerical modeling of approach slabs.

A transportation agency survey and a field crack survey conducted by the research team are also briefly described at the end of this chapter.

2.1 Literature Review

2.1.1 Select Studies of IABs

The behavior of IABs is not the primary focus of this study. However, due to the fact that integral abutments and approach slabs are generally connected and move together as the temperature changes, it is valuable to review the behavior of integral abutments and the temperature profiles of IABs as a reference for the analysis of approach slabs.

2.1.1.1 IAB Behaviour Due to Temperature Change

Representative studies of IAB behavior – in the form of field monitoring and numerical modeling – provide useful observations and findings.

Hoppe and Gomez (1996) instrumented an integral backwall (semi-integral) bridge in Virginia during construction and monitored it for 2.5 years, from the summer of 1993 to January 1996. The instrumentation included strain gages, temperature probes, and earth pressure cells that measured stresses at the bottom flange of steel girders and soil pressures behind the backwall and the abutment. Data were collected by three Campbell Scientific CR-10 dataloggers at the interval of 20 minutes. The results showed that the integral backwall bridge performed satisfactorily in the 2.5-year monitoring period. Settlement of bridge approaches was the dominant maintenance problem and was most likely magnified by cyclic movements of the integral backwall. Hoppe and Gomez (1996) suggested that the thermal movements of the superstructure need to be effectively accommodated in the adjacent embankment without causing undue settlement and distress in the bridge approach. Some horizontal rotation of the skewed bridge superstructure caused by non-collinear resultant soil forces at each abutment backwall was detected (Hoppe and Gomez 1996).

Arsoy et al. (1999) conducted finite element analysis to model a 302-ft (92-m) long, 82-ft (25-m) wide integral bridge with W44x285 steel girders using SAGE (Static Analysis of Geotechnical Engineering Problems). The bridge superstructure, abutment, approach fill, foundation piles, and the foundation soil are considered as a plain strain problem with simplification using symmetry. In addition to gravity load, the loads applied to the abutment represent the forces due to the superstructure thermal deformations. The study suggested that there was accumulated thermal expansion (growth) of the pavement due to the friction between pavement and subbase after repeated temperature cycles. Such pavement growth may need to be considered in bridge design

in the form of longitudinal compression. James et al. (1991) also conducted finite element analysis considering the longitudinal growth of the reinforced concrete pavement and concluded that such behavior can cause excessive pressure on the abutments.

A non-skewed IAB in Massachusetts was monitored for a period of three years (Breña et al. 2007). The bridge is 270 ft (82.3 m) long, with three spans: 80 ft (24.4 m) for exterior spans and 110 ft (33.5 m) for the interior span. The superstructure consists of a 8 in. (200 mm) concrete deck and four 48 in. (1,220 mm) deep steel girders. Longitudinal and transverse displacements of the bridge at the abutments, earth pressures behind the abutment walls, strains in flanges of exterior piles, and temperatures were measured and collected. Figure 2.1 presents the measured displacement components at the abutment-pile system.
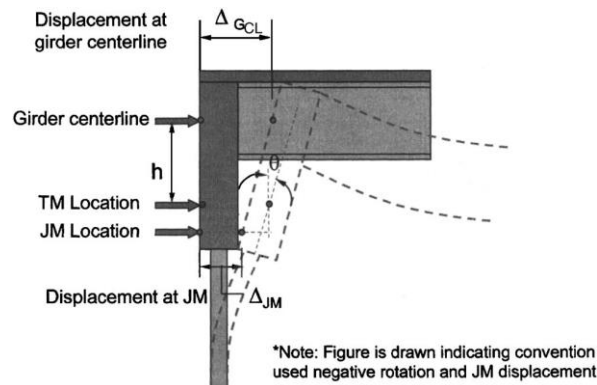
Figure 2.1 Displacement component at the abutment and piles (Breña et al. 2007).

Breña et al. (2007) found that the average thermal response of the bridge followed the ambient temperature variations closely. The trends of the longitudinal displacements of the abutments are approximately linear. Rapid and large temperature variations in early spring led to sudden bridge displacements and high backfill pressures. The abutment displacements and rotations affect the backfill pressures, pile moments, and superstructure stresses. The north abutment top displacement indicated negligible longitudinal restraint from the backfill, whereas higher longitudinal restraint was found at the south abutment, according to the abutment top displacement – temperature change relationship, as shown in Figure 2.2. Since the equivalent coefficients of thermal expansion for the north and south abutments were different, $6.0\times10^{-6}/$ °F vs. $5.0\times10^{-6}/$ °F ($10.8\times10^{-6}/$ °C vs. $9.0\times10^{-6}/$ °C), an elastically restrained bar model, shown in Figure 2.2, was used to estimate the backfill soil stiffness.
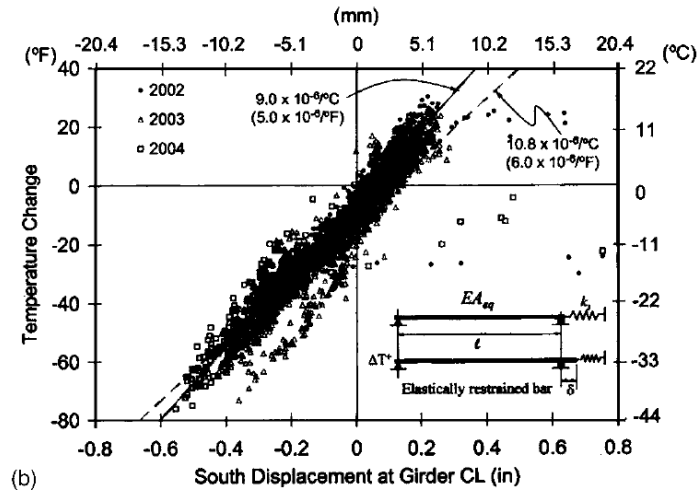
Figure 2.2 Temperature change vs. top displacement of south abutment (Breña et al. 2007).

Three years of the south abutment base displacement data might indicate that the initial differences in longitudinal restraints at abutment base due to different compaction conditions after construction were eliminated gradually (Breña et al. 2007). Tilt meter data showed accumulated rotation at zero temperature change, which may be attributed to backfill shifting into the void created by abutment movements during the bridge contraction phase. Data also indicated that after the longitudinal displacement of the abutment reached certain limits, the abutment rotations increase without an increase in longitudinal displacement near the abutment base. Inclinometer readings indicated that after the peak thermal contraction, abutment top displacement was controlled mainly by abutment rotation, which may be explained by the backfill falling into the void created by the bridge contraction restrained the rotations in the winter (Breña et al. 2007).

Horizontal extensometers, tiltmeters, and a total station were used to measure the abutment movements of a non-skewed IAB. This IAB, near Rochester, Minnesota, with 216.5 ft (66 m) total length and three spans, was monitored from the start of construction through several years of service. The bridge consists of four prestressed concrete girders. Lawver et al. (2000) claimed the bridge behavior was affected by the changes in air temperature and solar radiation. Different from the findings of Breña et al. (2007), readings taken bi-weekly indicated that the superstructure expansion and contraction were primarily accommodated by the horizontal translation of abutments, but not by abutment rotations (Lawver et al. 2000). The seasonal rotation of the abutment was measured to be as small as 0.06°. The double curvature of the piles was given as an explanation for the small rotation of the abutments.

There was an accumulated inward displacement of the abutments over time (Lawver et al. 2000). The inward movement in the first year could be attributed to the shrinkage of the deck. It was not certain why the inward displacement continued after the first year, but the possible explanation could be soil collection and compaction behind the abutments during winter, trapping of debris in the expansion joints of the approach slabs, or continued cambering of the superstructure. A coefficient of thermal expansion of $5.8 \times 10^{-6}/ °F$ ($10.5 \times 10^{-6}/°C$) was used to anticipate the bridge superstructure movements, leading to a 0.75 in. (19 mm) expected movement for the first six

months of monitoring, which was close to the measured displacement 0.71 in. (18 mm). The spot-weldable steel reinforcement strain gages at the interface between the abutment and the approach slab measured the change in strain of the reinforcement, which was controlled by seasonal superstructure movements. It was observed that in the summer, solar radiation influenced the bridge more significantly than the surrounding air by creating a thermal gradient across the width and depth of the bridge. However, in the winter, the solar radiation placed a smaller effect on the bridge due to the lower angle of the sun in the sky (Lawver et al. 2000).

Abendroth et al. (2007) reported that field monitoring data indicated a reasonable correlation between the change in bridge length and the average bridge temperature. However, the displacements of the abutments of the 110-ft (33.5-m) long, 30-ft (9.1-m) wide, single-span prestressed concrete girder IAB were different: almost all longitudinal displacements for the superstructure were from the east abutment. Since the soil backfill condition seemed to be the same for the abutments, it was believed that such differential abutment displacement was attributed to the 4.25 in. (108 mm) decrease in elevation for the east abutment, making the bridge pitched to the east abutment. The magnitude of these longitudinal movements fell into the lower bound of the predicted range for a bridge of this length. The change in position of the abutment consists of two parts: (1) the volume change of the concrete in the pile cap and abutment due to temperature variations, and (2) rigid-body translation and rotation of the abutment due to the thermal movements of the superstructure for a skewed IAB (Abendroth et al. 2007).

McBride (2005) validated the assumption of free of constraint for IAB subjected to thermal movements. Thermal effects on the superstructure stresses of the Evansville Bridge in Preston County, WV were investigated as well. Finite element modeling and field monitoring of the Evansville Bridge, a three-span IAB, indicated that full composite behavior was not achieved by the shear studs. IABs are not free to expand and contract fully with changes in temperature due to the constraints introduced by soil backfill, shear studs, and corrugated stay-in-place forms. The temperature-induced stresses, as well as stresses caused by constrained drying shrinkage, can increase the stress to a level indicating more cracks in the bridge deck.

Thippeswamy et al. (2002) conducted an analytical simulation of five jointless bridges considering various combinations of primary and secondary loads as well as a field monitoring of a three-span 177-ft (53.9-m) long jointless bridge in West Virginia. The results indicated that temperature gradient is the major contributor to total stresses in bridge superstructure. Concrete creep is helpful to reduce induced stresses in the superstructure. Shrinkage relieves creep partially.

The changes in temperature not only affect the bridge superstructure as well as the abutments, but also result in the volumetric changes and displacements of the backfill soil of the embankment that is behind the abutments.

In each annual (seasonal) cycle of temperature, when the temperature increases, the superstructure expands, pushing the abutments outward to the retained backfill soil; when the weather becomes colder, the superstructure contracts moving the abutments away from the backfill soil that the abutments retain, leading to the development of void at the interface of abutment and the backfill soil. Figure 2.3 illustrates the development of void near the abutment due to thermal movements of the IAB (Arsoy et al. 1999).
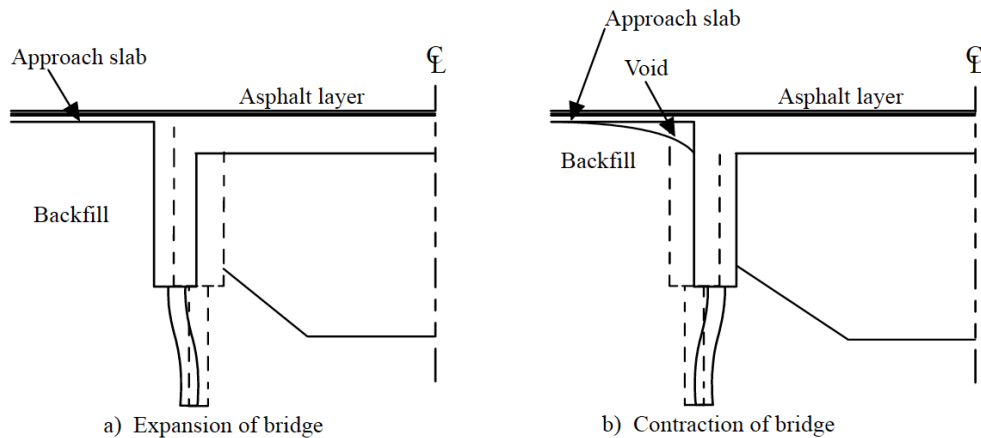
Figure 2.3 Void between the abutment and backfill soil due to abutment movement (Arsoy et al. 1999).

Different from the assessment made by Breña et al. (2007) that both the abutment translation and rotation have nonnegligible contributions to the movement of an abutment and the one stated by Lawver et al. (2000) that abutment movement primarily is made up of horizontal translations, Horvath (2000) suggested that the primary component of abutment movement is rotation about the bottom of the abutment. Horvath (2000) also mentioned that there is usually a net inward movement of the abutments that is away from the retained soil, as shown in Figure 2.4. Such net displacement is exacerbated when the girders of the superstructure are made of Portland cement concrete due to the inherent post-construction shrinkage effect (Horvath 2000). The net displacement is due to the nonlinear soil wedging and can lead to increasingly large horizontal earth pressure as much as the theoretical passive state (Horvath 2000). This behavior was referred to as "ratcheting", according to Horvath (2000).
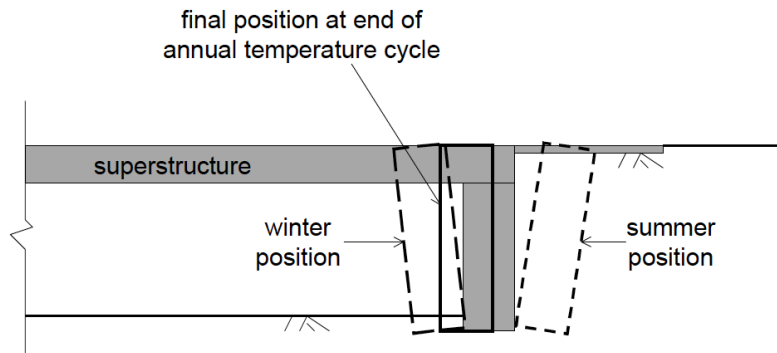
Note: Initial abutment position at start of annual temperature cycle shown by shaded area.

Figure 2.4 Abutment movement due to temperature changes (Horvath 2000).

2.1.1.2 Temperature Profiles of IABs

Studies on the temperature changes and distributions in IABs were conducted either with dedicated experiments or as a part of the field monitoring of IABs.

Emerson (1977) estimated the temperature distribution through the depth of concrete bridge decks and the concrete deck slabs of composite bridge based on empirical methods as well as field data. The study suggested that temperature differences will always exist in the deck slabs except during prolonged periods of overcast or during wet weather. The temperature distribution is attributable to the type of construction, the time of day, the time of year, the section depth, surfacing, and possibly the weather conditions of the previous one or two days for concrete structures. Figure 2.5 illustrates how the environmental factors affect the temperature distribution.
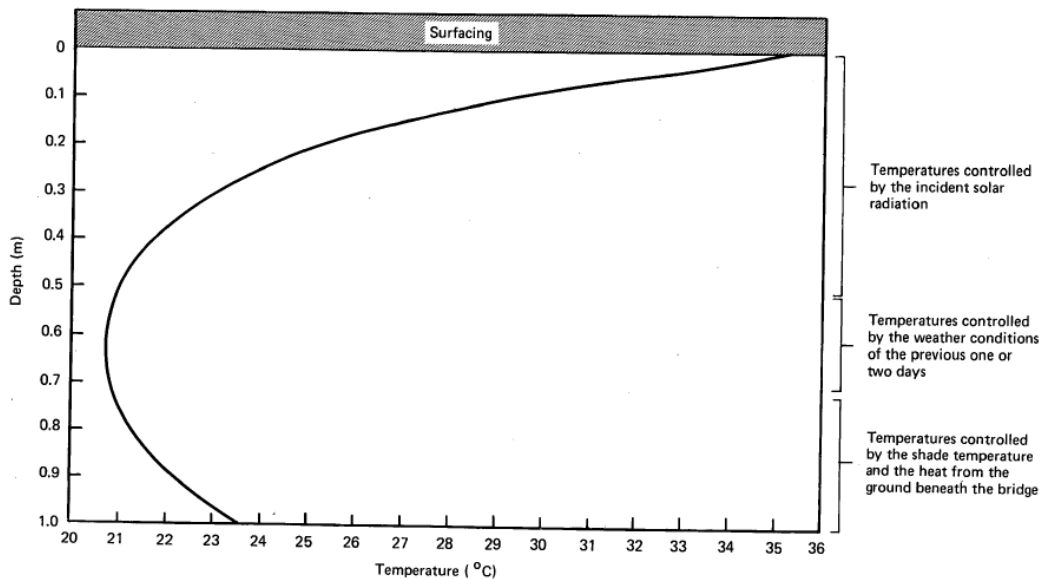
Figure 2.5 Temperature distribution of a bridge superstructure and controlling environmental conditions (Emerson 1977).

Oesterle et al. (1999) carried out experiments to address thermal movements and stresses, including creep and shrinkage movements. The concept of effective bridge temperatures is defined as the uniform temperature that would lead to the same change in bridge length as the nonlinear temperature distribution. The considered temperature variations included the effects of annual (seasonal) variation on the total bridge length and the effects of diurnal (daily) variation on the thermal gradient. It was found that the extreme effective temperatures can be effectively approximated by extreme shade air temperatures. The American Association of State Highway and Transportation Officials Load and Resistance Factor Design (AASHTO LRFD) specifications provides a more conservative estimate of extreme temperature gradient compared to experimental measurements. Tests also suggested that environment-dependent creep and shrinkage of concrete generally contributes to the relief of thermal stresses, by an average of 12% for nonwinter weather and 3% during winter (Oesterle et al. 1999).

In addition, a 415.9-ft (126.8-m) steel integral abutment bridge (the longest at the time) with a 59° skew in Tennessee was instrumented and monitored. The seasonal and diurnal thermal strain

changes were small compared to strains corresponding to the design allowable stresses (Oesterle et al. 1999).

According to Soltani and Kukreti (1992), Tennessee DOT claimed that the temperature cycling of concrete bridges seemed to reach lower peaks than steel bridges. Thippeswamy et al. (2002) suggested that a bilinear gradient with 30°F (16.7°C) at the top of the deck, 5°F (2.8°C) at the bottom of the deck, and 0°F (0°C) at the bottom of girders for summer conditions and a bilinear gradient -15°F (-8.3°C) at the top of the deck, 5°F (-2.8°C) at the bottom of the deck, and 0°F (0°C) at the bottom of girders for winter conditions can be used (all temperatures are compared to the ambient temperature). Abendroth et al. (2007) found that the measured thermal gradient through the depth of superstructure for the coldest day was stable and similar to the recommend thermal gradient in AASHTO.

2.1.2   Approach Slab Design, Problems, and Mitigation Methods

Just as the application of IABs has advanced, the design and performance of approach slabs have also changed over time. This section provides a review of the prevalent issues that the approach slabs or approach systems are facing, the findings of previous surveys and studies, and the potential mitigation methods for the problems.

2.1.2.1 Design Practice of Approach Slabs

There are several studies that contain the responses of agency surveys (Allen 1985, Kramer and Sajer 1991, Hoppe 1999, Kunin and Alampalli 2000, Greimann et al. 2008) or synthesize previously conducted surveys (Wahls 1990, Maruri and Petro 2005, White et al. 2005, Martin and Kang 2013) concerning the design practice and performance of approach slabs.

Allen (1985) found that among the 41 states responding to the survey, 34 states use reinforced approach slabs, and 26 among them rated the performance as good. The length of reinforced approach slabs ranges from 10 to 120 ft (3 to 36.6 m) with an average of 33 ft (10 m). Wahls (1990) reported that the approach slabs used by most state agencies are of uniform thickness, but some sections are thicker near the abutment to provide more flexural resistance. Hoppe (1999) synthesized survey responses from 39 states regarding the design, maintenance, and settlement problems of bridge approach slabs. Almost every state DOT utilizes a unique standard for the design, construction, and use of bridge approach slabs. The survey showed that 71% of responding states use mechanical connections between the approach slab and the integral abutment. Half of the respondents commonly make the slab length 20 ft (6.1 m), with an average thickness of 12 in. (0.30 m). Martin and Kang (2013) summarized the design practice for approach slabs among 21 states. The approach slab length ranges from 6.6 to 60 ft (2 to 18.3 m), with a majority between 20 to 30 ft (6.1 to 9.1 m). The thickness of the approach slab varies from 9.4 to 17 in. (240 to 432 mm), most of which are around 12 in. (305 mm).

The amount of reinforcement varies with the design loads and slab length. Most approach slab designs have top and bottom mats and are one-way slabs without intermediate support (Wahls 1990). Martin and Kang (2013) found that the longitudinal reinforcement ratio ranges from 0.55% to 1.23% among the 21 states in the U.S.

Approach slabs are attached rigidly to the abutment with a moment connection or only by a pinned connection (Oesterle et al. 1999). Similarly, Kunin and Alampalli (2000) mentioned three options for the approach slab-integral abutment interface: one uses reinforcement to connect the approach slab and the deck; another has reinforcing steel connecting the lip or the corbel of the abutment and the approach slab; the last does not use any connection. Seo et al. (2002) introduced approach slab design practice in Texas, where most bridges have stub abutments, and the approach slab is supported by the abutment backwall and the approach backfill. Greimann et al. (2008) conducted a survey on the specific practices of the approach slab among 8 states in the Midwestern United States. Seven out of the nine states used either horizontal or diagonal connections between the approach slab and the abutment. Only Illinois reported a transverse cracking problem with the approach slab.

The state agencies place the expansion joint at the far (pavement) end of the approach slab or between the abutment and approach slab, while other approach slabs have no expansion joints. The type of expansion joint is selected based on durability, movement capacity, easy maintenance, resistance to damage from snowplows, bridge length, and cost (Kunin and Alampalli 2000). An agency survey conducted by Maruri and Petro (2005) confirmed that 31% of the respondents used sleeper slabs, 26% did nothing but resting the slab on the fill, and 30% did both. It was found that approach slabs are tied to the abutment for most of the states, and sleeper slabs with an expansion joint are used on the pavement end of the approach slabs (Martin and Kang 2013).

2.1.2.2 Problems with Approach Slabs

White et al. (2007) summarized the frequent problems of approach systems observed at bridge sites in Iowa, as shown in Figure 2.6. The field study included 74 bridges in Iowa. At 25% of the bridges, thirteen of which were IABs, severe void development problems were observed. It was found that void development commonly occurs within one year of bridge approach slab construction. Severe soil erosion under the approach slab and around the bridge was observed at about 40% of the 74 bridges, fourteen of which were IABs (White et al. 2007).
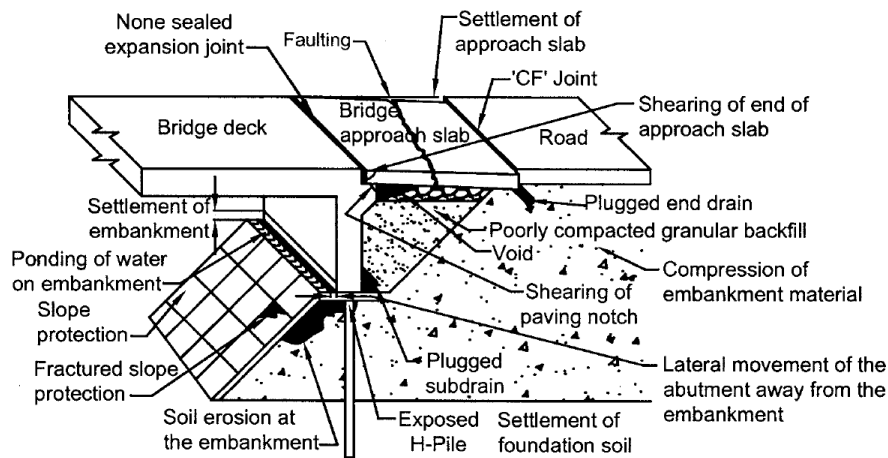
Figure 2.6 Frequent problems with approach system in Iowa (White et al. 2007).

One of the common problems that bridge approach systems face – regardless of the use of approach slabs – is the settlement and associated bump. Allen (1985) reported that 15 out of 41 states considered the settlement of the bridge approach as a major problem. Briaud et al. (1997) reported that about 150,000 bridges, 25 percent of all bridges, in the United States had approach settlement, leading to at least $100 million repair cost every year. In Texas, the state that has the highest number of bridges, 30 percent of bridges experienced the distress of settlement. Hoppe (1999) also reported that the majority of state DOTs consider bridge approach slab settlement as a serious and persistent maintenance problem. Seo et al. (2002) suggested that the bump problem due to settlement at the end of the bridge costs Texas DOT $7.0 million each year.

Briaud er al. (1997) ranked the factors that cause the bump problem in the order of importance:

1. Compression of the fill material (Hopkins 1969, Kramer and Sajer 1991, Arsoy et al. 1999, Puppala et al. 2009).
2. Settlement of the natural soil under the embankment (Hopkins 1969, Wahls 1990). Hopkins (1969) stated that such settlement can be attributed to (a) shear distortion, (b) bearing capacity failure, (c) compression or consolidation of the soil.
3. Poor construction practice (Long et al. 1998, White et al. 2007). White et al. (2007) found that the poor construction practices included poor approach pavement and paving notch construction, not using specified backfill materials, placing granular backfill in too thick of lifts and within the bulking moisture content range, and not placing the approach slab reinforcement steel as specified in the design.
4. High traffic loads (Laguros et al. 1990, Seo et al. 2002, Lenke 2006, Puppala et al. 2009). Seo et al. (2002) conducted a scaled circular track test with repeated vehicle load, concluding that the bump size is proportional to the number of load cycles on a log-log plot, and soil with higher compaction help reduce the bump effects. Lenke (2006) suggested that the bump problem increases with vehicle weight, vehicle velocity, and the number of load cycles. However, Hopkins (1969) stated that suggestive evidence indicates that traffic is not a major factor responsible for the settlement of bridge approaches. Field evaluation conducted by Bakeer et al. (2005a) suggested that speed limit and traffic may not have a significant impact on the performance of pile-supported approach slabs.
5. Poor drainage (Hoppe 1999, Puppala et al. 2009).
6. Poor fill material.
7. Loss of fill by erosion (Long et al. 1998, White et al 2007, Puppala et al. 2009).
8. Poor Joints.
9. Temperature cycles (Smith 1985, James et al. 1991, Burke 1993, Arsoy et al. 1999, Horvath 2005, White et al. 2005, Bakeer et al. 2005b). Smith (1985) claimed that cracking and bulking at the approach pavement are caused by lateral cyclic movement of the abutment from thermal movement-induced stresses at the bridge decks. Arsoy et al. (1999) and Horvath (2005) provide detailed explanations of how IAB thermal movements lead to void and approach slab distresses, as discussed in section 2.1.1. James et al. (1991) and Burke (1993) show a potential risk of pavement growth to the damage of approach slabs and abutments, as discussed in section 1.2.

Figure 2.7 also summarizes the factors that may contribute to the bump problem (Briaud et al. 1997).
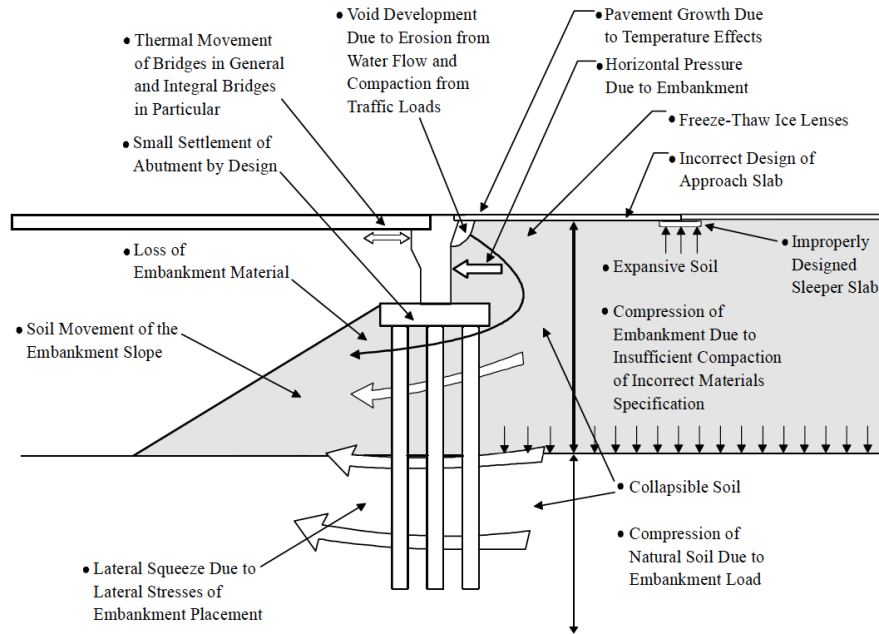
Figure 2.7 Factors that may contribute to the bump problem (Briaud et al. 1997).

In addition, the height of the embankment can also affect the approach settlement (Laguros et al. 1990).

Puppala et al. (2009) mentioned the following factors that are also relevant to the approach settlement:

1. Abutment type.
2. Age of approach slab (Laguros et al. 1990, Bakeer et al. 2005, Lenke 2006). Bakeer et al. (2005) inspected approach slabs built in the 1960s, 1970s, 1980s, and 1990s and found that generally newer pile- and soil-supported approach slabs were in better condition than the older ones.
3. Design of approach slabs. The difference in support method for both ends of approach slabs and insufficient length of approach slabs can result in the destruction of the approach slabs (Wahls 1990, Briaud et al. 1997).
4. Bridge skew (Laguros et al. 1990, Hoppe and Gomez 1996, Nassif 2002, Abendroth et al. 2007). Horizontal rotations of the abutment were observed, as discussed in section 2.1.1 (Hoppe and Gomez 1996, Abendroth et al. 2007). Nassif (2002) compared the performance of skewed and non-skewed approach slabs under the same truck load using finite element analysis. The results suggested that tensile stresses on the skewed approach slabs were 20 to 40 percent higher than those on un-skewed approach slabs.

Long et al. (1998) conducted a visual (drive-by) survey during the summer of 1994 on 1,191 bridge approaches in Illinois to evaluate the differential approach settlement. 27 percent of the inspected approaches exhibited a significant differential settlement at the approach embankment-bridge interface. Adjacent states, including Iowa, Wisconsin, Michigan, Ohio, Indiana, Missouri, and Kentucky, showed a similar percentage of approach embankment-bridge distress. It was found that, in Illinois, the differential settlement occurred at the approach embankment-abutment interface, at

the end of the approach slab, or at a break or crack in the approach slab. The authors believed the following factors are major causes of differential movement in Illinois: (1) local compression or erosion of soil at the approach embankment-abutment interface, (2) a broken approach slab, (3) compression of foundation soils, (4) compression or internal erosion of embankment soils, (5) poor construction grade control, and (6) areal distortion of foundation soils due to mine subsidence. It was also noted that structural distress such as cracked approach slabs can be caused by excessive traffic loads (overloads) when traffic volume or weight exceeds the originally intended service loading. Vertical movement, horizontal movement, and tilting of abutments can also lead to significant approach distress.

Martin and Kang (2013) summarized the structural problems of approach slabs based on reviewed agency surveys, as shown in Table 2.1. Kunin and Alampalli (2000) stated that transverse or longitudinal cracking and cracks in asphalt overlays at the end of approach slabs are also common problems of approach slabs. The performance of the approach slabs was found to depend on (1) the approach slab dimensions, (2) the steel reinforcement, (3) the use of a sleeper slab, (4) the type of connection between the approach slab and the bridge (White et al. 2005).

Table 2.1 Structural problems and their causes for approach slabs (Martin and Kang 2013).

Structural Problem	Causes
Concrete spalling of the approach slab	Poor construction
	Lack of tie between abutment and approach slab
Excessive deflection of the approach slab leading to an unsmooth transition to the bridge	Approach slab is not stiff enough
Water intrusion of approach slab and/or backfill material	Approach slab has excessive cracking
	Expansion joints are not properly maintained

2.1.2.3 Mitigation Methods

Based on the problems noted above for approach slabs, various efforts have been made to improve their performance.

Briaud et al. (1997) suggested that settlement calculations and corresponding design considerations are necessary for bridge approach system/slab. Hoppe (1999) recommended to design the approach slabs with a full width of the roadway and determine the length based on the expected settlement. Seo et al. (2002) determined the optimum width of the sleeper slab and support slab to be 1.5 m (5 ft), based on numerical analyses. A new approach slab design with 6 m (20 ft) length and 330 mm (13 in.) thickness was recommended (Seo et al. 2002). An expansion joint and a sleeper slab at the approach pavement interface were recommended to allow for thermal expansion (Briaud et al. 1997, Bakeer et al. 2005b). White et al. (2005) suggested to connect the approach slab to the abutment and support the approach slab on the pavement end with a 50.8 mm

(2 in.) sealed joint. A rubber V-shaped gland joint sealing system was recommended (White et al. 2005).

Bowders et al. (2003) investigated and evaluated a new approach slab design adopted in Missouri. The approach slab was 9 m (30 ft) long and supported by the bridge abutment and sleeper slab. A grid of holes was included in the slabs for pressure grouting (mudjacking) after some settlement was observed. However, the results showed that such a new design was not an effective solution.

Martin and Kang (2013) stated that although many bridge approach problems are due to geotechnical issues, appropriate structural design can elongate the service life and reduce maintenance costs. An anchor bar connection introduced by Greimann et al. (2008) was believed to be the most proper solution since such connection accommodates the rotation of the approach slab better when differential settlement is a concern, leading to less stress at the interface.

Puppala et al. (2009) summarized the ways of improving the performance of approach slabs in the aspect of embankment foundation and bridge design, which is presented in Table 2.2.

Table 2.2 Mitigation methods for approach settlement.

Embankment Soft Foundation Improvement Techniques			Design Improvements		
Mechanical		Excavation and Replacement	Bridge Foundation	Shallow Foundation	Spread Footings
		Preloading and Surcharge		Deep Foundation (more preferred)	Driven Piles and Drilled Shafts
		Dynamic Compaction	Integral Abutment	Compressible Elastic Materials behind Abutment	
Hydraulic		Sand Drains		Sufficient Drainage	
		Prefabricated Drains	Approach Slab	Length	Based on Maximum Slope of The Slab
		Surcharge Loading			> 20 ft.
Reinforcement	Columns	Stone and Lime Columns		Slope	< 1/200
		Geopiers			Sloped Slab in Its Length Direction
		Concrete Injected Columns		Thickness	Increase the Thickness
		Deep Soil Mixing Columns			Ribbed Slab
	Deep Foundations	In-situ: Compacted Piles		Width	Curb-to-curb
		Continuous Flight Auger (CFA) Cast Piles		Support	Appropriate Backfill Material
		Driven Piles: Timber and Concrete Piles			Sleeper Slab
	Geosynthetics	Geotextiles/ Geogrids			Pile Bent
		Geocells			
Material		Mechanically Stabilized Earth (MSE) Wall			
		Geosynthetic Reinforced Soils			
		Lightweight Fill			
		Flowable Fill			
		Grouting			

2.1.3 Field Monitoring of Approach Slabs

2.1.3.1 Rutgers University Study

Researchers at Rutgers University (Nassif et al. 2007) instrumented six approach slabs on the Doremus Avenue Bridge in Newark, New Jersey, and tested them prior to opening to traffic. The research aimed to recommend new design details based on static testing and long-term monitoring of approach slabs. The layout of the approach slabs at the Doremus Avenue Bridge is shown in Figure 2.8. The slabs were constructed such that they have varying lengths to study the effect of length of the slab while the thickness was kept constant at 18 in. The slabs were instrumented with up to 20 sensors of various types: strain gauges, thermistors, dynamic strain gages, pressure cells, settlement sensors, and deformation sensors. The 96 channels of data were collected every hour with data loggers. The maximum and minimum values incurred during each hour were also recorded. More sensors were provided at critical sections identified by prior 3-D FE analysis (Nassif et al. 2002) and near the abutment, as it had been observed that most of the approach slab cracking takes places near abutments.
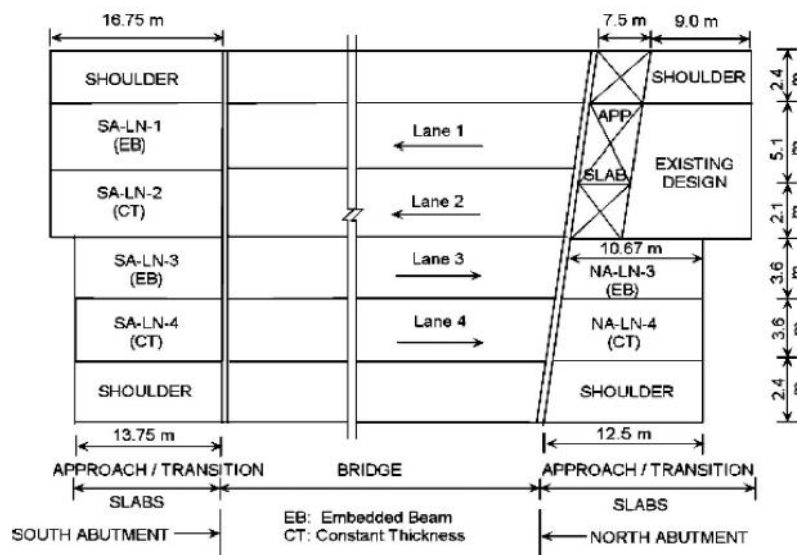
Figure 2.8 Layout of approach slabs on the bridge under investigation (Nassif et al. 2007).

The study showed that the approach slab strains exhibit a sharp initial decrease that is not recovered afterward. This strain change is attributed to the shrinkage of concrete. However, after the initial strain change, subsequent strain changes are observed to be proportional to the temperature of the slab. Typical strain and temperature response histories are shown in Figure 2.9.
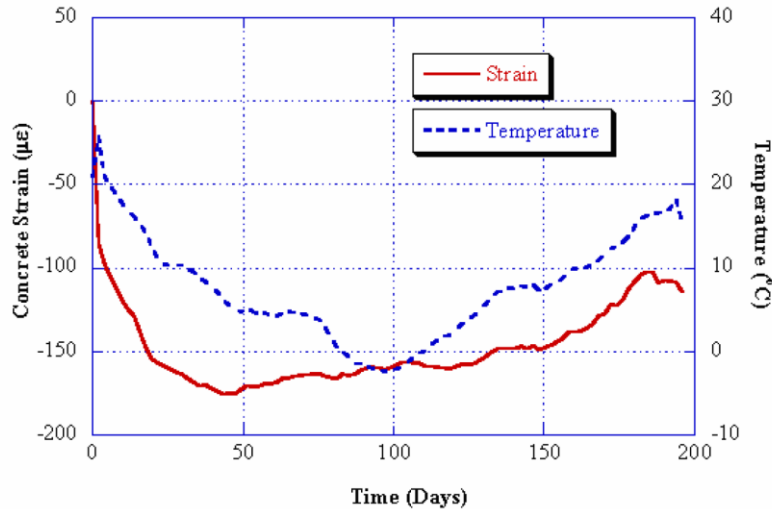
Figure 2.9 Approach slab strain and temperature profile with time (Nassif et al. 2007).

Static testing was performed on three slabs by placing a 3-axle truck on the slab at various positions, traveling in both directions. The strain data obtained from the static testing was used to calibrate the companion 3-D FE models.

2.1.3.2 Iowa State University Study

Researchers at Iowa State University instrumented two 3-span concrete girder bridges constructed in 2006 on the Iowa Highway 60 bypass in Sheldon, IA (Greimann et al. 2008). The objective of the study was to evaluate approach slab performance and the effects of connecting it integrally to the bridge. The northbound bridge has a 76 ft - 11 in. long precast approach slab, while the southbound bridge uses a 29 ft – 6 in. long cast-in-place approach slab. Both instrumented approach slabs have a 30º skew and 12 in. thickness. The support conditions for the two slabs differed significantly, with the precast slab supported continuously with a modified subbase used all along the bottom surface, while the cast-in-place slab is supported only at the ends, using a sleeper slab. The precast approach slab and cast-in-place approach slab are shown in Figures 2.10 and 2.11, respectively. Along with the approach slabs, other structural components, including the deck and piles, were also instrumented on the two bridges.

41
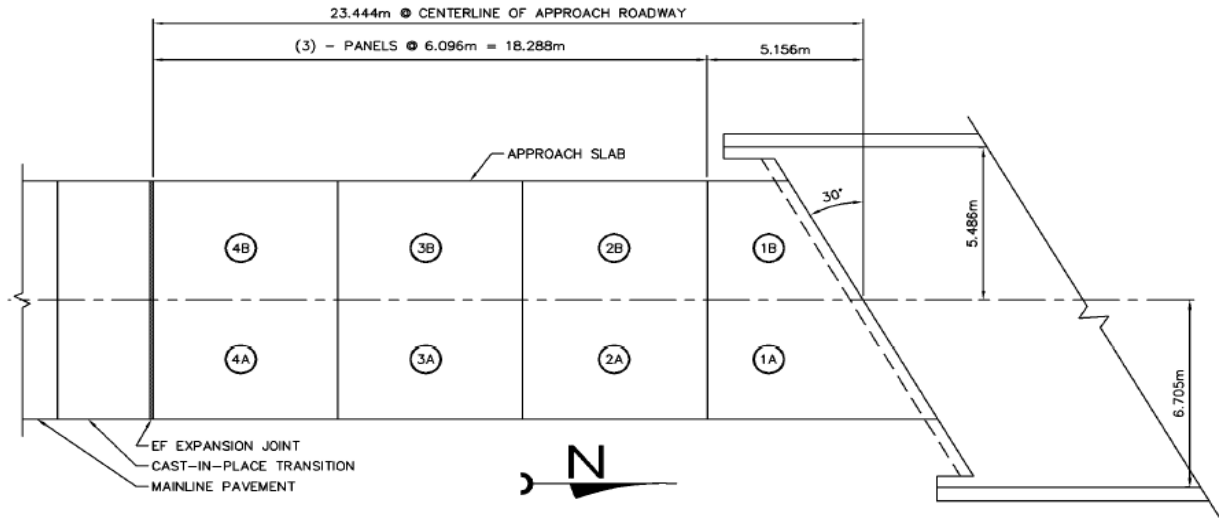
Figure 2.10 Plan view of northbound bridge precast approach slab (Greimann et al. 2008).
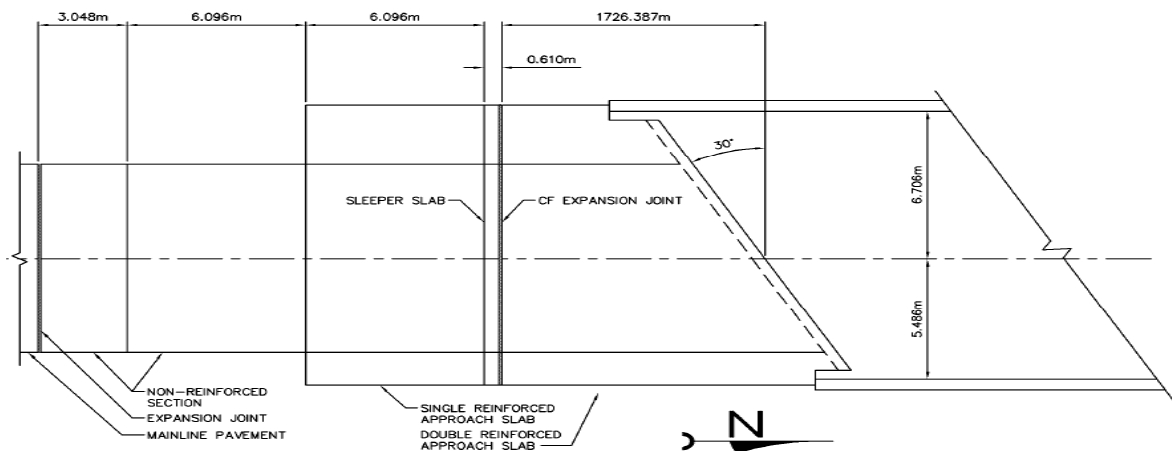
Figure 2.11 Plan view of southbound bridge cast-in-place approach slab (Greimann et al. 2008).

The strains were collected using strain gages installed along the middle of the approach slab arranged along the skew (northbound) and uniformly distributed in the slab (southbound). These were then averaged and elastic behavior of the slab was assumed to calculate slab forces. Both approach slabs showed long-term cyclic variation with each season while also exhibiting smaller short-term cycling behavior due to daily temperature variation, as observed in other studies. As shown in Figures 2.12 and 2.13, the average force in the precast slab was observed to have a clear proportional trend with temperature, but the cast-in-place approach slab showed no clear trend with average temperature, suggesting that the cast-in-place approach slab does not develop any load related strains. This phenomenon can be a result of a lack of restraints to the slab (Greimann et al. 2008).
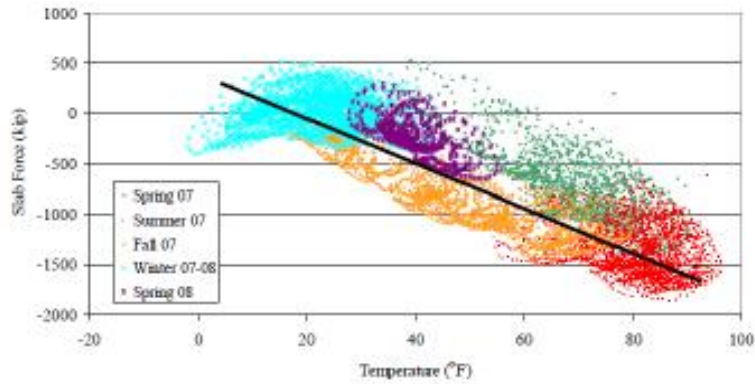
Figure 2.12 Northbound bridge precast approach slab average force (kips) with respect to slab temperature (ºF) (Greimann et al. 2008).
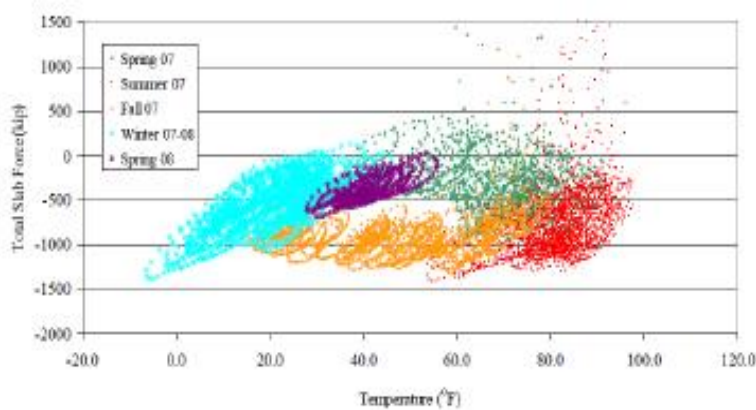
Figure 2.13 Southbound bridge cast-in-place slab average force (kips) with respect to slab temperature (ºF) (Greimann et al. 2008).

The precast approach slab was instrumented with displacement transducers installed across 5 joints (abutment to slab, Panel 1 to 2, Panel 2 to 3, Panel 3 to 4, and expansion joint between Panel 4 and pavement) along with strain transducers in the slab. It was observed that the longitudinal abutment displacement for the northbound bridge was lower than that of the southbound bridge (Farris 2009). This phenomenon was attributed to the difference in the length of approach slabs and the resulting difference in resistance to movement and rotation. However, the transverse abutment displacement for the northbound bridge was found to be higher (almost double) than that of the southbound bridge, and they were observed to have different trends over the year. The reason for this phenomenon was not resolved definitively. The displacement transducers also show negligible relative movement between the panels and between abutment and panels, while the maximum relative movement at the expansion joint was about 1 in. as shown in Figure 2.14 (Farris 2009). The expansion joint movement range for the cast-in-place slab was found to be slightly higher than that of the precast slab, but both slabs follow similar trends in joint opening with time (Greimann et al. 2008).

43
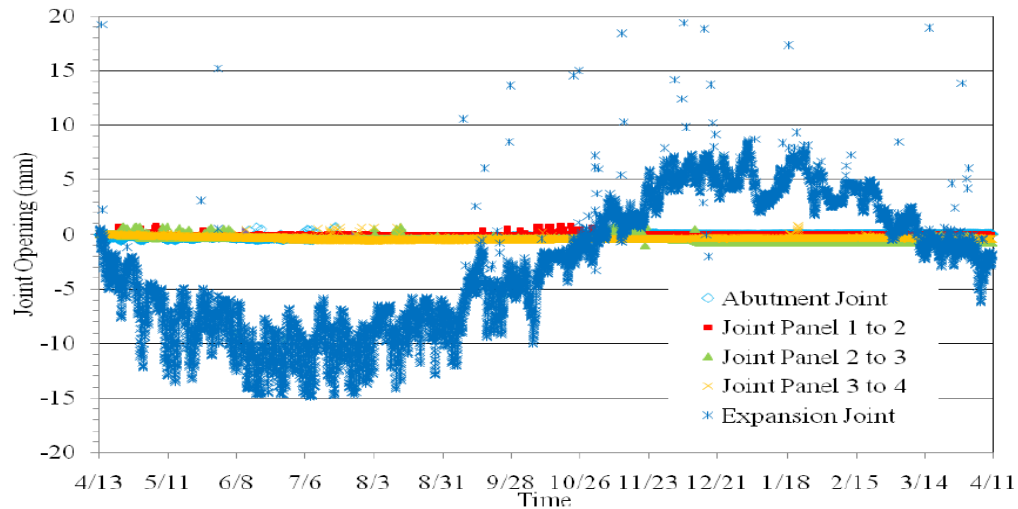
Figure 2.14 Northbound bridge approach slab joint movements (Farris 2009).

In another study (Nadderman and Greimann 2010), researchers at Iowa State University instrumented approach slabs on a bridge on U.S. 63, west of Denver, Iowa. The three-span concrete girder bridge was 161 ft × 40 ft (49 m × 12.2 m), with a skew of 2º29'52". The approach slab used both precast and cast-in-place shoulder sections. The study aimed to evaluate the performance of approach slabs along with a determination of forces that should be considered during the design of IAB approach slabs. Each approach slab consists of eight 12 in. (304.8 mm) thick precast prestressed panels, except at the abutment where the thickness was reduced to 9.5 in. The four panels at the bridge end of the approach slab are trapezoidal, while the ones at the pavement end are rectangular and dowelled to the pavement. The approach slab was monitored using 32 sensors (24 strain gages and 8 displacement transducers) to record the variation of strain in the approach slab along with the relative movement of approach slab joints. The approach slab dimensions and instrumentation scheme are shown in Figure 2.15.
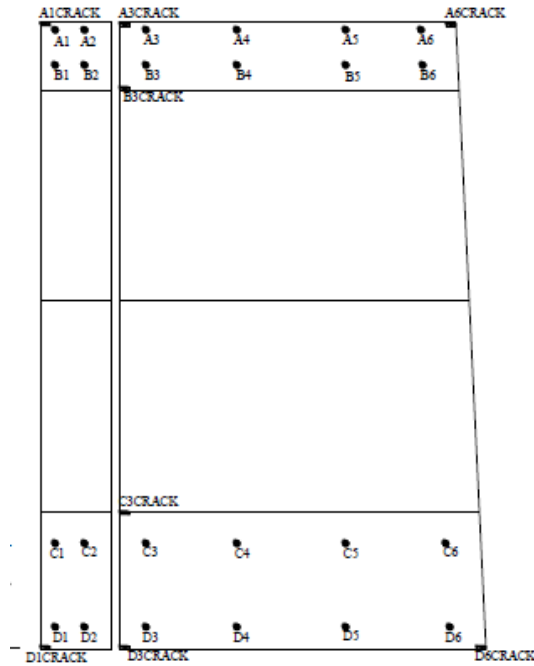
Figure 2.15 Instrumentation plan used for bridge on U.S. 63 near Denver, Iowa (Nadderman and Greimann 2010).

The research team defined load strain as the strain caused in the concrete by an applied load or restraints to expansion and calculated it by subtracting the strains caused by thermal expansion/contraction of the slab from the total strain observed at the sensors. They observed that as the temperature decreases, the load strain observed in the slab increases, such that the load strain moves towards compression in the summer season and tension in winter. The load strains vs. time observed for all the working gauges are shown in Figure 2.16.
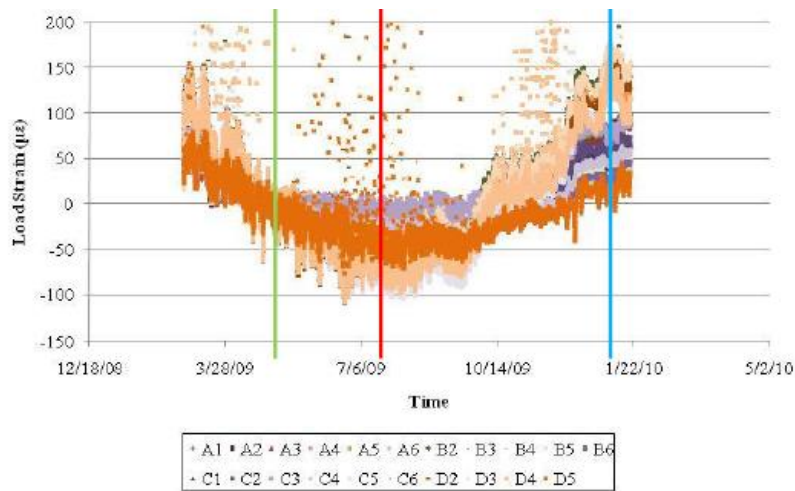
Figure 2.16 Load strain with respect to time for instrumented bridge (Nadderman and Greimann 2010).

45

The average load strain was calculated by averaging the load strains at each of the working sensors, which was in turn used to calculate the average slab force. This was plotted against the average temperature of the slab, and it was observed that the average slab force follows a cyclic pattern. The change in force in the slab ranged from -1166 kips in the summer to 2996 kips in the winter (where tension is negative), showing significant forces applied due to live load and constraints from the boundary conditions, as shown in Figure 2.17.

(a)

(b)

Season	Dates	Color
Winter 2009	2/25 to 3/21	
Spring	3/22 to 6/21	
Summer	6/21 to 9/21	
Fall	9/22 to 12/21	
Winter 2010	12/22 to 1/19	
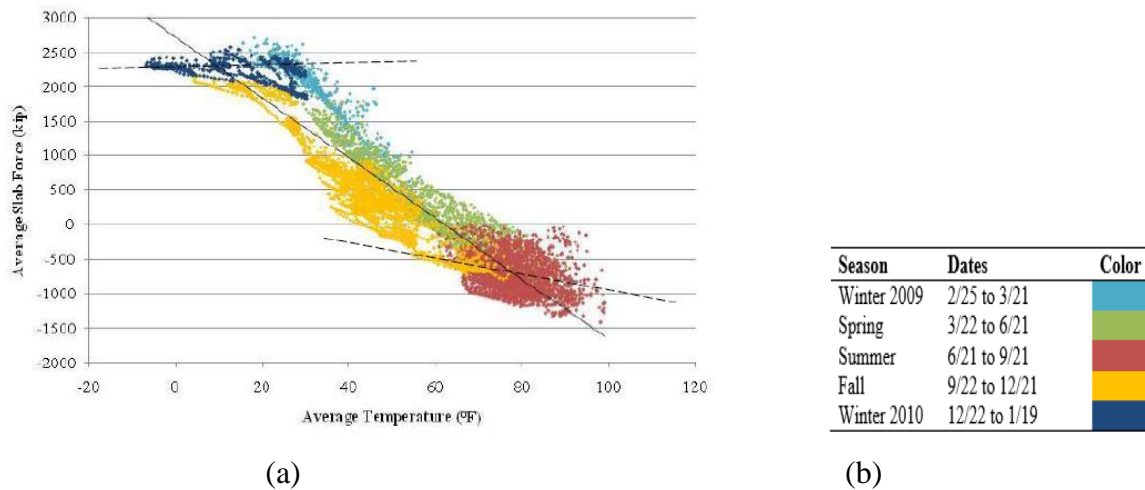
Figure 2.17 (a) Average slab force with respect to average temperature; (b) Legend (Nadderman and Greimann 2010).

2.1.3.3 Penn State University Study

Researchers instrumented 4 IABs and installed a weather station in central Pennsylvania, and then monitored the bridges over a period of seven years (from 2002-2009) to record the long-term behavior of the IABs. Details of the instrumented bridges are given in Table 2.3. The study archives long-term IAB response data and trends for abutment displacement, backfill pressure, abutment rotation, girder rotation, girder bending moment, girder axial force, pile moment, pile axial force, and approach slab strains.

Table 2.3 Details of instrumented bridges (Kim and Laman 2014).

Bridge No.	Girder type	Integral abutment	Abutment height m (ft-in.)	Span lengths Total length m (ft)	Number of instruments
109	PennDOT 28/78[a]	Both	3.5 (11-6)	26.8 – 37.2 – 37.2 – 26.8 = 128.0 (88 – 122 – 122 – 88 = 420)	64
203	AASHTO V	North only south fixed	5.8 (19-0)	14.3 – 26.8 – 11.3 = 52.4 (47 – 88 – 37 = 172)	64
211	PennDOT 28/78[a]	Both	4.3 (14-1)	34.7 (114)	64
222	PennDOT 24/48[a]	Both	4.0 (13-1)	18.9 (62)	48

For this study, we can focus on the approach slab strain data and trends. The researchers observed that approach slab strain decreases initially (by approximately 100 $\mu\varepsilon$), likely caused by the actions of creep and shrinkage. This decrease in strain was not recovered, however as the time went by

46

the compressive strains decreased, as seen especially prominently for Bridge 203, which was designed and constructed following AASHTO specifications and had only one end of the bridge with an integral abutment. This phenomenon was much less pronounced in other bridges, with both sides having integral abutments. Approach slab strains for the 4 bridges are shown in Figure 2.18.
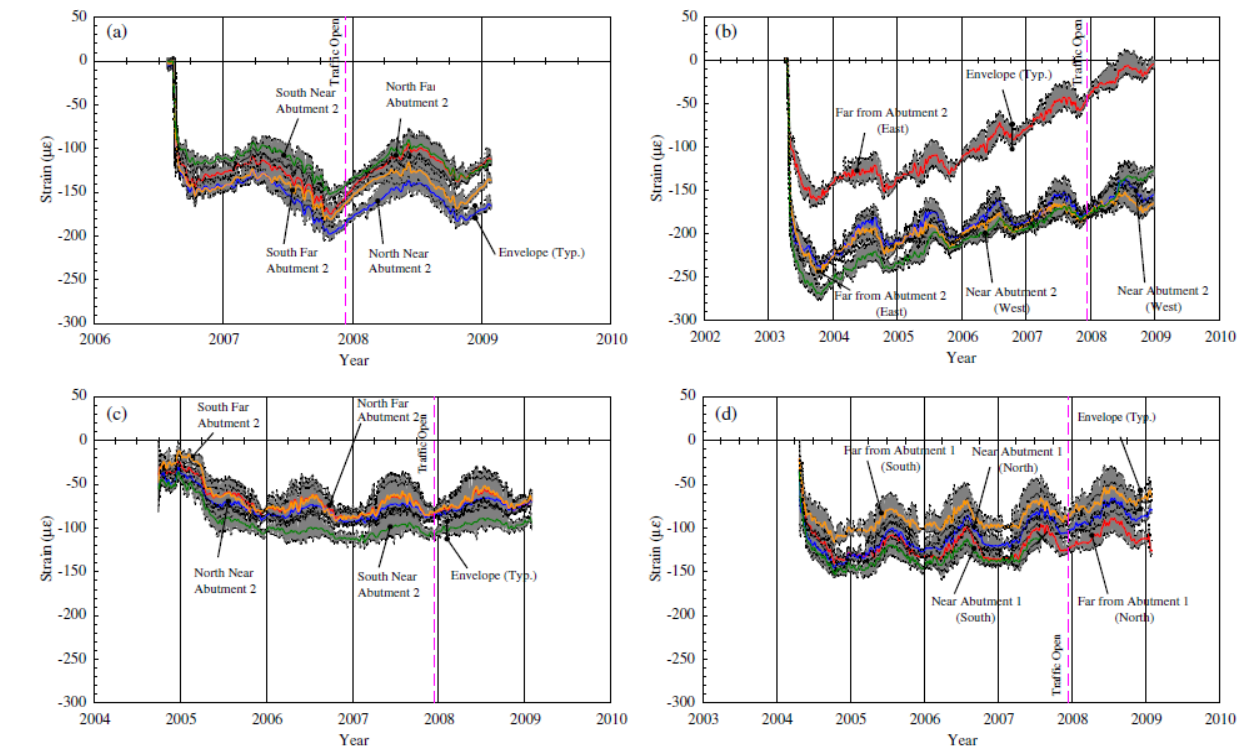
Figure 2.18 Approach slab strains near abutment 2: (a) bridge 109; (b) bridge 203; (c) bridge 211; (d) bridge 222 (Kim and Laman 2014).

2.1.3.4 University of Illinois Study

The structural response of IAB superstructures and substructures was studied at the University of Illinois (LaFave et al. 2016, 2017). The field monitoring program included collecting data about: (a) global bridge movements; (b) pile, deck, girder, and approach-slab strains; and (c) rotations at different abutment interfaces. The superstructure and substructure of the Union Pacific Railroad (UPRR) and Kishwaukee River bridges (I-90 mainline bridges) were instrumented with strain gages on girders and piles, tiltmeters, and displacement transducers. The instrumentation plan used for the longer bridge in the study is given in Figure 2.19.

47
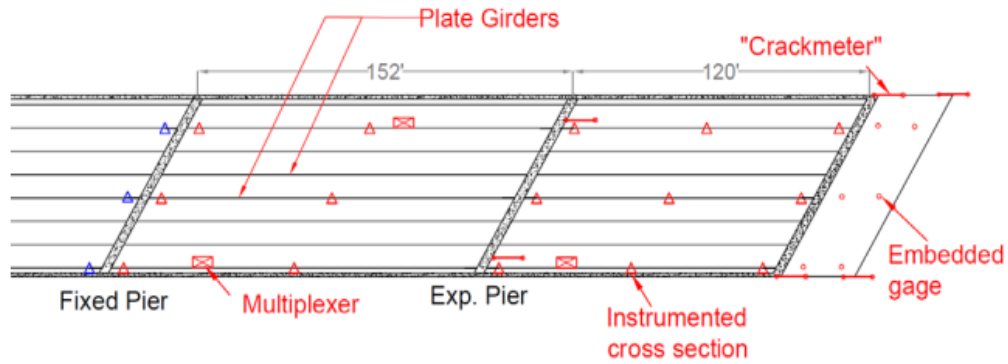
Figure 2.19 Instrumentation plan for Kishwaukee River Bridge (LaFave et al. 2017).

Displacement transducer data showed that the change in length of the joints followed a linear trend with respect to the temperature of the slab, as seen in Figure 2.20. The approach slab-transition slab interface showed the largest displacement magnitudes, as expected, as it is the location of the expansion joint where relative displacements are intended to occur. The data can be observed to follow distinct lines with almost the same slope but a significant shift, which happened after a full year of data collection. This was attributed to the bridge overcoming some resistance and thus closing the joint to a new permanent displacement. The other end of the slab (at the abutment) showed a much lower magnitude of relative displacement, which was expected due to reinforcing steel continuity across this construction joint.
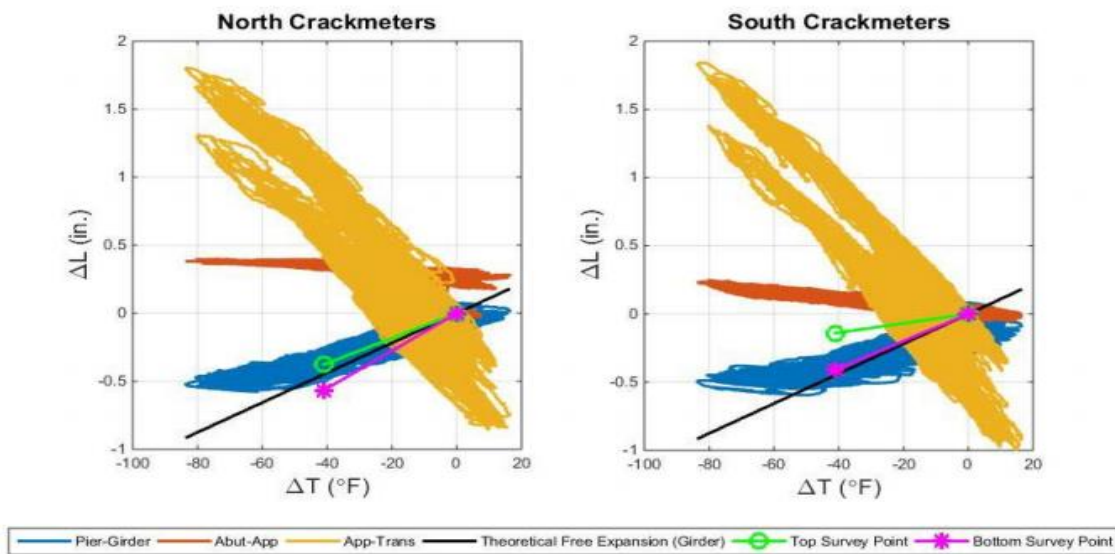
Figure 2.20 Kishwaukee River Bridge displacement transducer data (LaFave et al. 2017).

The strain developed in the approach slab was observed to be highly correlated to the temperature variation, which follows the findings of previous studies covered in this chapter. The variation of strain with change in temperature is shown in Figure 2.21.

48
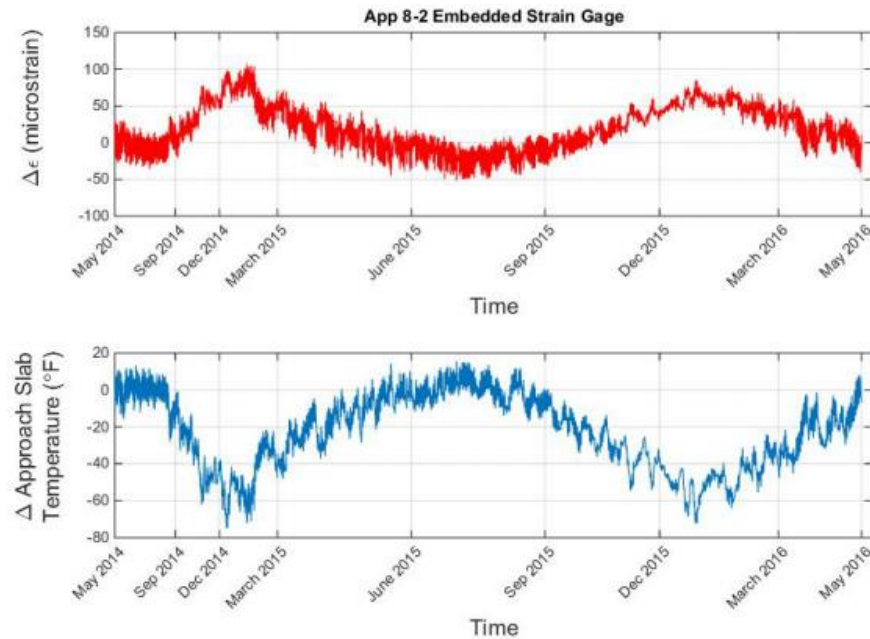
Figure 2.21 Variation of approach slab gauge strain and temperature with time for the
Kishwaukee River Bridge (LaFave et al. 2017).

The slab was assumed to be in the elastic regime, and using the recorded strains, the load related
stresses were calculated for the approach slab. The stress was observed to follow a different trend
for the first four months of data collection. This was attributed to the construction activity. In
subsequent months, the data followed a linear trend with a change in temperature. However, the
slope of the stress vs. temperature plot decreased after each summer. The decrease in slope
signified the approach slab becoming less constrained, likely due to soil settlement causing a
friction reduction beneath the slab (LaFave et al. 2017). Figure 2.22 shows the stress calculated in
the slab with respect to the slab temperature.

Table 2.4 summarizes the related field monitoring studies. The research affiliation, year of
publication, site conditions, means of monitoring, and significant results are provided as essential
information.
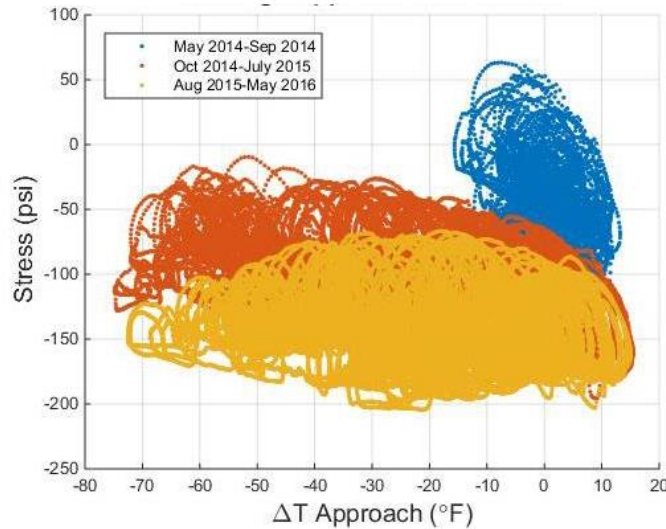
Figure 2.22 Kishwaukee River Bridge approach slab stress with respect to change in temperature (LaFave et al. 2017).

Table 2.4 Summary of field monitoring studies

Research Group Location	Year	Site Conditions	Monitoring Approach	Important Results
Rutgers University (Nassif et al. 2007).	2007	Six approach slabs with varying lengths and skew angles	20 sensors of various types: strain gauges, thermistors, dynamic strain gauges, pressure cells, settlement sensors, and deformation sensors placed in critical areas. Data collected for a year	An initial drop in strains observed, caused by shrinkage After the initial drop, strain is proportional to the temperature
Iowa State University (Greimann et al. 2008) and (Nadderman and Greimann 2010).	2008	Precast approach slab: 77 ft long Cast in place slab: 30 ft long Skew for both the slabs: 30º	Embedded strain gages placed in the approach slab along with deck and piles. Displacement transducers placed at each joint in the precast slab. Data collected for a year.	Along with the long-term cycle, stress developed in the slabs also follows short-term cycles, attributed to friction ratcheting. Negligible movement in joint on the abutment side and between the panels of the precast slab. Expansion joint movements were highly related to temperature, with a

				maximum magnitude of about 1 in.
	2010	Precast approach slab constructed using 8 12 in precast panels and one 9.5 in one with a skew of about 2º29'52".	Embedded strain gages placed towards the boundaries of the slab. Displacement transducers placed at each corner of the slab.	The load caused by restraints was defined and observed to be tensile in Winter and compressive in the Summer season. Average Slab force was defined and observed to have long- and short-term cycles.
Pennsylvania State University (Kim and Laman 2014)	2014	Four bridges of different specifications	Instrumented the bridge to find abutment displacement, backfill pressure, abutment rotation, girder rotation, girder bending moment, girder axial force, pile moment, pile axial force, and approach slab strains. Data collected for 7 years.	An initial increase in compressive strain was observed. For the IAB approach slab, the strain follows the change in temperature and does not recover the initial change. However, for the bridge with one end fixed instead of integral, the compressive strain was recovered by the end of 7 years.
University of Illinois Urbana-Champaign (LaFave et al. 2016, 2017)	2017	30ft approach slab with a skew of 30º	6 embedded strain gages placed uniformly in the slab. 4 displacement transducers at each corner of the slab.	The change in length of the joints at the ends of the approach slab follows a linear trend with respect to the temperature of the slab. Strain highly dependent on temperature. The slope of strain vs. temperature decreases each summer, caused by the removal of some restraint due to possible settlement

2.1.4   Numerical Modelling of Approach Slabs

2.1.4.1 Rutgers University Study

Nassif et al. (2007) aimed to find the possible causes of cracking, the location of cracks, and factors influencing crack development in approach and transition slabs. A 3-D model was developed using typical NJ specifications with the approach slab shaped like a parallelogram with a length of 25 ft (7.62 m) and a width of 12 ft (3.66 m). The transition slab is modeled as a trapezoid with a smaller base of 30 ft (9.14 m) and a width of 12 ft (3.66 m). The reinforced concrete slab is modeled using a four-node, reduced integration shell element (S4R). The soil underneath the approach and transition slab is modeled using Spring 1 type elements (linear elastic springs with constant stiffness), and the boundary condition at abutment and approach slab are taken as simply supported, as shown in Figure 2.23. The soil was assumed to be silty medium dense sand with stiffness of 0.092 kip/in/in^2 (25000 kN/m/m^2). Figure 2.24 shows the plan view of the spring elements in the FE model.
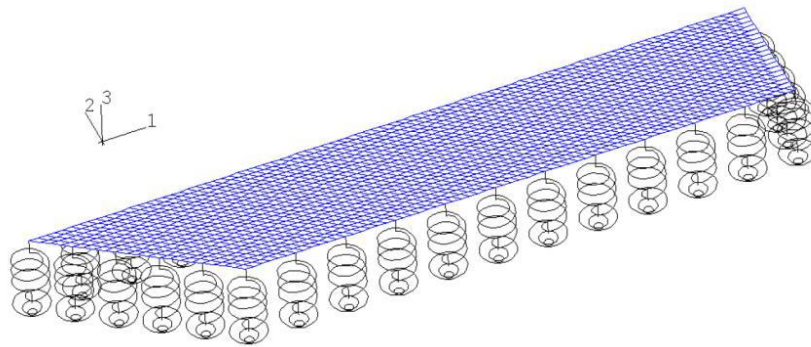
Figure 2.23 The approach slab with edge springs for soil-structure interaction (Nassif et al. 2007).
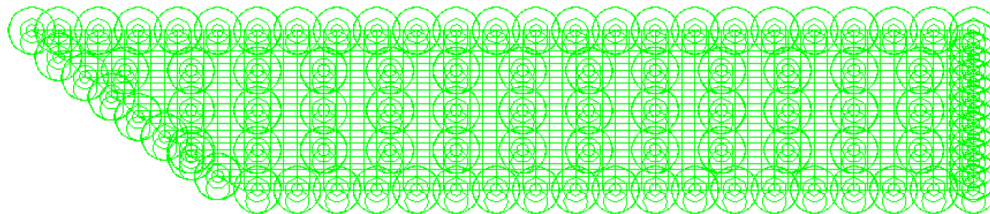
Figure 2.24 Plan view of the spring elements representing soil-structure interaction (Nassif et al. 2007).

The slab was subjected to multiples of HS-20 bridge design truck loading, which has three axles and a Gross Vehicle Weight of 72 kips (320.27 kN). If the truck enters from pavement to bridge, the required load for first cracking is 1.66 times the HS-20 design truck, but it increases to 4.3 times the design truck load if the truck exits the bridge. It was found that a thicker slab helps increase the strength of the slab, so a heavier load is required to crack the approach slab. Additionally, since the slab is skewed, the distribution of the axle loads is uneven. The pinned connection at the edge of the approach slab prevents any displacement along the edge, increasing the strength in this region.

The effects of skew angle were also examined in the study. For the same loading conditions and at the same location, a skewed approach slab has higher tensile stresses than a straight slab. Parametric study for skewed slabs showed that 1) increasing the concrete compressive strength increases the cracking

load capacity, but not very efficiently; 2) increasing the steel reinforcement yielding stress or area has no effect on neither cracking load capacity nor the stresses in the critical elements; 3) increasing the thickness of approach slab is an effective way to improve the cracking load capacity.

2.1.4.2 Louisiana State University Study

The study conducted by researchers at Louisiana State University (Cai et al. 2005) focused on the 3-D finite element analysis of approach slabs. For this study 20, 40, and 60 ft (6.1, 12.19, and 18.29 m) long approach slabs were studied. The width of the slab is 40 ft (12.19 m). A sleeper slab, which provides an additional transition to the roadway pavement, as shown in Figure 2.25, is used in this model to minimize the possibility of differential settlement at the approach slab-roadway interface. The dimension of the embankment and natural soil L5, W2, and H5 are determined through a finite element analysis, particularly to reduce the sensitivity of the approach slab analysis to these parameters. For the sensitivity analysis, two truckloads on two lanes and slab self-weight were applied to the approach slab, and values of L5, W2, and H5 (see Figure 2.18) were found so that the effect of these parameters is minimized in the system.
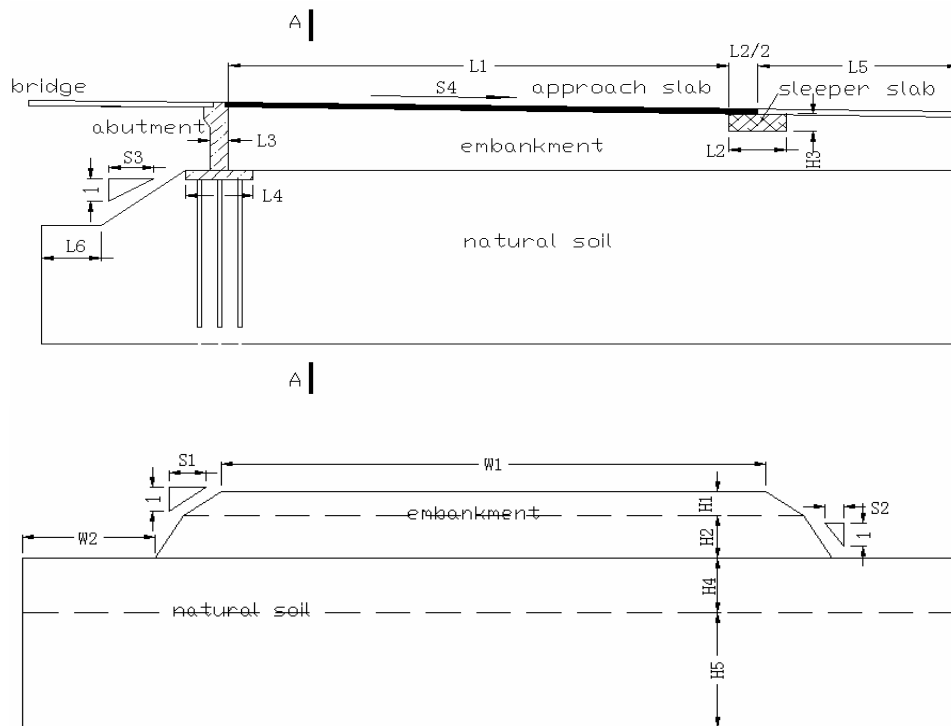
Figure 2.25 Elevation and section view of the abutment (Cai et al. 2005).

The 3-D finite element model was developed, as shown in Figure 2.26. Eight-node hexahedron elements (ANSYS Solid 45) were used to form the finite element mesh. A contact and target pair surface element was used to help simulate the real interaction between slab and soil. The dead load (DL) was applied first, and the dead load and live load were applied together. It was reported that the deflections and internal moments of the beam, and reaction of the beam at the sleeper beam corresponding to maximum moment increase with the increase of the embankment settlement. The

boundary condition of the slab changes from "fully supported across the span" to "simply supported". Figure 2.27 shows the distribution of the coefficient for maximum bending moments in the slab.
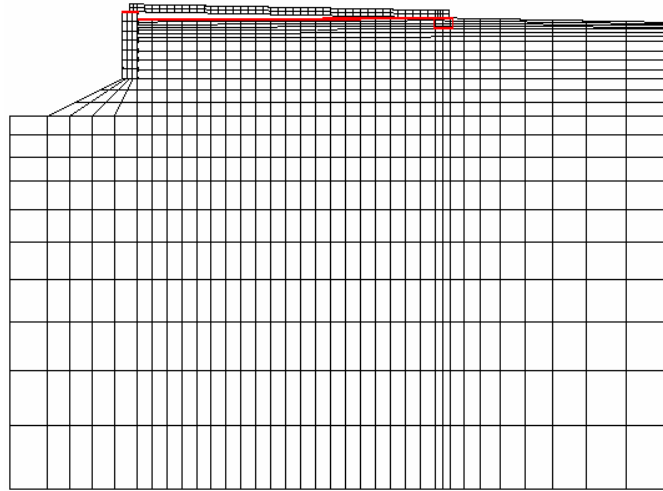
Figure 2.26 Typical finite element mesh (Cai et al. 2005).
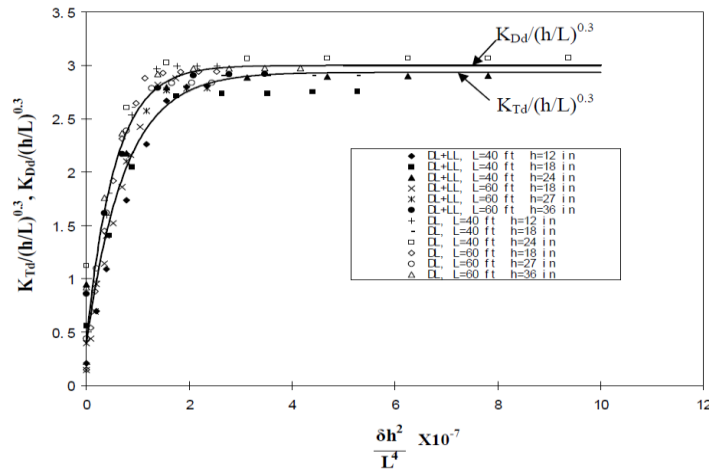
Figure 2.27 Design equations based on parametric study (Cai et al. 2005).

2.1.4.3 University of Missouri-Columbia Study

The study conducted by the researchers at the University of Missouri-Columbia focused on the development of equations for the uniaxial and biaxial bending behavior of a slab on elastic soil support. The wash-out of soil, which is similar to void development, was considered in the research. The approach slab was modeled as a 38 ft × 25 ft (11.58 m × 7.62 m) plate and discretized into 0.5 ft × 0.5 ft (0.15 m × 0.15 m) elements. Figure 2.28 shows the approach slab model. For a simply-supported edge, bending moment perpendicular to the edge and displacement is zero; for a soil supported edge, bending moment and shear are zero; for corner nodes, the twisting moment is zero.
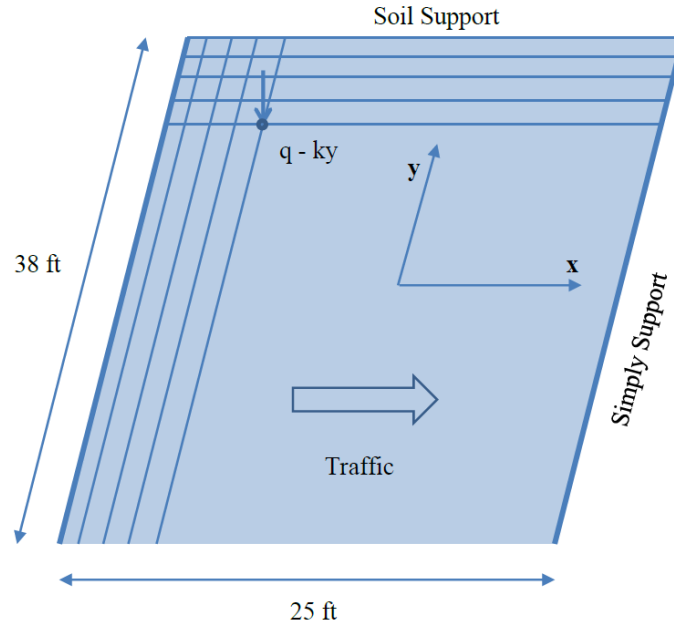
Figure 2.28 Plan view of the approach slab model (Ma 2011).

Lane load, design truck, and design tandem in AASHTO specification were used. Two tandem loads were applied because there were two lanes in the slab (Ma 2011). Two kinds of soil washout were considered: strip washout simulating a strip through the width of the slab and circular washout simulating localized voids, which have been observed at many approach slab sites. It was concluded that the finite difference method could effectively analyze the behavior of the approach slab with unsymmetrical cases and washouts. The uniaxial bending solutions are generally more conservative when compared to biaxial bending. Finite element analysis of approach slabs was conducted in the study using SAP 2000.

Thiagarajan et al. (2010) used 3-D FE analysis to come up with structural solutions for approach slabs for typical approach slab specifications in the state of Missouri. The typical approach slab in the state of Missouri is 25 ft (7.62 m) long, 12 in (304.8 mm) thick. The total width of the slab model was 38 ft (11.58 m), including 2-12 ft (2-3.66 m) lanes, 4 ft (1.22 m) wide inside shoulder, and 10 ft (3.05 m) wide outside shoulder. Simple support, slab on grade, and washout boundary conditions were considered. No sleeper beam with full slab on grade support was also considered. Figure 2.29 shows the detailed boundary conditions of all models.

Case	Span	Depth	File Name	Support Conditions	
				SET 1 - Std Missouri BAS	
1	25'	12"	BAS-25-12-SSS	SS- Standard Missouri BAS	
2	25'	12"	BAS-25-12-ES-25-18.4	SS with linear springs over L with ks=18.4 lb/in3	
3	25'	12"	BAS-25-12-ES-21.25-18.4	SS with linear springs over 85% L	
4	25'	12"	BAS-25-12-ES-18.75-18.4	SS with linear springs over 75% L	
5	25'	12"	BAS-25-12-ES-25-18.4-NS	without sleeper slab	
				SET 2 - Missouri Modified BAS	
1	25'	12"	MODBAS-25-12-SSS	Modified BAS for Missouri	
2	25'	12"	MODBAS-25-12-ES-25-18.4	SS with linear springs over L with ks=18.4 lb/in3	
3	25'	12"	MODBAS-25-12-ES-21.25-18.	SS with linear springs over 85% L	
4	25'	12"	MODBAS-25-12-ES-18.75-18.	SS with linear springs over 75% L	
5	25'	12"	MODBAS-25-12-ES-25-18.4-N	without sleeper slab	
				SET 3 - Idaho BAS	
1	20'	12"	ID-BAS-20-12-SSS	SS- Standard Missouri BAS	
2	20'	12"	ID-BAS-20-12-ES-20-18.4	SS with linear springs over L with ks=18.4 lb/in3	
3	20'	12"	ID-BAS-20-12-ES-17-18.4	SS with linear springs over 85% L	
4	20'	12"	ID-BAS-20-12-ES-15-18.4	SS with linear springs over 75% L	
5	20'	12"	ID-BAS-20-12-ES-20-18.4-NS	without sleeper slab	
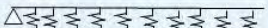
SSS-Simply Supported Slab

Figure 2.29 Finite element model matrix (Thiagarajan et al. 2010).

A very poor soil condition with subgrade modulus of 18.4 lb/in/in^2 (2.89 kN/m/m^2) was selected. The loading of the model was based on AASHTO LRFD specifications. The design truck with three axles and a gross weight of 72 kips (320.27 kN) was considered along with the design lane load. The tandem load was also considered along with the lane load. The design truck was 6 ft wide, and the distance between the front axle and middle axle was 14 ft (4.27 m). The distance between the middle axle and the rear axle was considered as 14 ft (4.27 m) as the span of the approach slab modeled was either 20 ft (6.1) or 25 ft (7.62 m). The loading has been applied in steps, with three design trucks entering the slab at the slab-pavement end and then traversing the slab. Figure 2.30 shows the location of critical loads with simply supported boundary conditions.
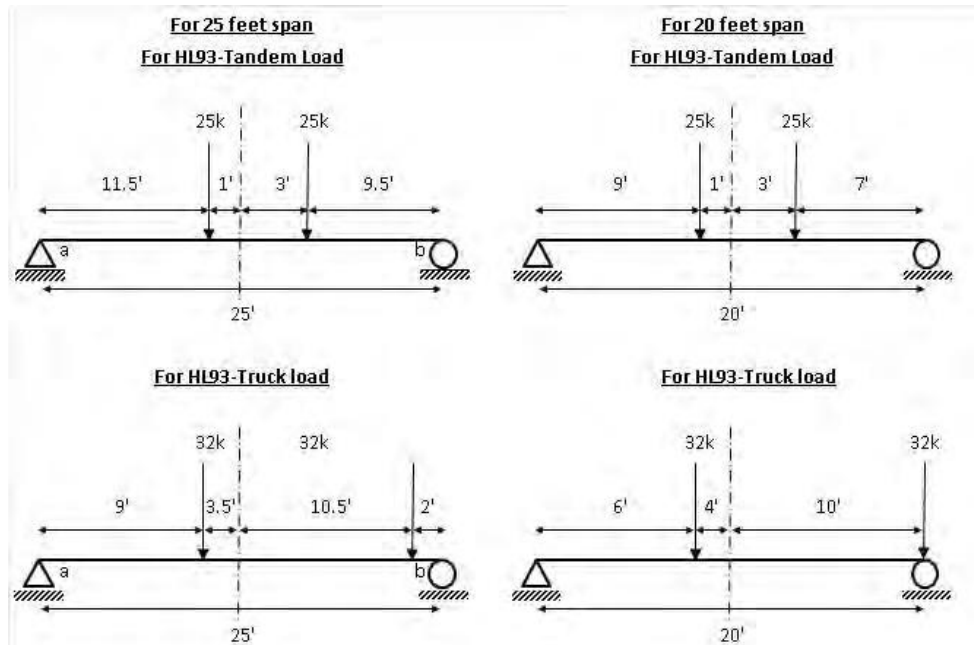
Figure 2.30 Load locations for maximum bending moment in simply supported slabs
(Thiagarajan et al. 2010).

It was reported that the maximum deflection at the center for the Standard Missouri approach slab is 0.63 in. for the simply supported case, whereas the maximum deflection of modified Missouri approach slab is 0.68 in (16 mm). It can be found that Idaho slab deflection was found to be 0.36" for simply supported condition. The maximum deflection value for slab on grade with a given percentage of voids was observed to be 0.3 in (7.62 mm). The maximum moment for the simply supported condition was observed to be 134.52 kips·ft/ft (598.37 kN·m/m) for the standard MO-BAS. In contrast, the maximum moment for the slab on grade option was found to be 63.15 kips·ft/ft (280.91 kN·m/m). For all the models, the rebar bottom and rebar top stresses are observed to be much lower than the yield limits of the reinforcement. The values for concrete and rebar stresses for slab on grade conditions seemed to be lower than that of simply-supported conditions.

In all, the discussed prior relevant work carried out by other research groups is summarized in Table 2.5 with locations, year of publication, approach slab conditions, modeling approach, and important results included.

Table 2.5 Summary of analytical studies

Research Group Location	Year	Conditions	Modeling Approach	Important Results
Louisiana State University (Cai et al. 2005)	2005	20, 40, and 60 ft approach slabs modeled with a width of 40 ft.	Eight-node hexahedron elements in ANSYS were used. Contact target pair used to model soil-structure interaction.	Increasing the thickness of the slab and reinforcement reduces the cracking in the slab. The use of ribbed slabs (similar to slab-on-beam bridge decks) was recommended for better performance than a flat slab.
Rutgers University (Nassif et al. 2007)	2007	Approach Slab modeled as a parallelogram of dimensions 25 ft × 12 ft.	S4R elements were used to model the slab in ABAQUS. Soil structure interaction modeled using linear elastic spring elements. Loading is done using HS-20 truck load, applied in the middle of the lane	The load required to induce a crack is 2.5 times higher if the truck is leaving the bridge than when the truck is entering from the pavement of the bridge. Skewed approach slabs have higher tensile stress than straight slabs. Increasing the slab thickness was identified as the most effective way to reduce cracking.
University of Missouri-Columbia (Thiagarajan et al. 2010) and (Ma 2011)	2010	Typical approach slabs used in Missouri used. (20 to 25 ft long with low skew)	Simple support, slab on grade, and washout boundary conditions were studied. Loading is done using the HL-93 design truck.	For all the models, the rebar bottom and rebar top stresses are observed to be much lower than the yield limits of the reinforcement. Deflection of the slab in simply supported conditions is about 0.63 in while that in case of slab on grade condition becomes 0.3 in.
	2011	Focused on developing uniaxial and biaxial bending behavior of slab on elastic soil support. Soil washout also considered	The approach slab is modeled as a 38 ft × 25 ft plate in SAP2000. The ends of the slab were assumed to be simply supported, and soil support was assumed to be continuous. Loading done using the HL-93 truck.	A span of 20 ft with a thickness of 12 in was recommended to be optimal design configuration. Pretensioned precast approach slabs with transverse ties were recommended.

2.2 Agency Survey and Crack Survey

To gain the most current understanding of the relevant approach slab behavior, design, and construction practices at the start of the present study, the research team conducted a nationwide transportation agency survey. Key responses are summarized below.

Only Illinois, Nebraska, and Vermont have used precast and cast-in-place approach slabs in both conventional bridges and IABs. Texas has used cast-in-place, and precast approach slabs in conventional bridges but did not comment on the type of approach slab used in the 1% of bridges that are IABs in Texas. Out of these four states that have used precast approach slabs, only Vermont did not have any issues with approach slab cracking. However, pavement cracking at the end of the approach slab is still present in Vermont.

Illinois, Missouri, North Dakota, New Jersey, and Iowa indicated that approach slab cracking is an issue in their state and that they have instrumented or studied approach slabs. The survey indicated that 50% or more of bridges in Illinois, Missouri, and New Jersey exhibit approach slab cracking. Oklahoma, Nebraska, Michigan, Nevada, Delaware, Texas, Minnesota, and Indiana all indicated cracking as a primary issue, but they have not instrumented or studied approach slabs. Ohio, Louisiana, and Wisconsin did not indicate approach slab cracking as a primary problem, but approach slab cracking is still present.

There are no major patterns across many states that would clearly relate bridge parameters and approach slab cracking. Designs for bridges in one state may be prone to cracks, whereas cracking may not be present in another state using a seemingly similar design. For example, aside from South Dakota, Alabama, and Montana, all the other states that have used sleeper slabs as the support type for the transition/pavement end of the approach slab have had problems with approach slab cracking. However, one clear pattern across states with approach slabs that are at least 30 feet in length is that they have issues with approach slab cracking. An increase in reinforcement is the most common method among the states to minimize cracks in approach slabs.

The structural drawings and available field inspection photos of approach slab cracking for 46 Illinois Tollway bridges were studied to identify cracking patterns and bridge design and construction parameters that may influence approach slab cracking. The generally observed patterns are as follows:

1. For skew less than 30°, mainline bridge approach slabs have cracks near the corners and shoulders, whereas crossroad bridge approach slabs have cracks in the travel lanes that propagate in the direction of traffic.
2. For skew of 30° and greater, many diagonal cracks extend out of the obtuse corners and across the acute corners of approach slab travel lanes and shoulders, and other cracks originate from both the expansion and construction joints (roughly perpendicular to those joints).

The severity of cracking for the inspected approach slabs at a particular bridge can be categorized as follows:

- Severe: there are on average 3 or more cracks per approach slab;
- Moderate: there are on average 1 or 2 cracks per approach slab;
- Uncracked: there are no cracks.

By looking at design and construction parameters among these different categories of bridge approach slabs in terms of cracking, it is found that skew over 20°, staged construction, and presence of wingwalls may be linked to severe cracking on approach slabs of mainline bridges. Even so, nearly half of all surveyed mainline bridges had uncracked approach slabs, whereas all mainline bridges with greater than 46° skew had severe approach slab cracking. For crossroad bridges, severe cracking was observed more frequently at IABs and approach slabs with wingwalls.

More details of the transportation agency survey and field inspection (crack survey) can be found in Appendix A and Appendix B, respectively.

3 Bridge Descriptions and Instrumentation Details

The details of the two instrumented bridges for the present research, as well as the data acquisition method, are presented in this chapter. The instrumentation employs many sensors, which are all discussed in detail in the following sections.

3.1 Instrumented Bridge Approach Slabs

Approach slabs at two mainline IABs on Illinois Route 390 in Itasca, IL, were instrumented for long-term strain and global movement monitoring. The Eastbound-West (EB-W) approach slab of the Illinois Route 390 Bridge over Arlington Heights Road and Eastbound-East (EB-E) approach slab of the Illinois Route 390 Bridge over Prospect Avenue were chosen. Details of the bridge and approach slab geometry are given in Table 3.1.

Table 3.1 Bridge and approach slab details

Parameter	Arlington Heights Road	Prospect Avenue
Spans	129'-11 ¼"	124'-6" – 103'-1" (West to East)
Total Length	133'-8 ⅛"	227'-7"
Width	100'-8 ¼" at approach slab	Varies 66'-10" to 67'-3 ⅜"
Abutment Skew	10°40'22''	16°9'32''
Approach Slab Type	Cast-in-place	Precast
App. Slab Thickness	15"	16"
App. Slab Length	30'	30'
Expansion Joint	3" opening at transition slab side	2.5" opening at transition slab side
Support at Exp. Joint	Pile bent under the slab	Pile bent under the slab

The geometry of the precast EB-E approach slab of the Illinois Route 390 Bridge over Prospect Avenue is similar to the EB-W approach slab of the Illinois Route 390 Bridge over Arlington Heights in terms of width, skew magnitude, and thickness. The support under the slab at the expansion joint is a pile bent, which is widely applied in the mainline bridge approach slabs in Illinois. The fabrication of the precast slab began in April 2017, allowing the research team to install all the embedded strain gages.

In addition to the geometric similarities between the approach slabs at Prospect Avenue and at Arlington Heights Road, several bridge parameters were taken into consideration in selecting a bridge with cast-in-place approach slabs for instrumentation. The key reasons why this structure was preferred over the other candidate, IL-23 over I-90 (structure number 605), were that the approach slabs at Arlington Heights were not staged constructed slabs and the construction schedule for the EB Illinois Route 390 Bridge over Arlington Heights Road was more favorable for the research group to install all sensors in the slab. Moreover, the EB Illinois Route 390 Bridge over Arlington Heights Road was connected in series to the EB Illinois Route 390 Bridge over Prospect Avenue, where both structures will experience similar loading conditions. Furthermore, the support of the IL-23 approach slab at the expansion joint is an approach footing rather than an

approach bent, making a direct comparison between precast and cast-in-place slabs difficult. Lastly, the IL-23 Bridge is a crossroad bridge where the width and loading conditions differ more from the EB Illinois Route 390 Bridge over Prospect than the EB Illinois Route 390 Bridge over Arlington Heights Road.

The EB-W approach slab of the Illinois Route 390 Bridge over Arlington Heights Road (cast-in-place) was selected for instrumentation; the location of the slab is highlighted in Figure 3.1. This approach slab consists of seven sections: North Shoulder (NS), Lane 1 (L1), Lane 2 (L2), Lane 3 (L3), Gore (G), Ramp (R), and South Shoulder (SS). Concrete for all sections of the slab was poured integrally.
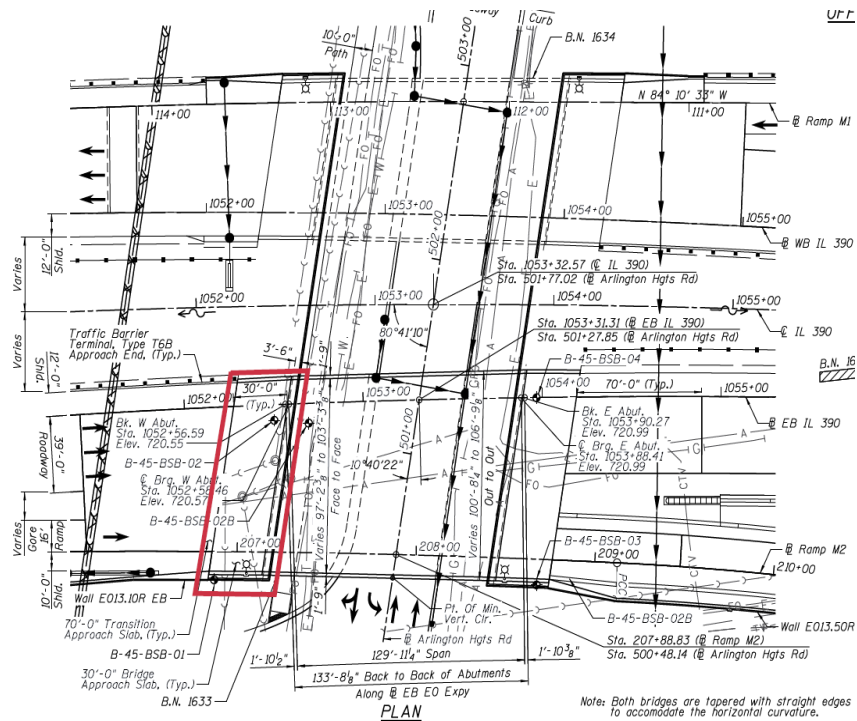
Figure 3.1 Instrumented EB-W approach slab at Arlington Heights Road (cast-in-place).

The EB-E approach slab of the Illinois Route 390 Bridge over Prospect Avenue (precast) was also selected for instrumentation; the location of the slab is highlighted in Figure 3.2. The approach slab consists of 5 sections: North Shoulder (NS), Lane 1 (L1), Lane 2 (L2), Lane 3 (L3), and South Shoulder (SS). The slab was constructed with five precast concrete sections connected with tie bars along the longitudinal joints, as shown in Figure 3.3.
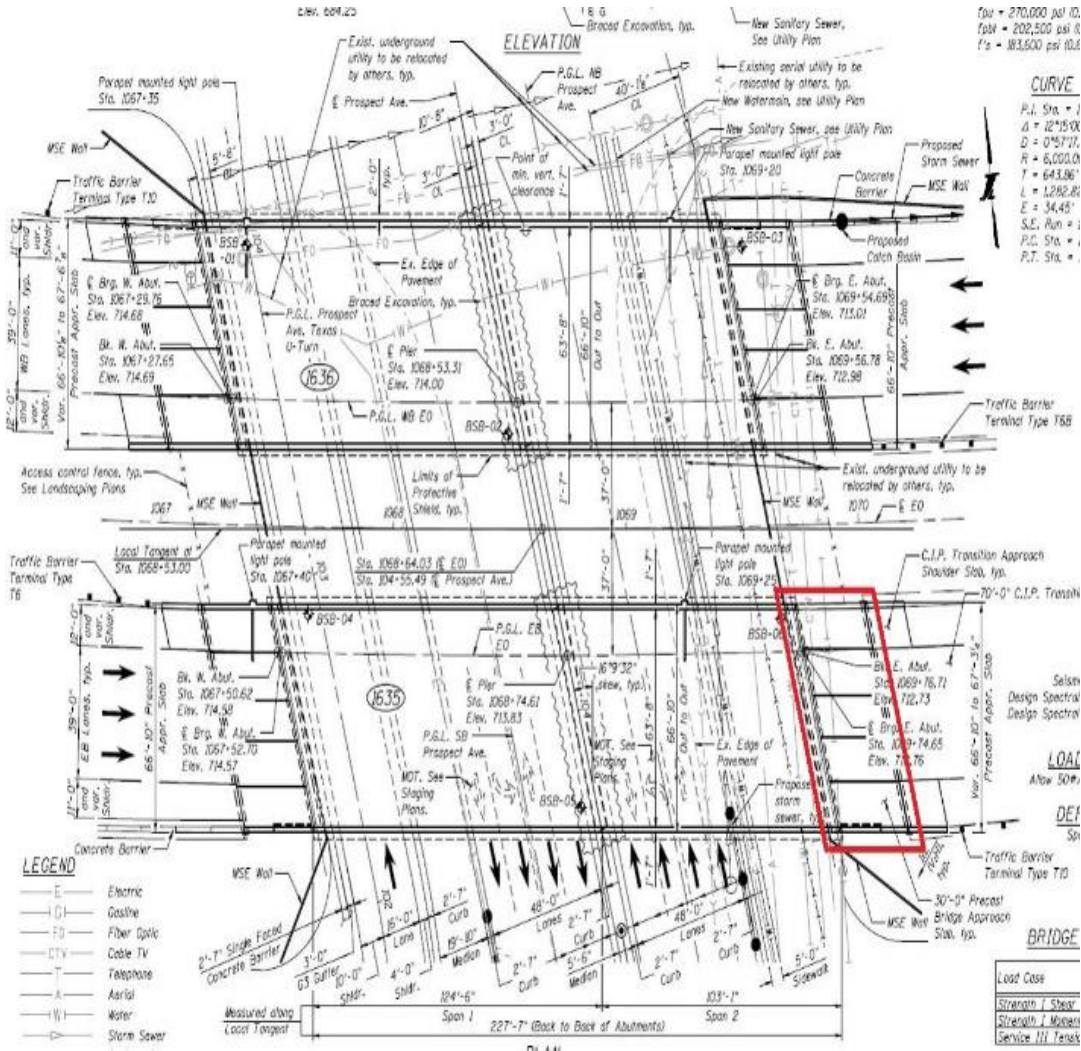
Figure 3.2 Instrumented EB-E approach slab at Prospect Avenue (precast).
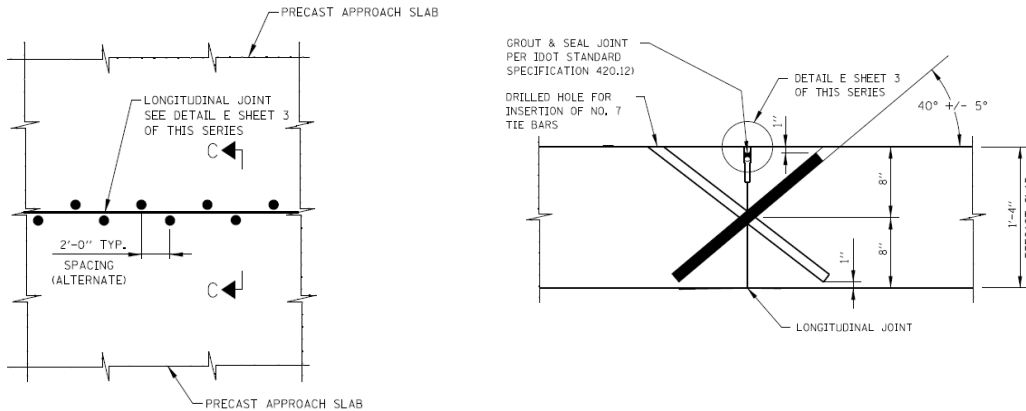
(a) Plan view of longitudinal joint   (b) Section view of longitudinal joint

Figure 3.3 Longitudinal joint of EB-E approach slab at Prospect Avenue (precast).

There is a granular subbase under both instrumented approach slabs between the abutment support and pile bent, as shown in Figure 3.4. The granular subbase of the cast-in-place slab is 4 inches thick, whereas the thickness of that for the precast slab is uncertain on the design drawing. Note that after placement of the precast slab sections, grout injections were employed under the slab in order to fill the potential gaps between the slab and subbase.
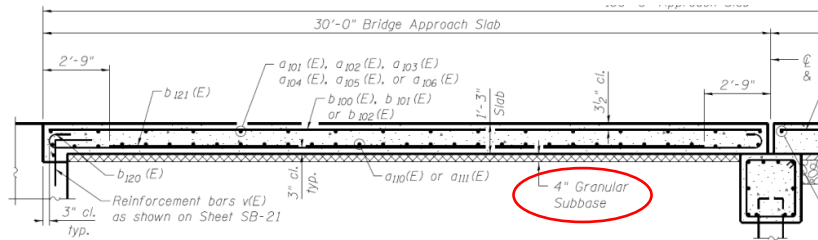
(a) Arlington Heights Road (cast-in-place)
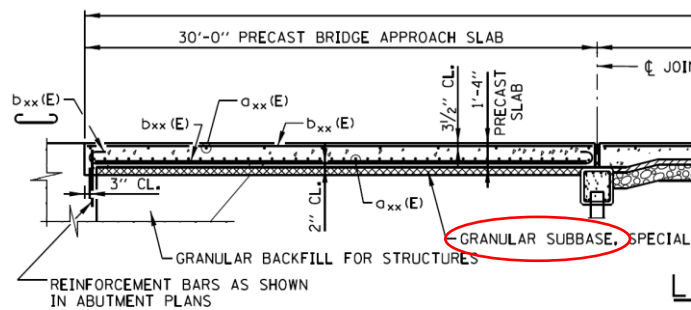
(b) Prospect Avenue (precast)

Figure 3.4 Longitudinal cross-sections of instrumented approach slabs.

3.2 Instrumentation Goals

The instrumentation aims to develop an understanding of global approach slab behavior, which includes the stresses developed in the slab at different positions, as well as global approach slab movement. Moreover, the field monitoring can also validate the numerical approach slab models.

The strain in the concrete slab is one of the most significant concerns in the study because it relates to the live loads applied to the slab and the thermal stresses developed in the slab due to its thermal deformation and restraints. Embedded gages were deliberately distributed in each lane/panel of the slab at different locations. Each embedded gage can provide the concrete strain in one direction and the temperature. A temperature compensation beam was utilized to measure the coefficient of thermal expansion for each slab.

Thermal expansion or contraction of each component of the bridge structure, such as the deck, abutment, and approach slab, will produce volumetric changes and lead to an overall approach slab displacement in the longitudinal direction. The global movement is accommodated by the expansion joint between the approach slab and transition slab. Displacement transducers or "crackmeters" placed at the abutment-approach slab and approach slab-transition slab interfaces, help measure these overall movements. Note that since there is no fixed reference point selected for the bridge and slab, the measurements are the relative displacement between the two ends of the displacement transducer.

3.3 Equipment Description

Based on the performance of similar instruments (from Geokon, Inc.) used in a previous IAB project (LaFave et al. 2016), all instruments and data acquisition equipment in this project were procured from Geokon, Inc. as well. The basic specifications of the instruments used, such as model number, range, resolution, and accuracy, are tabulated in Table 3.2.

Table 3.2 Basic specifications of the instruments

Instrument Name	Model Number	Range	Resolution	Accuracy
Vibrating Wire (VW) Strain Gage	4200	3000 $\mu\varepsilon$	1.0 $\mu\varepsilon$	+/- 0.5%
Displacement Transducer	4420	+/- 6"	0.025%	+/- 0.1%
Displacement Transducer	4420	+/- 3"	0.025%	+/- 0.1%
Datalogger	8600-1	N/A	0.001 Hz RMS	+/ 0.013%
Multiplexer	8032-16	Can connect 16 instruments with temperature reading		
Multiplexer	8032-32	Can connect 32 instruments without temperature reading		

3.4 Instrumentation Layout

3.4.1 Gage Orientations

The embedded gages were installed in three different configurations – namely, longitudinal top (T), longitudinal bottom (B), and transverse top (R). A longitudinal top gage is installed at the top mat of reinforcement under a longitudinal reinforcing bar; a longitudinal bottom gage is installed at the bottom mat of reinforcement above a longitudinal reinforcing bar; a transverse top gage is installed at the top mat of reinforcement under a top transverse rebar. In this study, five possible combinations of the configurations described above were used at various locations, as indicated in Figure 3.5.

☆ - 2 longitudinal (TB), 1 transverse (R)
⬠ - 2 longitudinal (TB)
□ - 1 longitudinal (T), 1 transverse (R)
▷ - 1 longitudinal (T)
○ - 1 transverse (R)

Figure 3.5 Symbol of gage location combinations.

A star combination includes one top longitudinal gage, one bottom longitudinal gage, and a transverse gage at the top. There is one top longitudinal gage and one bottom longitudinal gage in a pentagon combination. The square configuration consists of a top longitudinal gage and a transverse gage. The triangle indicates the installation of one longitudinal top gage. Lastly, a circle means there is only a transverse gage. Figure 3.4 shows the cross-sectional views for each of the four gage combinations. Note that the first four combinations are the ways in which gages were installed, but the additional circle is a result of the longitudinal top (T) gage, which is L1-3-1T at Prospect Avenue (precast), from a "TR" combination malfunctioning. Figure 3.6 shows the cross-sectional view for each of the five gage combinations.

☆ Combination (3 Gages)

Longitudinal Direction   Transverse Direction

⬠ Combination (2 Gages)   ▷ Combination (1 Gage)

Longitudinal Direction   Longitudinal Direction

□ Combination (2 Gages)

Longitudinal Direction   Transverse Direction

○ Combination (1 Gage)

Transverse Direction
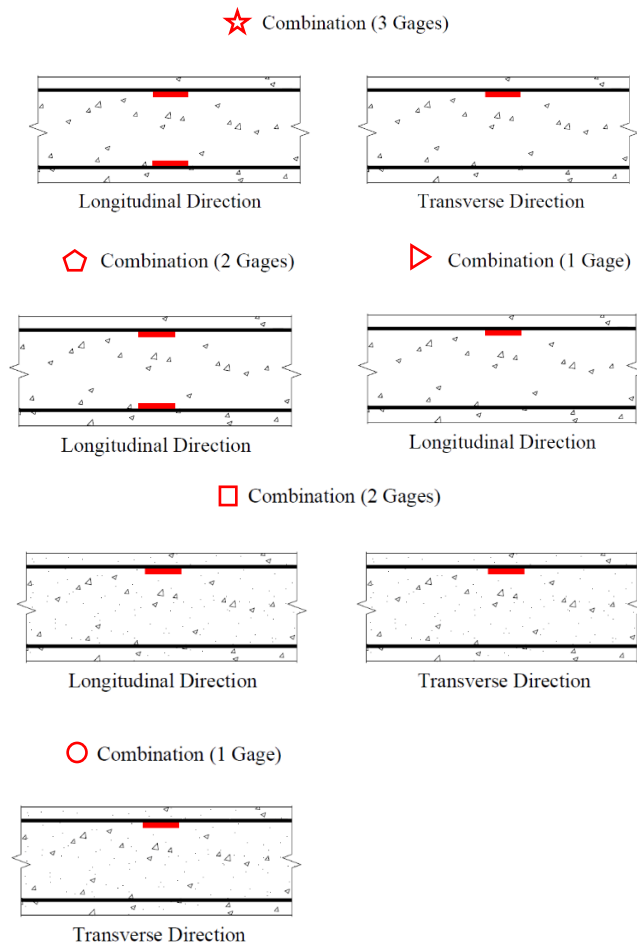
Figure 3.6 Gage configuration combinations.

66

3.4.2 Sensor Locations

Forty-three vibrating wire embedded strain gages from Geokon Inc. were installed in the EB-E approach slab on the bridge over Arlington Heights Road. The layout of the gages is shown in Figure 3.7. Strain gages were placed along two longitudinal lines in the NS and SS sections and one longitudinal line in the L1, L2, L3, G, and R sections. The longitudinal lines in each section were at approximately either the third points or the middle point of the section width. For each longitudinal line, the gages were placed approximately at the quarter points along the length of the slab, numbered from 1 to 3, beginning from the west side of the slab to the east side of the slab. A displacement transducer was installed at each corner of the approach slab (4 in total), and the data acquisition instruments were mounted on two posts on the north side of the slab.

Similarly, for the approach slab at the bridge over Prospect Avenue, forty-four vibrating wire embedded strain gages from Geokon Inc. were used to monitor strains in the slab. These were used in all 5 panels of the approach slab, and the layout of the gages is shown in Figure 3.6. Strain gages were placed along two longitudinal lines in the NS and SS panels and one longitudinal line in the L1, L2, and L3 sections. The longitudinal lines in each section were at either approximately the third points or the middle point of the section width. For each longitudinal line, the gages were placed approximately at the $1/5^{th}$ points along the slab length, numbered from 1 to 4, beginning from the west side of the slab to the east side of the slab. A displacement transducer was installed at each corner of the approach slab.

In addition, the selection of certain sensors to read temperature is made to measure the temperature in as wide a range of the slab plan as possible, in conjunction with several top and bottom pairs at the same plan locations to monitor the temperature difference in the slab thickness direction. The north and south displacement transducers at the abutment side of the slab were selected to measure the temperature outside the concrete (assumed as the ambient temperature on both sides of the slab). All sensors selected to record temperature data are highlighted with solid symbols and names in Figures 3.7. Note that to keep the annotations in Figure 3.7 (a) and (b) as similar size, the plans of the two slabs are not on the same scale. The spans of the two slabs are both about 30 feet.
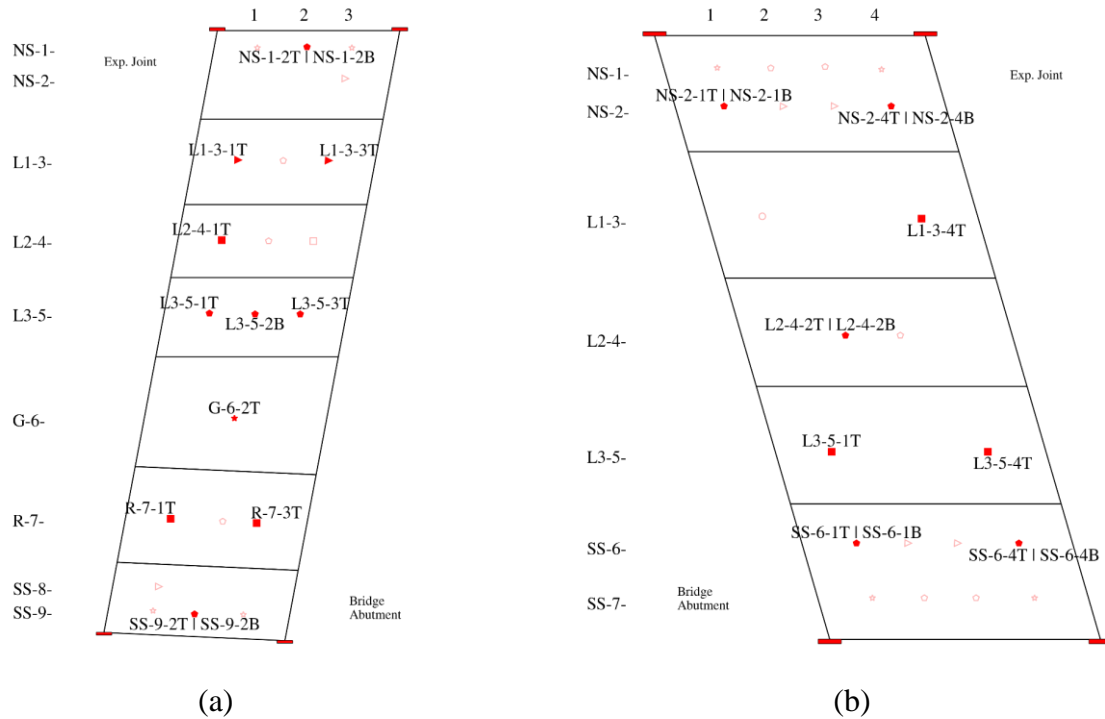
Figure 3.7 Instrumentation plan for approach slabs at (a) Arlington Heights Road; (b) Prospect Avenue.

3.4.3 Naming Convention for Sensors

The naming convention for each gage location follows the rule of "panel-longitudinal line (row number in the layout)-longitudinal position (column number in the layout)-T/R/B." For example, NS-1-3T means the embedded gage located in the north shoulder, on the first longitudinal line (row 1), in the third longitudinal position (column 3), and attached to the top mat of reinforcement in the longitudinal direction (as shown in Figures 3.7). The displacement transducers were named according to the direction of the corner where they are installed, followed by CM (for crackmeter). Thus, the displacement transducer at the northeast corner of the slab is represented as NE CM. Tables 3.4 and 3.5 detail all the sensors used in the cast-in-place and precast slabs, respectively.

Table 3.3 Instrument details for cast-in-place slab (Arlington Heights Road)

Location	Instrument ID	Type	Remarks
	NE CM	Crackmeter	Temperature data recorded as well
North Shoulder	NW CM	Crackmeter	
	NS-1-1T	VW strain gage	
	NS-1-1B	VW strain gage	
	NS-1-1R	VW strain gage	
	NS-1-2T	VW strain gage	Temperature data recorded as well

68

	NS-1-2B	VW strain gage	Temperature data recorded as well
	NS-1-3T	VW strain gage	
	NS-1-3B	VW strain gage	
	NS-1-4T	VW strain gage	
	NS-1-4B	VW strain gage	
	NS-1-4R	VW strain gage	
	NS-2-3T	VW strain gage	
Lane 1	L1-3-1T	VW strain gage	Temperature data recorded as well
	L1-3-2T	VW strain gage	
	L1-3-2B	VW strain gage	
	L1-3-3T	VW strain gage	Temperature data recorded as well
Lane 2	L2-4-1T	VW strain gage	Temperature data recorded as well
	L2-4-1R	VW strain gage	
	L2-4-2T	VW strain gage	
	L2-4-2B	VW strain gage	
	L2-4-3T	VW strain gage	
	L2-4-3R	VW strain gage	
Lane 3	L3-5-1T	VW strain gage	Temperature data recorded as well
	L3-5-1B	VW strain gage	
	L3-5-2T	VW strain gage	
	L3-5-2B	VW strain gage	Temperature data recorded as well
	L3-5-3T	VW strain gage	Temperature data recorded as well
	L3-5-3B	VW strain gage	
Gore	G-6-2T	VW strain gage	Temperature data recorded as well
	G-6-2B	VW strain gage	
	G-6-2R	VW strain gage	
Ramp	R-7-1T	VW strain gage	Temperature data recorded as well
	R-7-1R	VW strain gage	
	R-7-2T	VW strain gage	
	R-7-2B	VW strain gage	
	R-7-3T	VW strain gage	Temperature data recorded as well
	R-7-3R	VW strain gage	
South Shoulder	SS-8-1T	VW strain gage	
	SS-9-1T	VW strain gage	
	SS-9-1B	VW strain gage	
	SS-9-1R	VW strain gage	

	SS-9-2T	VW strain gage	
	SS-9-2B	VW strain gage	Temperature data recorded as well
	SS-9-3T	VW strain gage	
	SS-9-3B	VW strain gage	
	SS-9-3R	VW strain gage	
	SE CM	Crackmeter	Temperature data recorded as well
	SW CM	Crackmeter	
Near North Shoulder	Temp Beam	VW strain gage	Temperature data recorded as well

Table 3.4 Instrument details for precast slab (Prospect Avenue)

Location	Instrument ID	Type	Description
North Shoulder	NE CM	Crackmeter	
	NW CM	Crackmeter	Temperature data recorded as well
	NS-1-1T	VW strain gage	
	NS-1-1B	VW strain gage	
	NS-1-1R	VW strain gage	
	NS-1-2T	VW strain gage	
	NS-1-2B	VW strain gage	
	NS-1-3T	VW strain gage	
	NS-1-3B	VW strain gage	
	NS-1-3R	VW strain gage	
	NS-2-1T	VW strain gage	Temperature data recorded as well
	NS-2-1B	VW strain gage	Temperature data recorded as well
	NS-2-2T	VW strain gage	
	NS-2-3T	VW strain gage	
	NS-2-4T	VW strain gage	Temperature data recorded as well
	NS-2-4B	VW strain gage	Temperature data recorded as well
	NS-2-4R	VW strain gage	
Lane 1	L1-3-1T	VW strain gage	Malfunctioned, no data available
	L1-3-1R	VW strain gage	
	L1-3-4T	VW strain gage	Temperature data recorded as well
	L1-3-4R	VW strain gage	
Lane 2	L2-4-2T	VW strain gage	Temperature data recorded as well

	L2-4-2B	VW strain gage	Temperature data recorded as well
	L2-4-4T	VW strain gage	
	L2-4-4B	VW strain gage	
Lane 3	L3-5-1T	VW strain gage	Temperature data recorded as well
	L3-5-1R	VW strain gage	
	L3-5-3T	VW strain gage	
	L3-5-3R	VW strain gage	
South Shoulder	SS-6-1T	VW strain gage	Temperature data recorded as well
	SS-6-1B	VW strain gage	Temperature data recorded as well
	SS-6-2T	VW strain gage	
	SS-6-3T	VW strain gage	
	SS-6-4T	VW strain gage	Temperature data recorded as well
	SS-6-4B	VW strain gage	Temperature data recorded as well
	SS-7-1T	VW strain gage	
	SS-7-1B	VW strain gage	
	SS-7-1R	VW strain gage	
	SS-7-2T	VW strain gage	
	SS-7-2B	VW strain gage	
	SS-7-3T	VW strain gage	
	SS-7-3B	VW strain gage	
	SS-7-4T	VW strain gage	
	SS-7-4B	VW strain gage	
	SS-7-4R	VW strain gage	
	SE CM	Crackmeter	
	SW CM	Crackmeter	Temperature data recorded as well
Near North Shoulder	Temp Beam	VW strain gage	Temperature data recorded as well

3.5 Installation Details

3.5.1 Temperature Beam

Two temperature compensation beams were fabricated as the bridges were constructed, as shown in Figure 3.8. The 6 in. × 6 in. × 30 in. beams have a longitudinal bottom #8 bar, similar to the reinforcement used in the slabs. The temperature beams were cast with an embedded strain sensor mounted on the reinforcement to record the strain and temperature of the beam. These beams were used to estimate the coefficient of thermal expansion of both slabs.

<center>(a)</center> <center>(b)</center>

Figure 3.8 (a) Temperature beam with embedded gage and reinforcement bars; (b) the temperature compensation beams being cast.

3.5.2 Strain Gage Installation

Both cast-in-place and precast approach slabs were instrumented with embedded strain gages having top, bottom, and transverse orientations, as indicated in Figure 3.9 (a), which shows an instance in a precast section. To place the gages in the desired positions, all the gages were mounted with the help of stackable chairs from Polylok Inc., as shown in Figure 3.9 (b), which was taken from the cast-in-place approach slab. Note that the zip tie tails seen in Figure 3.9 (b) were eliminated and disposed of before the concrete pour.

<center>(a)</center> <center>(b)</center>
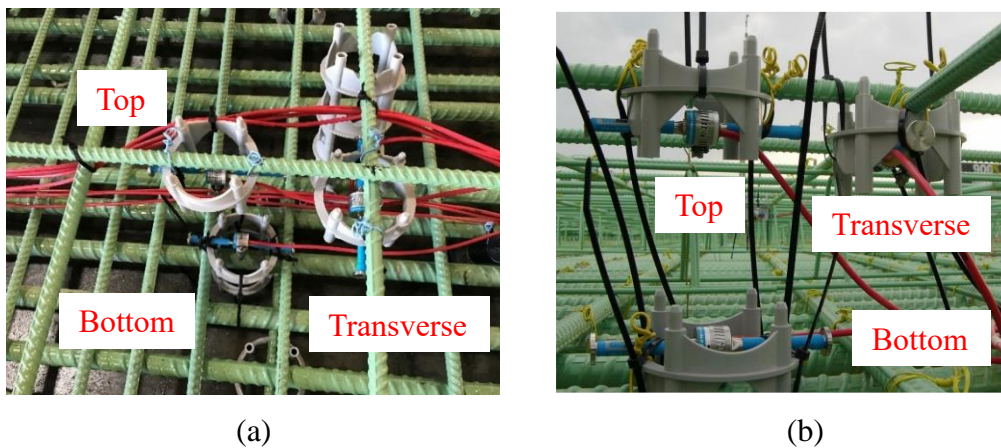
Figure 3.9 (a) Plastic chairs used in all three gage locations at NS-1-4 (precast); (b) Plastic chairs used in all three gage locations at NS-1-4 (precast).

3.5.3 Displacement Transducers

Four displacement transducers were installed on each bridge – one at every corner. These displacement transducers were designed to be installed at mid-depth of the approach slab, ideally using groutable anchors on both ends of the sensor. One end should be mounted onto the approach

<center>72</center>

slab, whereas the other end should be mounted onto the transition slab or the abutment, which was achieved at most of the locations. Cover plates were used to keep these sensors from any physical damage, as shown in Figure 3.10. A gap between the two plates allows them to move freely with respect to one another as the slab expands or contracts. However, due to the actual condition of each corner of the slabs, the following modifications were made:

- At the North side of the approach slab for the Arlington Heights Road bridge, a regular Tollway asphalt shoulder was constructed on the other side of the expansion joint. Therefore, the displacement transducer (6 in. range) at the northwest end was anchored to the slab, and the pile bent.
- At the southwest corner of the slab for Arlington Heights Road Bridge, the approach slab was not accessible for instrumentation. Therefore, the displacement transducer was anchored at the barrier of the approach slab and moment slab.

(a)   (b)

Figure 3.10 (a) Installation of NW displacement transducer (Arlington Heights Road); (b) Cover plates of NW displacement transducer (Arlington Heights Road).

3.5.4 Data Collection and Transmission

A datalogger, two multiplexers, and a solar panel were installed on posts at each bridge, using the same installation plan for both slabs. Two multiplexers were mounted below the datalogger, which was under the solar panel. The terminal boxes were mounted on three pieces of 4 in. by 6 in. pressure-treated lumber, as shown in Figure 3.11. The solar panel was installed at the top of one post, with the tilt of the panel set to be approximately equal to the latitude at the location (about 41.9°) in order to yield the maximum solar energy throughout the year. The temperature compensation beam was placed on top of gravel between the posts at each bridge. All wires were connected to two multiplexers based on the selection of certain sensors to also provide temperature readings. The modem for remote communication was installed in the datalogger box, as shown in Figures 3.12.
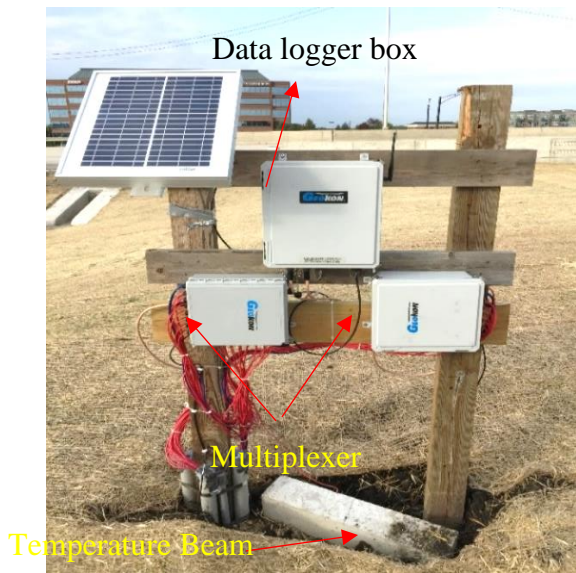
(a)   (b)

Figure 3.11 (a) The multiplexer, datalogger, solar panel and temperature beam at Arlington Heights Road (cast-in-place); (b) The multiplexer and datalogger at Prospect Avenue (precast).
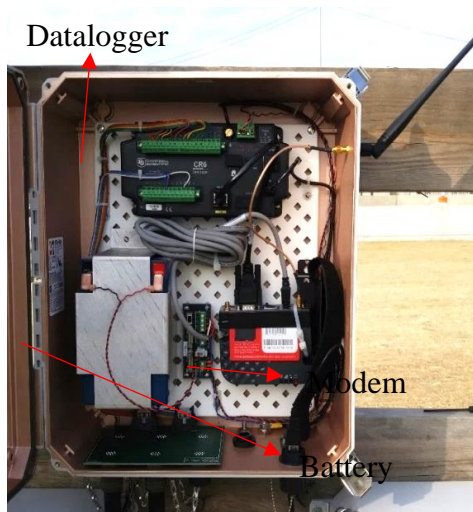
(a)   (b)

Figure 3.12 (a) Inside of datalogger after modem was installed at Arlington Heights Road (cast-in-place); (b) Inside of datalogger after the modem was installed at Prospect Avenue (precast).

4 Field Monitoring Results

4.1 Approach Slab Temperature

Strains in an IAB approach slab can be affected by temperature change in the slab (LaFave et al. 2016), and so temperatures in both monitored slabs were recorded at 15 strain gage locations (including 2 crackmeters), where sensors with both strain and temperature gaging capabilities were installed. Temperatures were also recorded at strain gages placed in the supplementary beams located at both bridges (referred to as "temperature beams").

As a reference for the temperatures in the slab and ambient temperature near the bridges, data from the NOAA weather database were collected as well. The specific station is the Chicago O'Hare International Airport station, of which the latitude is 41.96019°, the longitude is -87.93162°, and the elevation is 201.8 m. It is located approximately 4 miles from the bridges, as shown in Figure 4.1.
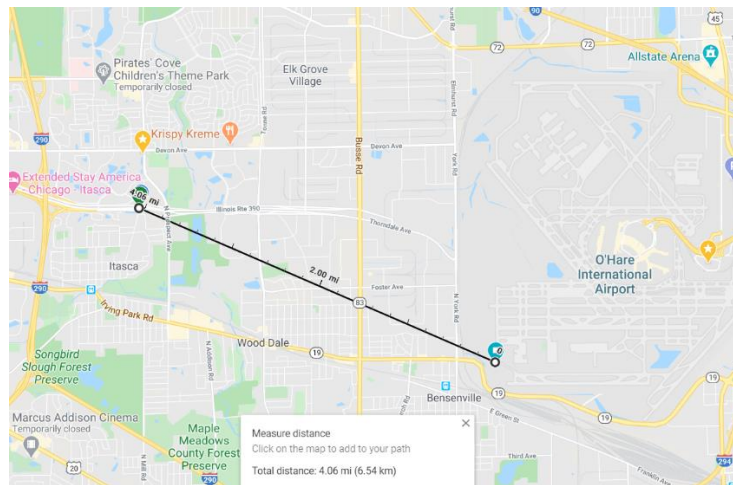
Figure 4.1 Location of monitored bridges and Chicago O'Hare International Airport temperature station.

The data indicate that temperatures obtained from the sensors generally share similar trends with the dry-bulb temperature readings from the O'Hare station. The dry-bulb temperature is usually thought of as being the measured air temperature. Figures 4.2 and 4.3 present the differences between each set of 16 temperature readings and the O'Hare station readings, for Arlington Heights Road and Prospect Avenue, respectively. There are a few gaps with no data in both Figures 4.2 and 4.3; during these periods of time, data collection was interrupted for either all (micro-strain and temperature) channels or just the channels that collect temperature readings. Since the temperature is such a significant factor in this study, estimated temperature data will be used to replace those missing data, as discussed in detail later in this chapter.

For the cast-in-place approach slab at Arlington Heights Road, the temperature beam's recorded temperature did not track well with the data obtained by other sensors from roughly January to March of 2018, as it was accidentally buried in the ground. However, after the beam was uncovered, its temperature reading started to again track well with the other sensors (as well as with ambient temperature).
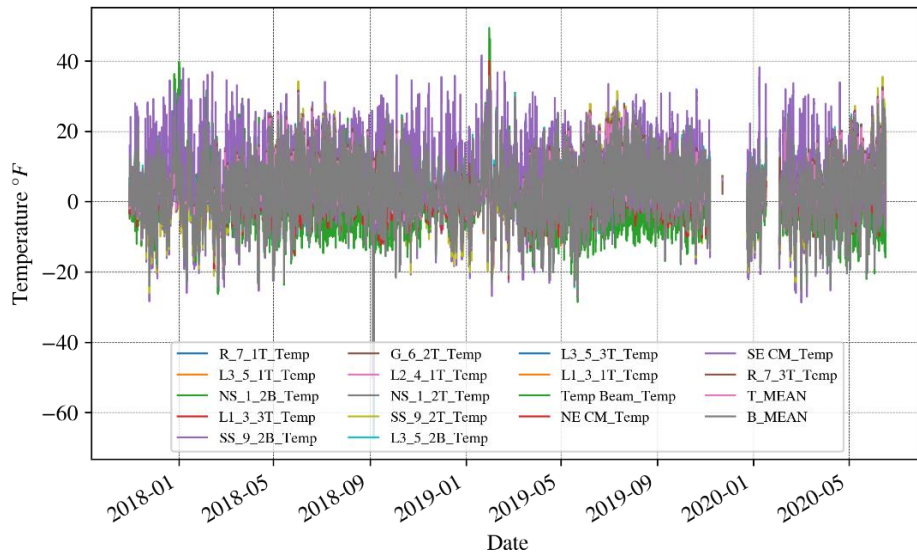
Figure 4.2 Difference between sensor temperatures and O'Hare station dry-bulb temperature (Arlington Heights Road).
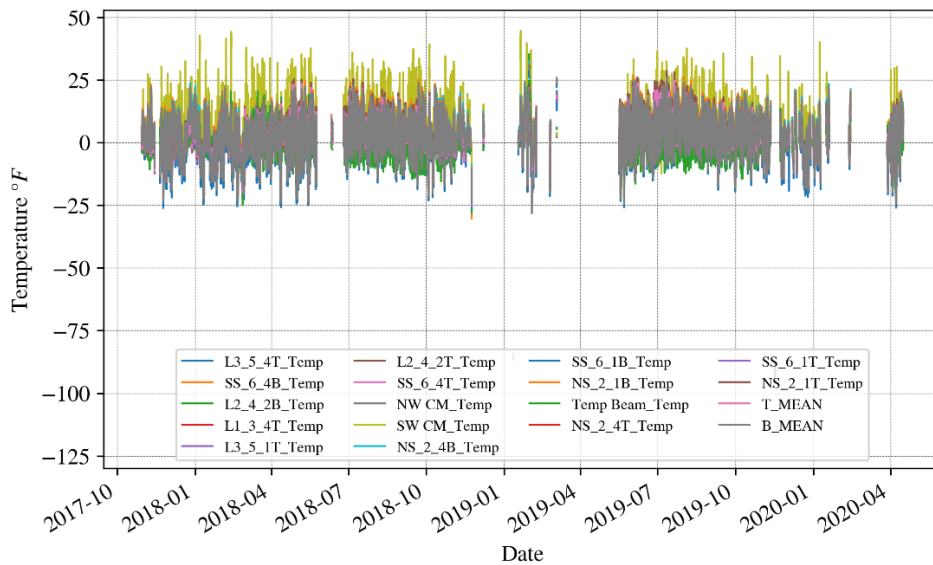
Figure 4.3 Difference between sensor temperatures and O'Hare station dry-bulb temperature (Prospect Avenue).

To better learn how frequently the various magnitudes of temperature difference occur, the estimated probability density function of such differences for each sensor at the two monitored slabs is shown in Figures 4.4 and 4.5. These distributions are obtained solely from valid data (not including any missing / replacement data). For embedded gages in the slabs, most of the difference remains in the range of ±10 ºF, with a slight (less than 3 ºF) positive bias. For temperatures measured from crackmeters and the temperature beams, the difference is more densely distributed around 0 ºF, which is attributed to more direct exposure to the air and solar radiation.
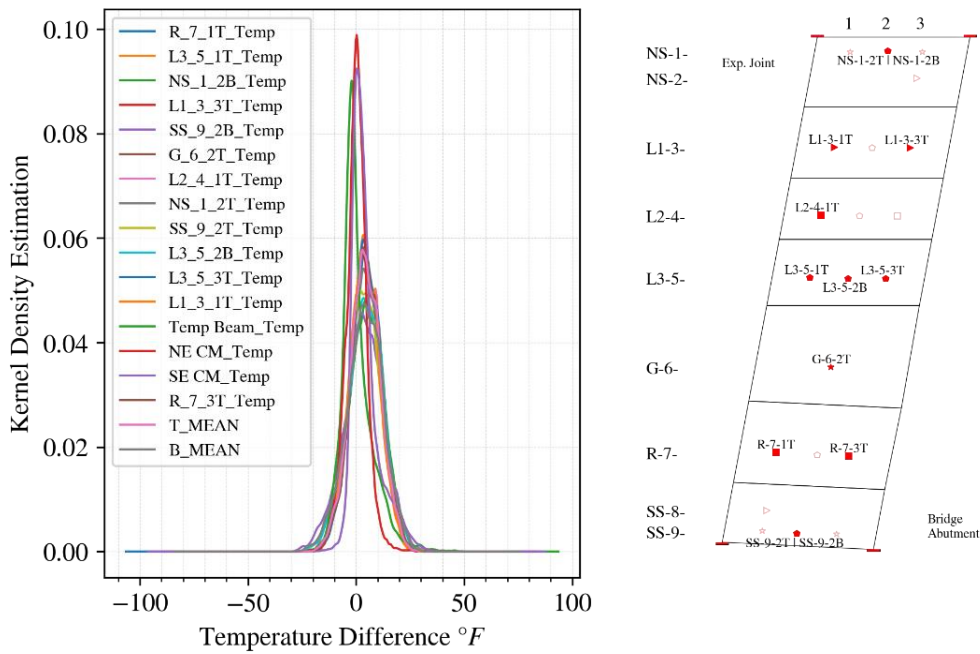
Figure 4.4 Distribution of difference between sensor temperatures and O'Hare dry-bulb temperature (Arlington Heights Road).
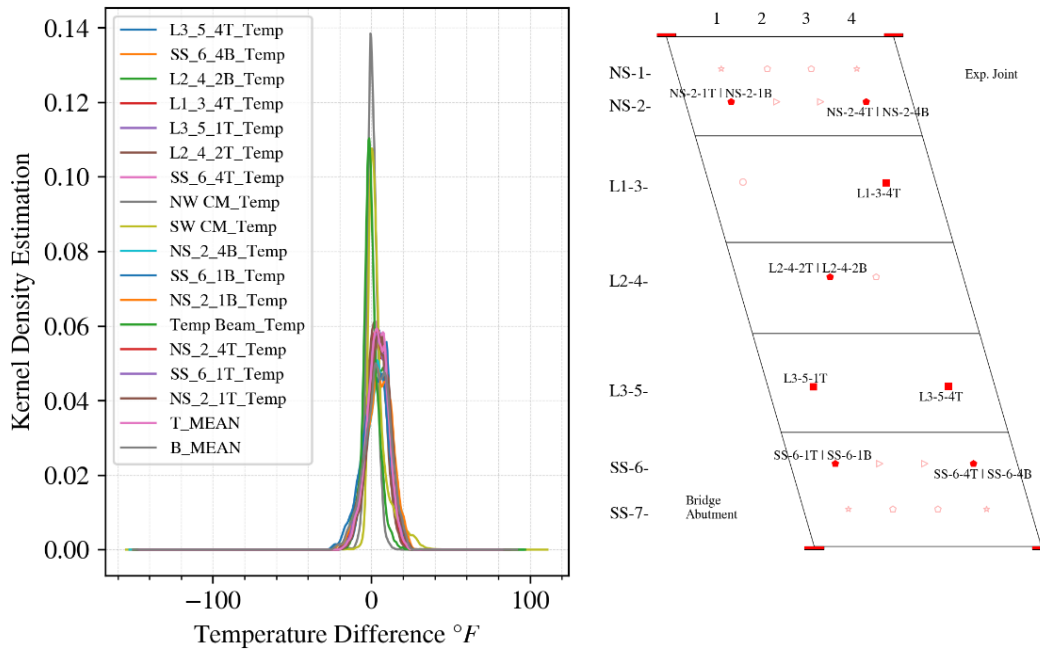
Figure 4.5 Distribution of difference between sensor temperatures and O'Hare dry-bulb temperature (Arlington Heights Road).

In-plane spatial variation of temperature is relatively small; the coefficients of correlation for temperatures measured at the same vertical position (T or B) are generally greater than 0.98, suggesting strong agreement of the temperature trends from these two differently-positioned sets of gages with respect to time.

However, the temperatures from top gages were observed to change more drastically when the ambient environmental conditions changed – two instances are shown in Figures 4.6 and 4.7, which present the time history of all measured temperatures from embedded gages at the instrumented approach slabs from 12:00 PM on 10/29/2017 to 12:00 PM on 10/30/2017. The higher temperature position through the slab thickness alternated during the day. Generally, the temperatures at top gages get higher than the bottom ones in the afternoon. Hence, the temperatures measured from top gages appear to be more sensitive to ambient conditions such as solar radiation, wind, and precipitation.
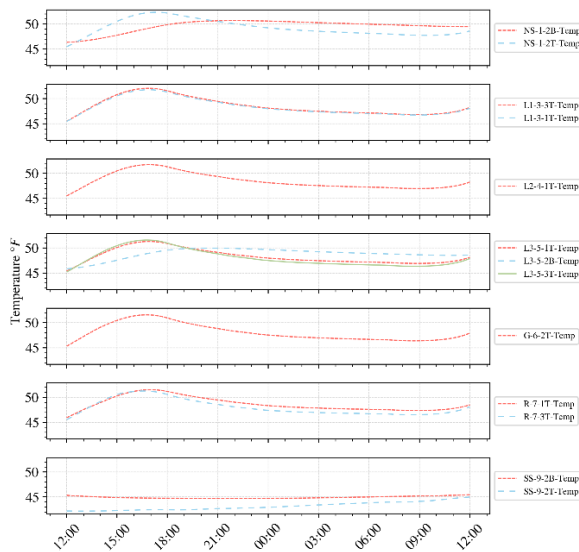
Figure 4.6 Temperature history from noon on 10/29/2017 to noon on 10/30/2017 (Arlington Heights Road).
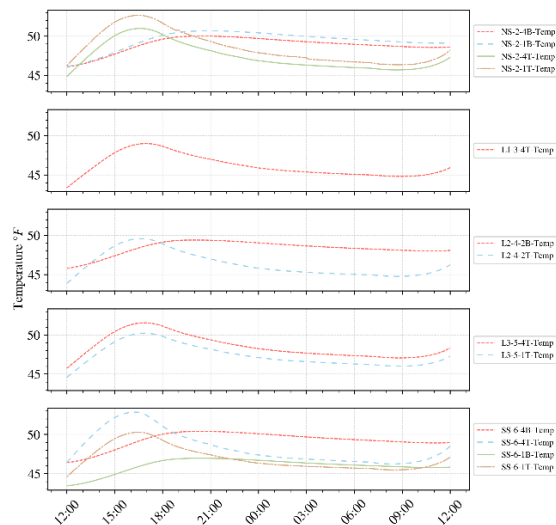
Figure 4.7 Temperature history from noon on 10/29/2017 to noon on 10/30/2017 (Prospect Avenue).

To compare the top and bottom gage temperatures, the difference in temperature between the top and bottom gages at the same plan locations can be used. A positive difference in temperature means the measured temperature is higher at the top gage than at the bottom, and vice versa for a negative difference. If the temperature variation through the thickness of the slab is investigated by computing the top-bottom temperature difference vs. time (in the range from 12:00 AM to 11:59 PM), the trends of the temperature difference between top and bottom gages during a day can be obtained, as shown in Figures 4.8 and 4.9, where the lines represent averages of temperature difference. The shaded areas behind the lines are the regions within ±2 standard deviations.

It can be observed that the temperature difference for most top-bottom gage pairs in the instrumented slabs exhibits similar trends during a day – top gages generally measure higher temperatures than bottom gages from 12:00 PM to 8:00 PM. Magnitudes of the standard deviations

78

are comparable to the averages due to the fact that such top-bottom temperature differences can vary significantly in different weather conditions or seasons. The upper and lower bounds of the enveloped areas can be employed as worst-case temperature gradients in the numerical modeling of these approach slabs, which will be discussed later in this report.
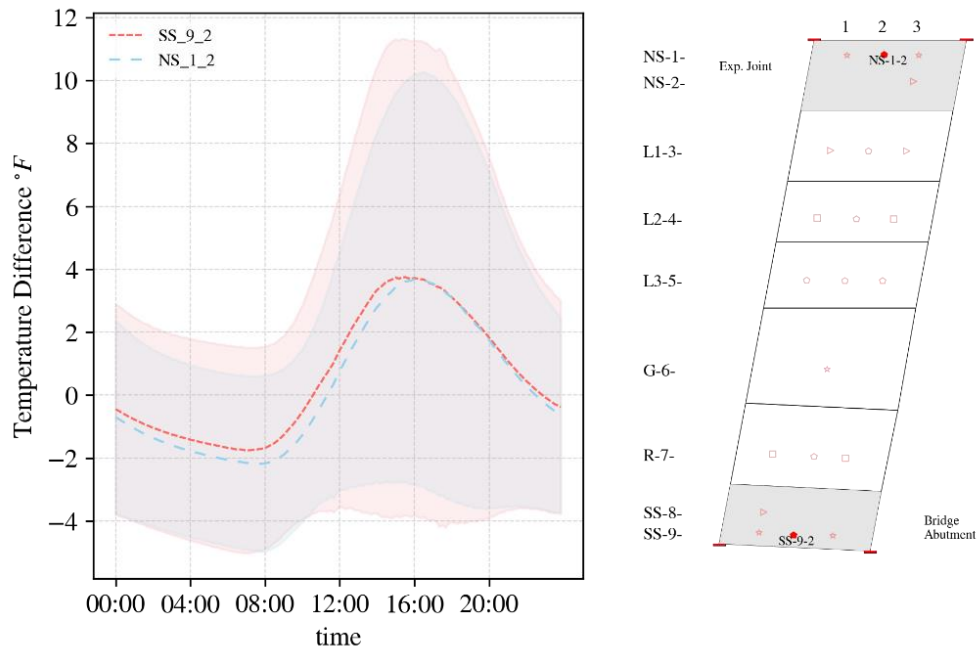
Figure 4.8 Top-bottom temperature difference trend (Arlington Heights Road).
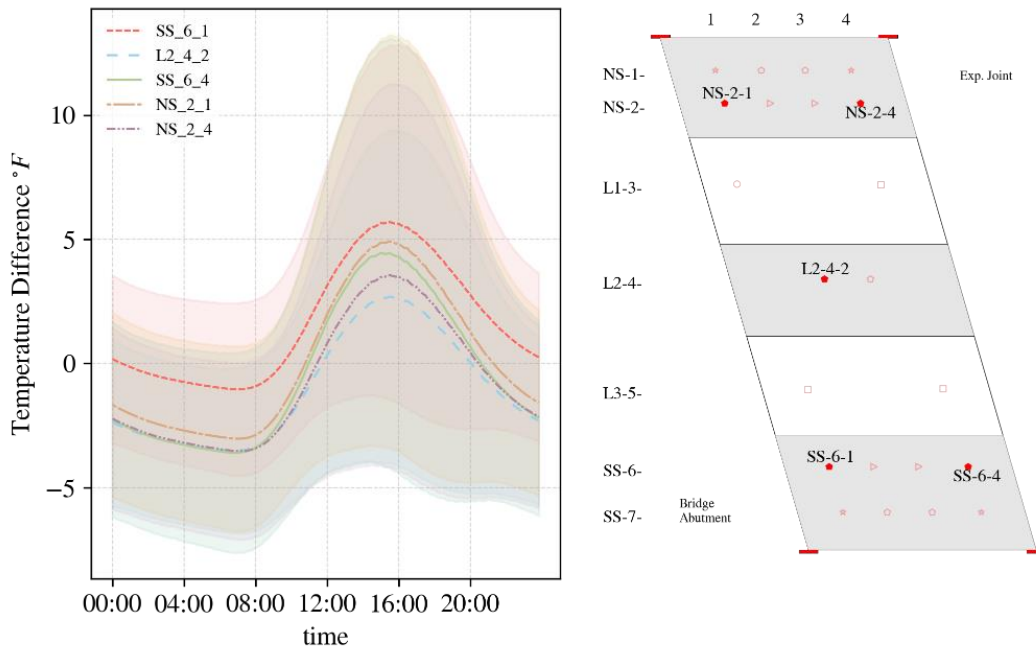
Figure 4.9 Top-bottom temperature difference trend (Prospect Avenue).

Due to high similarities among embedded gage temperatures in the same vertical position (T or B) and apparent difference between top and bottom gage temperatures, average slab temperatures for top and bottom gages, which are denoted as "T_MEAN" and "B_MEAN" in the figures, are calculated respectively by averaging all valid gage temperature readings from the same vertical positions, as shown in Figures 4.10 and 4.11. The gaps in the time history plots reflect the missing data due to data collection interruptions. For both monitored slabs, top average temperature tracks bottom average temperature during most of the time when there are valid readings. Nevertheless, the top average temperature is more likely to be the local maxima and minima among the two average temperatures.

As representative variables, average top and bottom temperatures for embedded gages are used in many ways. For example, they provide a simplified manner to develop a regression relationship between sensor temperature readings and the O'Hare station data, which can be utilized to get estimated temperatures as an alternative to those missing temperature data. Moreover, average top and bottom temperatures are simple but reasonable metrics to find the timestamps of hottest and coldest weather.
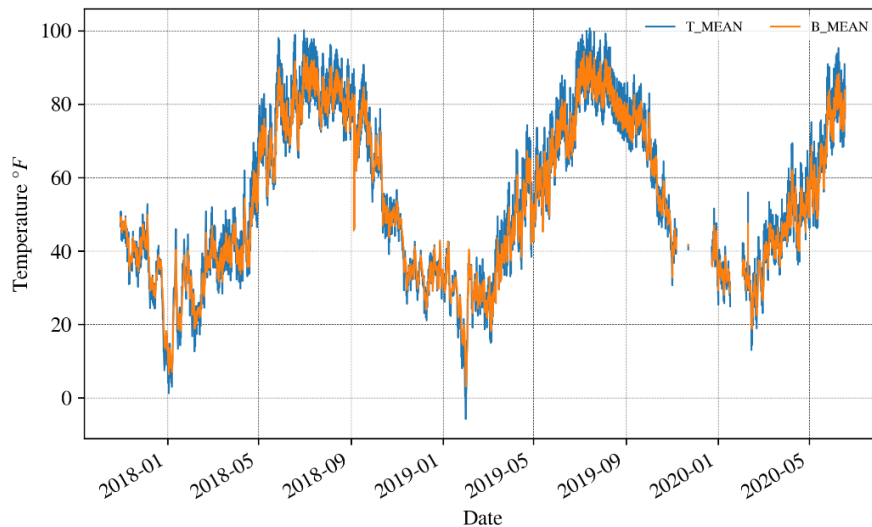
Figure 4.10 Top and bottom average temperature time history (Arlington Heights Road).

Figure 4.11 Top and bottom average temperature time history (Prospect Avenue).

As indicated by the gaps in Figures 4.10 and 4.11, there are time periods when there were no valid temperature readings, especially for the instrumented slab at Prospect Avenue. However, lack of temperature readings from Prospect Avenue does not necessarily indicate there were no data collected at all. In fact, for many of the time windows when there were no temperature readings, there were stable strain readings from most of the embedded gages, as well as the crackmeters. The mix of missing temperatures and valid gage strain or displacement readings emphasizes the need to recover those missing temperatures since relationships between temperature and strains/stresses, as well as displacements, are important in this study.

The missing top and bottom temperature readings are estimated by a regression model between the top or bottom average temperature and the O'Hare station data, including dry-bulb temperature, precipitation, relative humidity, wind speed, visibility, and station pressure. The regression model is trained by all valid temperature readings collected from the embedded gages. In comparison to Figures 4.2 and 4.3, Figures 4.12 and 4.13 are the temperature time histories with the estimated temperature readings included for time periods where temperature measurements are missing.
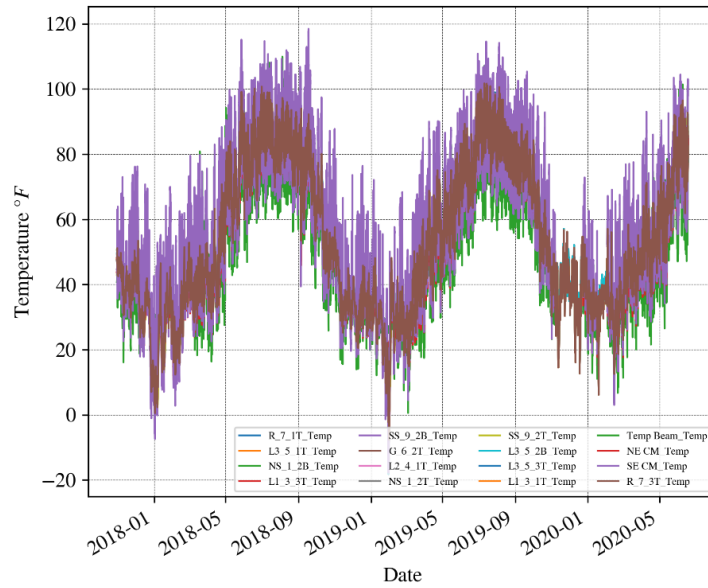
Figure 4.12 Time history of temperatures with estimated temperature data filling gaps (Arlington Heights Road).
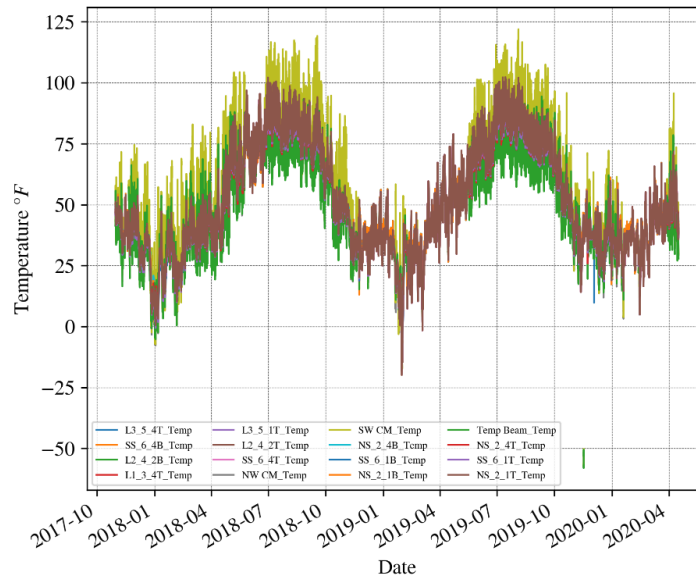
Figure 4.13 Time history of temperatures with estimated temperature data filling gaps (Prospect Avenue).

4.2 Coefficient of Thermal Expansion

The coefficient of thermal expansion was calculated using the strain and temperature readings obtained from the temperature beams for both bridges. The strain was plotted against temperature, and the slopes of the plots were calculated, which gives the thermal expansion coefficient. The coefficient estimated using the temperature beam data from Arlington Heights Road and Prospect

Avenue is 11 µε/ºC (see details in Appendix D). These results agree reasonably well with the commonly accepted thermal expansion coefficient of concrete, which is 10 µε/ºC.

4.3 Approach Slab Strains

Strain readings for all slab gages were collected every 10 minutes for most of the monitoring program. This interval was decreased to 2 and 3 minutes during static load testing and then restored after completion of those tests. The raw data that were obtained were post-processed to estimate the change in strain with respect to a reference time, which is 12:00 AM 10/30/2017, due to thermal effects as well as live loads and restraints caused by boundary conditions. The main reason such reference time is selected is that stable data collection from both instrumented slabs started shortly before the reference time. Figures 4.14 and 4.15 prove that the micro-strain readings from the embedded gages were stable at the reference time for both monitored slabs. Strain in this report refers to strain in the longitudinal direction unless stated otherwise.
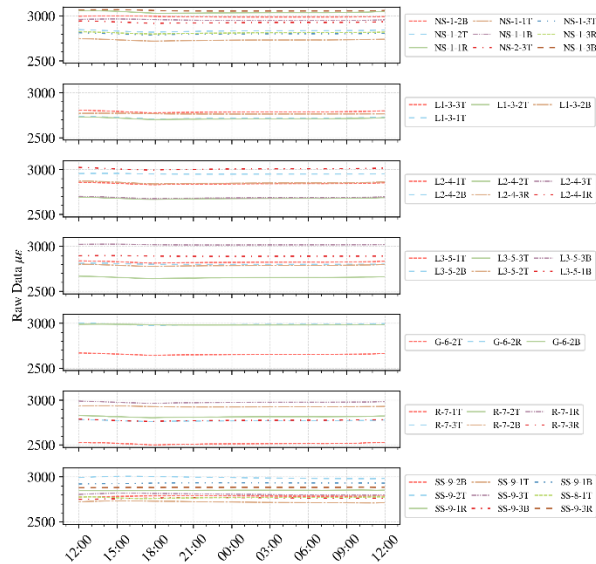
Figure 4.14 Raw data response history from 12 hours before to 12 hours after the reference time (Arlington Heights Road).
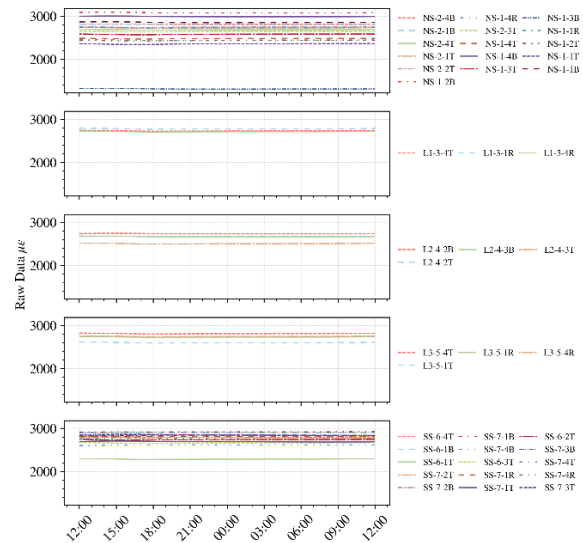
Figure 4.15 Raw data response history from 12 hours before to 12 hours after the reference time (Prospect Avenue).

Reliable data were collected from the approach slab at Arlington Heights Road, with several exceptions: 1) channel L1-3-2B worked well until July 2018, after which no data were collected; 2) channel R-7-2T stopped recording readings in January 2019; 3) all channels were interrupted from mid-November 2019 to January 2020 due to an issue with the solar panel; 4) there are occasional outliers from many channels for both strain/displacement and temperature readings and these outliers were removed through filtering. The raw micro-strain readings from all embedded gages without the apparent outliers are shown in Figure 4.16.

For Prospect Avenue, data collection was interrupted for about a month during the summer season of 2018 due to a damaged circuit board in the data acquisition system, which was replaced. The channel of L1-3-1T stopped collecting strain and temperature data during data collection, while

83

the sensor at SS-6-4B only provided temperature data. The raw micro-strain readings from all embedded gages are shown in Figure 4.17.
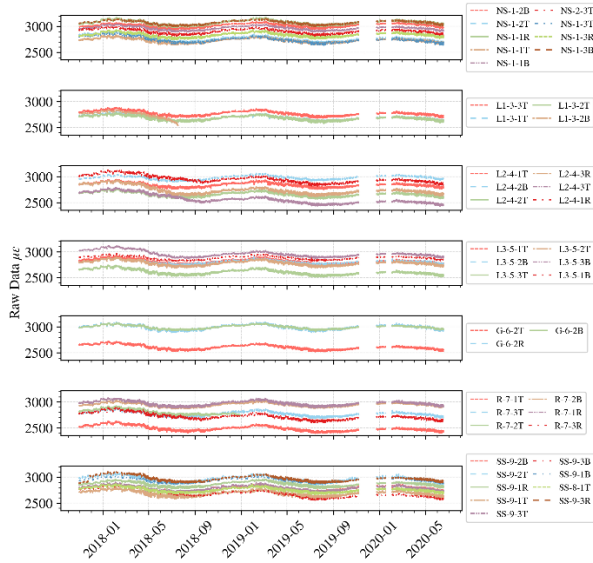
Figure 4.16 Raw data time history from embedded gages (Arlington Heights Road).
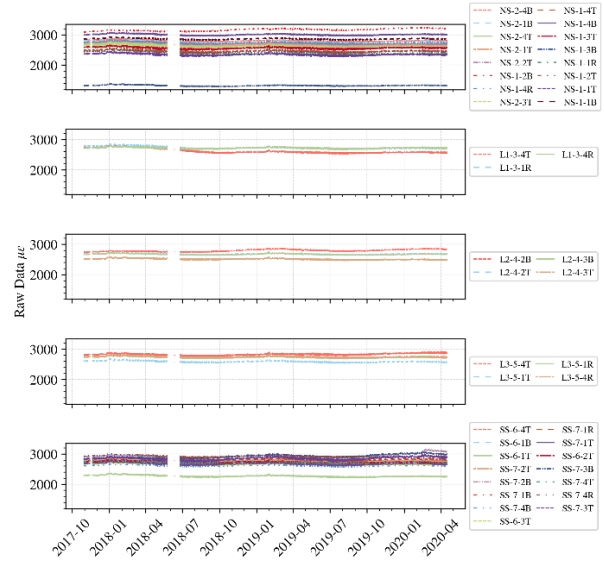
Figure 4.17 Raw data time history from embedded gages (Prospect Avenue).

4.3.1 Actual Strains

Actual strain is defined as the strain (unit change in length) observed in the slab due to all the effects in the slab. The actual strains were calculated from the raw data of the gages using the formula below:

$$\varepsilon_{actual} = (R_1 - R_0)B + (T_1 - T_0)C_1$$

where:

R₀ is the initial (reference) strain gage reading;
R₁ is the current strain gage reading;
B is the batch gage factor supplied by Geokon;
T₀ is the initial (reference) temperature;
T₁ is the current temperature; and
C₁ is the coefficient of thermal expansion of steel (12.2 με/°C).

This correction to get actual strain from raw measured strain accounts for the change in length of the vibrating wire within the strain gage. This strain represents a value that would be obtained by an instrument attached to the concrete surface. For example:

- In a case where there is no external load or restraint, ε_actual will be the unrestrained thermal expansion/contraction of the slab.
- In a case where there is no external load and the slab is restrained between rigid blocks, ε_actual will be zero.

84

4.3.1.1 Lane-wise variation of actual strains

The actual strain change for both the cast-in-place (Arlington Heights Road) and precast (Prospect Avenue) slab was observed to be closely affected by the change in temperature, as the strain variations in both slabs in general track proportionally with temperature change, which can be readily observed in Figures 4.18 and 4.19, respectively. All the magnitudes reflect the relative change compared to the fixed reference time, which means everything starts as zero at the reference time.

Tensile strain is represented as positive, while a compressive strain is presented as negative in the figures. The actual strain was observed to become more compressive as the temperature decreased, and vice versa. This trend was consistent for top longitudinal, bottom longitudinal, and transverse gages. Magnitudes of actual strain change at most of the corresponding locations were observed to be similar for the two approach slabs. The actual strain change in all panels/sections have similar ranges of magnitude for each instrumented approach slab, with the exception of the sensor located at SS-9-3R (Figure 4.18 (g)) at Arlington Heights Road, which showed a sudden jump in strain change shortly after the reference time. No evidence of physical phenomenon was observed to cause such a change in strain at this location, and thus the change may be attributed to initial spurious readings. From Figure 4.18 (b), it can also be observed that the gage L1-3-2B at Arlington Heights Road malfunctioned during the summer of 2018 with a large decrease in actual strain and stopped recording data afterward, as highlighted in the figure. In addition, one exception in the range of strain change at Prospect Avenue is gage NS-1-2B, which is more tensile than the other gages in the slab, as shown in Figure 4.19 (a).

Plots of individual actual strain change time history for all embedded gages at both instrumented slabs are included in the appendix.

Figure 4.18 (a) Arlington Heights Road, North Shoulder

85

Figure 4.18 (b) Arlington Heights Road, Lane 1

Figure 4.18 (c) Arlington Heights Road, Lane 2

Figure 4.18 (d) Arlington Heights Road, Lane 3

Figure 4.18 (e) Arlington Heights Road, Gore

Figure 4.18 (f) Arlington Heights Road, Ramp

(g) Arlington Heights Road, South Shoulder

Figure 4.18 Actual strain change time history (Arlington Heights Road): (a) North Shoulder; (b) Lane 1; (c) Lane 2; (d) Lane 3; (e) Gore; (f) Ramp; (g) South Shoulder.
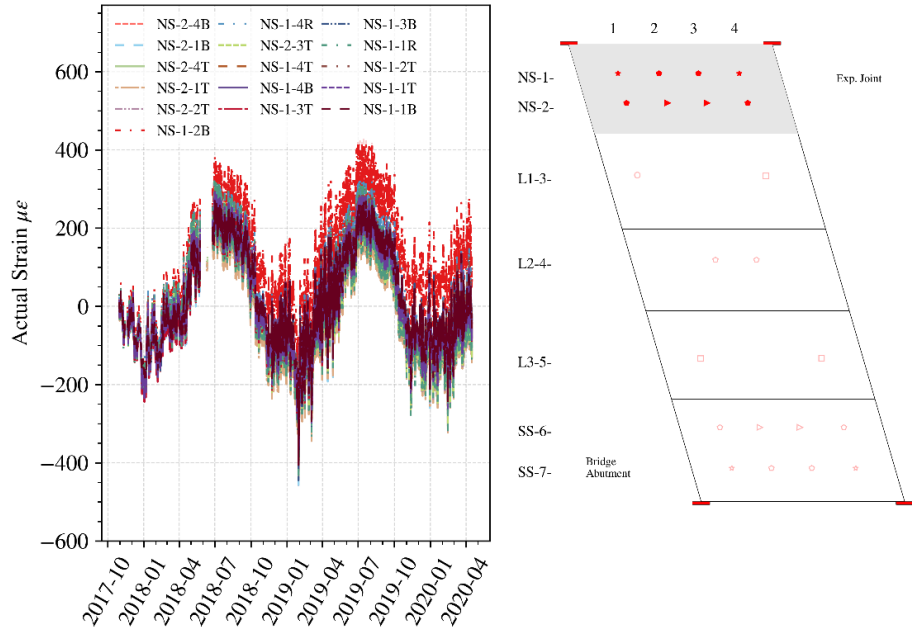
Figure 4.19 (a) Prospect Avenue, North Shoulder
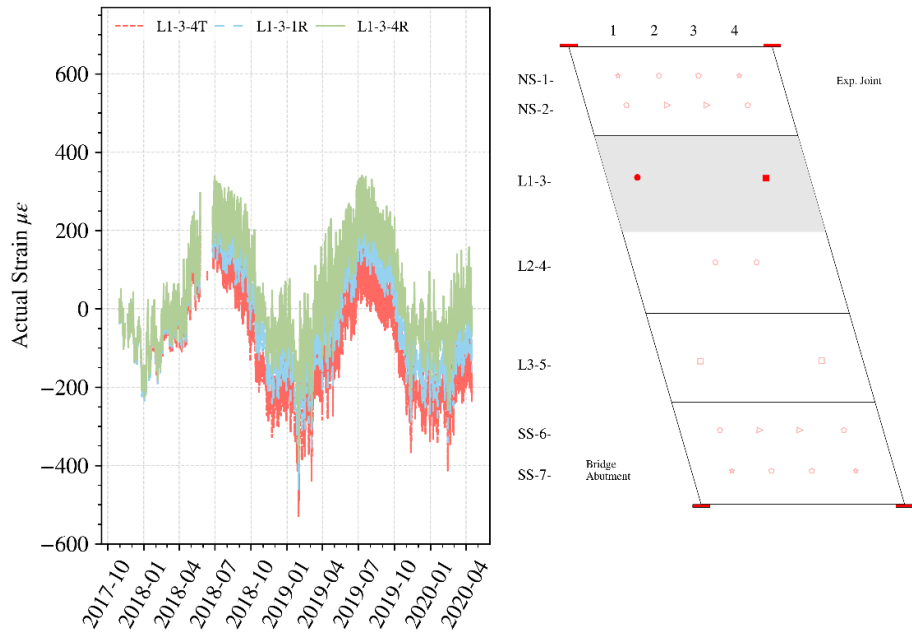
Figure 4.19 (b) Prospect Avenue, Lane 1
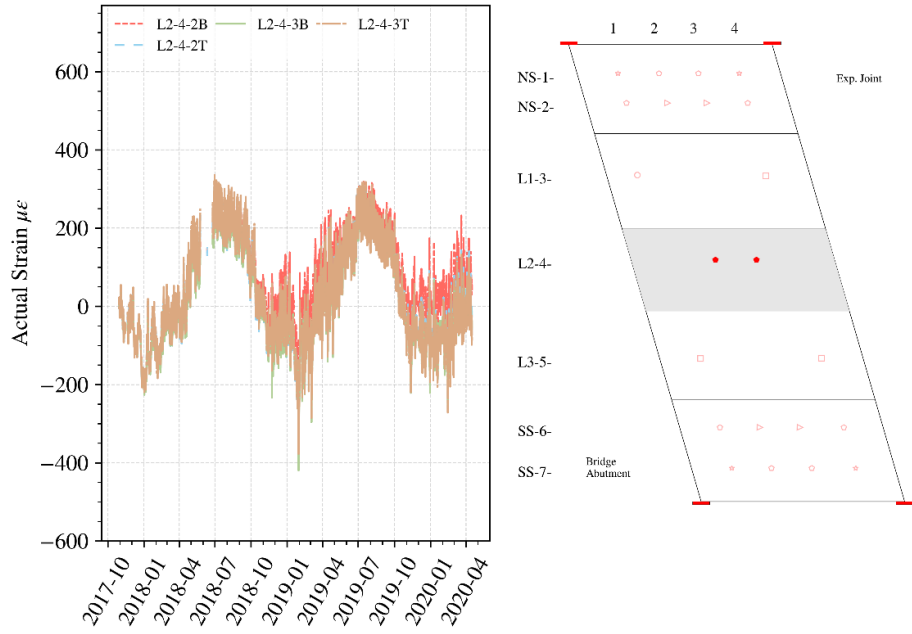
Figure 4.19 (c) Prospect Avenue, Lane 2
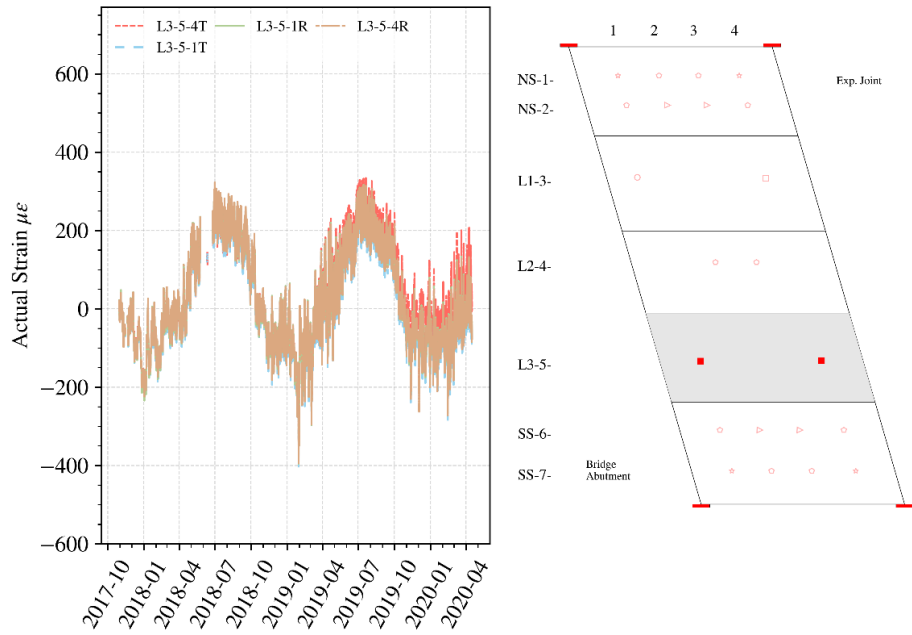
Figure 4.19 (d) Prospect Avenue, Lane 3
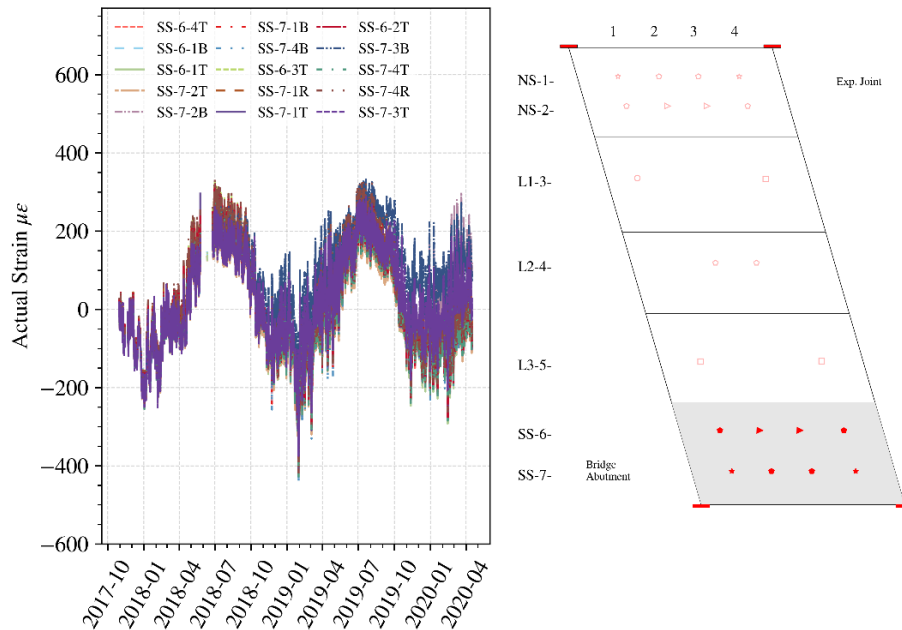
(e) Prospect Avenue, South Shoulder

Figure 4.19 Actual strain change time history (Prospect Avenue): (a) North Shoulder; (b) Lane 1; (c) Lane 2; (d) Lane 3; (e) South Shoulder.

4.3.1.2 Variation of strains with respect to slab temperature

The actual strain was observed to vary almost linearly with respect to temperature for many of the sensors at both the cast-in-place and precast approach slabs. The temperature herein is not the average temperature but the actual temperature at the gage of interest if its temperature readings are collected; otherwise, the closest gage to the one of interest in the same reinforcement mat, meaning the temperature difference through the slab thickness is already taken into account. Examples of generally observed slab behavior for cast-in-place and precast approach slabs are given in Figures 4.20 and 4.21. In each of the figures, year 1 means the period from the reference time to 365 days after it, so on and so forth. In this report, the year refers to the time window based on the reference time but not the calendar year, if not otherwise specified.

Arrows with a number around each of them provide an idea of how the variable in the vertical axis (actual strain change in this case) evolves over time. Each arrow is set to represent a time window of 90 days. The detailed mappings between the arrow number and the start as well as end time are summarized in Table 4.1. All times shown in the table are by default at the start of the day (12:00 AM). Note that some of the arrows may not be presented in some figures in the report as there were missing data at either side or both sides of the arrow. In Figures 4.20 and 4.21, the actual strain vs temperature relationship exhibits strong linear correlations such that the numbered arrows overlap with each other significantly, making it challenging to identify the path of the arrows. This is a sign of consistent actual strain behavior of the approach slab, and the path of the arrows is not as significant as the case where there are obvious variations in slab behavior every 3 months.

91

Table 4.1 Mappings between arrow number and start/end time

Arrow Number	Start Time	End Time	Arrow Number	Start Time	End Time
1	10/30/2017	01/28/2018	6	01/23/2019	04/23/2019
2	01/28/2018	04/28/2018	7	04/23/2019	07/22/2019
3	04/28/2018	07/27/2018	8	07/22/2019	10/20/2019
4	07/27/2018	10/25/2018	9	10/20/2019	01/28/2020
5	10/25/2018	01/23/2019	10	01/28/2020	04/27/2020
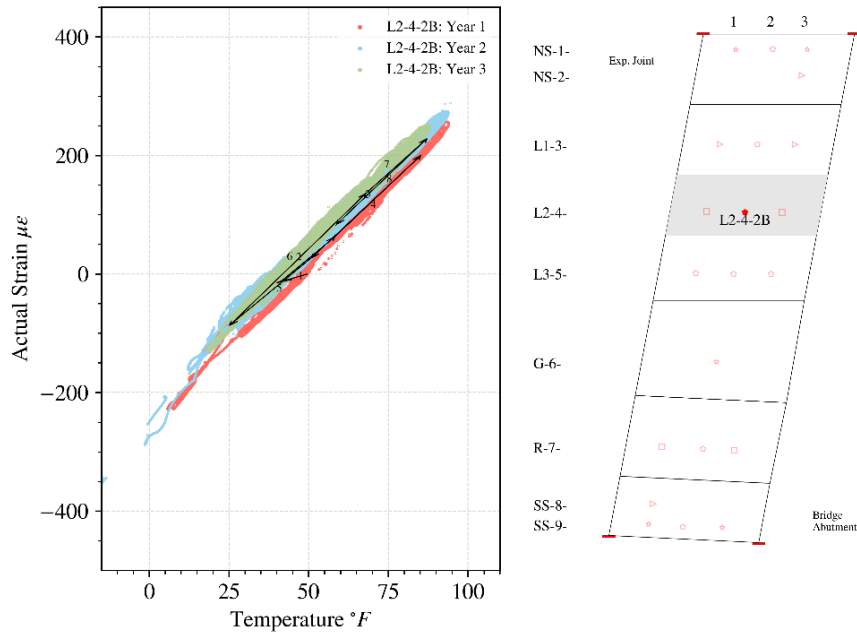
Figure 4.20 Typical actual strain change vs. temperature relationship (Arlington Heights Road).
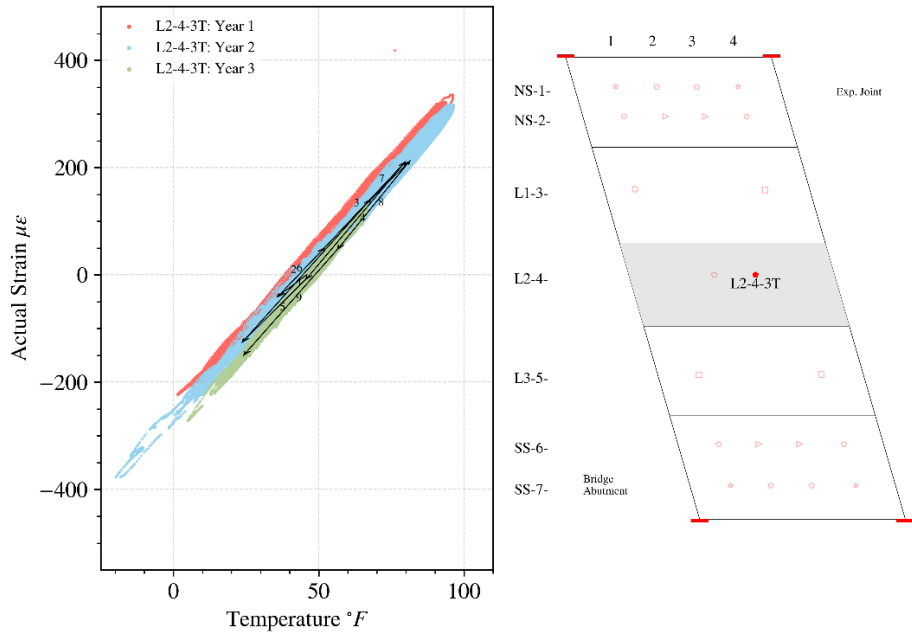
Figure 4.21 Typical actual strain change vs. temperature relationship (Prospect Avenue).

Since there are fewer sensors that do not follow the linear trend, for clarity in the plots, those gages not following a clear linear trend are labeled in Figures 4.22 and 4.23. Plots of individual actual strain change with respect to temperature for all embedded gages at both instrumented slabs are included in the appendix.
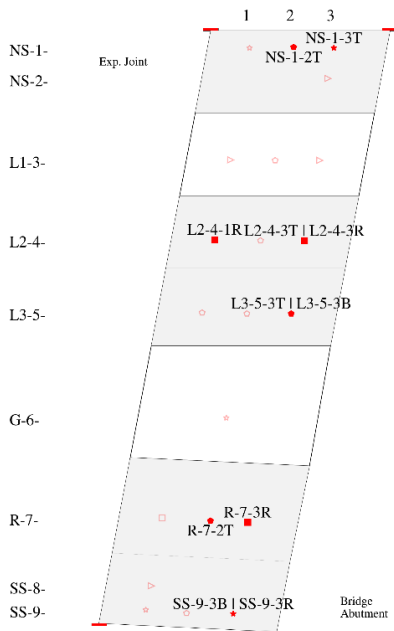
Figure 4.22 Sensor locations exhibiting a non-linear trend vs. temperature (Arlington Heights Road).
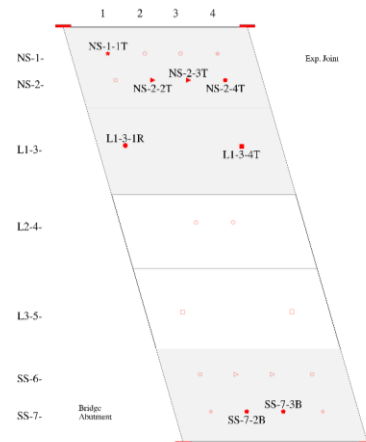
Figure 4.23 Sensor locations exhibiting a non-linear trend vs. temperature (Prospect Avenue).

93

4.3.1.3 Strain profiles of approach slabs on hottest and coldest days

In addition to individual response at each sensor, in-plane spatial variation of actual strain change in the slabs was studied to get comprehensive details about slab behavior. Especially for IAB approach slabs, there is a lack of information about the behavior near the abutment end. Additionally, Figures 4.22 and 4.23 suggest that it is more likely to observe nonlinear behaviors from the gages near the abutment. To study this, the strain variations along the abutment were plotted for the hottest and the coldest days of the year. Table 4.2 provides details of the dates and temperatures considered in this section. In each of the figures, lanes are marked using dashed lines for ease of understanding.

The "hottest time" and "coldest time" are determined by looking at the maximum and minimum values of the top and bottom average temperatures in year 1 and year 2. Although there are temperature readings in year 3, the highest and lowest temperature are less extreme by more than 15°F compared to the first two years, making it not comparable to year 1 and 2. Thus, the data for year 3 are omitted in Table 4.2. It can be easily observed that the extreme temperatures (highest and lowest) always occur at the top embedded gages. All of the corresponding hottest and coldest times for the two monitored slabs are on the same days with a difference of hours. The extreme temperatures among the two slabs during the same year are close to each other, with a difference less than 2°F, which confirms the fact that these two bridges experience essentially the same weather conditions as they are less than a mile away from each other. The highest temperatures of year 1 and 2 are very similar, whereas the lowest temperatures in year 2 are more than 6°F lower than year 1.

Table 4.2 Dates and temperatures during hottest and coldest data points

Slab	Year	Gage Position	Date and Time	Temperature (°F)	Remark
Arlington Heights Road	Year 1	Top	**06/30/2018 19:10:00**	**100.08**	Hottest time
			01/02/2018 20:50:00	**1.22**	Coldest time
		Bottom	06/30/2018 21:50:00	93.52	
			01/02/2018 11:00:00	6.33	
	Year 2	Top	**07/14/2019 17:50:00**	**100.63**	Hottest time
			01/31/2019 08:40:00	**-5.78**	Coldest time
		Bottom	07/06/2019 18:00:00	94.26	
			01/31/2019 12:00:00	3.07	
Prospect Avenue	Year 1	Top	**06/30/2018 17:50:00**	**98.62**	Hottest time
			01/02/2018 09:00:00	**1.27**	Coldest time
		Bottom	06/30/2018 21:30:00	91.84	
			01/02/2018 11:00:00	7.32	
	Year 2	Top	**07/14/2019 17:40:00**	**99.00**	Hottest time
			01/31/2019 09:50:00	**-7.40**	Coldest time
		Bottom	07/14/2019 20:50:00	91.81	
			01/31/2019 11:00:00	-0.88	

4.3.1.3.1   Cast-in-place Slab (Arlington Heights Road)

The variations of actual strain along the transverse direction (the columns in the plan view) are presented in this section. The result of the hottest or coldest time in year 1 and 2 are plotted with red diamonds, plus 4 additional lines for each year, giving the result of 4 and 2 hours before and after the target time, respectively.

For top sensors close to the abutment end of the approach slab on the hottest day (Figure 4.24), the maximum tensile strain is observed in the Ramp during year 1 and 2, while the least strain is observed in the North Shoulder in year 1 and Lane 2 in year 2. There are small variations between year 1 and 2, except for gage L2-4-3T having a significant decrease in tensile strain. The North and South Shoulder strains are not close in magnitude, exhibiting higher tensile strains near the South Shoulder. This suggests unsymmetrical deformations of the slab near the abutment, which can be attributed to uneven restraints.

The bottom layer sensors show a similar trend between year 1 and 2, except for the South Shoulder getting less tensile strain over time, as shown in Figure 4.25. In year 1, the actual strain remains similar in the shoulders, which is attributed to the proximity of similar boundary conditions and loads, while there is a less tensile strain in the load-bearing section, Lane 2.
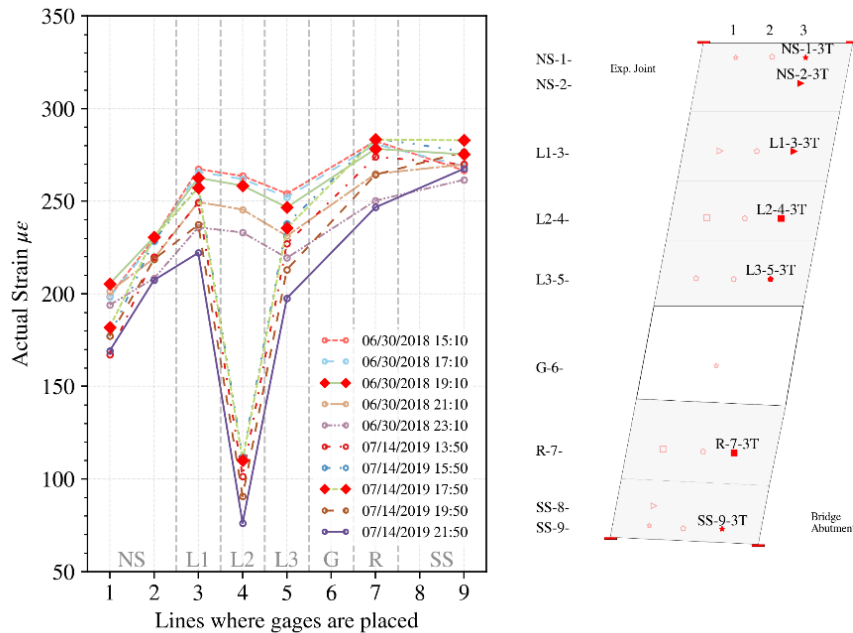
Figure 4.24 Top actual strain changes along the bridge abutment end during the hottest time (Arlington Heights Road).
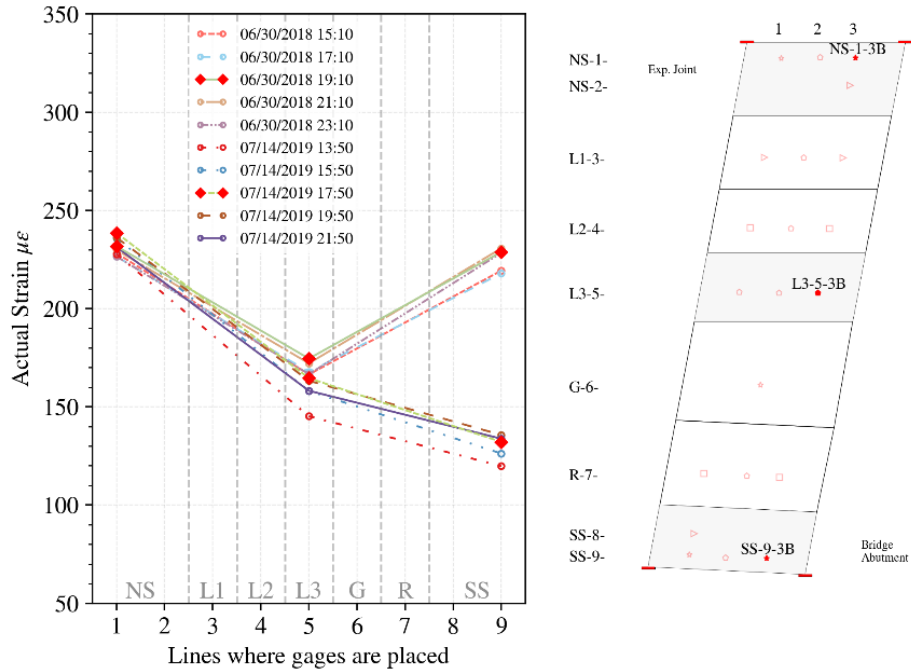
Figure 4.25 Bottom actual strain changes along the bridge abutment end during the hottest time (Arlington Heights Road).

At the coldest time observed (Figure 4.26), all the strains were compressive in nature, in contrast to all tensile in the case of hottest time. For the top longitudinal sensors, the higher compressive actual strains are generally observed in loaded sections like Lane 1, 2, and 3, as well as the Ramp, while smaller compressive strains were found at the shoulders. Year 2 data also seem more compressive than year 1, which agrees with the pattern for the hottest time but have a greater increase towards compression than the hottest time. Similar to the case of hottest time, there was a significant strain increase towards compression at Lane 2 in year 2. It is found that such a sharp increase in compressive strain at gage L2-4-3T happened just around the target coldest time due to the extreme cold weather.
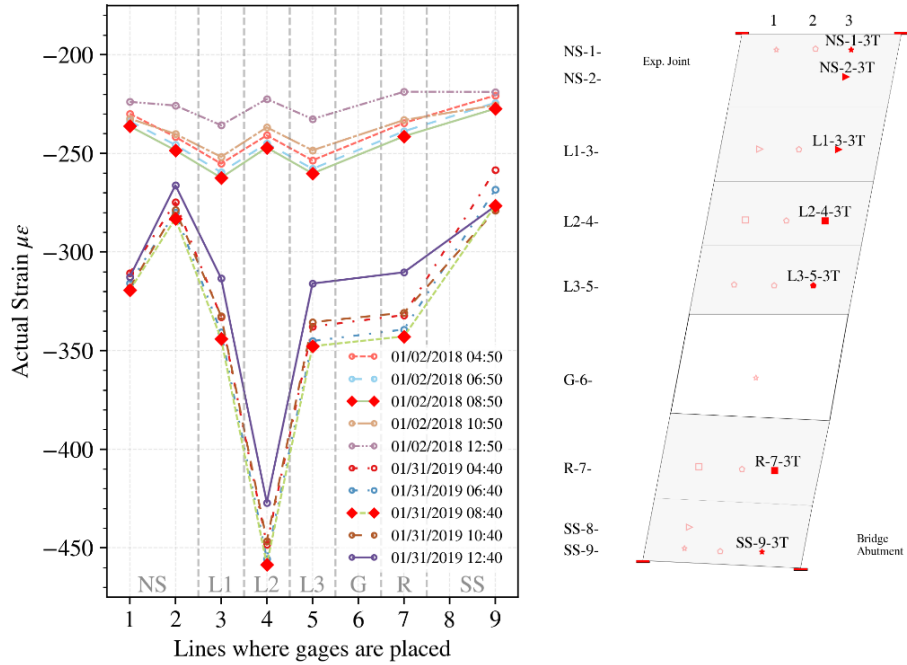
Figure 4.26 Top actual strain changes along the bridge abutment end during the coldest time (Arlington Heights Road).

For the bottom longitudinal sensors in Figure 4.27, Lane 3 incurs more compressive strain, especially in year 2, with the North Shoulder strain more tensile than that observed in the South Shoulder, which is similar to what was observed at the hottest time as well. The actual strain remains almost unchanged at sensor NS-1-3B, different from the other two bottom sensors. Again, this phenomenon may suggest a difference in restraints around these sensor locations.
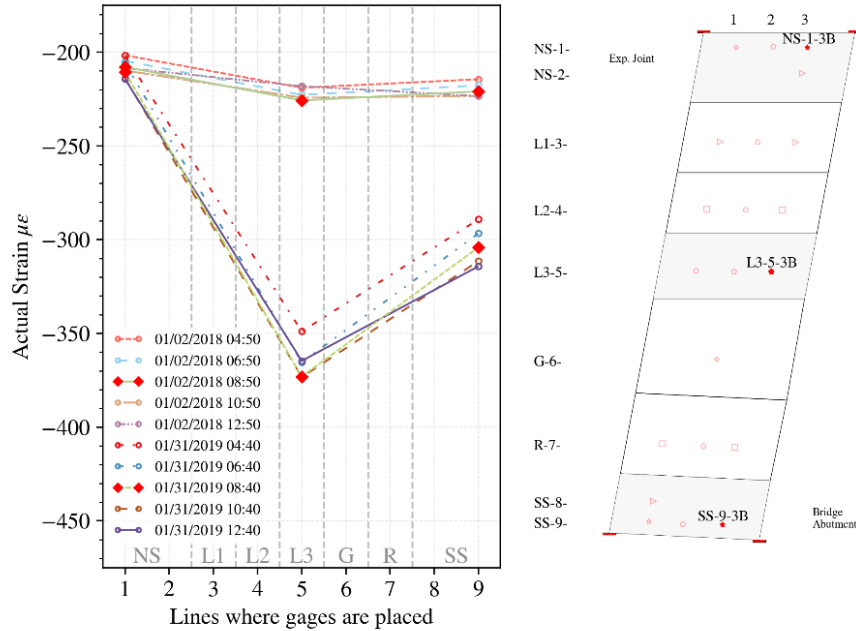
Figure 4.27 Bottom actual strain changes along the bridge abutment end during the coldest time (Arlington Heights Road).

4.3.1.3.2   Precast Slab (Prospect Avenue)

Figures 4.28 and 4.29 provide the actual strain distribution along the transverse direction for the hottest time. Different from the cast-in-place slab at Arlington Heights Road, the actual strains at both top and bottom layer of sensors exhibit stronger consistency between year 1 and 2. Top actual strains show more decrease in tension in year 2, which is attributed to greater temperature variation in the top layer of gages. The difference in actual strain between the North and South Shoulder is smaller than that of the cast-in-place slab as the precast slab possesses simpler geometry and possibly less complex restraint distribution under the slab. It is interesting to note that for both shoulders, the north half always tends to be more tensile than the south half, and it holds for top and bottom sensors layers. This is not only found at the hottest time but at the coldest time as well.
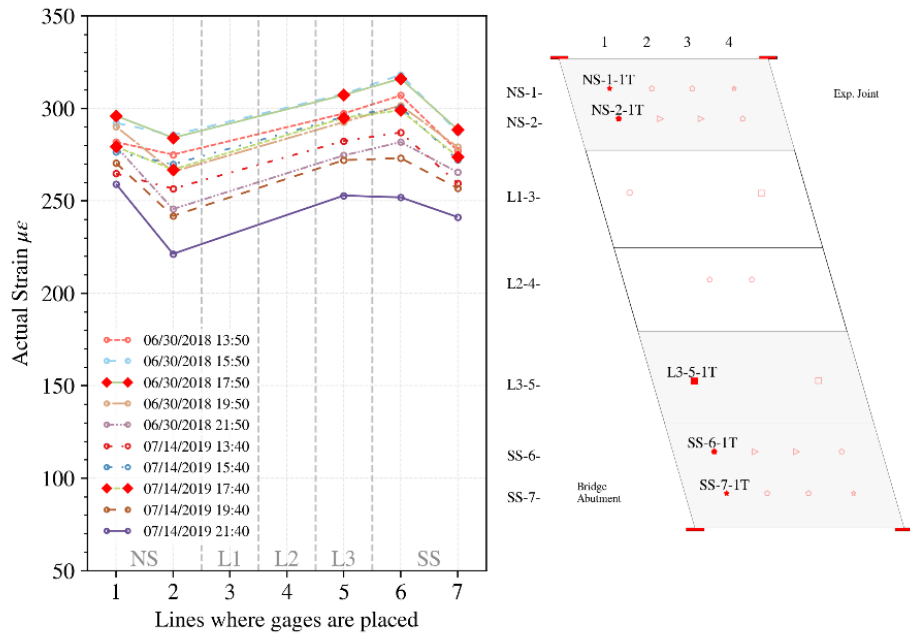
Figure 4.28 Top actual strain changes along the bridge abutment end during the hottest time (Prospect Avenue).
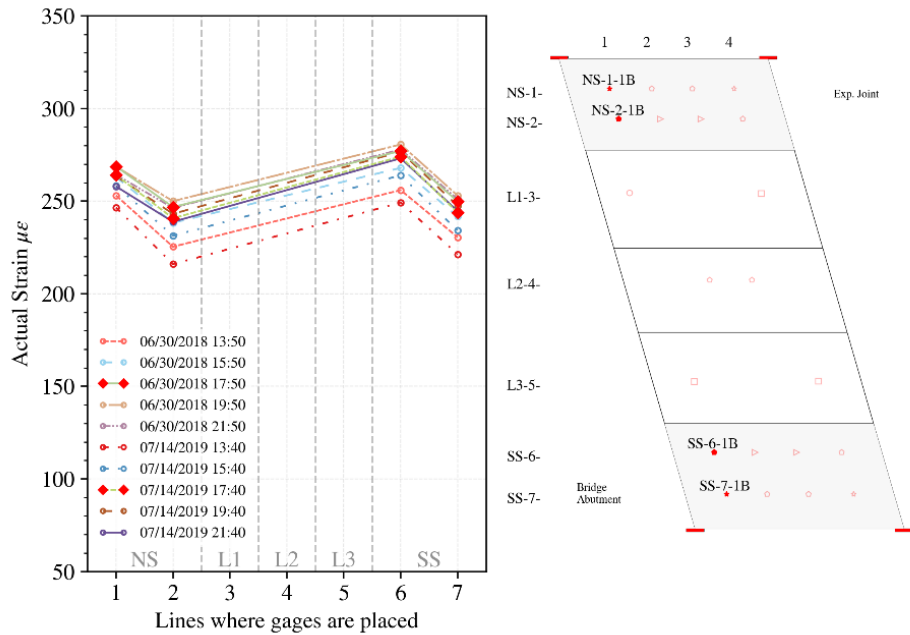
Figure 4.29 Bottom actual strain changes along the bridge abutment end during the hottest time (Prospect Avenue).

During the coldest time (Figures 4.30 and 4.31), the behavior of the top and bottom layer gages was similar to that observed during the hottest time, with a larger increase towards compression. This phenomenon matches most of the sensors in the cast-in-place slab. A larger variation in actual strain was found in year 2 within the North Shoulder. Both the top and bottom layers experienced

a quicker decrease in compression from 4 hours before to 4 hours after the coldest time in year 2, indicating that the extreme strain/deformation does not always coincide with the extreme temperature as the compressive strain may be compensated by the pulling effects the bridge abutment applied to the slab when there were frictional restraints around the slab.
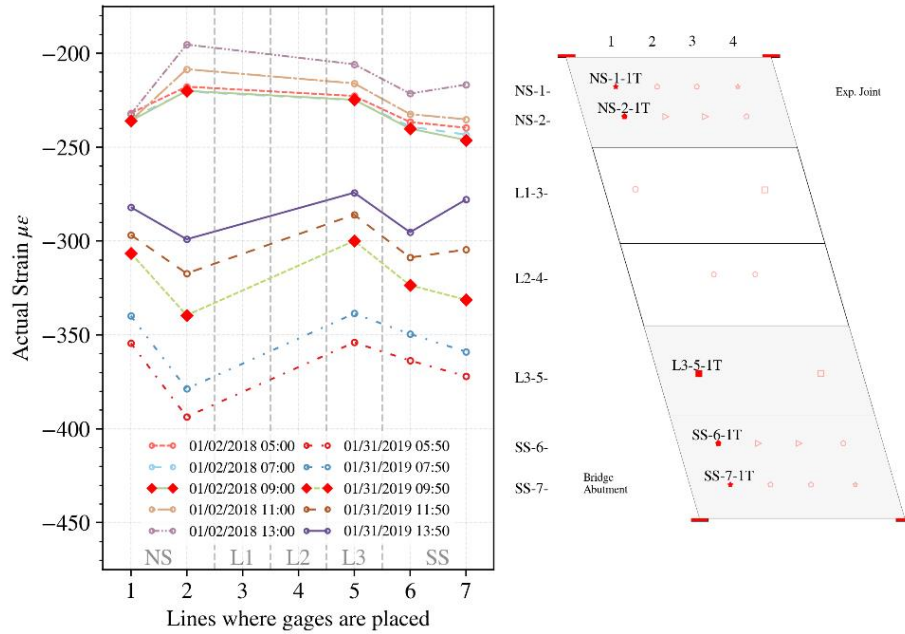
Figure 4.30 Top actual strain changes along the bridge abutment end during the coldest time (Prospect Avenue).
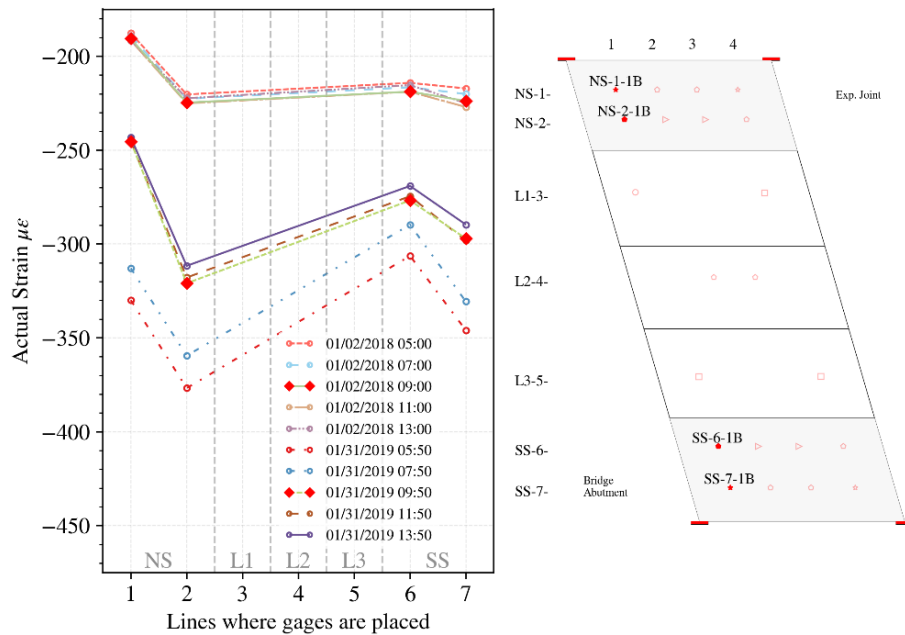
Figure 4.31 Bottom actual strain changes along the bridge abutment end during the coldest time (Prospect Avenue).

4.3.2 Load-related strains

The load-related strain is defined as the strain observed due to external loading or by demands imposed due to restraint of deformation that occurs after the selected reference time. In other words, the load-related strain is the strain directly related to the stress in the structure. For instance, if the structural component remains in its elastic range, the stress can be estimated as the product of load-related strain and modulus of elasticity. It is calculated by subtracting the strains caused by the thermal expansion of concrete from the actual strains calculated earlier. The load-related strain for any sensor can be calculated using the following equation (See more details in Appendix D):

$$\varepsilon_{load} = (R_1 - R_0)B + (T_1 - T_0)(C_1 - C_2)$$

where:

R_0 is the initial (reference) strain gage reading;
R_1 is the current strain gage reading;
B is the batch gage factor supplied by Geokon;
T_0 is the initial (reference) temperature;
T_1 is the current temperature;
C_1 is the coefficient of thermal expansion of steel (12.2 $\mu\varepsilon$/°C); and
C_2 is the coefficient of thermal expansion of concrete.

Like all other strain values reported in this study, load-related strain is defined as a change compared to the value at the chosen reference time.

4.3.2.1 Lane-wise variation of load-related strains

For both instrumented approach slabs, the load-related strains were observed to have lower magnitudes than actual strains, varying with the daily temperature to a modest extent compared to the total range observed for actual strains. The major bands in the response history of load-related strains roughly represent the daily variations due to temperature fluctuations plus live loads, in which the magnitude of the load-related strains caused by thermal load dominate, as will be shown in detail in Chapter 5. The magnitudes of most sensor strains track well with other sensors in the same lane and have averages close to zero, with tensile strain (stress) developed in lower temperature conditions and compressive strain (stress) in months with higher temperature, as shown in Figures 4.32 and 4.33, respectively.

The cast-in-place slab experienced a larger increase in compressive load-related strains, followed immediately by a sharp increase in tensile load-related stains, during the first two winters after construction (December 2017 to January 2018, January 2019), which was not observed as much in the precast slab. Moreover, in the cast-in-place slab, eleven gages out of forty-three mostly located close to the abutment of the bridge, reported large increasing compressive strain from May 2018 to August 2018. A similar significant increase in compressive load-related strains are observed in the precast slab, but with only two gages out of forty-two: L1-3-4T and L1-3-1R, as boxed in Figure 4.33 (b). The increased compressive strain at the sensors just mentioned suggests that local compressive stress was developed. The detailed list of gages mentioned above will be presented in conjunction with the discussion of load-related strains versus temperature.

Significant increases in tensile strains, with which the load-related strain reaches over 100 µε, were observed in six sensors out of forty-two at the precast approach slab. Gage NS-1-2B (boxed in Figure 4.33 (a)) was found to be the earliest one (since fall 2017) that started accumulating tensile strain. About a year later, during fall 2018, gages L2-4-2B (boxed in Figure 4.33 (c)) and SS-7-3B (red box in Figure 4.33 (e)) recorded a large increase in tensile strain. The load-related strain at L3-5-4T (boxed in Figure 4.33 (d)) remained tensile in spring 2019, while the other gages in the same section (Lane 3) developed more compressive strains. Lastly, two gages in the South Shoulder, SS-7-2B and SS-7-3T (yellow box in Figure 4.33 (e)), detected a sharp increase in tensile load-related strains during fall 2019. The strain at all six gages except for SS-7-3T was not recovered since the initiation of the increase, regardless of the increase in temperature, suggesting that local tensile stress developed at these gages.

As observed in the case of actual strains, the load-related strain of L1-3-2B at Arlington Heights Road (highlighted by a red box in Figure 4.32 (b)) undergoes a large and sudden change, most likely caused by malfunction of the sensor. (There is no data obtained from the sensor after it recorded the highest compressive strain, and the corresponding top sensor, L1-3-2T, keeps delivering continuous and stable data since then.) The sensor at SS-9-3R (highlighted by a red box in Figure 4.32 (g) experienced a sudden increase in tensile strain (about 100 µε) in December 2017, which was not recovered as time progressed. Instead, the recorded strains followed the regular trend as in the other sensors.
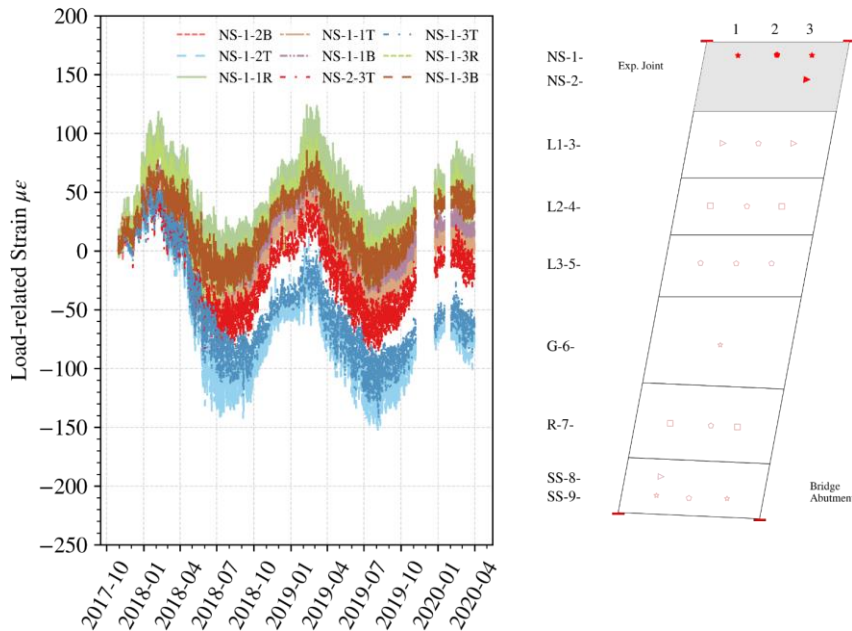
Figure 4.32 (a) Arlington Heights Road, North Shoulder
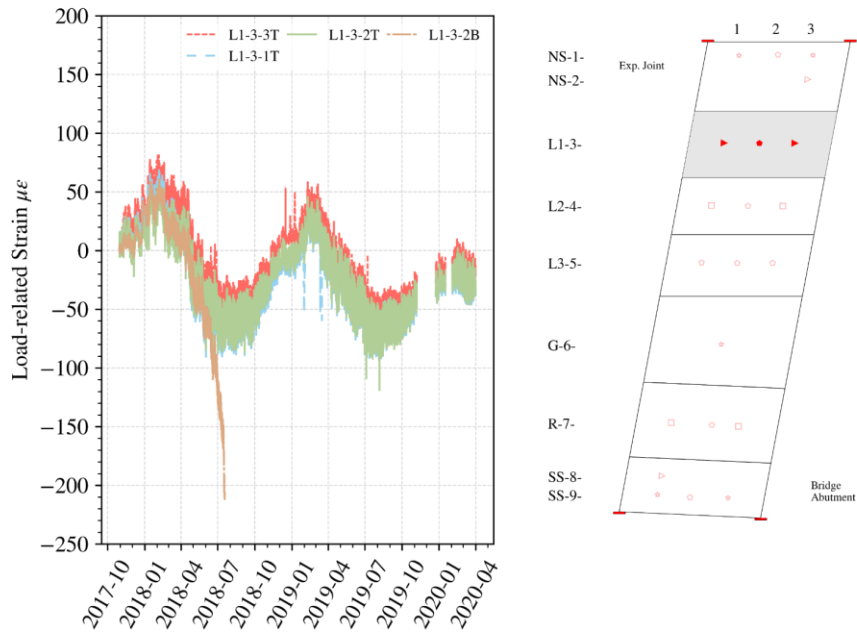
Figure 4.32 (b) Arlington Heights Road, Lane 1
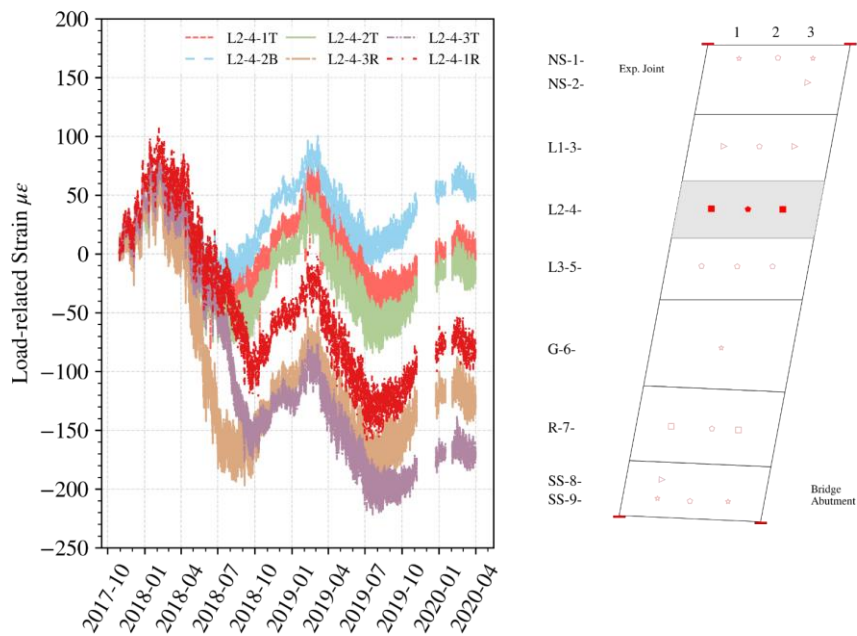
Figure 4.32 (c) Arlington Heights Road, Lane 2
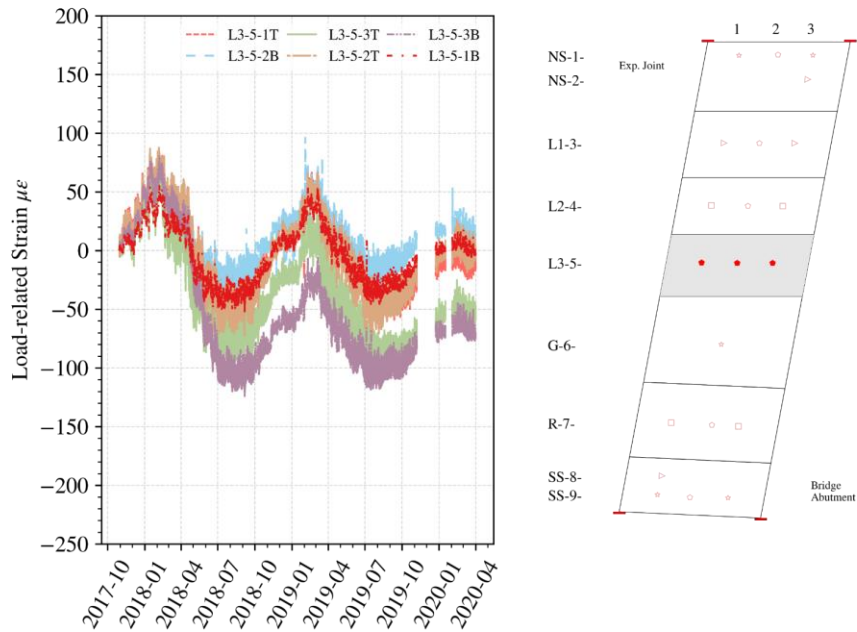
Figure 4.32 (d) Arlington Heights Road, Lane 3
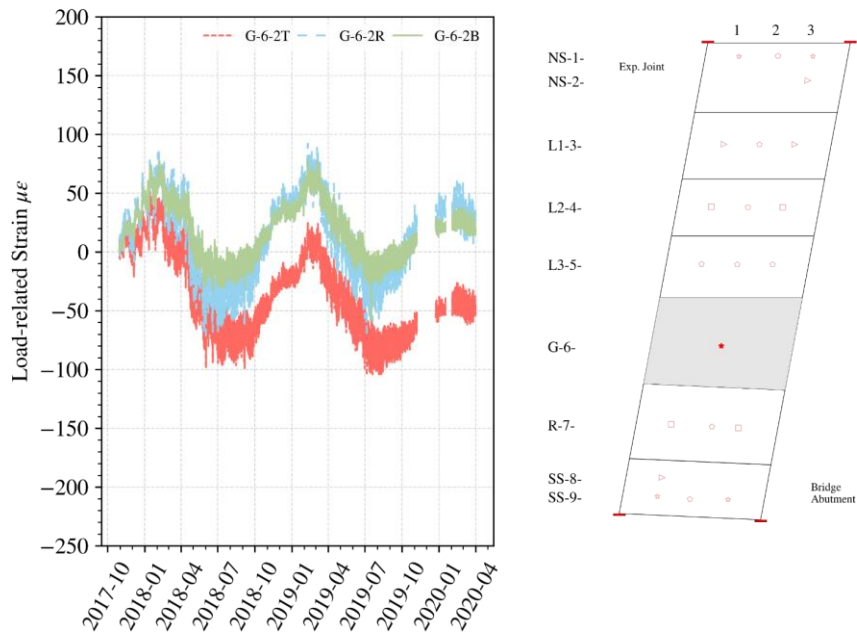

Figure 4.32 (e) Arlington Heights Road, Gore
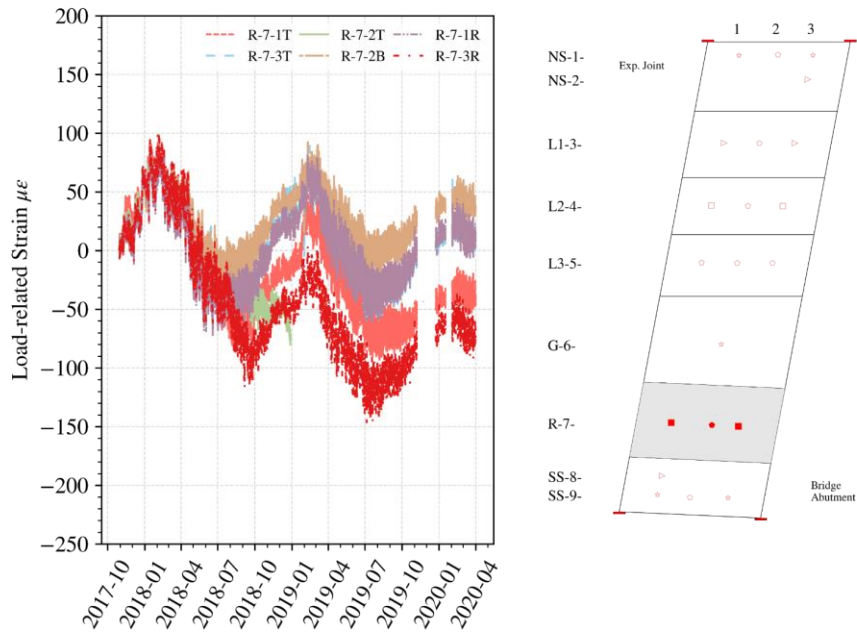
Figure 4.32 (f) Arlington Heights Road, Ramp
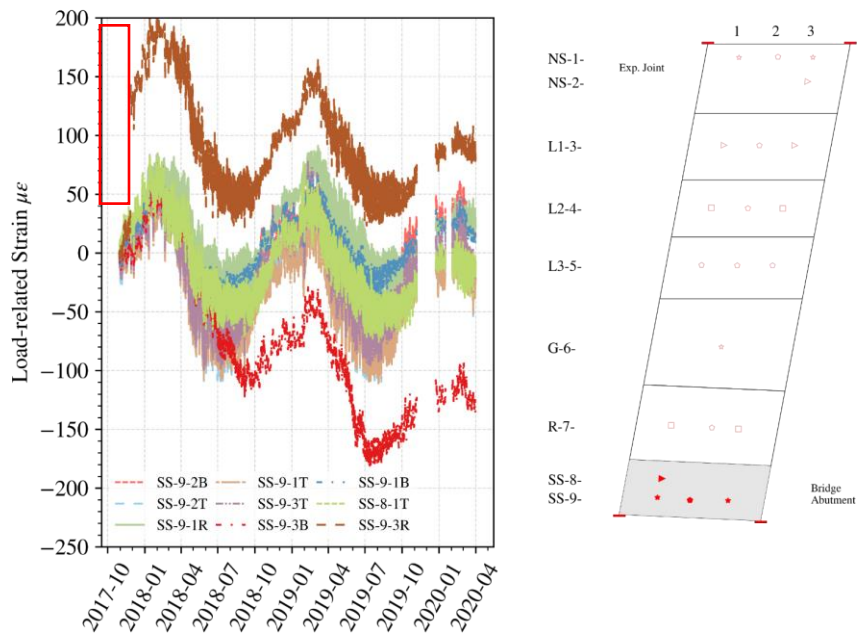
(g) Arlington Heights Road, South Shoulder

Figure 4.32 Load-related strain time history (Arlington Heights Road): (a) North Shoulder; (b) Lane 1; (c) Lane 2; (d) Lane 3; (e) Gore; (f) Ramp; (g) South Shoulder.

105
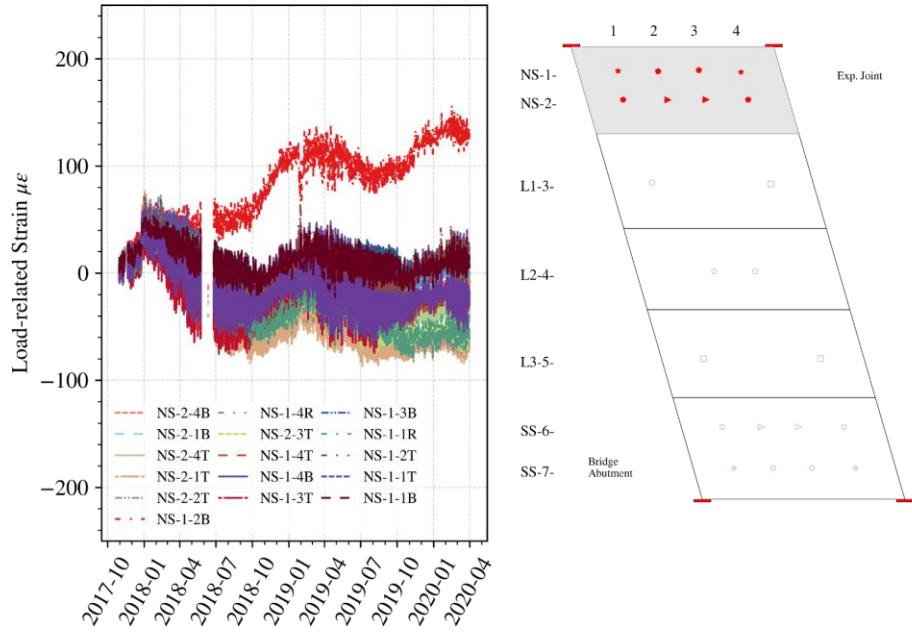
Figure 4.33 (a) Prospect Avenue, North Shoulder
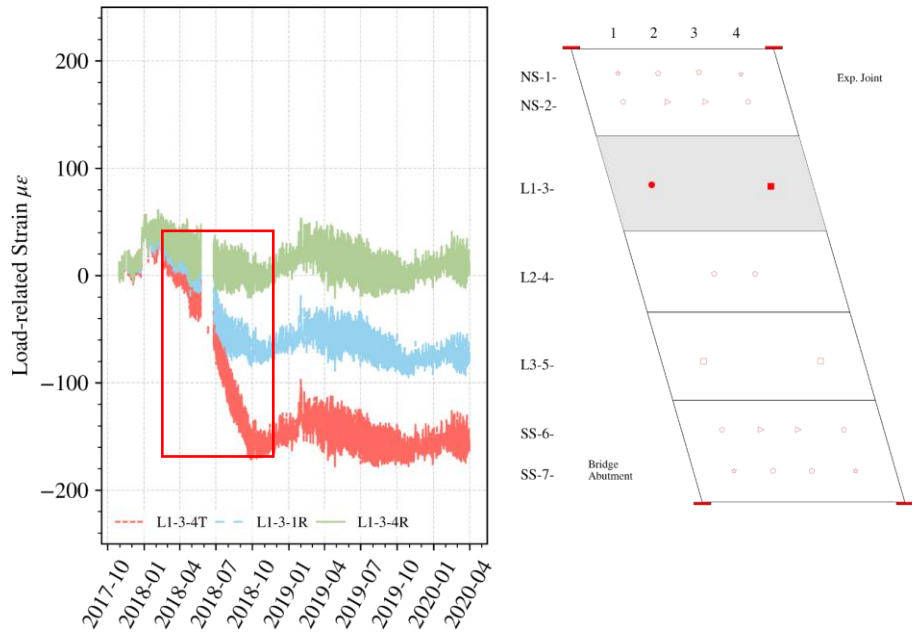
Figure 4.33 (b) Prospect Avenue, Lane 1

106
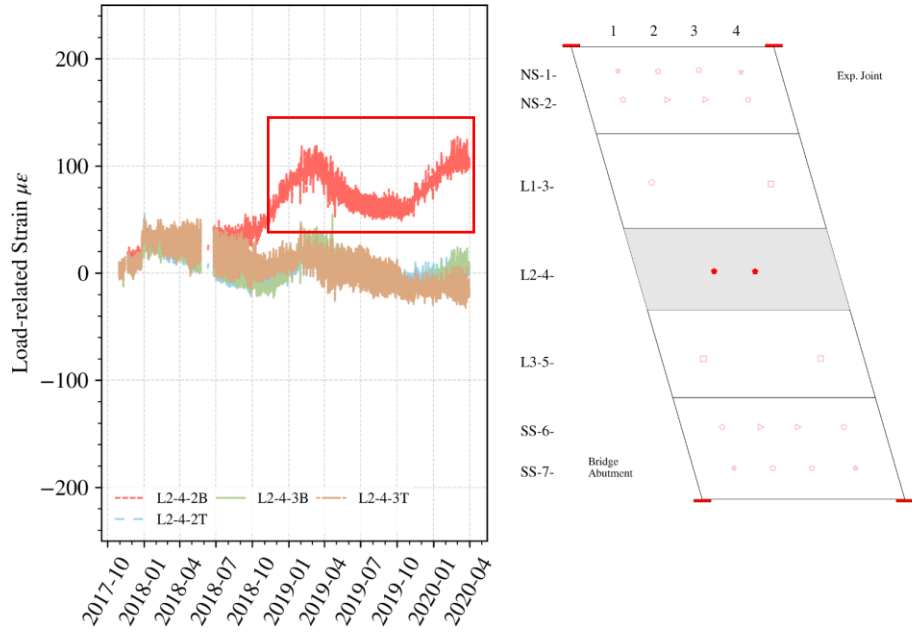
Figure 4.33 (c) Prospect Avenue, Lane 2
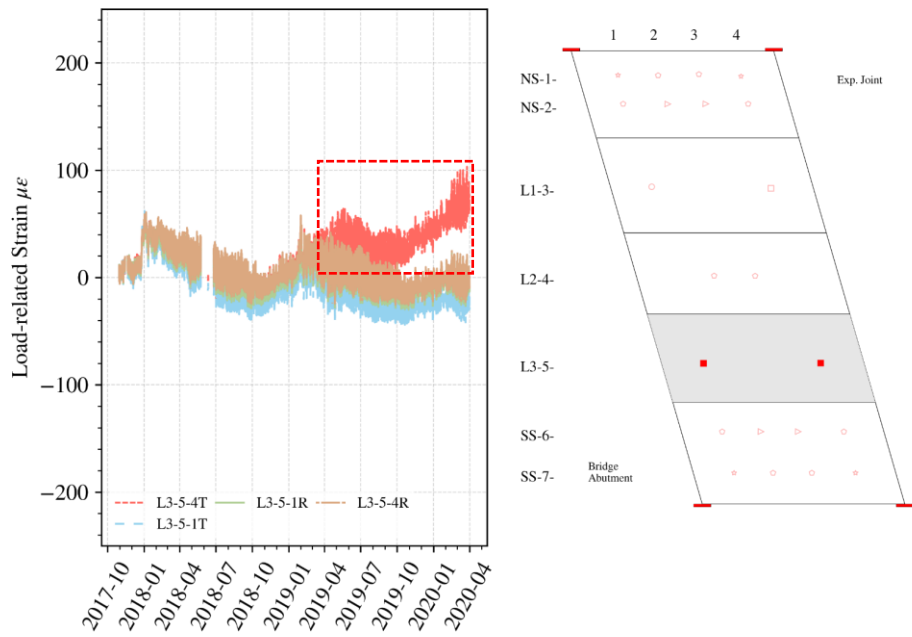
Figure 4.33 (d) Prospect Avenue, Lane 3

107
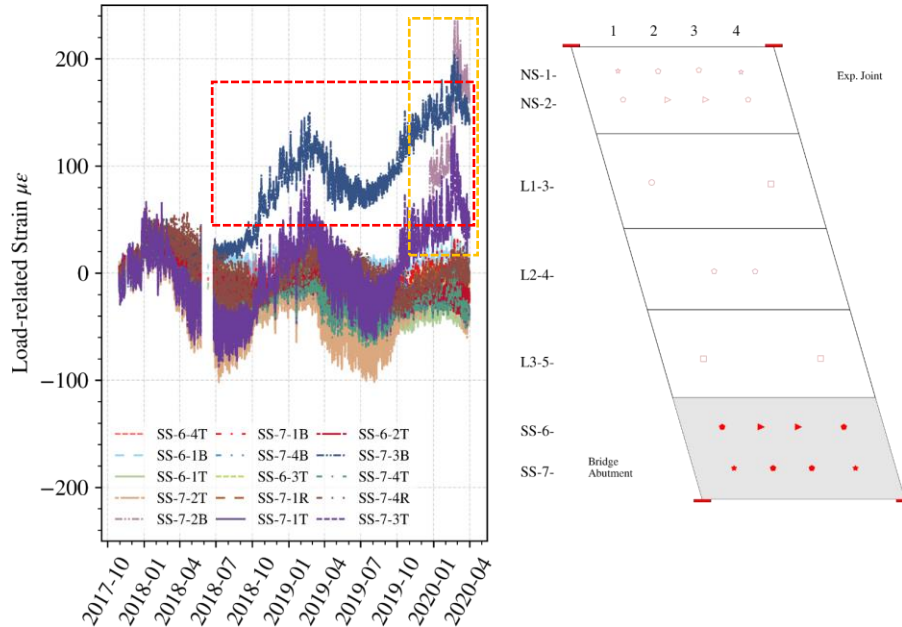
(e) Prospect Avenue, South Shoulder

Figure 4.33 Load-related strain time history (Prospect Avenue): (a) North Shoulder; (b) Lane 1; (c) Lane 2; (d) Lane 3; (e) South Shoulder.

In addition to those gages exhibiting apparent accumulated compressive or tensile load-related strain, there are gages in both monitored slabs that have a gradual accumulation of compressive or tensile strain. Since the temperature variation has a significant impact on the load-related strains in the slabs and the temperature history varies among different years, it is more reliable to evaluate these gages when the load-related strain is studied with respect to temperature.

4.3.2.2 Variation of strains with respect to slab temperature

The behavior of load-related strain with respect to temperature can be categorized into three broad groups:

1) **Group 1**: the load-related strain exhibits a roughly linear trend versus the temperature, with a smaller slope than that of the actual strains; there are no significant deviations between year 1, 2, and 3, in other words, each year's data form a concentrated cluster, and all three clusters overlap each other heavily.

2) **Group 2**: the load-related strain remains a linear relation to the temperature for each year; there are moderate deviations between year 1, 2, and 3, meaning each year's data form a concentrated cluster and there are gaps between these clusters. This group of behavior corresponds to the gages with gradual accumulation in compressive or tensile strain (mentioned at the end of the last section).

3) **Group 3**: the load-related strain experiences a significant change in magnitude at some time and keeps approximately linear with respect to the temperature otherwise; there are large changes in strain within a small range of temperature.

Figures 4.34 and 4.35 give examples of Group 1 strain at a top longitudinal, bottom longitudinal, and a top transverse gage in the cast-in-place and precast approach slabs, respectively. All gages show approximately consistent cyclic strain behaviors with moderate variation among years if there is any. Group 1 behavior suggests that the stress level remains in the relatively stable state, and there is no significant change in restraints around the gage locations.

Again, tensile strain change is taken as positive, while a negative sign represents compressive strain change, both compared with the reference data. It can be observed that, along with having a general linear trend with temperature, the load-related strain changes also have smaller local cycles with slopes slightly different from the general trend. Each loop involves the thermal deformation of the slab and a process of global displacement induced by the abutment (as the bridge superstructure expansion and contraction move the abutment); in such process, the slab only moves once it overcomes the frictional restraint, mostly under the slab, leading to the flattened ends of the local loops and all the local loops, in turn, contribute the overall behavior of the load-related strain changes.

(a)

109
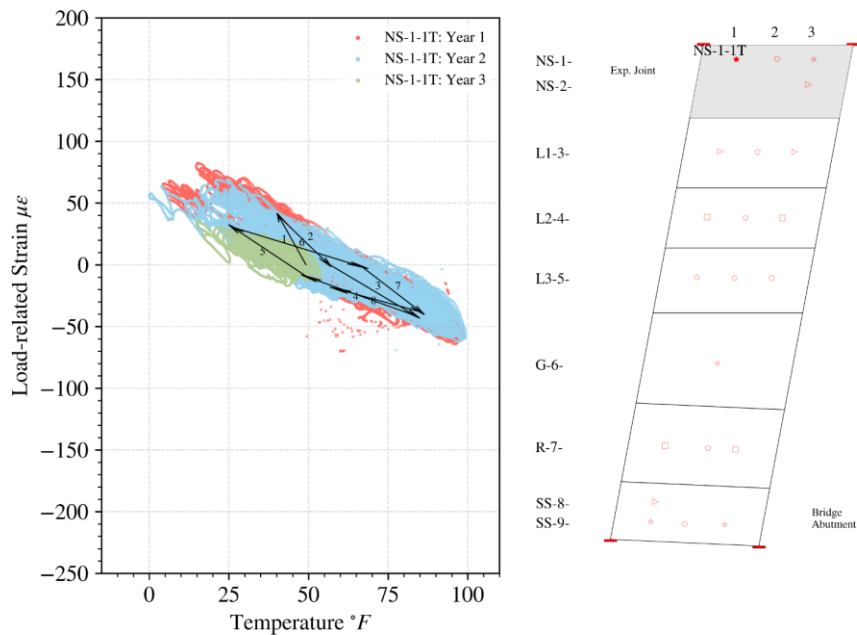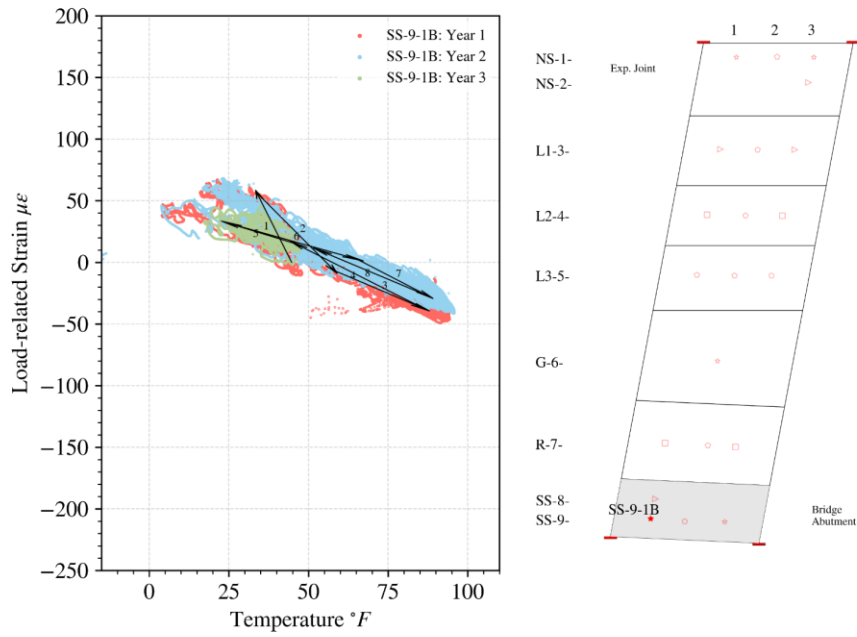
(b)
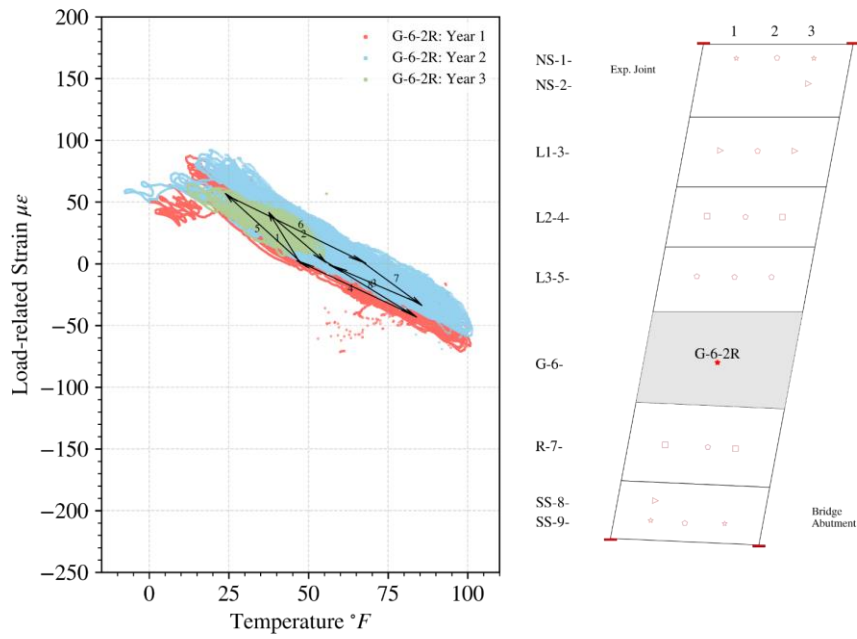
(c)

Figure 4.34 Examples of Group 1 load-related strain (Arlington Heights Road): (a) NS-1-1T; (b) SS-9-1B; (c) R-7-1R.
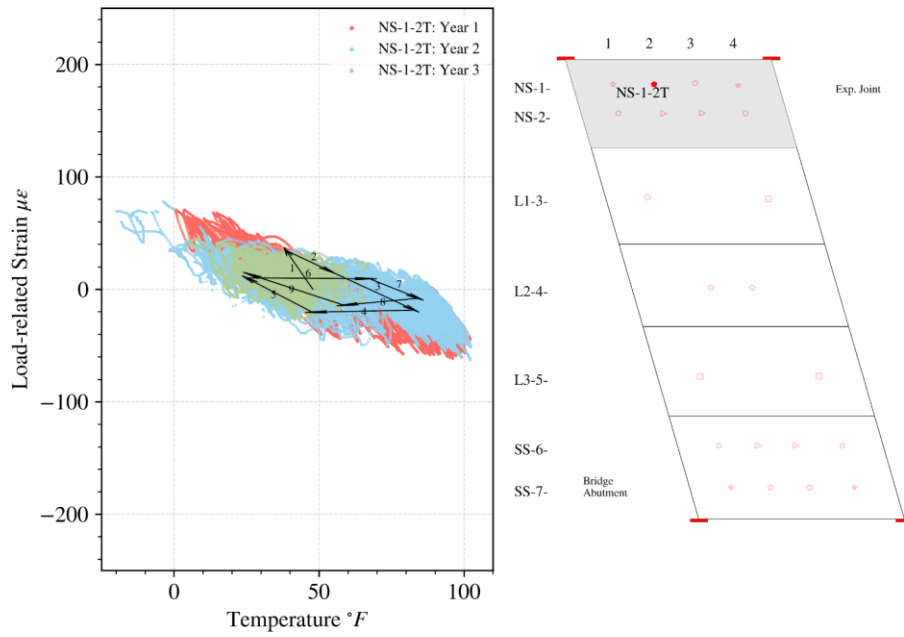
(a)
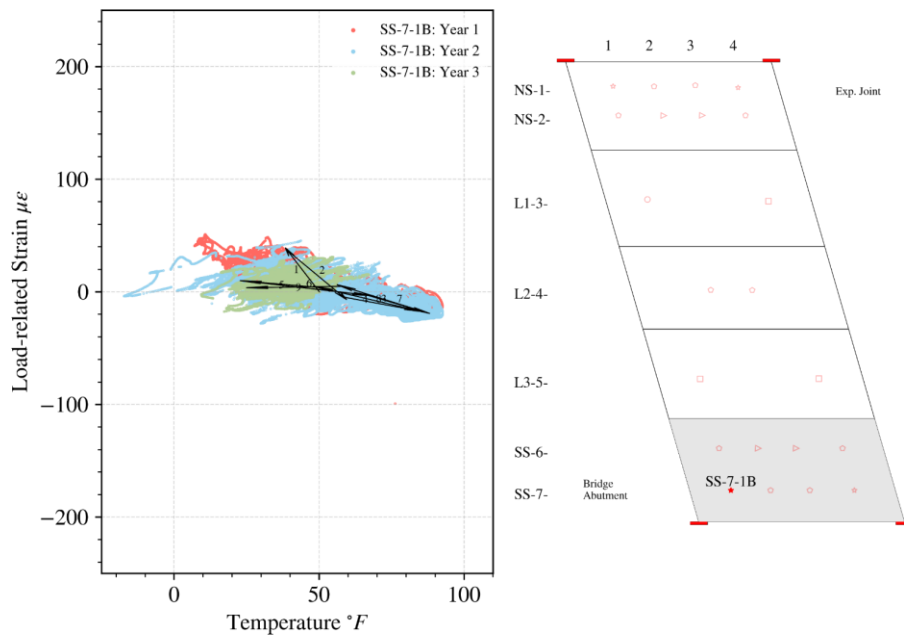
(b)
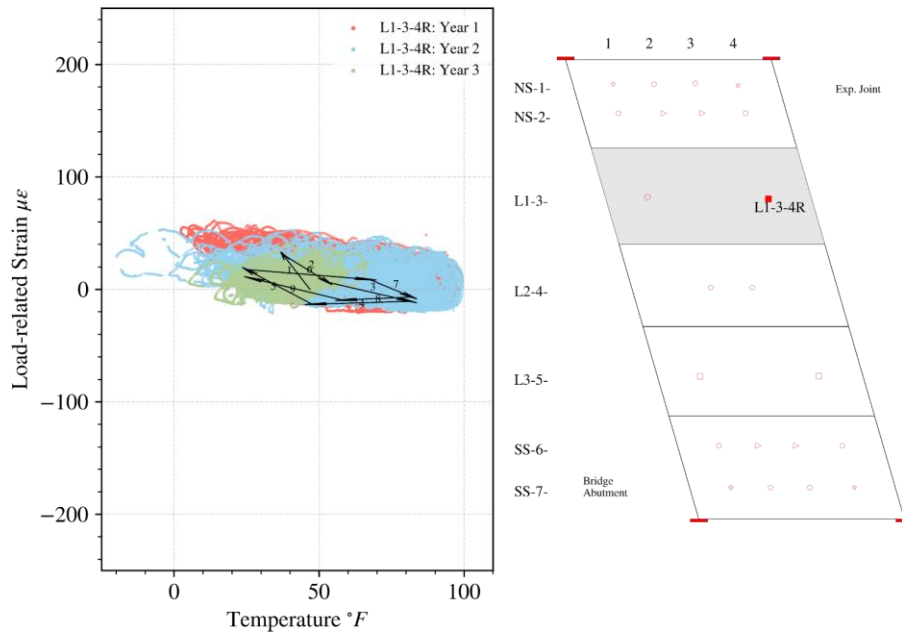
(c)

Figure 4.35 Examples of Group 1 load-related strain (Prospect Avenue): (a) NS-1-2T; (b) SS-7-1B; (c) L1-3-4R.

Maps of gage locations where Group 1 strain behavior is observed for the cast-in-place and precast slabs are shown in Figures 4.36 and 4.37, respectively. There are more gages in the cast-in-place slab than in the precast that belongs to Group 1. In both slabs, Group 1 strain behavior tends to occur at the shoulders rather than the load-bearing sections. In the cast-in-place slab, there are more gages close to the expansion joint end or at the midspan that exhibit consistent behavior. However, seldom do the gages near the expansion joint end at the precast slab show Group 1 strain behavior.
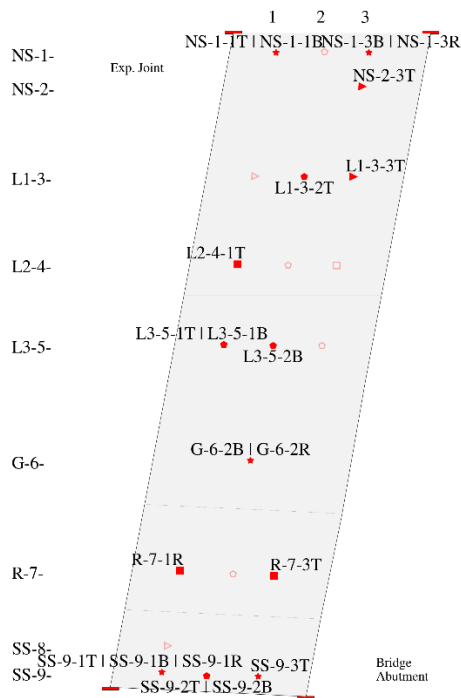
Figure 4.36 Gages with Group 1 strain behavior (Arlington Heights Road).
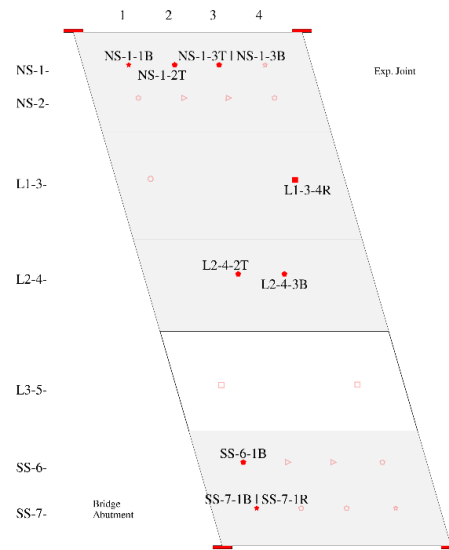
Figure 4.37 Gages with Group 1 strain behavior (Prospect Avenue).

As for Group 2 strain behavior, accumulation in compressive and tensile strains are both observed from the gages at the cast-in-place slab, whereas only compressive accumulated strains are observed at the precast slab. Figures 4.38 and 4.39 present examples of Group 2 strain behavior for the cast-in-place and precast slabs, respectively.

As indicated by the numbered arrows in the figures, though cyclic behaviors are found, there are clear translations between the year clusters either upwards or downwards. A pair of top and bottom gages in the longitudinal direction is selected in Figure 4.38, where the top gage has accumulated compressive strain and bottom gage tensile, which suggests that there is an increase in positive bending caused by the gradual decrease in the subbase support under the cast-in-place slab. Figure 4.39 gives examples of gradual accumulation in compressive strain in both longitudinal and transverse directions. Some of the gradual accumulations primarily occurred between year 1 and 2 (SS-7-4R); the others keep growing throughout the three years (SS-7-4T), as indicated by the numbered arrows.
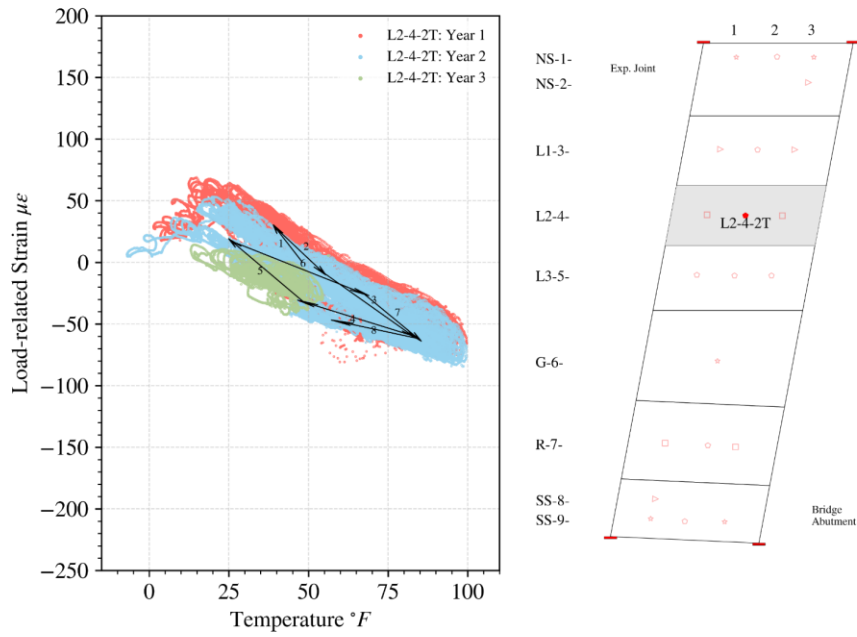
(a)
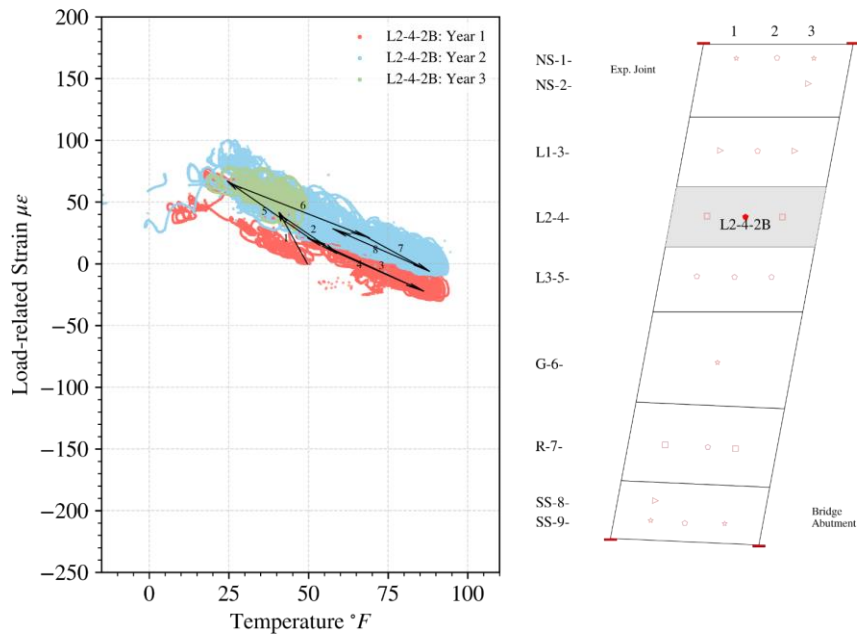
(b)

Figure 4.38 Examples of Group 2 strain behavior (Arlington Heights Road): (a) L2-4-2T with accumulation in compressive strain; (b) L2-4-2B with accumulation in tensile strain.

114
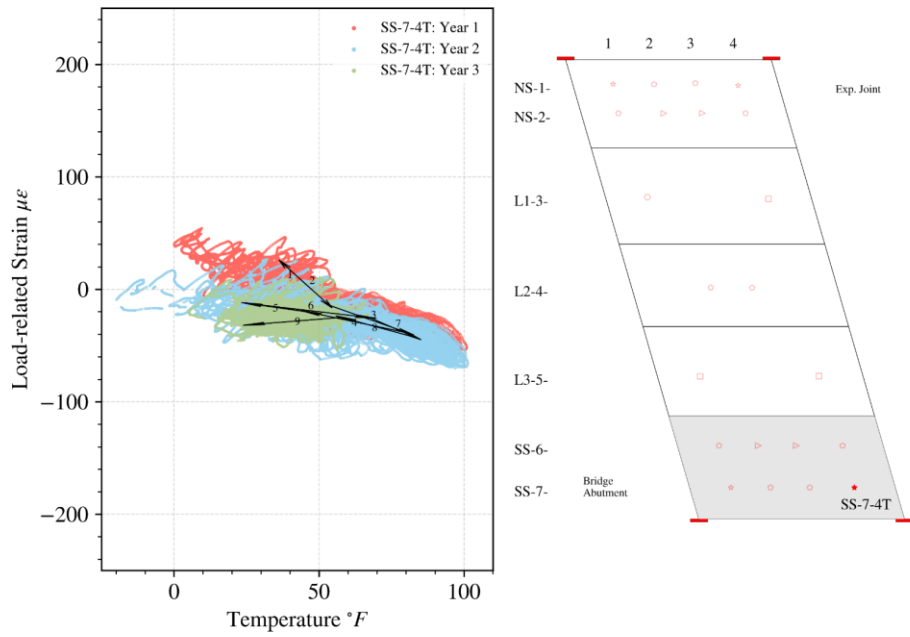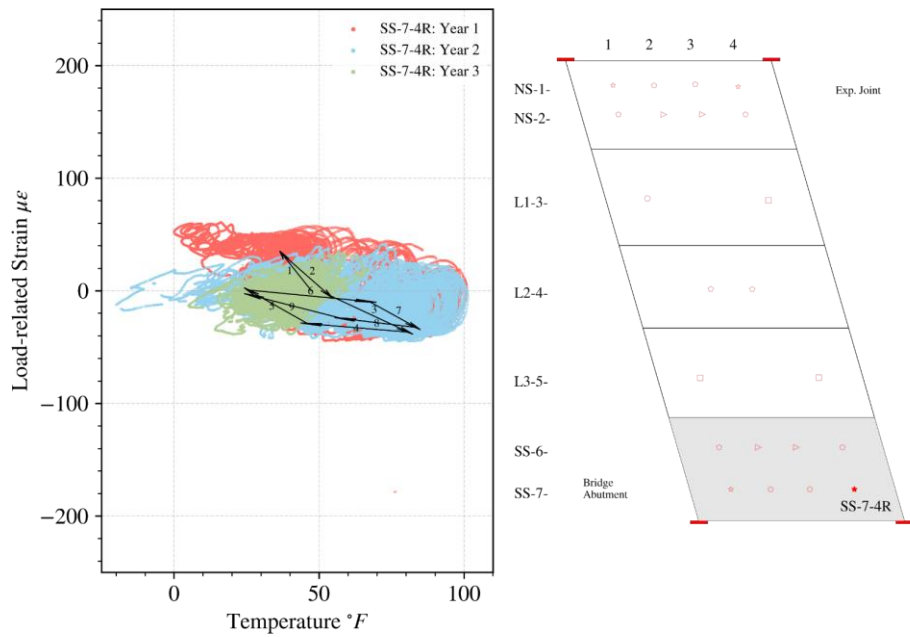
Figure 4.39 Examples of Group 2 strain behavior (Prospect Avenue): (a) SS-7-4T; b) SS-7-4R, both gages with accumulation in compressive strain.

The distribution of gages with Group 2 strain behavior at the cast-in-place slab is shown in Figure 4.40. For the precast slab, all gages belonging to Group 2 are labeled in Figure 4.41. In the cast-

in-place slab, those gages that have a gradual increase in compressive strain are all located at the top reinforcement mat in the longitudinal direction. Four out of five gages that experience an increase in tensile strain are bottom gages. For the precast slab, the majority of gages showing increasing compressive strain are top gages.

(a)

(b)
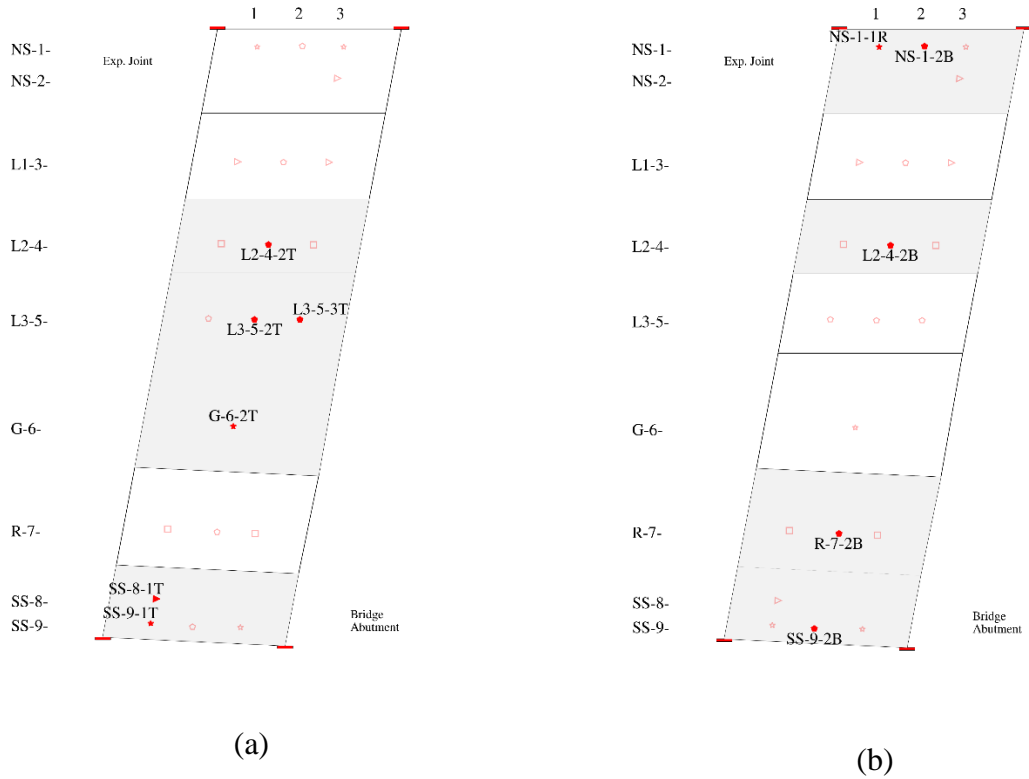
Figure 4.40 Gages with Group 2 strain behavior (Arlington Heights Road): (a) accumulated compression; (b) accumulated tension.
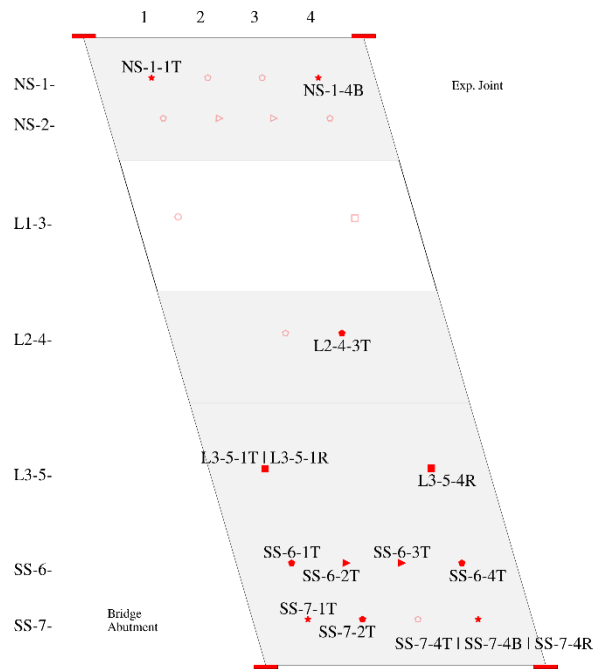
Figure 4.41 Gages with Group 2 strain behavior (Prospect Avenue).

Gages in Group 3 record a drastic increase in compressive or tensile strain during the time of field monitoring. Figure 4.42 gives examples of such behavior at a top longitudinal, bottom longitudinal, and a top transverse gage at the cast-in-place slab. All three presented strain behaviors experienced a noticeable increase in compressive strain in the hot days in year 1 and as time passes, the slope of the load-related strain with respect to temperature becomes smaller, which is indicative of a change of boundary conditions under the slab. Possible causes are that during the hot days in year 1 (summer 2018), the slab portion close to the abutment was pushed by the bridge expansion and restrained by subbase friction, leading to an increase in compression. As the temperature decreased, the support of the subbase to the slab decreased due to settlement, so the positive bending moment increased, making the load-related strain remain at a similar compressive level.

A similar phenomenon was observed in the precast slab, but to a lesser extent, as shown in Figure 4.43 (a) – (c). Accumulation in tension was observed as well, of which two examples are included in Figure 4.43 (d) and (e). In general, the load-related strain slopes versus temperature for the precast slab are smaller than those of the cast-in-place slabs, but it is still unclear why positive slopes develop in the precast slabs, meaning as the temperature increased, tension developed in the slab, and vice versa.

117
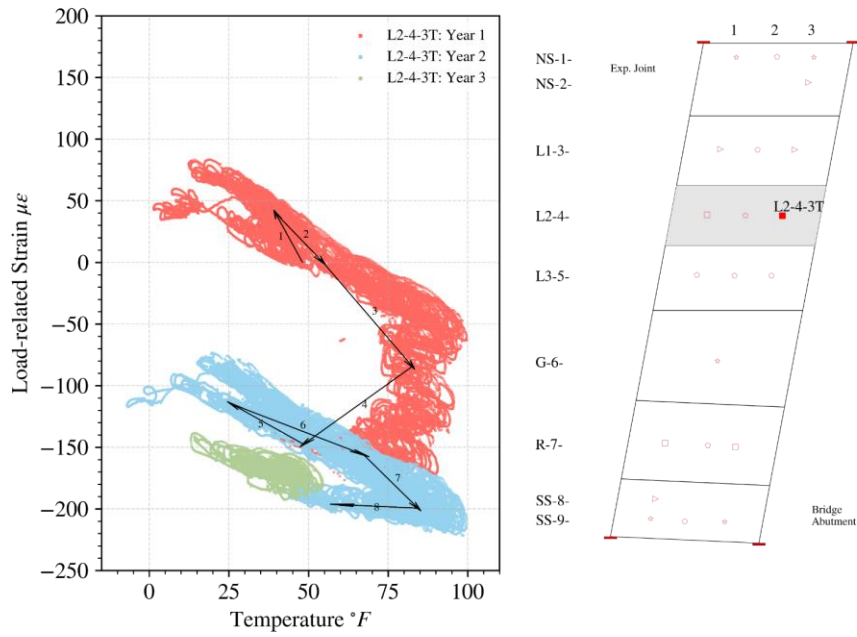
Figure 4.42 (a) Arlington Heights Road, L2-4-3T
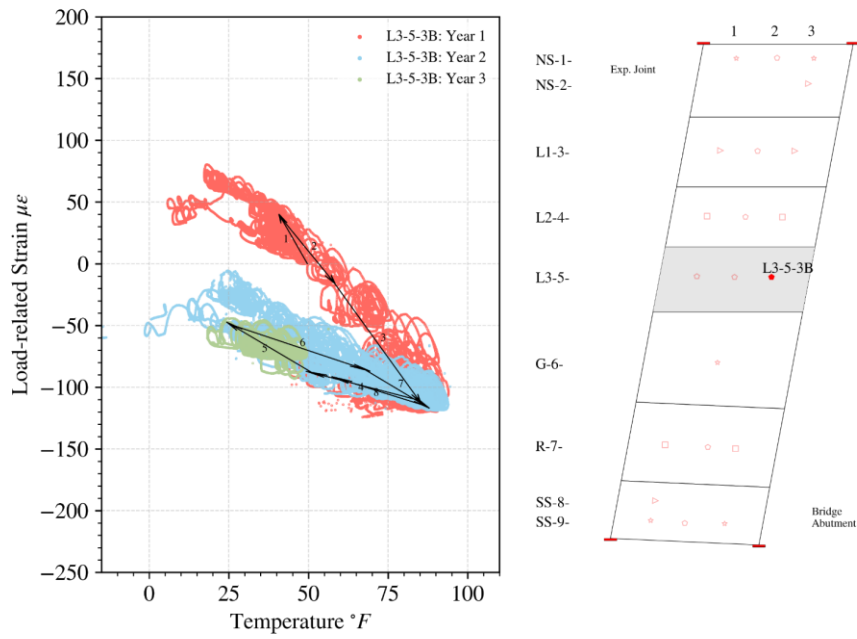
Figure 4.42 (b) Arlington Heights Road, L3-5-3B
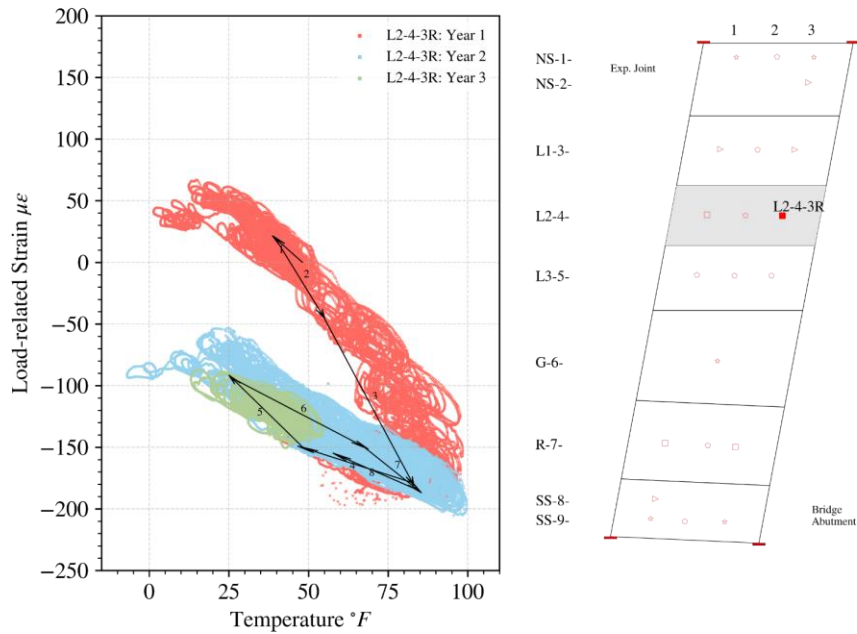
(c) Arlington Heights Road, L2-4-3R

Figure 4.42 Examples of Group 3 strain behavior (Arlington Heights Road): (a) L2-4-3T; (b) L3-5-3B; (c) L2-4-3R
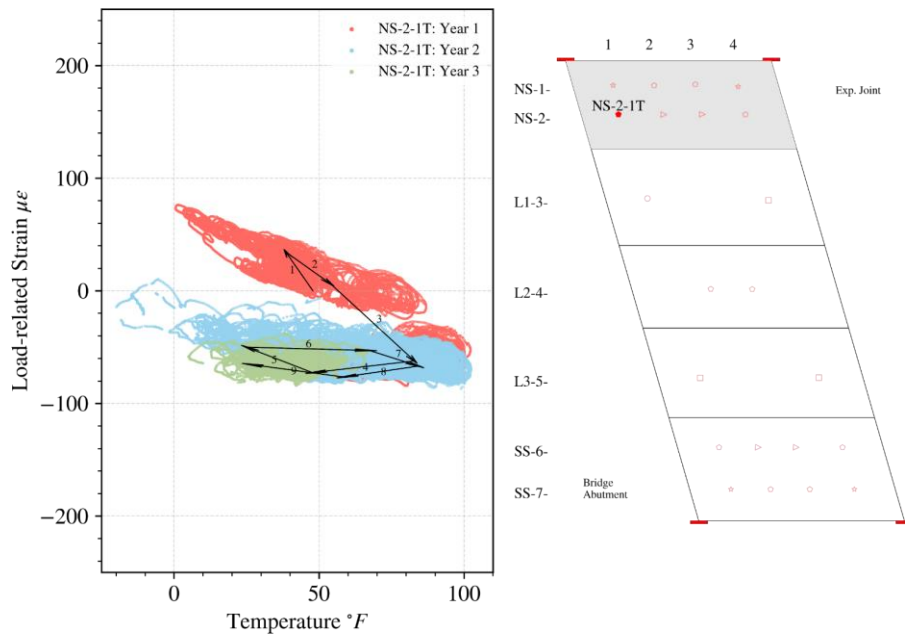
Figure 4.43 (a) Prospect Avenue, NS-2-1T
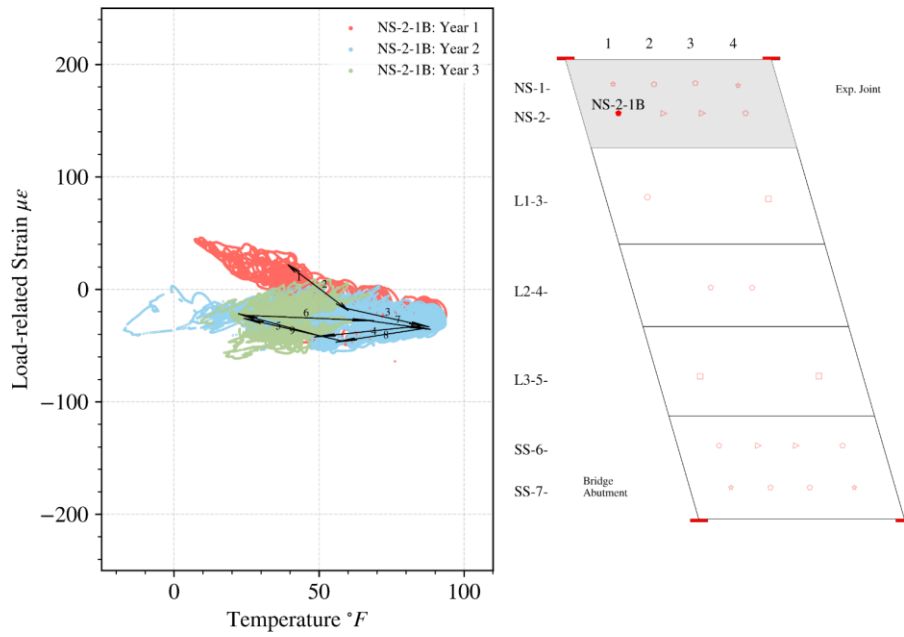
Figure 4.43 (b) Prospect Avenue, NS-2-1B
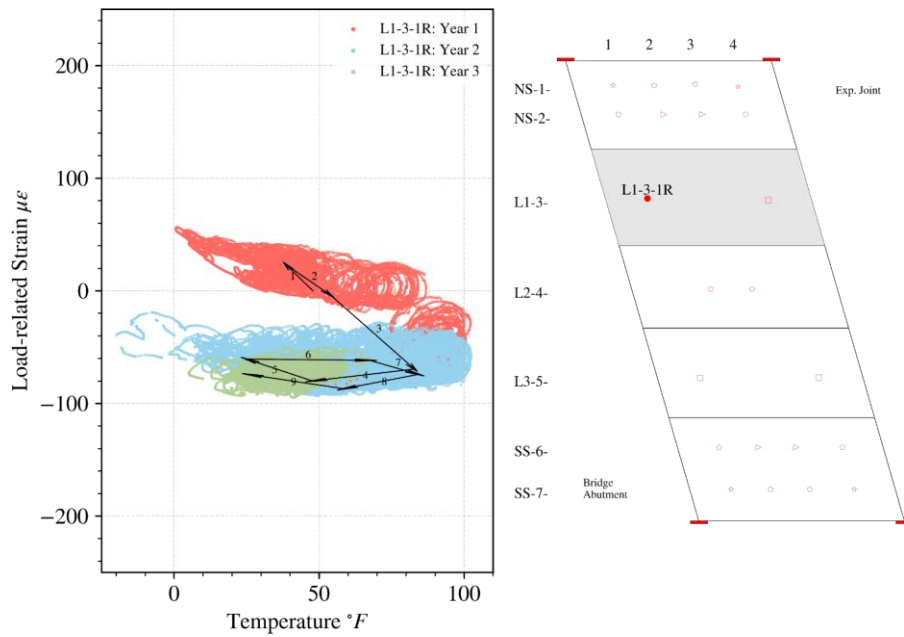
Figure 4.43 (c) Prospect Avenue, L1-3-1R

120
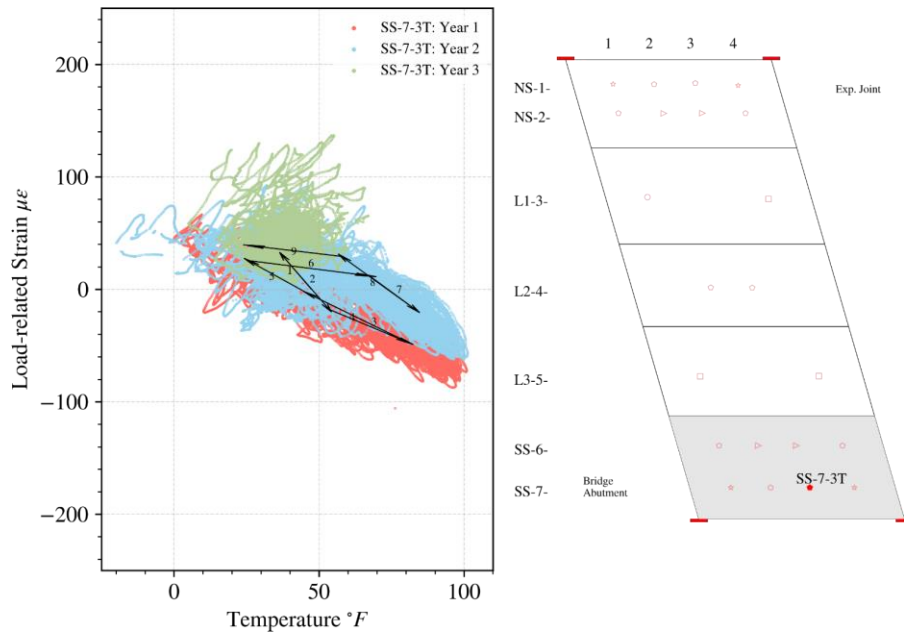
Figure 4.43 (d) Prospect Avenue, SS-7-3T
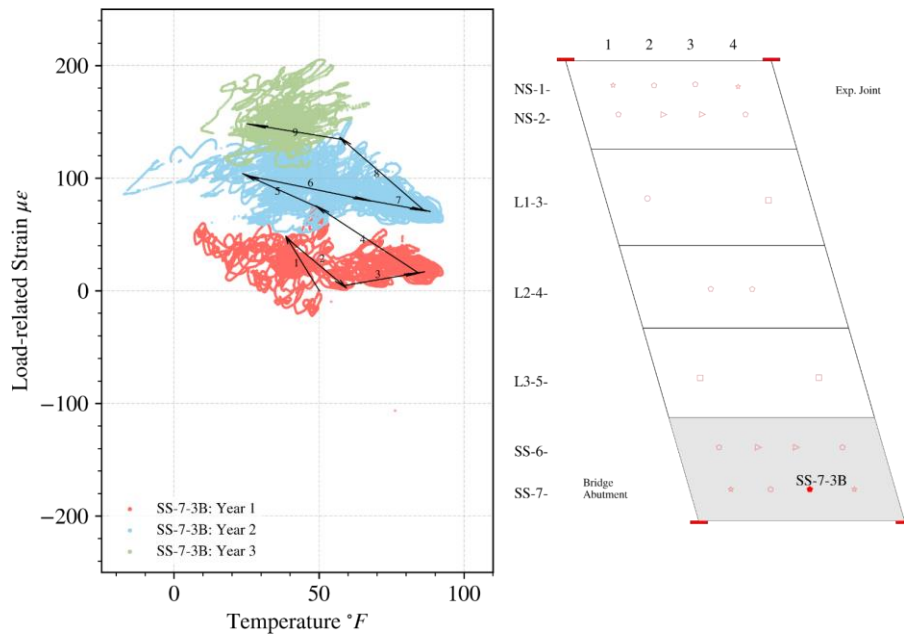
(e) Prospect Avenue, SS-7-3B

Figure 4.43 Examples of Group 3 strain behavior (Prospect Avenue): (a) NS-2-1T; (b) NS-2-1B; (c) L1-3-1R; (d) SS-7-3T; (e) SS-7-3B.

Figures 4.43 and 4.44 provide the distribution of gages of Group 3 for cast-in-place and precast slab, respectively. Most of the Group 3 gages in the cast-in-place slab are located close to the

121

abutment or mid-span. However, such a pattern is not observed in similar locations of the precast slab. Instead, two sections (North Shoulder and Lane 1) on the north side of the slab exhibit accumulated compression, whereas the rest of the sections have accumulated tensile strains, which is suggestive of global in-plane rotation of the slab due to the differential displacement of the bridge abutment. Also, note that the bridge at Prospect Avenue has two spans and is longer than the one at Arlington Heights Road.

It is also observed that gages in the same precast section, such as North Shoulder, Lane 2, and South Shoulder, have very similar strain behaviors. This is indicative of a uniform or symmetric distribution of restraints under the slab.
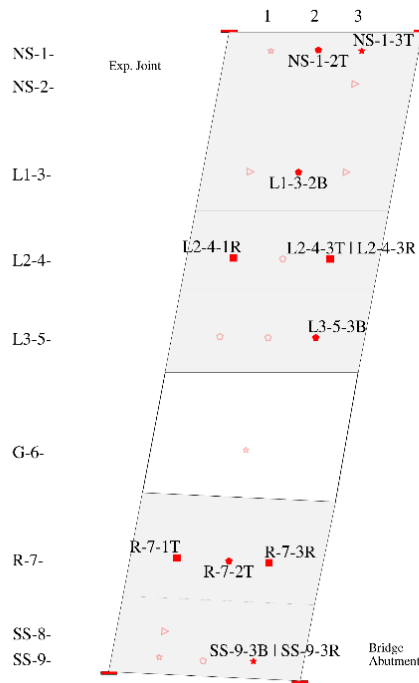
Figure 4.44 Gages with Group 3 strain behavior (Arlington Heights Road): accumulation in compression.

(a)   (b)
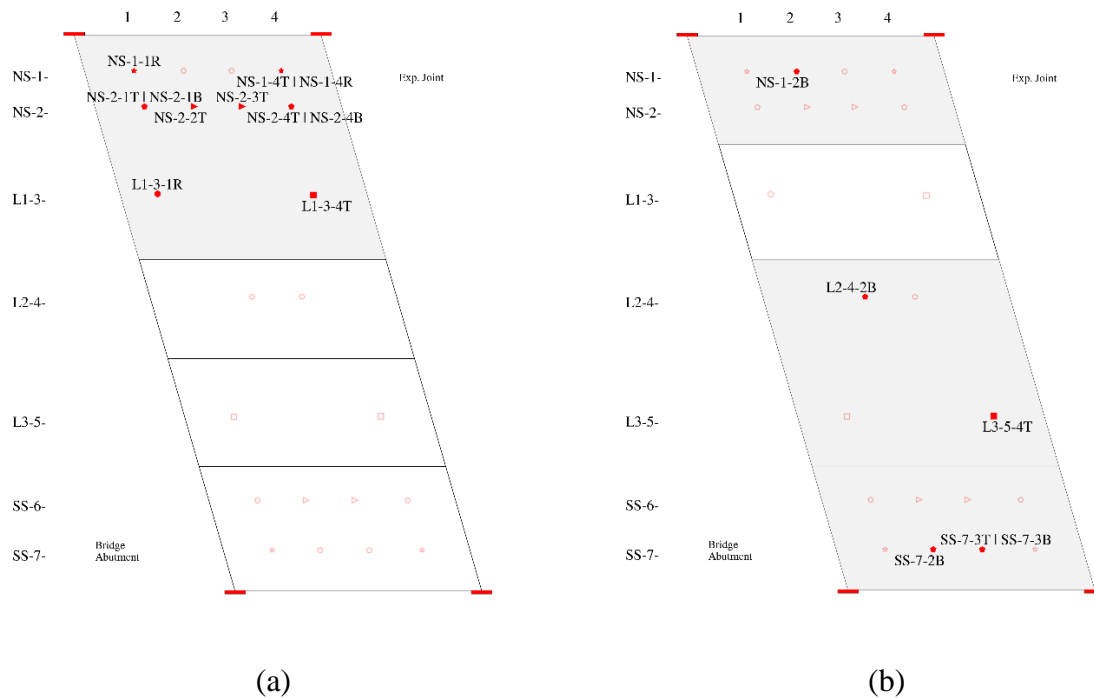
Figure 4.45 Gages with Group 3 strain behavior (Prospect Avenue): (a) accumulation in compression; (b) accumulation in tension.

Table 4.3 summarizes the number of gages in each group for both instrumented slabs.

Table 4.3 Count of gages in three groups of strain behavior.

	Arlington Heights Road (cast-in-place)		Prospect Avenue (precast)	
Group 1	21		10	
Group 2	Compressive	Tensile	Compressive	Tensile
	6	5	15	0
Group 3	Compressive	Tensile	Compressive	Tensile
	11	0	11	6

4.3.2.3 Strain Profiles of Approach Slabs on Hottest and Coldest Days

4.3.2.3.1   Cast-in-place Slab (Arlington Heights Road)

At the hottest time, the strain variation along the abutment end (Figures 4.46 and 4.47) generally follows the same trend as that observed in the actual strains, with the least compressive strain in the Ramp and the most compressive strain in Lane 2. In addition, as observed earlier, the strains in the North Shoulder were more compressive at the top reinforcement mat and more tensile at the bottom mat than in the South Shoulder. For the bottom layer, there is the maximum compressive

123

strain at Lane 3 and tensile strains in the North Shoulder. A significant increase in compressive strain occurred at *L2-4-3T* and *SS-9-3B* during year 2.
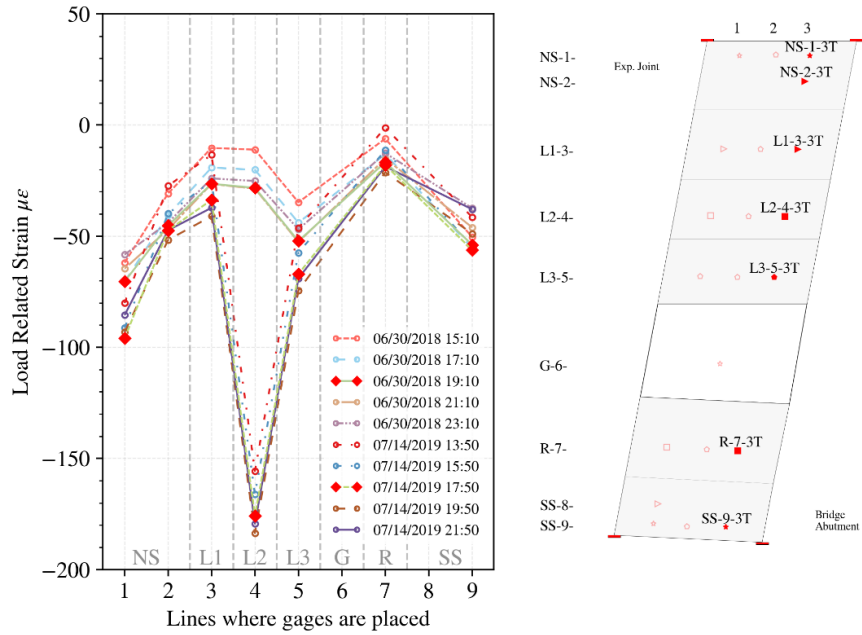
Figure 4.46 Top load-related strain changes along the bridge abutment end during the hottest time (Arlington Heights Road).
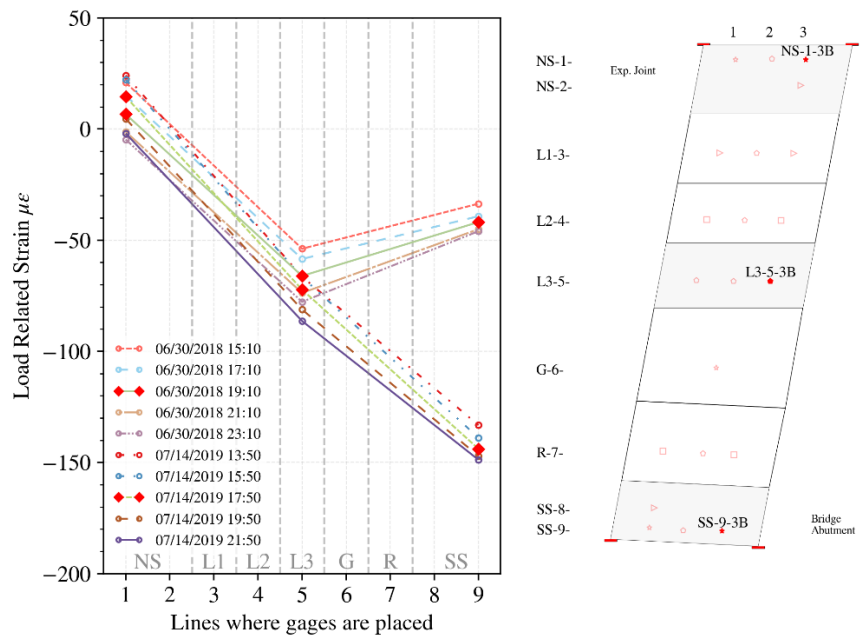
Figure 4.47 Bottom load-related strain changes along the bridge abutment end during the hottest time (Arlington Heights Road).

At the coldest time, the abutment side load-related strains for the cast-in-place approach slab are shown in Figures 4.48 and 4.49. The strains observed across the slab at the top mat of reinforcement are mainly constant, except for a significant increase in compressive strain in Lane 2. The strain at NS-2-3T did not change much at the two coldest times. Similar to the hottest time, there was no significant change in strain for *NS-1-3B,* whereas the load-related strain at L3-5-2B and SS-9-3B turned from tensile to compressive.
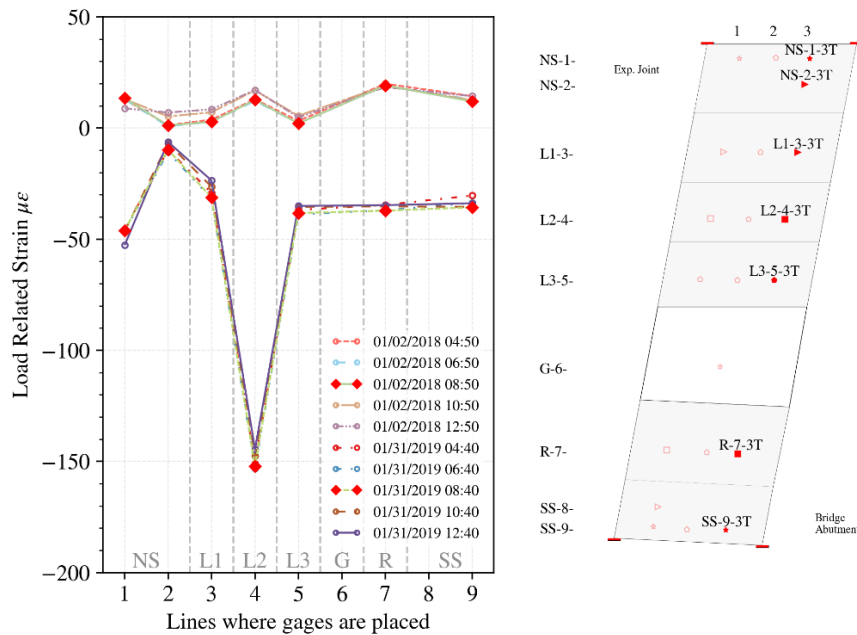
Figure 4.48 Top load-related strain changes along the bridge abutment end during the coldest time (Arlington Heights Road).
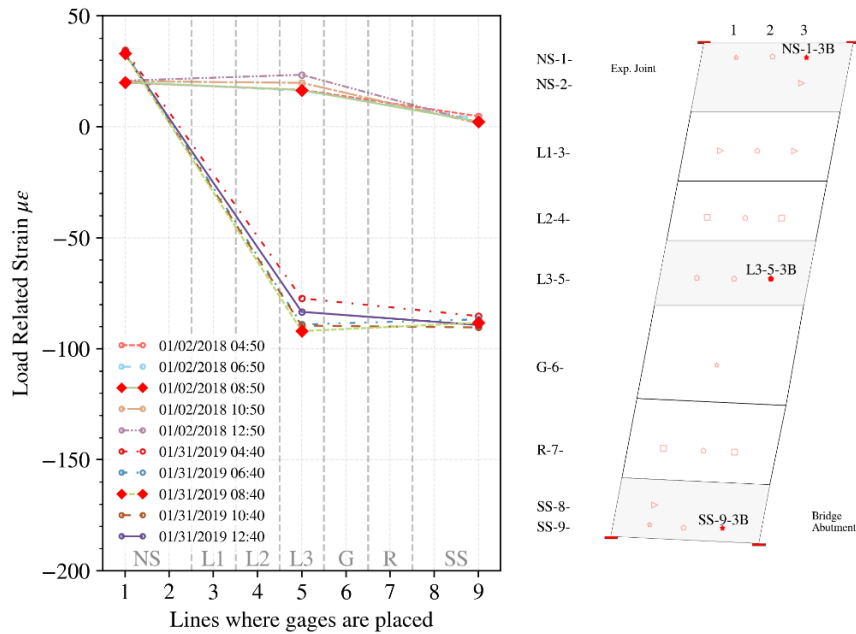
Figure 4.49 Bottom load-related strain changes along the bridge abutment end during the coldest time (Arlington Heights Road).

4.3.2.3.2 Precast Slab (Prospect Avenue)

The strain variations observed on the abutment end of the precast slab were similar to the actual strain, with a smaller variation before and after the hottest/coldest time. The strain changes at the hottest time are shown in Figures 4.50 and 4.51. In addition, the case of the coldest time is presented in Figures 4.52 and 4.53.
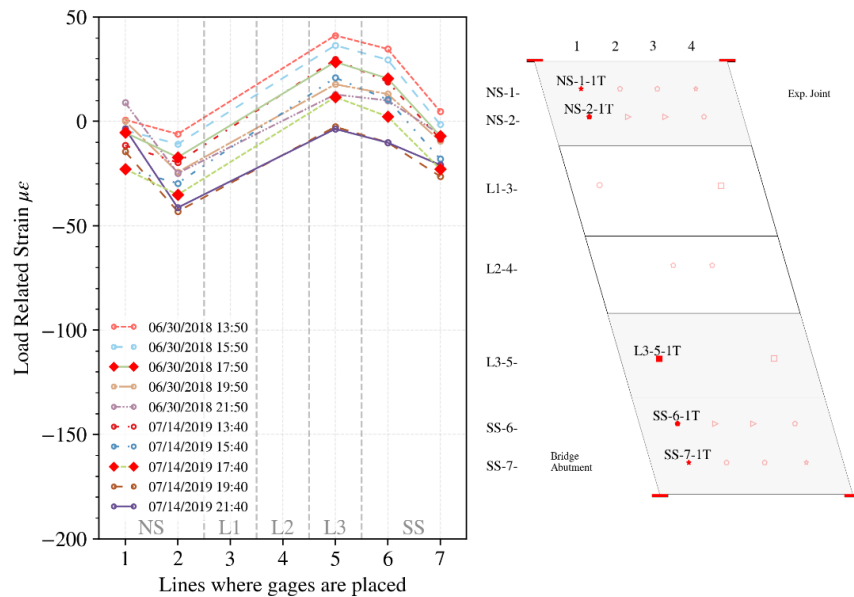
Figure 4.50 Top load-related strain changes along the bridge abutment end during the hottest time (Prospect Avenue).

126
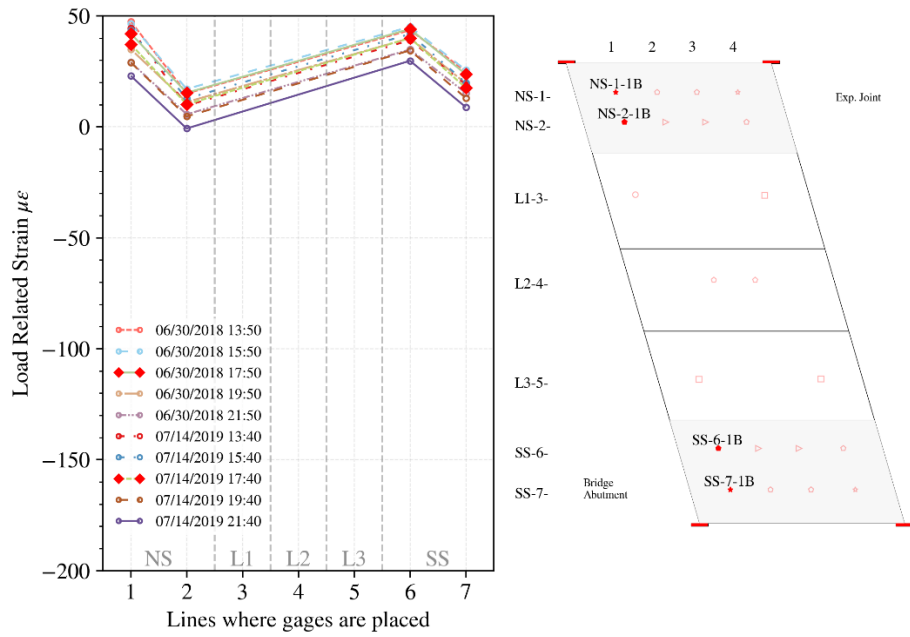
Figure 4.51 Bottom load-related strain changes along the bridge abutment end during the hottest time (Prospect Avenue).
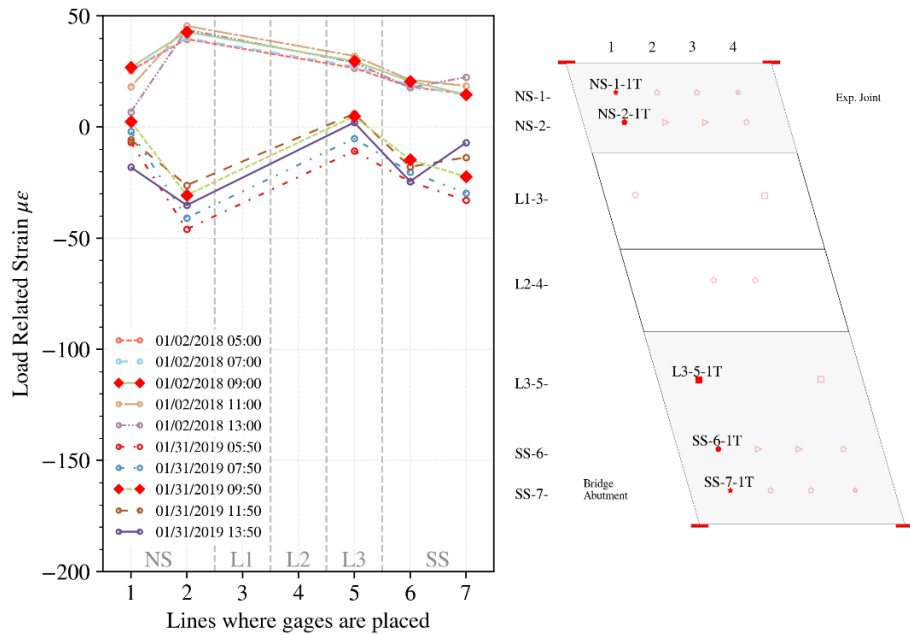
Figure 4.52 Top load-related strain changes along the bridge abutment end during the coldest time (Prospect Avenue).
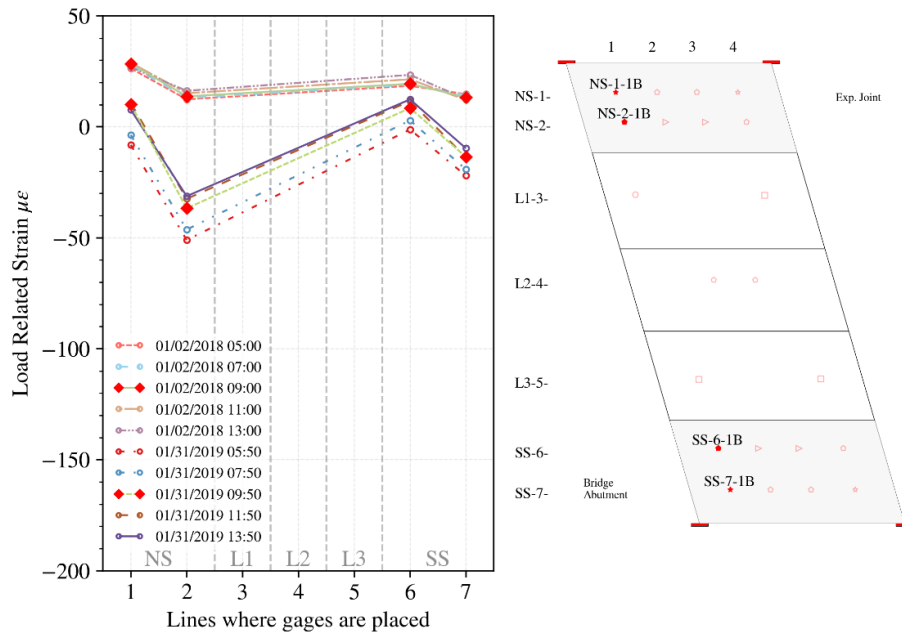
Figure 4.53 Bottom load-related strain changes along the bridge abutment end during the coldest time (Prospect Avenue).

4.4 Approach Slab Stresses

Cracking of approach slabs is the most common problem identified by the Illinois Tollway and confirmed more broadly through the agency survey reported above. For the field data, extreme-fiber stresses were estimated to better understand slab behavior and determine any potential for undesirable slab response.

4.4.1 Calculation of Approach Slab Extreme Fiber Stresses

The change in load-related stress can be estimated as the product of load-related strain and elastic modulus if elastic behavior is assumed and Poisson effects due to three-dimensional behavior are neglected. This approximation of normal stress in the direction of the measured strain is the only feasible approach since the full three-dimensional state of strain is not measured. Here, we use the change in load-related strain calculated in the previous section to calculate the approximate change of stress. Thus, the stress change shown hereafter represents the effects caused by live load and constraints on movement. To obtain the extreme fiber strains for the slabs, which can then be used to calculate extreme fiber stresses, the measurement locations that have both and top and bottom longitudinal sensors were used. The strains at the top and bottom are then extrapolated to the surface, assuming a linear variation of strains across the slab, as shown in Figure 4.54. For the schematic scenario shown in Figure 4.54, the top and bottom gages have strains of opposite signs, but there are also cases where the top and bottom gages have strains of the same sign.

128
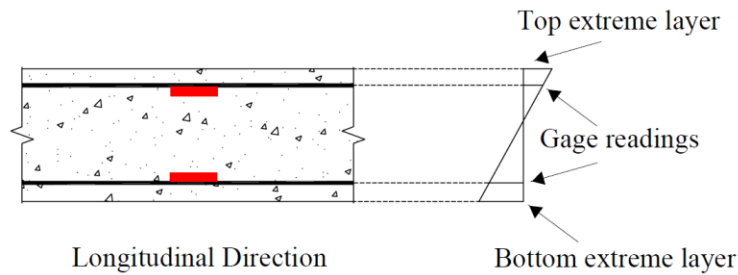
Figure 4.54 Schematic of stresses in slab section (longitudinal).

4.4.2 Extreme Fiber Stress Variation

Since the stresses are calculated using the load-related strains presented before, the stresses follow the same general trends as already discussed for the load-related strains.

The average modulus of rupture values obtained from 56-day plain concrete tests for the cast-in-place slab and sections of the precast slab are shown in Table 4.4.

Table 4.4 Average modulus of rupture (ksi).

Cast-in-place (Arlington Heights Road)	Precast (Prospect Avenue)				
	North Shoulder	Lane 1	Lane 2	Lane 3	South Shoulder
0.900	1.128	1.275	1.090	1.060	1.103

The variations of extreme fiber stresses for the cast-in-place slab are given in Figure 4.55. In the cast-in-place slab at Arlington Heights Road, the stresses observed in the sensors in certain sections (North Shoulder, Lane 2, Gore, Ramp, and South Shoulder) began to diverge in magnitude starting as early as October 2017. This phenomenon is most evident in the North Shoulder (Figure 4.55 (a)) where each location experiences different stress variations. Here, the variation of Lane 1 sensors is not presented since the sensor at L1-3-2B malfunctioned after the summer of 2018. The calculated extreme fiber stresses are compared with the estimated modulus of rupture (Table 3.2) from material characterization. As judged by this metric, only one gage, NS-1-2B, shows the potential risk of cracking since 2019, as indicated in Figure 4.56.

129
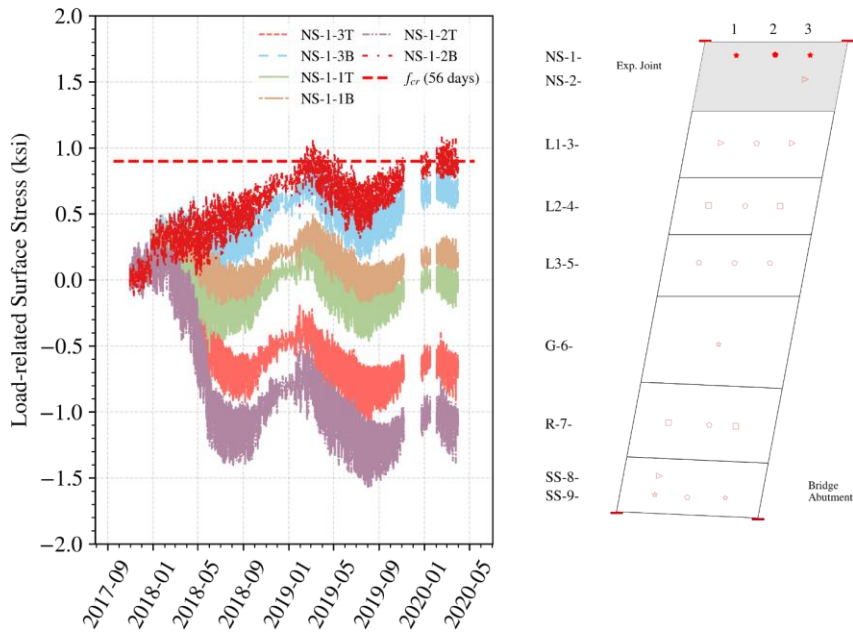
Figure 4.55 (a) Arlington Heights Road, North Shoulder
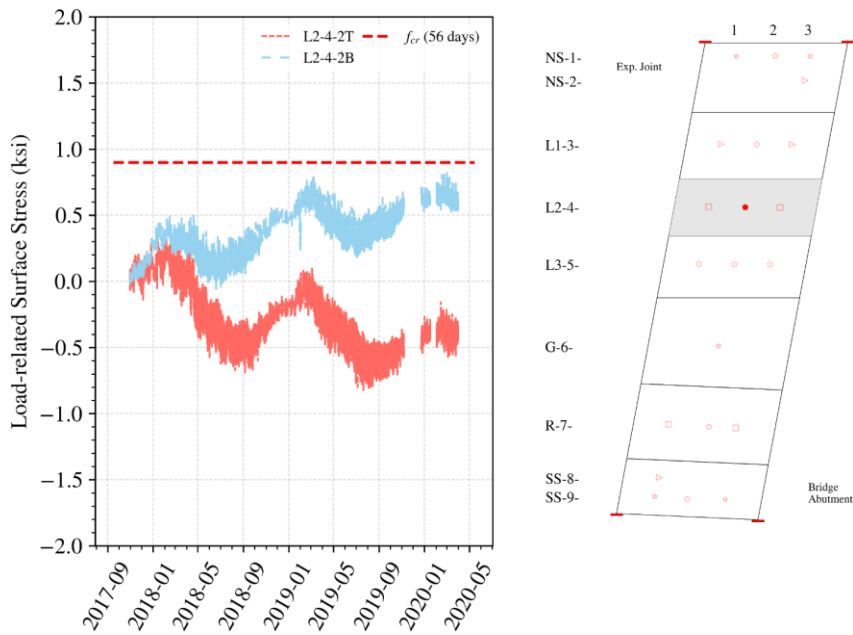
Figure 4.55 (b) Arlington Heights Road, Lane 2
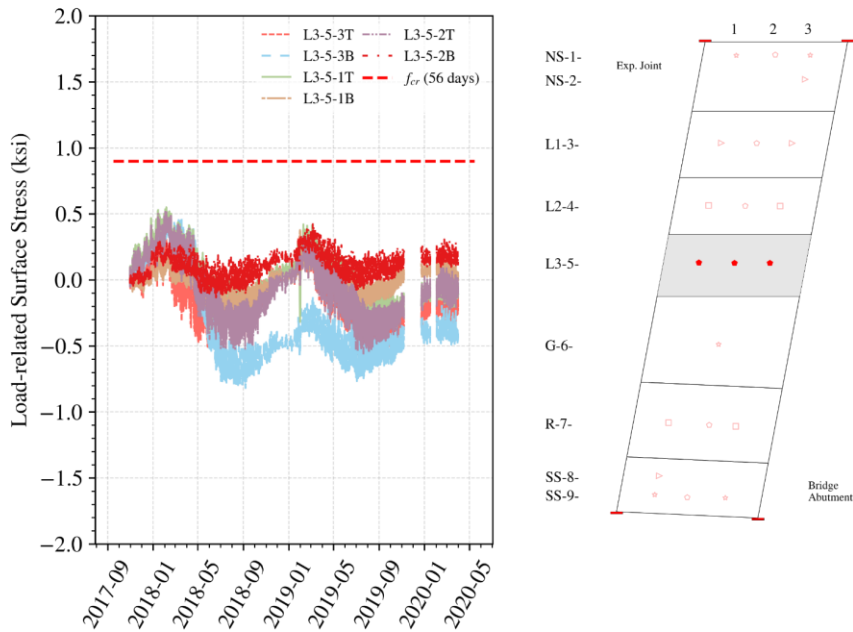
Figure 4.55 (c) Arlington Heights Road, Lane 3
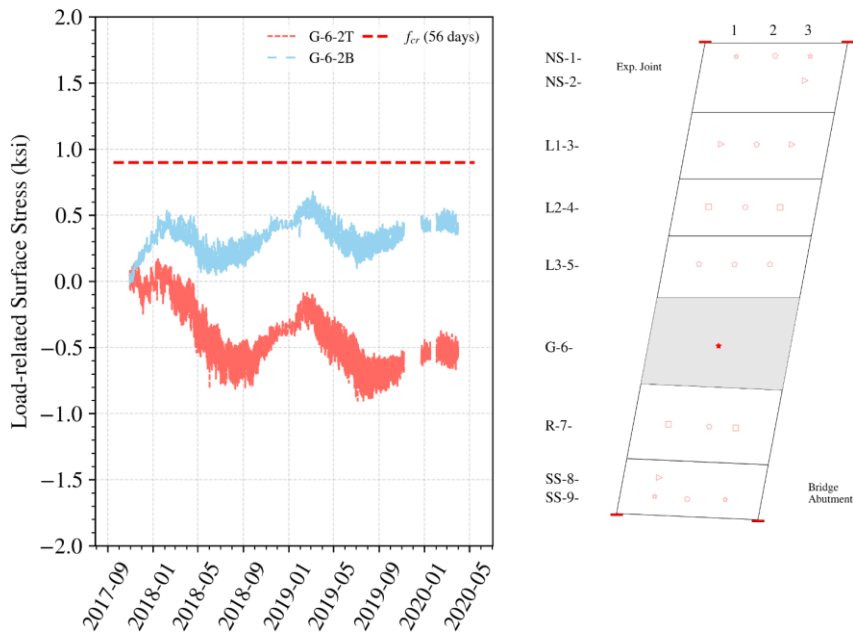

Figure 4.55 (d) Arlington Heights Road, Gore

131
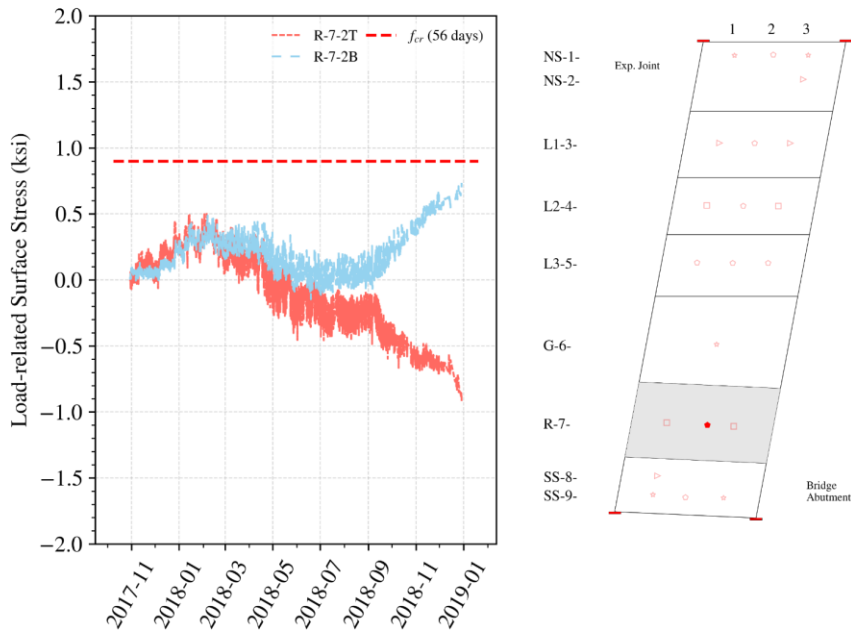
Figure 4.55 (e) Arlington Heights Road, Ramp
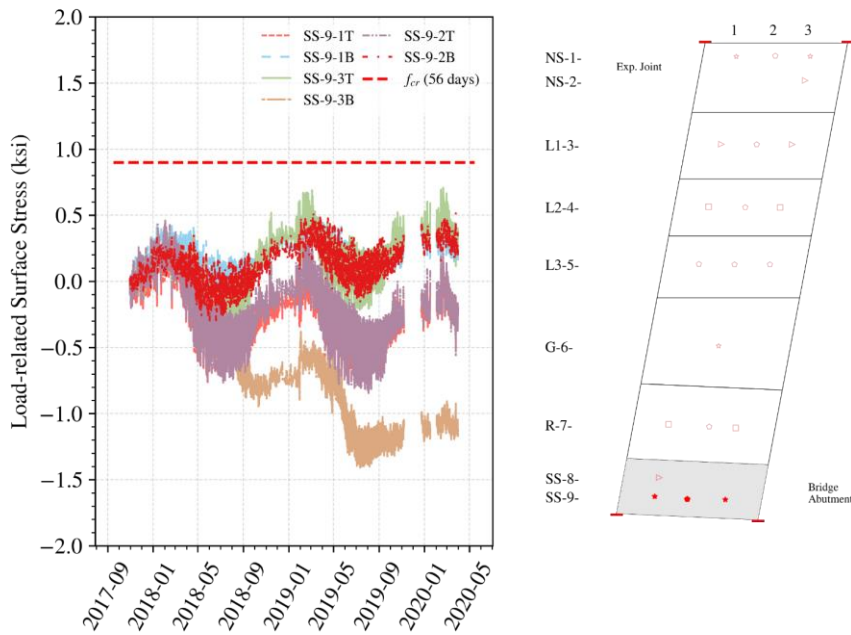
(f) Arlington Heights Road, South Shoulder

Figure 4.55 Load-related surface stresses (Arlington Heights Road): (a) North Shoulder; (b) Lane 2; (c) Lane 3; (d) Gore; (e) Ramp; (f) South Shoulder.
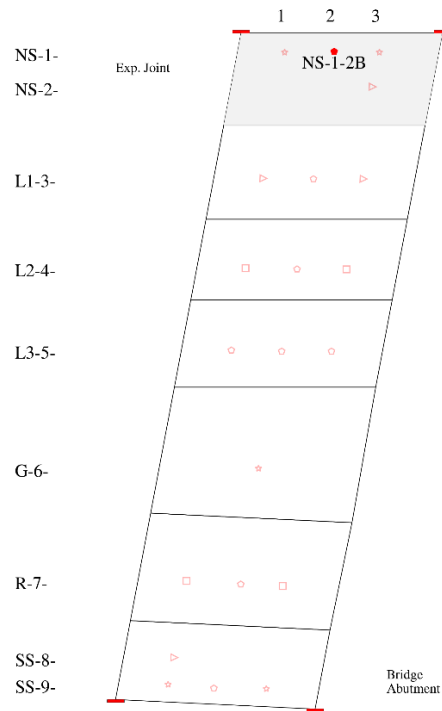
Figure 4.56 Locations with potential risk of cracking (Arlington Heights Road).

In the precast slab (Figure 4.57), the extreme fiber stresses were observed to diverge since spring 2018. The top surface location stresses were observed to get more and more compressive, while the bottom surface stresses were observed to get more tensile. The bottom slab surface at four gage locations, NS-1-2B, L2-4-2B, SS-7-2B, and SS-7-3B, are prone to cracking based on the calculations, as shown in Figure 4.58.
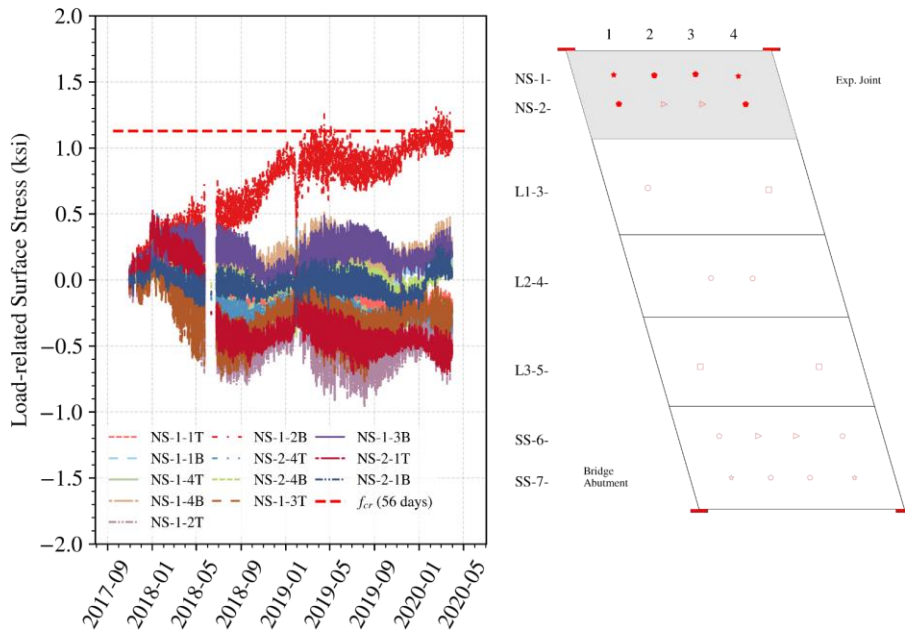
Figure 4.57 (a) Prospect Avenue, North Shoulder
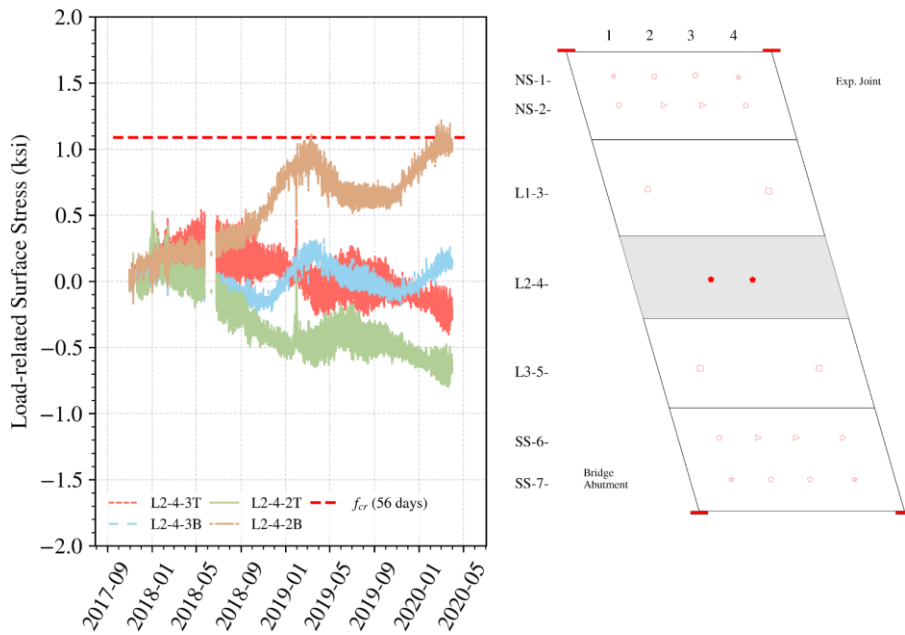
Figure 4.57 (b) Prospect Avenue, Lane 2
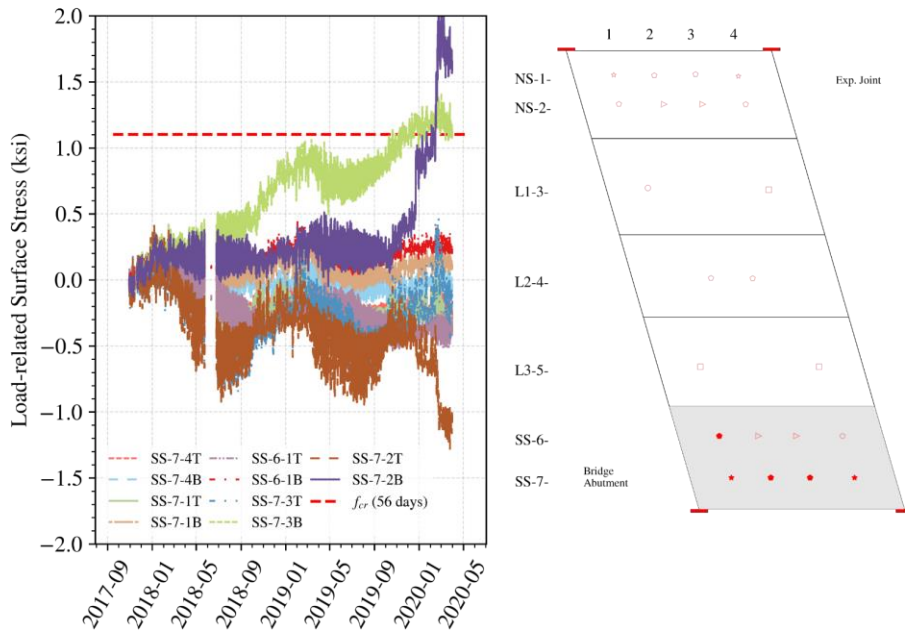
(c) Prospect Avenue, South Shoulder

Figure 4.57 Load-related surface stresses (Prospect Avenue): (a) North Shoulder; (b) Lane 2; (c) South Shoulder.
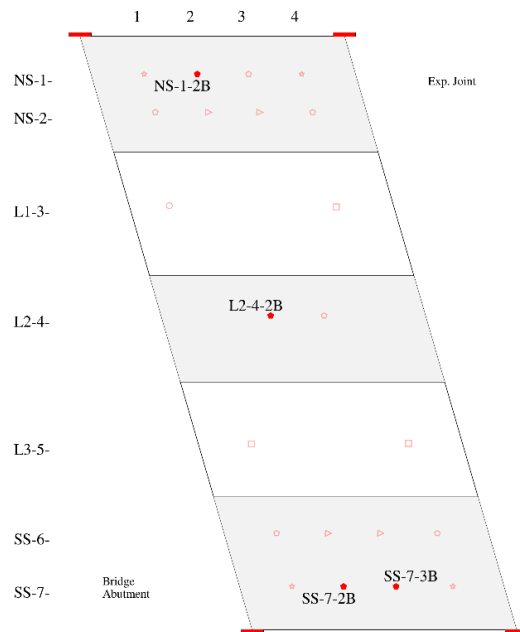
Figure 4.58 Locations with potential risk of cracking (Prospect Avenue).

4.5   Approach Slab Displacements

Global longitudinal movement of the approach slab was studied using four displacement transducers installed at the corners of both approach slabs. The displacement transducers recorded relative displacements – between the approach slabs and adjacent components. The displacement transducers were typically installed horizontally near the mid-depth of the approach slab section. The displacement recorded for each of the transducers shows that the slab movement depends primarily on the change in temperature, with an increase in temperature leading to the closing of the gap between the two components, and vice versa. This was true for both the cast-in-place and precast slabs, as shown in Figure 4.59. However, the displacement transducer readings for the Northwest corner at the cast-in-place slab do not follow this observation. This is a result of a different installation method used for this sensor (as discussed in Chapter 3). The displacements were observed to be close to zero near the abutment for both of the bridges, while the significant movement was observed at the expansion joint end, as expected. The displacement of the slab at the expansion joint was observed to be marginally higher at the precast slab than at the cast-in-place slab, which is partially attributed to the larger bridge span for the precast slab.
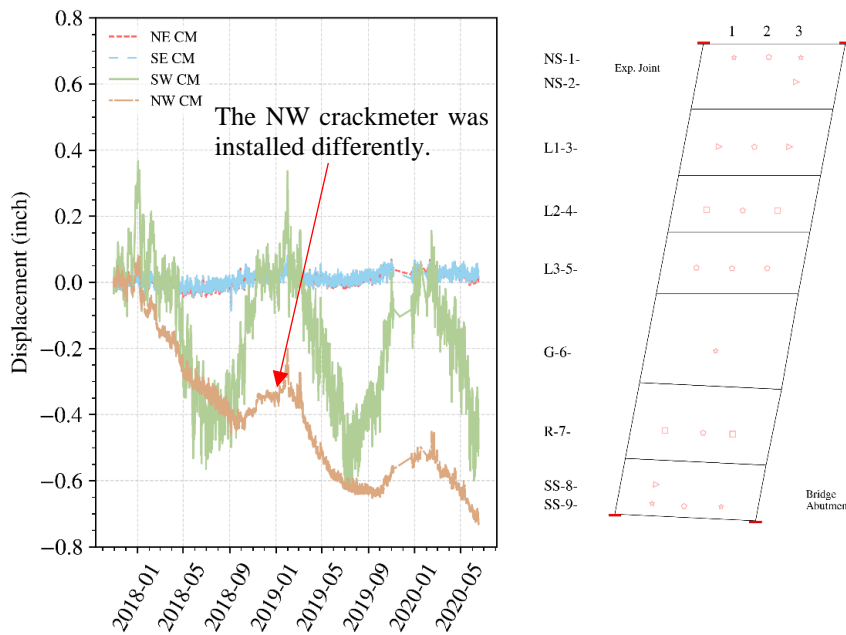
(a)
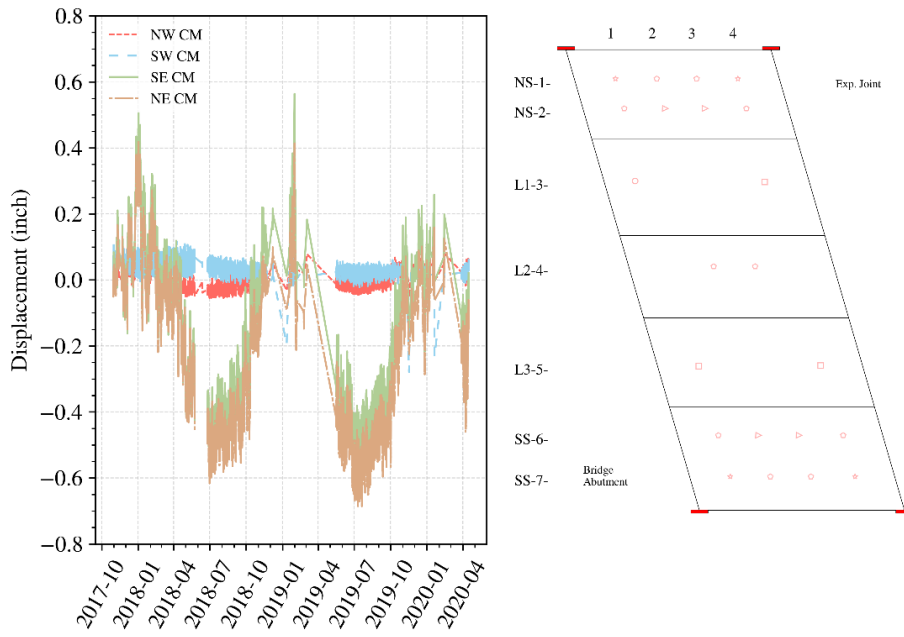
(b)

Figure 4.59 Displacements recorded at: (a) cast-in-place slab; (b) precast slab.

To gain a better understanding of the displacements of the approach slabs, the displacements were plotted against temperature. Figure 4.60 shows the variation of displacements at the four corners of the cast-in-place slab. As expected, all the displacements vary approximately linearly with temperature, except at the Northwest corner of the cast-in-place slab, where the displacement transducer is mounted between the approach slab and pile bent. The displacements at the abutment ends are close to zero, as the approach slab is connected to the abutment using rebar dowels. At the expansion joint, the Southwest corner experienced a total movement of about one inch, with 1 ℉ change in temperature leading to about 0.01-inch change in displacement.
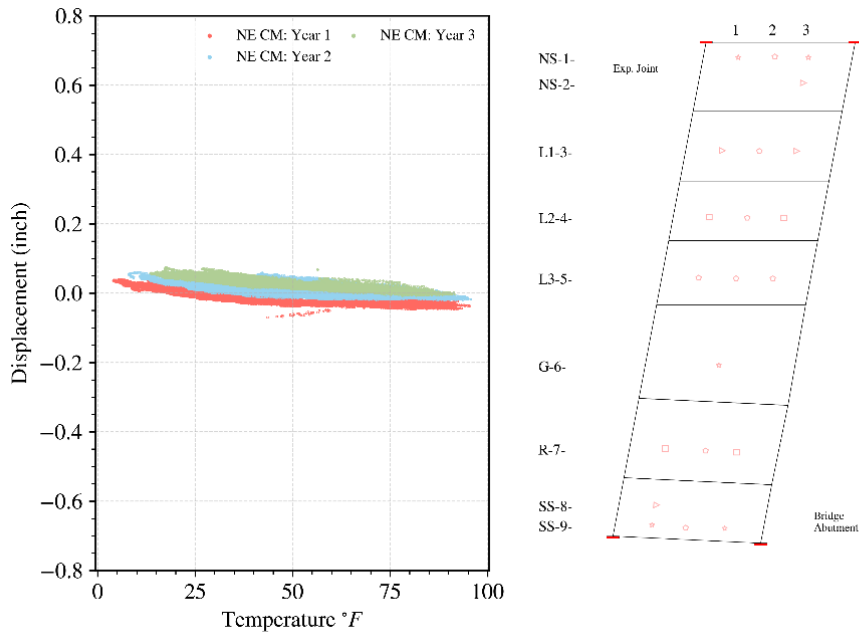
Figure 4.60 (a) Arlington Heights, Northeast Corner
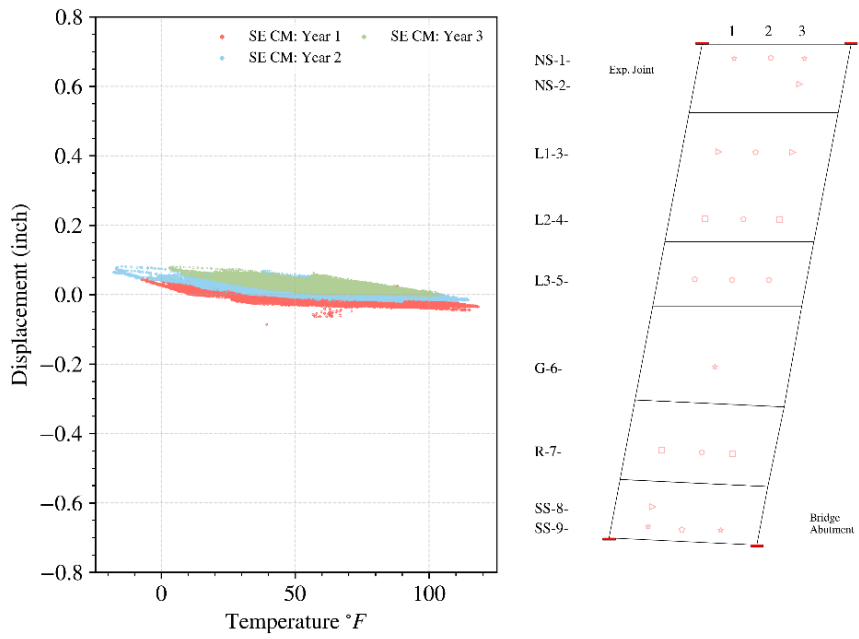
Figure 4.60 (b) Arlington Heights, Southeast Corner
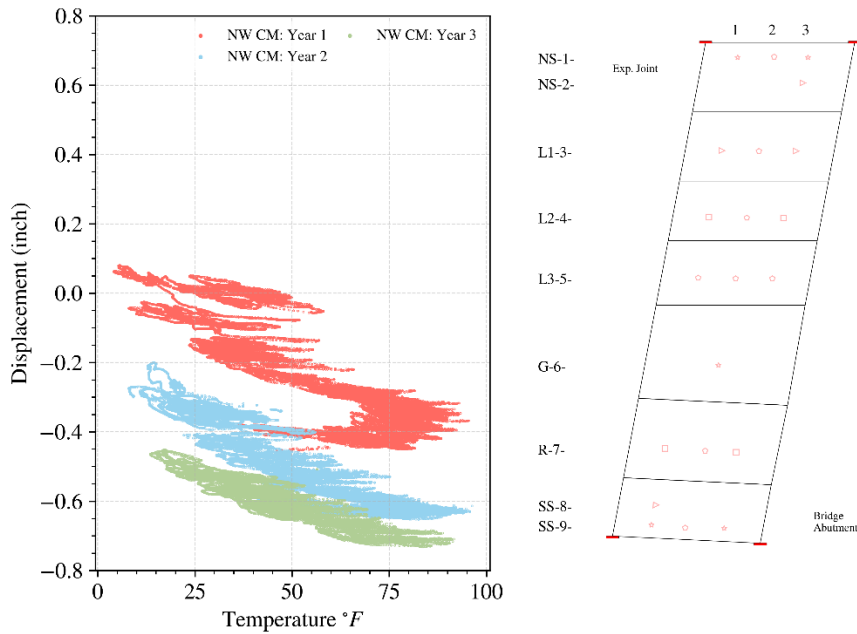
Figure 4.60 (c) Arlington Heights, Northwest Corner
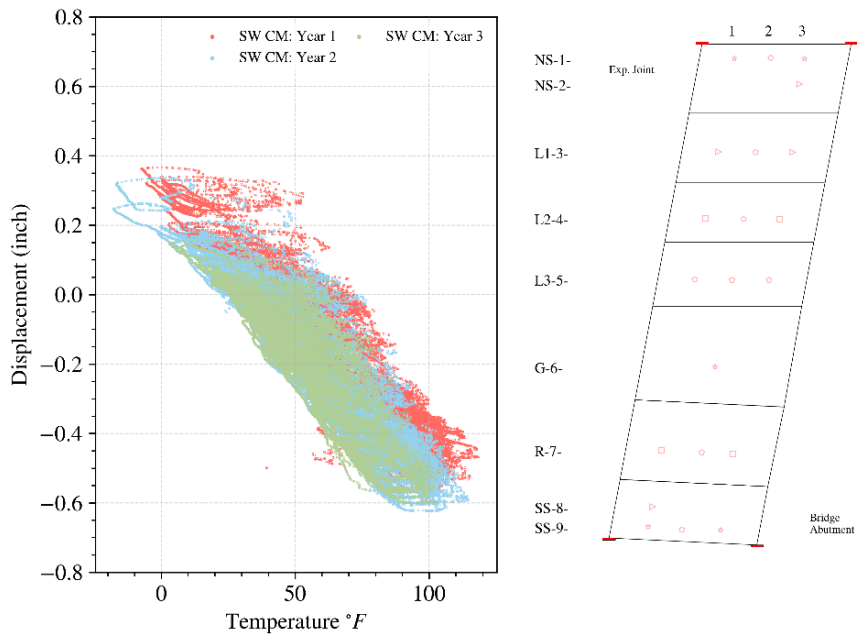
(d) Arlington Heights Road, Southwest Corner

Figure 4.60 Displacement transducer displacements versus temperature (Arlington Heights Road) at (a) NE; (b) SE; (c) NW; (d) SW corner of the slab.

For the precast slab, the displacements were also observed to follow similar trends, with a roughly linear relationship between temperature and displacements. The displacements at the abutment end

139

(NW and SW corners) show a total movement of about 0.1 inches, while the expansion joint moves more than 1 inch during the same time. There are differences between the displacements on the north and south side. The relative displacement between the bridge abutment and the approach slab on the north side is more sensitive to the temperature (larger slope) and has a mean closer to zero compared to the one on the south side. Similarly, the opening between the approach slab and the transition slab on the north side is always smaller than that on the south side. This observation may suggest that the abutment on the north side tends to push more than it does on the south side, which corresponds to the result that North Shoulder and Lane 1 have more accumulated compressive strains. In other words, there appears to be moderate clockwise in-plane rotation in the entire precast approach slab. The variation of displacement observed for the precast slab is shown in Figure 4.61.
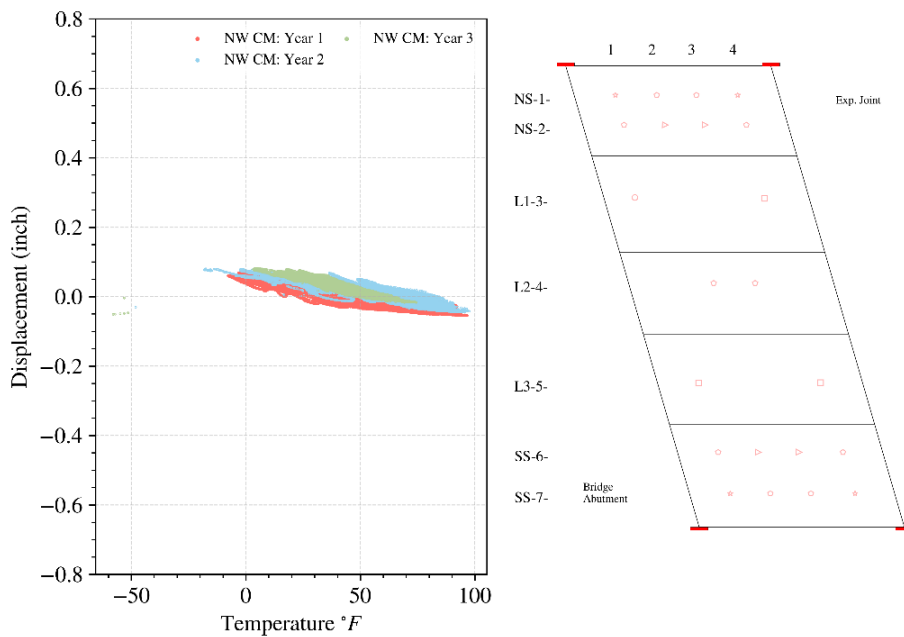
Figure 4.61 (a) Prospect Avenue, Northwest Corner

140
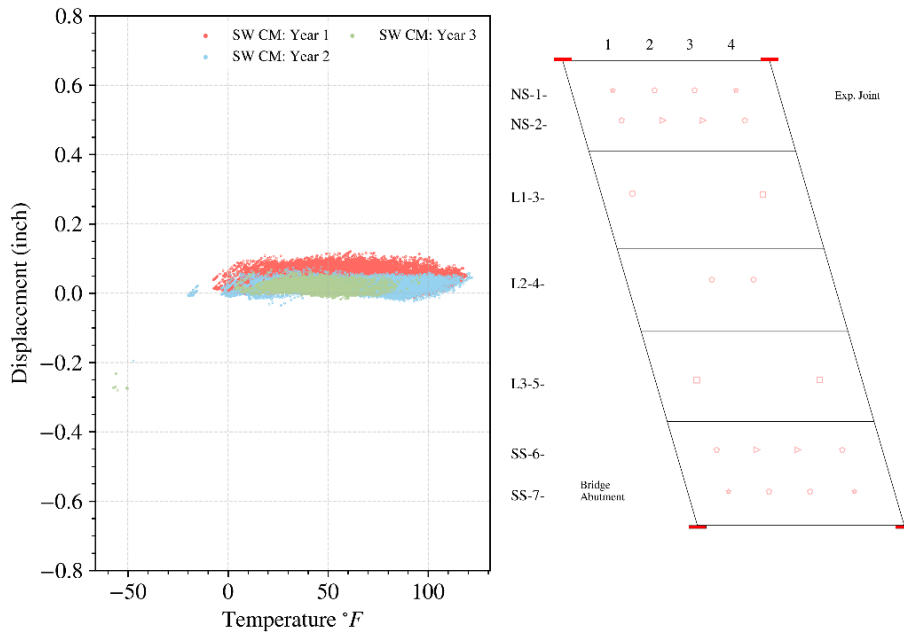
Figure 4.61 (b) Prospect Avenue, Southwest Corner
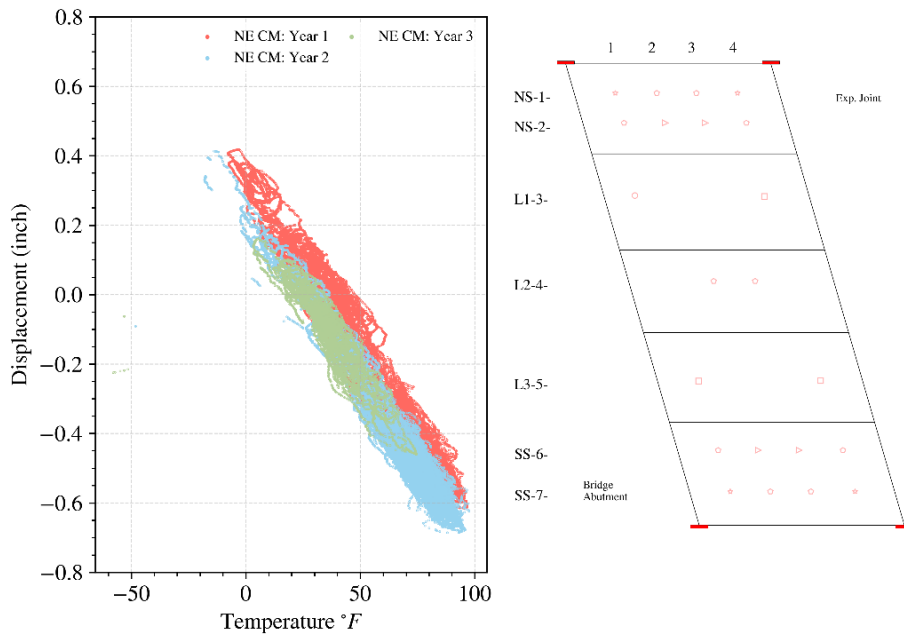
Figure 4.61 (c) Prospect Avenue, Northeast Corner
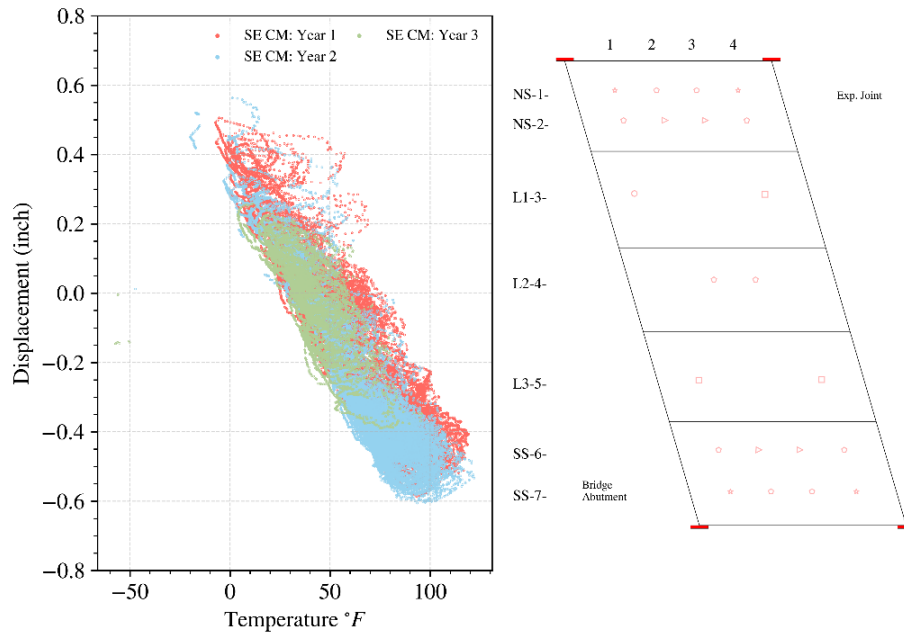
(d) Prospect Avenue, Southeast Corner

Figure 4.61 Displacement transducer displacements versus temperature (Prospect Avenue) at (a) NW; (b) SW; (c) NE; (d) SE corner of the slab.

4.6 Observations from Field Visits

Field visits were made by the University of Illinois research team in order to maintain the data acquisition systems as well as to conduct inspections on the instrumented approach slabs. The dates of the field visits, excluding static truck loading testing, include 03/09/2018, 06/01/2018, 06/25/2018, 01/17/2019, 02/07/2019, 05/17/2019, 05/31/2019, 06/14/2019, 11/22/2019, 12/23/2019, 01/19/2020, and 02/02/2020.

Only one very small crack was first observed on 03/09/2018 at the entrance side of the ramp at Arlington Heights Road, the cast-in-place slab, as shown in Figure 4.62. There were no other cracks found by visual inspection from the shoulders during the visits listed above.

Figure 4.62 Crack found at the entrance of ramp (Arlington Heights Road) on 03/09/2018.

More recent field visits found that voids developed at least near the north or south boundary of both slabs, as shown in Figure 4.65. The condition of slab bottom surface still remains unknown.
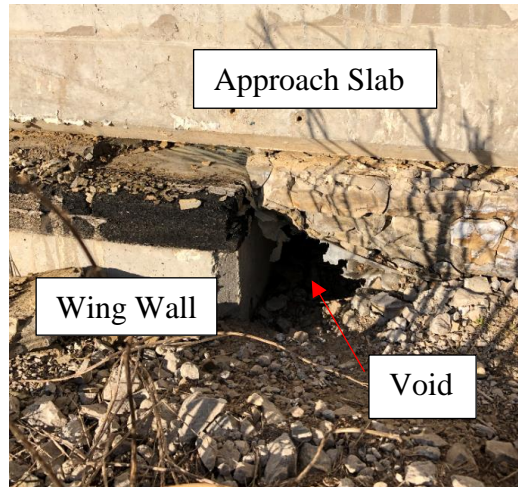
(a)   (b)

Figure 4.63 Inspected voids at: (a) northwest corner of the cast-in-place slab (Arlington Heights Road) as of 12/23/2019; (b) south side of the precast slab (Prospect Avenue) near the midspan as of 11/22/2019.

143

4.7   Summary of Field Observations and Measurements

The major findings from the data processing are summarized as follows:

- Two monitored approach slabs experience very similar weather and traffic conditions.
- Field data suggest that top gage temperatures tend to fluctuate more than the bottom gage temperatures as gages at the top reinforcement mat are more sensitive to the ambient environmental changes. In general, top gage temperatures are higher than the bottom ones in the afternoon of a day.
- Actual strain is defined as the strain observed in the slab due to all effects, including slab dead load, live load, thermal load, bridge abutment displacement, and restraints under the slab. Load-related strain is defined as the stress-causing strain observed due to live load, thermal load, abutment displacement, and restraints under the slab. It is calculated by subtracting the strains caused by the thermal expansion of concrete from the actual strains calculated earlier.
- The actual strain for the cast-in-place slab at Arlington Heights Road ranged from about 400 $\mu\varepsilon$ in compression to 400 $\mu\varepsilon$ in tension. For the precast slab at Prospect Avenue, the actual strain ranged between 400 $\mu\varepsilon$ in compression to 350 $\mu\varepsilon$ in tension.
- The load-related strains for the cast-in-place slab at Arlington Heights Road ranged from about 200 $\mu\varepsilon$ in compression to 200 $\mu\varepsilon$ in tension, while for the precast slab, the range was 200 $\mu\varepsilon$ in compression to 240 $\mu\varepsilon$ in tension.
- The actual strain change tends to be tensile during periods with temperatures higher than reference temperature (summer season) and compressive during the period with temperature lower than the reference temperature. However, tensile load-related strains are observed during the time when the temperature is lower than the reference and compressive load-related strain are observed during the time when temperature is higher than the reference at most of the gages in the cast-in-place slab and some gages in the precast slab.
- The load-related strain at twenty-one of forty-three gages at the cast-in-place slab as well as ten out of forty-two gages at the precast slab exhibit rough linear trends versus temperature and strong consistency among year 1, 2, and 3. No particular pattern of gage locations was found in either instrumented slab as these gages are scattered through the whole slabs.
- Eleven gages at the cast-in-place slab and fifteen gages at the precast slab maintain a linear relation to the temperature for each year, and there are gradual accumulations in compression for the cast-in-place slab gages. Both compression and tension accumulations occur for the precast gages. For the cast-in-place slab, it is found that top longitudinal gages at the midspan tend to accumulate compressive load-related strains, as well as bottom longitudinal gages at the midspan are more likely to gain accumulation in tensile load-related strains, indicating there was an increase in positive bending at the cast-in-place slab.
- Eleven gages at the cast-in-place slab and seventeen gages at the precast slab experience a significant change in load-related strain magnitude at some time and keeps approximately linear with respect to the temperature otherwise; there are large changes in strain within a small range of temperature. For the cast-in-place slab, only a significant increase in

compression is observed, and it appears more frequently at the gages close to the abutment side. For the precast slab, a noticeable increase in compression is widely found in the two sections on the north side (North Shoulder and Lane 1), and a large increase in tension occurred at the remaining three sections, suggesting the possibility of clockwise global rotation of the whole approach slab.

- The behavior of the slab under the highest and lowest temperature during the first 2 years appears to be similar, with a higher magnitude (tensile) load-related strain observed during the lowest temperature.
- Load-related strain changes were used to calculate the stress changes by assuming the slabs to be linear elastic. The stresses thus calculated were extrapolated to the surface to get an estimate of the extreme layer stress on the slab. By comparing the estimated modulus of rupture, several bottom gage locations at both instrumented slabs are found to have the potential risk of cracking.
- The variation of extreme layer stress with time shows that the stress is uniform in each lane of the slab for the initial period, but the stress diverges as the slab experiences more temperature variation cycles.
- The relative movement of the slab with respect to the abutment and transition slab was recorded using displacement transducers at four corners of each slab. The movements observed were as expected, with about 1 inch of movement at the transition slab end (due to the expansion joint) and about 0.1 inch at the abutment end (since the slab and abutment are connected using dowel bars). The opening between the abutment and the approach slab, as well as the opening between the approach slab and the transition slab, are always smaller on the north side than on the south side at the precast slab, indicating that there may be moderate clockwise in-plane rotations at the precast slab.

5 Finite Element Analysis for Instrumented Slabs

5.1 General Strategy

5.1.1 Analysis Tool

To simulate and analyze the behavior of bridge approach slabs, finite element analyses (FEA) were carried out in Abaqus 2017 (Dassault Systems 2017), which allows for user-defined live loads and temperature fields to be implemented in the numerical models.

5.1.2 Modeling of Slab

Planar shell elements S8R in Abaqus (Dassault Systems 2017) are used to model the approach slabs. The S8R element has 8 nodes with reduced integration points, enabling second-order interpolation. Hence, the S8R element is sufficient to capture the flexural behavior of the approach slab and possible transverse shear deformations.

The geometry of the numerical models follows the corresponding bridge drawings. For the cast-in-place instrumented approach slab at Arlington Heights Road, the slab is modeled as a whole part, as shown in Figure 5.1 (a). The model for the precast approach slab at Prospect Avenue consists of five slab parts, each representing one actual precast slab section, as shown in Figure 5.1 (b).

(a)   (b)
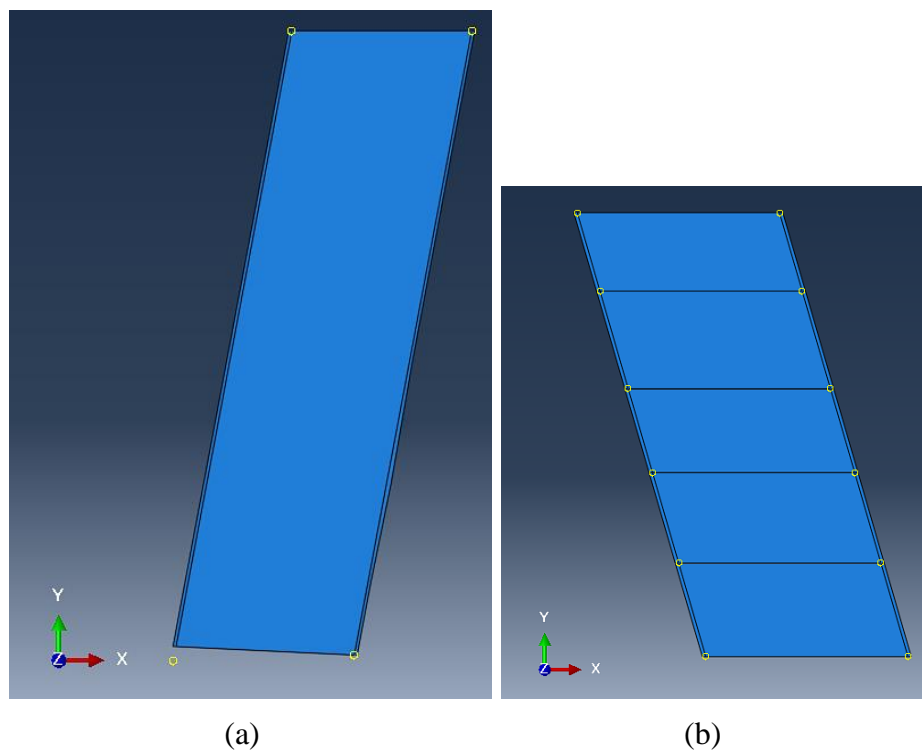
Figure 5.1 Plan view of numerical models for (a) cast-in-place slab at Arlington Heights Road, (b) precast slab at Prospect Avenue.

146

Between the sections of the precast approach slab, diagonal dowel bars shown in Figure 5.2 are placed to connect the adjacent sections. The dowel bars limit the relative movement in the three translational degrees of freedom. Hence, tie constraints in Abaqus (Dassault Systems 2017) are used to incorporate the movement restraint between the adjacent precast slab sections, leading to no relative translation between the slab sections.

GROUT & SEAL JOINT
PER IDOT STANDARD
SPECIFICATION 420.12)

DETAIL E SHEET 3
OF THIS SERIES

DRILLED HOLE FOR
INSERTION OF NO. 7
TIE BARS

40° +/- 5°

PRECAST SLAB

1'-4"

8"

8"

LONGITUDINAL JOINT

SECTION C-C
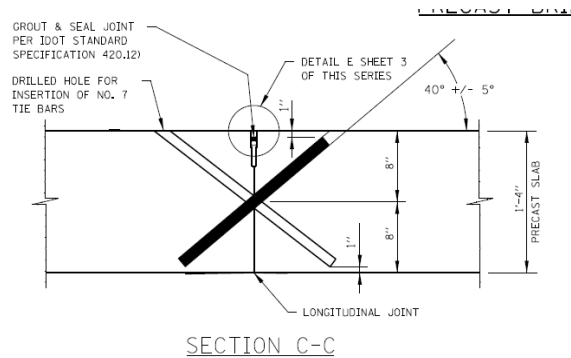
Figure 5.2 Precast slab dowel bars at the longitudinal joint.

The materials of the slab, including the concrete and steel, are assumed to be elastic and isotropic as serviceability is the primary focus of the study. The Poisson's ratio for the concrete is defined as 0.15. The concrete modulus of elasticity values is defined based on the 28-day compressive strength or modulus of elasticity test data, as shown in Table 5.1. The modulus of elasticity values for the precast sections was obtained directly from the samples made during the concrete pour. For the cast-in-place approach slab, since only the compressive strength test data were available, the modulus of elasticity is computed based on the equation recommended by AASHTO for estimating the modulus of elasticity of normal weight concrete:

$$E_c = 1860\sqrt{f_c'}$$

Where f_c' is compressive strength of the concrete sample (in ksi) and E_c is the modulus of elasticity (ksi).

Table 5.1 Concrete properties for both instrumented slabs.

Approach Slab		f_c' (ksi)	E_c (ksi)
Arlington Heights Road		6.724	4823
Prospect Avenue	North Shoulder	7.641	5100
	Lane 1	7.548	5275
	Lane 2	7.671	5350
	Lane 3	7.773	5375
	South Shoulder	7.942	5275

The reinforcing steel modulus of elasticity is assumed to be 29,000 ksi, and Poisson's ratio is taken as 0.3. Table 5.2 summarizes the reinforcement mats for both instrumented approach slabs.

Table 5.2 Reinforcement of the instrumented approach slabs.

Slab	Arlington Heights Road	Prospect Avenue
Top Longitudinal Mat	#5 @ 12"	#5 @ 12"
Top Transverse Mat	#4 @ 15"	#5 @ 12"
Bottom Transverse Mat	#6 @ 9"	#5 @ 6"
Bottom Longitudinal Mat	#9 @ 4"	#9 @ 4"
Top Concrete Cover	3.5"	3.5"
Bottom Concrete Cover	3"	2"

5.1.3 Boundary Conditions

The approach slabs are typically supported by the abutment and pile bent at the two ends. At the abutment-approach slab interface, there are vertical (or inclined) dowel bars connecting the abutment and the approach slab, as shown in Figure 5.3 (a) for cast-in-place slabs and (b) for precast slabs. At the approach slab-transition slab interface, there is an expansion joint for IABs. The approach slabs rest on the pile bent, and there are friction reduction measures at the interface such as elastomeric sheets and polyethylene sheets, as shown in Figure 5.4 (a) for cast-in-place slabs and (b) for precast slabs. Although there can be wingwalls in the longitudinal direction from the abutment, the approach slabs are not typically supported vertically by the wingwalls since there is a 2" preformed joint filler that does not transmit significant forces, as shown in Figure 5.5 (a) for cast-in-place slabs and (b) for precast slabs.

(a)   (b)
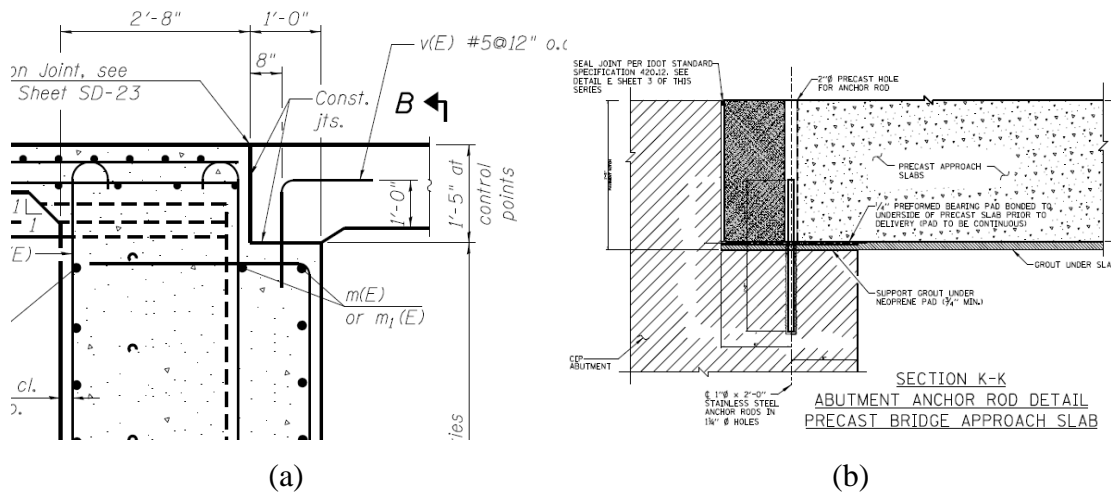
Figure 5.3 Details of dowel bars at the abutment-approach slab interface: (a) cast-in-place, (b) precast.

148

(a)   (b)
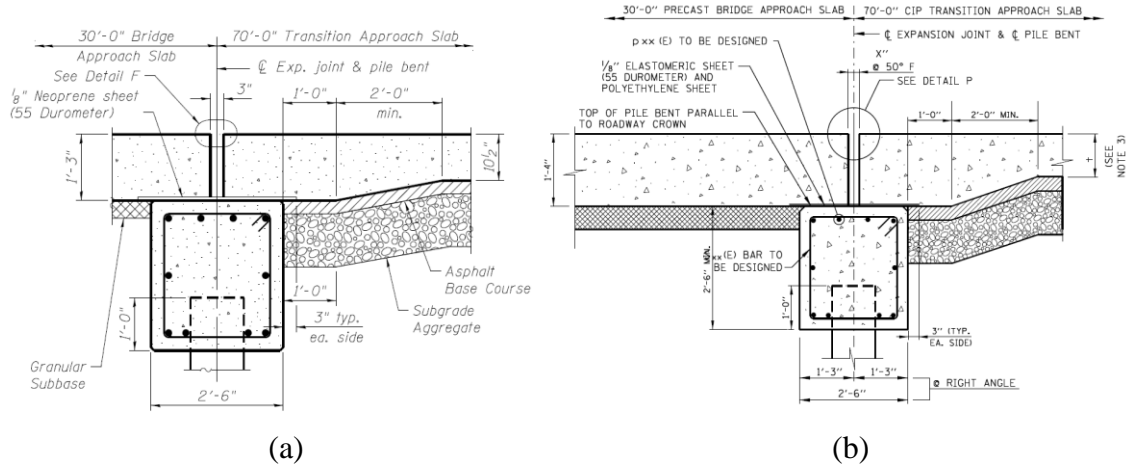
Figure 5.4 Details of the approach slab-transition slab interface: (a) cast-in-place, (b) precast.

(a)   (b)
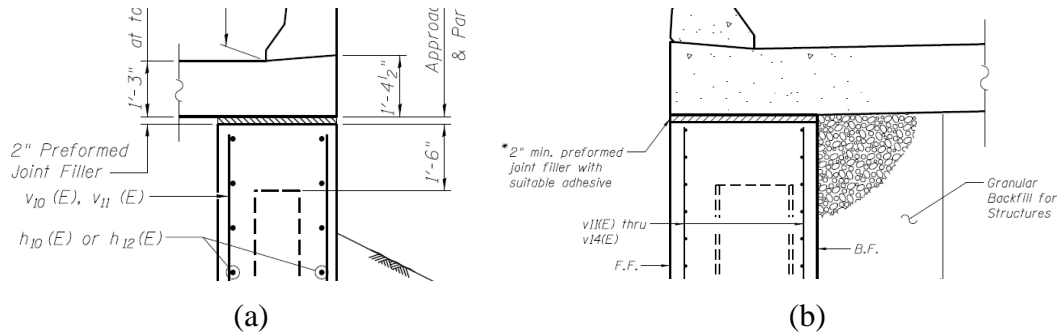
Figure 5.5 Details of the approach slab-wingwall interface: (a) cast-in-place, (b) precast.

(a)   (b)
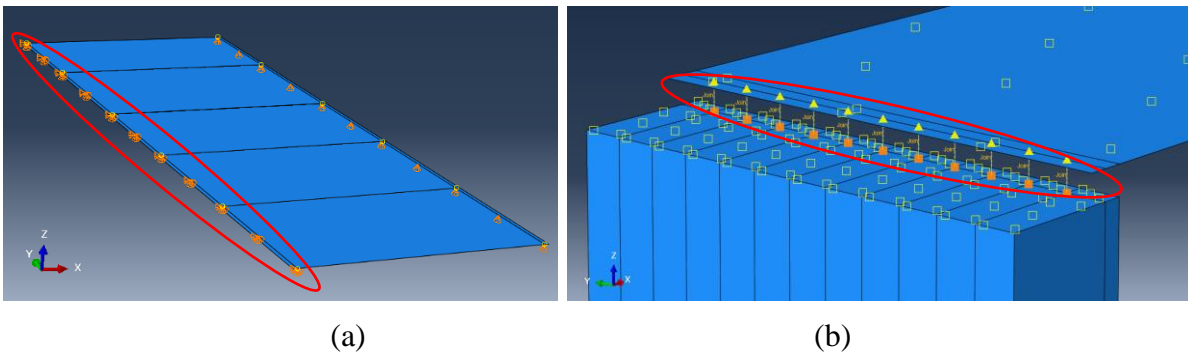
Figure 5.6 Boundary conditions at the abutment-approach slab interface: (a) hinge, (b) connectors.

One simplified modeling approach to the boundary conditions at the abutment-approach slab interface is a hinge, i.e., the translational degrees of freedom (U1, U2, and U3) are restricted to be zero, as shown in Figure 5.6 (a), resembling a simply-supported beam scenario. Another way to incorporate the restraint that the abutment applies to the approach slab is to explicitly model the dowel bars with connector elements and the abutment with solid elements, as shown in Figure 5.6 (b). The relative translation in the three directions is then restricted at those dowel bar locations.

149

The potential friction at the abutment-approach slab interface can also be incorporated explicitly in the model.

The boundary conditions at the abutment-pile bent interface can be simplified as rollers if friction between the approach slab and pile bent is ignored, representing the case of a simply-supported beam, as shown in Figure 5.7 (a). The interaction of the approach slab and the pile bent can be captured in a more detailed manner, which considers the area that the slab and pile bent may be in contact with and the corresponding friction at the interface, as shown in Figure 5.7 (b).

(a)   (b)
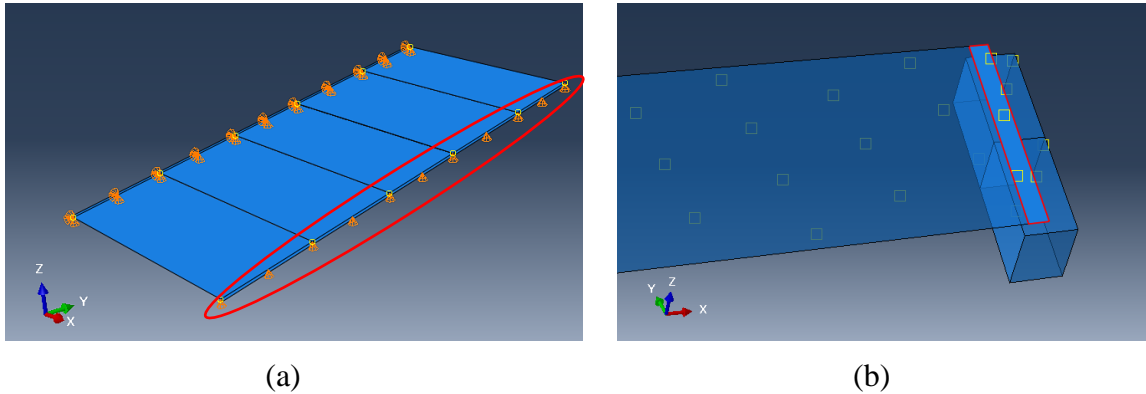
Figure 5.7 Boundary conditions at the approach slab-pile bent interface: (a) roller, (b) surface interaction.

It is also possible that the approach slab is supported within its span by the subbase below it. The interaction between the approach slab and the subbase can involve vertical (upward) support and friction between the approach slab and the subbase in the tangential direction of the slab bottom surface. If only the vertical support from the subbase is considered, such interaction can be implemented by an "elastic foundation" in the interaction module of Abaqus (Dassault Systems 2017). If the friction is considered as well, both interactions can be incorporated by the connector elements that join the slab and the ground. This is accomplished through compression-only springs in the vertical direction (Z-direction) and horizontal springs (X- and Y-direction).

5.1.4   Live Loads

As the length of the approach slab is typically 30 feet, the HL-93 tandem truck and the rear three axles of IL-120 are the primary truck loading cases of interest for the approach slabs, as shown in Figures 5.8 and 5.9, respectively. Additionally, for both cases, the design lane load is applied to all traffic lanes of the approach slabs. As will be discussed in Chapter 6, another set of truckload is specifically considered and implemented in the numerical models for the static truck loading test.
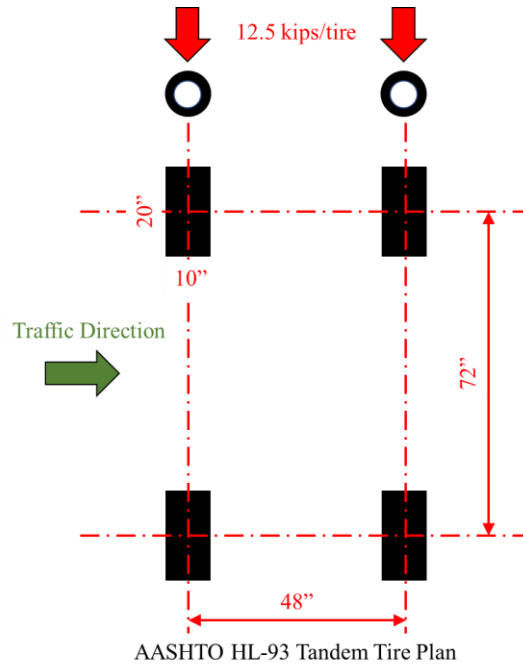
Figure 5.8 AASHTO HL-93 design tandem.
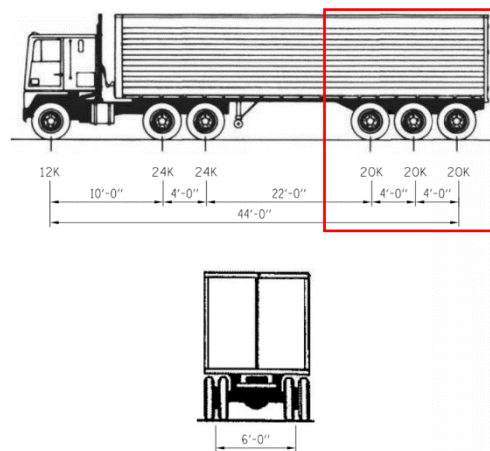
Figure 5.9 IL-120 design truck.

5.1.5 Temperature Field

In the Abaqus (Dassault Systems 2017) models, the temperature field is defined as (1) uniform temperature change in the whole slab and (2) uniform temperature change at the middle surface of the shell element section together with a linear temperature variation through the thickness of the slab, i.e., a linear temperature gradient in the Z direction. The values of the uniform temperature change and linear temperature gradient in the numerical models are discussed in Chapter 7.

5.1.6 Mesh Size

The mesh size of the approach slab shell elements needs to be carefully determined to achieve a stable numerical accuracy for all approach slab models and an acceptable efficiency in terms of time and memory. Hence, a set of experiments was conducted to examine the influence of mesh size on the numerical modeling results. As the analytical solution to the problem where a skewed reinforced concrete slab is loaded by design trucks or subjected to thermal loading is not easily accessible, the convergence of the numerical modeling results with various mesh sizes is chosen as the criterion of selecting the mesh size.

A set of slabs – where each slab has 5 sections and various skew values, loaded by the IL-120 design truck at the midspan – was developed. Variation in mesh size was considered with the following element sizes (inches): 40, 20, 10, 5, 2. The maximum principal stress of each model was recorded and compared in a log scale to obtain the maximum reliable mesh size, as shown in Figure 5.10. For all the considered skew values in Figure 5.10, the maximum principal stress fluctuates significantly as the mesh size decreases from 40 inches to 5 inches. Table 5.3 details the relative difference of the maximum principal stresses compared to the case of the 5-inch mesh size. When the mesh size varies from 5 inches to 2 inches, the stresses tend to be stable for most of the selected skew values, with a maximum relative difference of -6.83%. Consequently, the convergence of the maximum principal stress suggests a reliable mesh size no greater than 5 inches. The subsequent numerical models in this study adopt a mesh size of 5 inches.
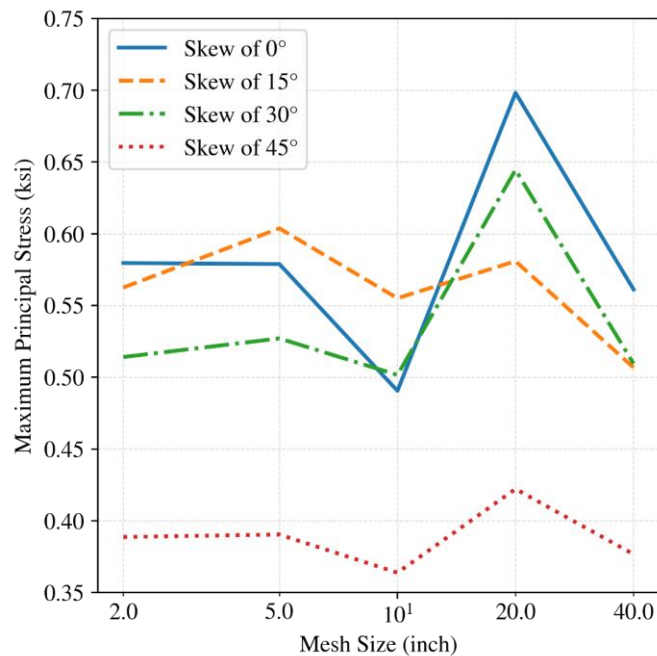
Figure 5.10 Maximum principal stresses vs. mesh size.

Table 5.3 Relative difference of the maximum principal stresses.

Skew	Mesh Size (inch)				
	2	5	10	20	40
0°	0.12%	0.00%	-15.26%	20.61%	-3.06%
15°	-6.83%	0.00%	-8.06%	-3.79%	-16.07%
30°	-2.46%	0.00%	-4.83%	22.29%	-3.33%
45°	-0.44%	0.00%	-6.82%	8.13%	-3.52%

5.2 Modeling and Analysis Automation Process

To effectively create, run, and extract the results from a number of numerical models in Abaqus (Dassault Systems 2017), a set of Python scripts was created for the Abaqus Python Development Environment (Abaqus PDE). In addition, Python scripts that can automatically change the variable values in the scripts for Abaqus PDE were created for the parametric study. Python scripts that post-process the numerical model results were also developed in Jupyter Notebook for analyzing and visualizing the numerical model results.

6 Study of Short-Term Behavior with Static Load Tests

Field monitoring of the instrumented approach slabs records the slab strain changes due to the combined effects of live loads, slab temperature changes, and restraints at the ends and bottom of the slab. To better understand the slab behavior under live load, it is necessary to carry out experiments with controlled conditions, such as placing trucks with known weights at controlled locations for a short window of time in which the temperature effects are not significant or can be properly excluded. Observing the slab behaviors in terms of strain, displacement, and temperature at a higher sampling rate (a scan interval of 3 minutes from 9/14/2018 to 9/22/2018) provides a chance to understand how vehicular live loads and thermal effects influence the approach slabs.

Both monitored slabs were loaded with a test truck at various positions to understand slab behavior under truck loads and to calibrate numerical models. The North Shoulder, Lane 1, Lane 3, and South shoulder of both approach slabs (at Arlington Heights Road and Prospect Avenue) were loaded as a part of this experiment, along with an additional test done on the Gore of the slab at Arlington Heights Road. For loading of a section (lane or shoulder), a single truck was placed statically for a short period of time (several minutes) at three locations defined by the rear axle locations. These locations are for the center of the rear axle at the quarter points and at the midpoint of the slab, as shown in Figure 6.1, where the truck tires are represented by red boxes. (The test truck had a double rear axle, so the noted "axle" locations are actually for the midpoint of the two rear axles.) The truck and loading conformed to the IDOT/Tollway specifications of legal dimension and weights. The loads applied at both the front and rear axles were measured after the tests to obtain reliable estimates of the load on the slab. This load data also served as input for the truck loads in the corresponding numerical simulations. Testing was performed with the help of lane closures at the lanes under investigation and was conducted on two days (on 9/14/2018 and 9/21/2018), with 7 tests in total conducted on the cast-in-place slab (numbered 1-7) and 12 on the precast slab (numbered 1-12).

Truck Tests on 9/14/2018 at Arlington Heights Rd
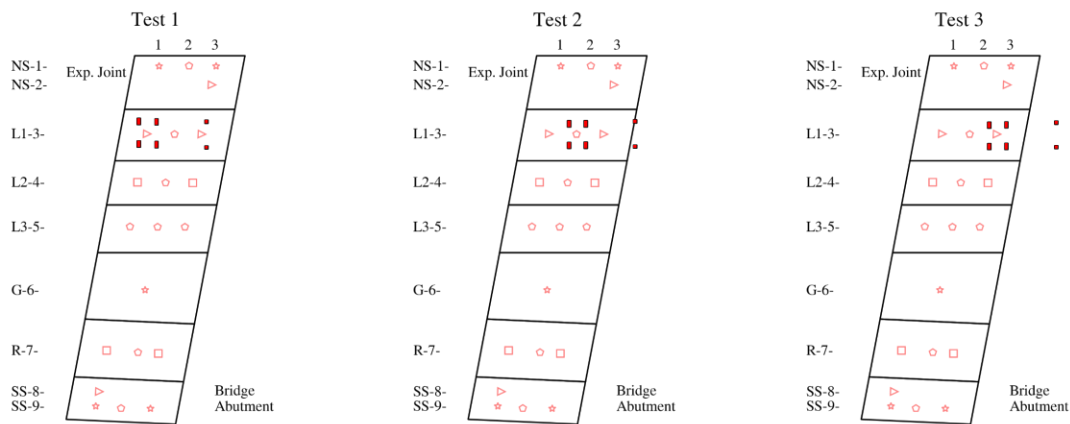
(a)

Truck Tests on 9/21/2018 at Arlington Heights Rd

(b)

Truck Tests on 9/14/2018 at Prospect Ave

(c)

155
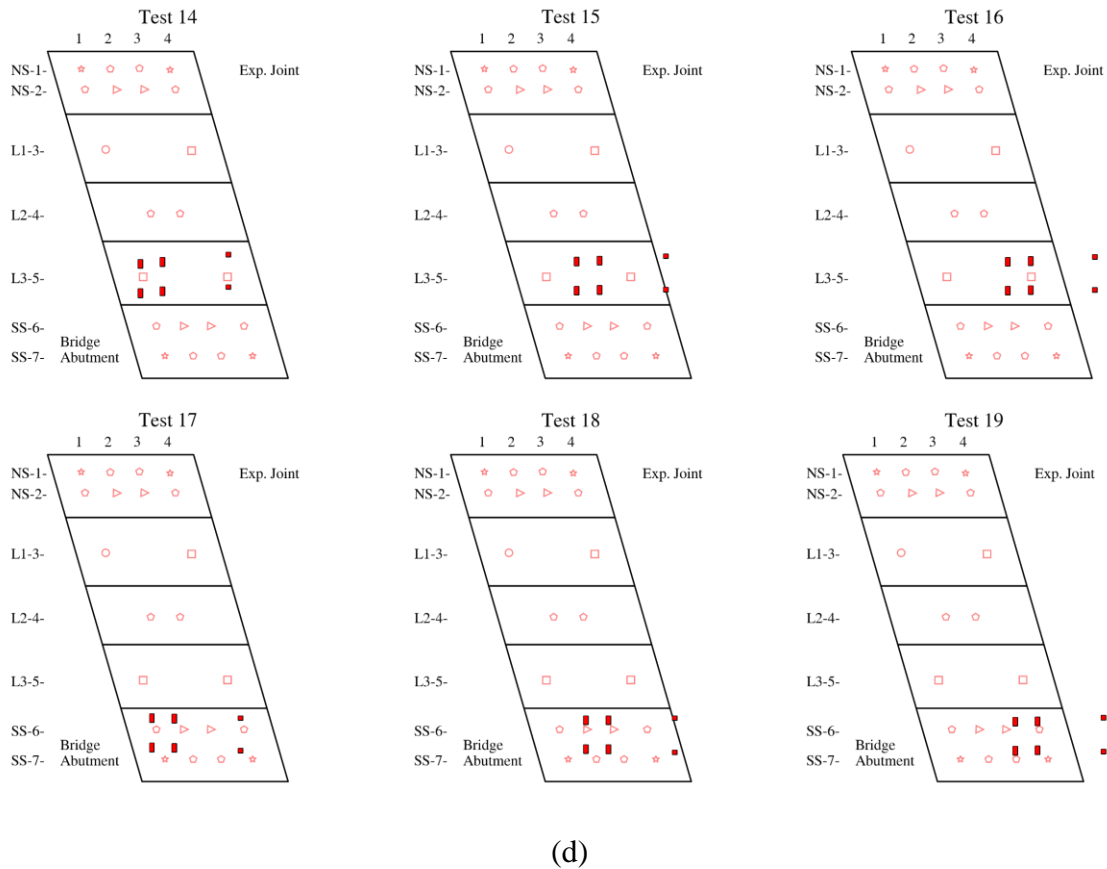
Figure 6.1 Static truck load locations at: (a) Arlington Heights Road on 9/14/2018, (b) Arlington Heights Road on 9/21/2018, (c) Prospect Avenue on 9/14/2018, and (d) Prospect Avenue on 9/21/2018.

6.1 Test Procedure

The following procedure was adopted by the research team to perform a test on each selected section (lane or shoulder):

1) The truck remained outside of the approach slab to get several stable unloaded data sets as reference readings. Then the truck was placed at a selected location, and the time of placement was recorded.
2) The truck remained parked at the selected location (quarter points of span or midspan) of the slab for a duration of at least two sets of sensor readings collection so that the multiplexer and datalogger could record data from all the sensors.
3) The exact locations of the truck axles were recorded for each test location to facilitate numerical modeling of the corresponding test.
4) The truck was then driven off the approach slab, and the time was recorded.
5) The truck was kept out of the slab for at least two data scan intervals so that the strain in the sensors could return to their unloaded level. The readings of the sensors at this point

156

were again recorded and served as the new reference readings. The above steps were then repeated in their sequence for the next test location.

6) The recorded data sets were post-processed to obtain strain changes caused only by the applied live load.

The axles of the truck were weighed after the tests; those loads are presented in Table 6.1.

Table 6.1 Weighed loads of the static test trucks.

Date	Front Axle Load (kips)	Rear Axle Load (kips)
9/14/2018	12.66	35.10
9/21/2018	12.70	34.78

(a)

(b)

(c)

(d)

Figure 6.2 Research team conducting static truck loading test: (a) U of I research team (b) testing location with the team working on truck placement and data collection; (c) measurement of rear axle location; (d) measurement of front axle location.

Figure 6.2 (a) to (d) show the process of the static loading truck test carried out by the research team on 9/14/2018.

6.2 Field Results on Test Days

In addition to the long-term behavior of the approach slabs over 2.5 years, it is beneficial to also examine the daily response of the approach slabs as they experience roughly one cycle of temperature change due to solar radiation and other ambient environmental factors within a day. As was the case for long-term behaviors, both actual strains and load related strains are again discussed herein. Displacements of the approach slabs are also studied against temperature.

6.2.1 Actual Strain

Actual strain measures the deformation of the approach slab due to all combined effects, including live loads and thermal loads. The variations of actual strains with time during the two test days, 9/14/2018 and 9/21/2018, are computed with the reference readings set at the approximate sunrise time of the day, which is 6:00 AM. The main consideration behind the reference reading selection is that solar radiation can have significant impacts on approach slab behavior.

6.2.1.1 Test Day of 9/14/2018

On 9/14/2018, it was sunny, and hence there was stable and sufficient solar radiation during the daytime. Figure 6.3 compares the actual strains at all gages in each of the transverse lines in the gage layout at Prospect Avenue (precast slab). The vertical blue and red dashed lines around noon in Figure 6.3 represent the start and end of each static truck test during the day. The piecewise function-like behaviors during the truck tests, for example NS-2-1B in Figure 6.3 (a), reflect the strains/deformations caused by the controlled truck load.

It can be observed that after sunrise all gages experienced an expansion of the concrete at different levels, which can be clustered in the descending order of actual strain increase: transverse gages in the top mat (R), longitudinal gages in the top mat (T), and longitudinal gages in the bottom mat (B), as can be found by the three groups of curves in Figure 6.3. This may be indicative of less restraint in the transverse direction compared to the longitudinal restraint of the approach slab.

There are only small variations in the strains of the same gage position among different transverse lines of the gage layout, indicating that the approach slab thermal deformations are consistent in the longitudinal direction. A greater increase in actual strains for gages in the top mat suggests that the thermal deformations of approach slabs are affected more substantially by the temperature distribution through the slab thickness, i.e., temperature gradient.

As the approach slab started to cool down, beginning 2 to 3 hours before the sunset (which was around 7:30 PM), the concrete expansion decreased gradually for all gages in the top mat. However, such behavior is observed 1 to 2 hours later for the gages in the bottom mat, which is because of the smaller sensitivity of the temperature at the bottom mat to the solar radiation and ambient environment.
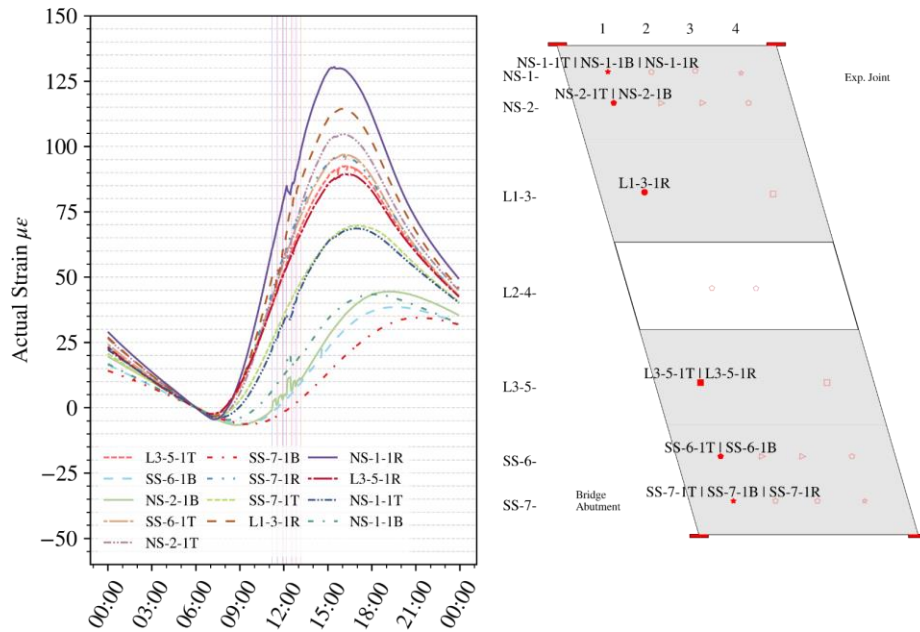
Figure 6.3 (a)
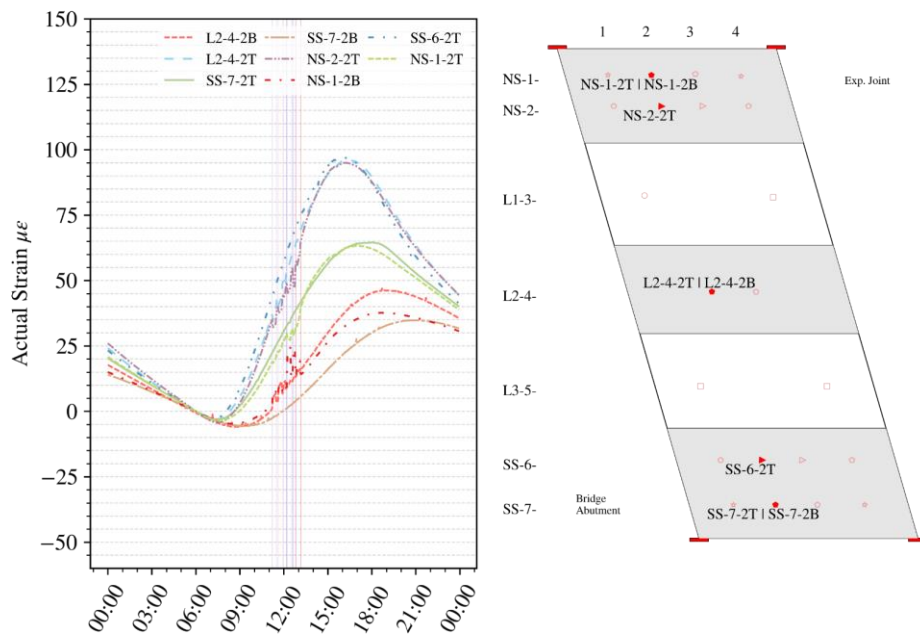
Figure 6.3 (b)
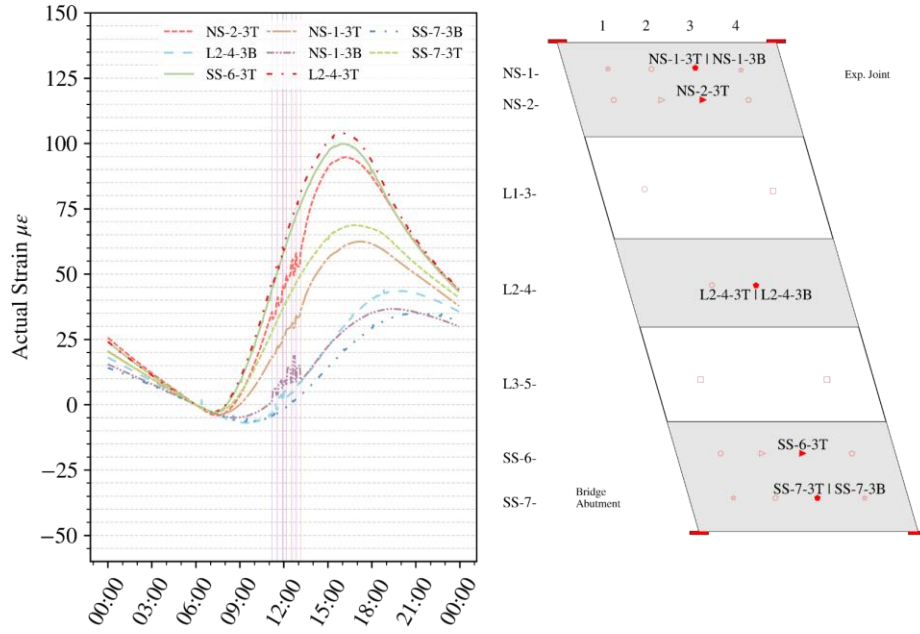
(c)
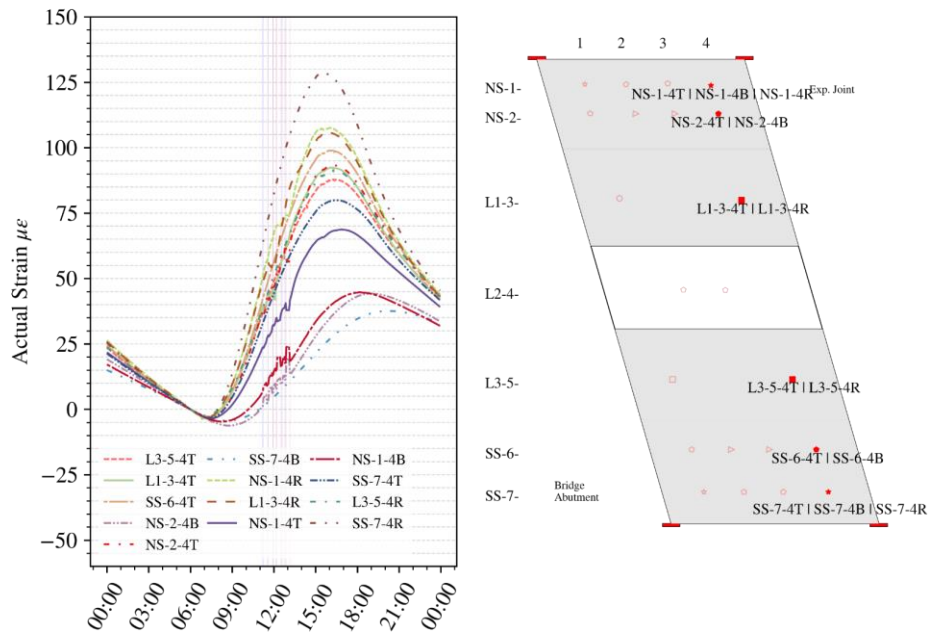
(d)

Figure 6.3 Actual strains at Prospect Avenue on 9/14/2018 at (a) transverse line 1, (b) transverse line 2, (c) transverse line 3, and (d) transverse line 4.

160

For the cast-in-place approach slab at Arlington Heights Road, the actual strains, as shown in Figure 6.4, share most of the trends observed from the precast approach slab: concrete expansion at all gages; consistent thermal deformations along the longitudinal direction of the slab; top gages having more increase in strains; and decrease of concrete expansion before sunset. Additionally, the maximum increase in actual strains for the cast-in-place slab is less than that of the precast slab, which may indicate more restraint at the cast-in-place slab than the precast slab.
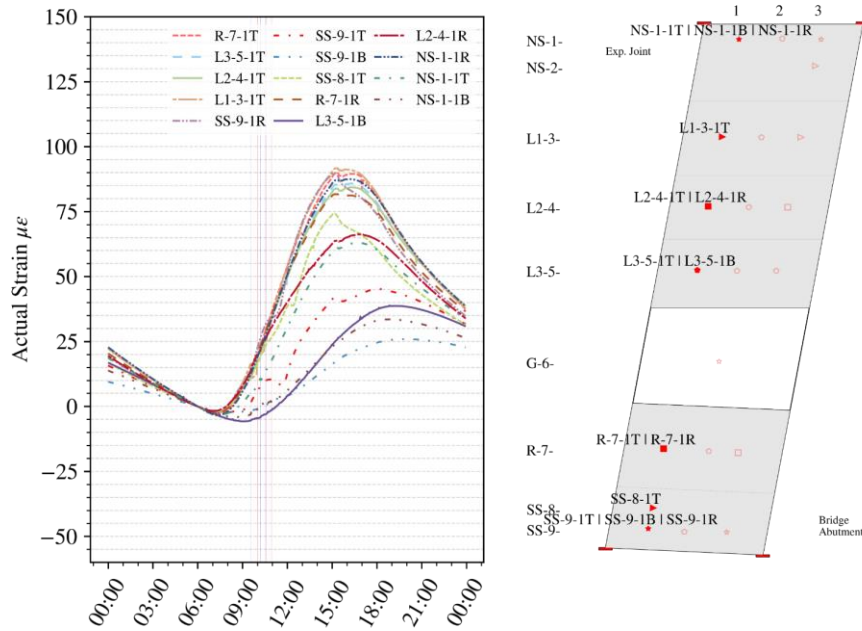
Figure 6.4 (a)

Figure 6.4 (b)

161

(c)
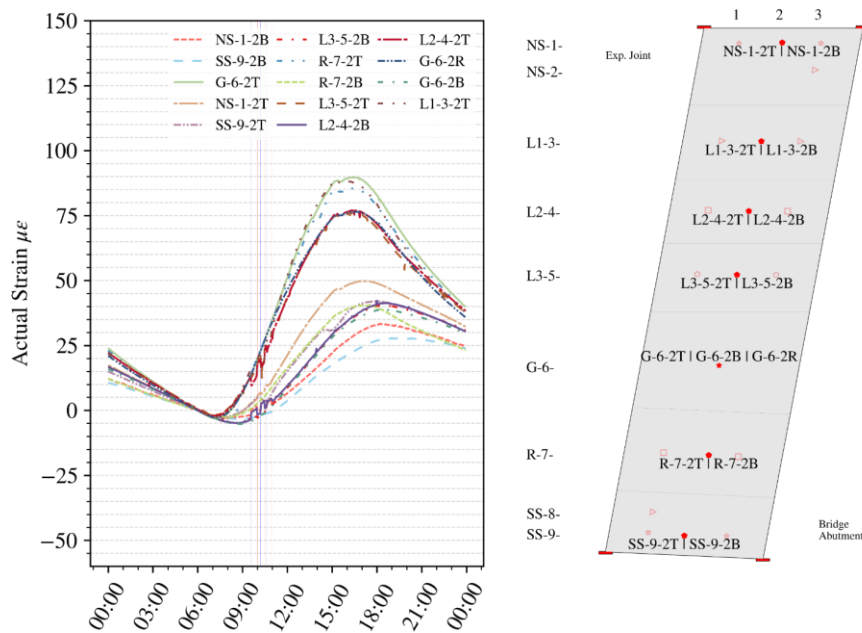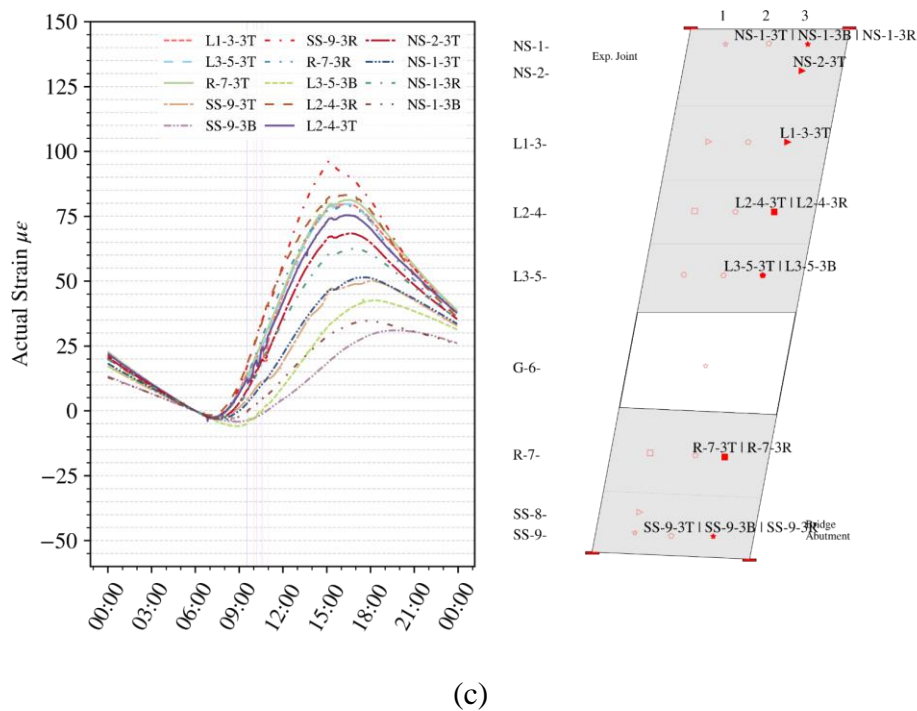
Figure 6.4 Actual Strains at Arlington Heights Road on 9/14/2018 at (a) transverse line 1, (b) transverse line 2, and (c) transverse line 3.

The longitudinal actual strains at the top reinforcing mat for gages at the exterior locations of the shoulders (i.e., longitudinal line NS-1 and SS-7 for the precast slab, as well as NS-1 and SS-9 for the cast-in-place slab) indicated less concrete expansion during daytime compared to the counterpart inner locations, as shown in Figure 6.5. For example, considering the precast approach slab, the actual strain of NS-1-1T in Figure 6.5 (a) was less than that of L2-4-3T in Figure 6.5 (b), which resembled NS-1-4R in Figure 6.5 (a). Such difference may be caused by the boundary conditions at the exterior edges of the shoulders, including the effect of parapets and the support under the slab.

162
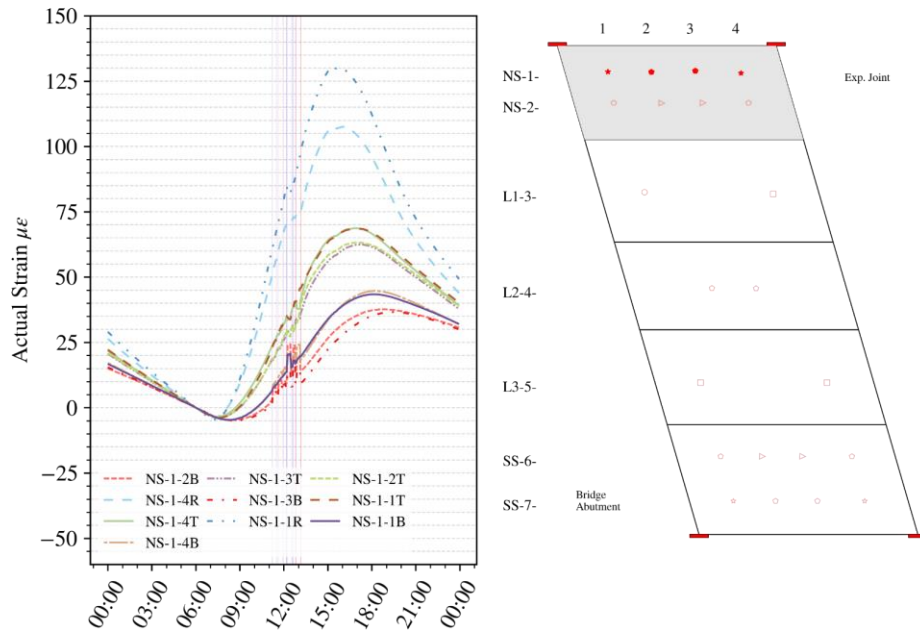
Figure 6.5 (a)

Figure 6.5 (b)

163
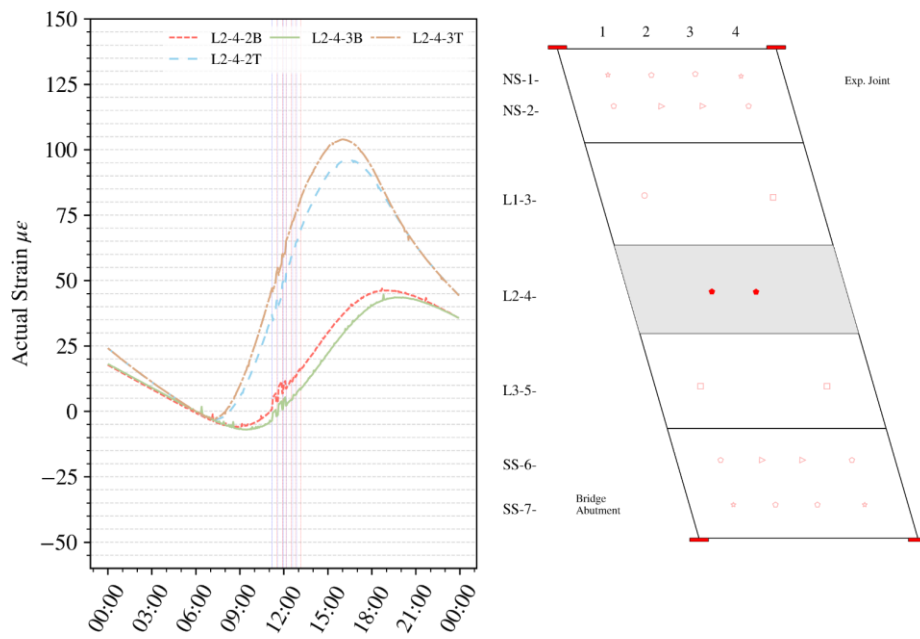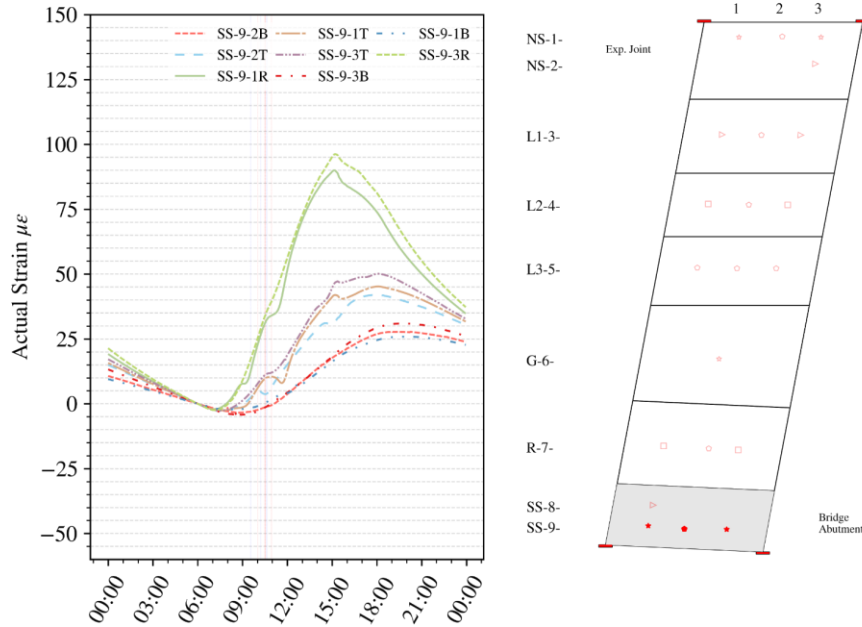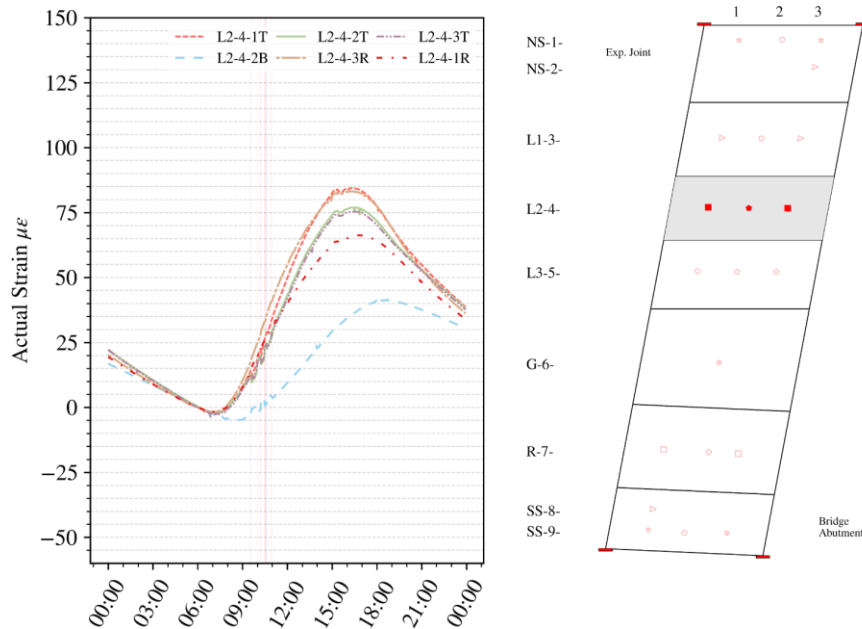
Figure 6.5 (c)

(d)

Figure 6.5 Selected actual strain comparisons between (a) exterior locations at Prospect Avenue, (b) interior locations at Prospect Avenue, (c) exterior locations at Arlington Heights Road, and (d) interior locations at Arlington Heights Road.

The trend of actual strain vs. temperature remains approximately linear among all gages in both slabs, with only slight differences in the slope of the strain vs. temperature relationships. Figure 6.6 and Figure 6.7 show the detailed trends for Prospect Avenue and Arlington Heights Road, respectively. On top of the actual strain vs. temperatures relationship, the estimated distribution of temperatures during the test day, 9/14/2018, is also plotted to illustrate the temporal distribution of temperatures at different gages.

The higher the temperature density is at a certain temperature value, the more temperature readings were recorded near that value; i.e., the temperature changed relatively slowly. For the actual strain-temperature relationship during the complete day, it traversed the plotted line in the clockwise direction, corresponding to the process of temperature decreasing-increasing-decreasing throughout the day. One can observe that the low-temperature range of the day generally has slightly greater density, which is indicative of slow temperature change. After sunrise, as the solar radiation increased, the temperature tends to vary faster.

The actual strains trend approximately linearly with the temperatures during the day except for the maximum and minimum temperature ranges, where there are additional changes in actual strains that lead to two different actual strain values for a single temperature at most gages in the slabs. The differential behavior is believed to be related to solar radiation and can be explained by the apparent strains (or raw readings) presented later in section 6.2.2.
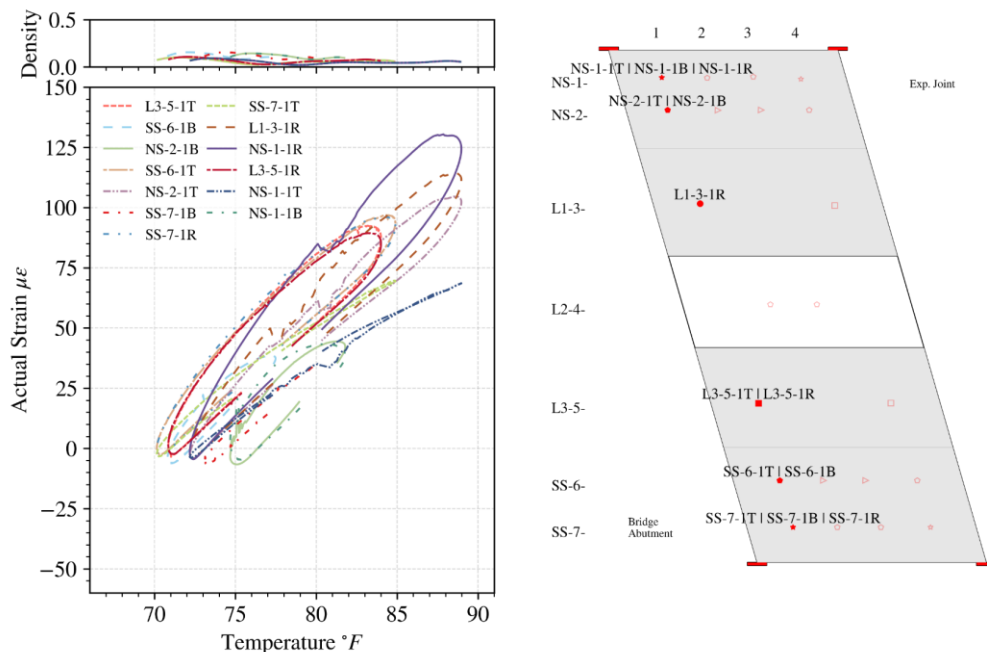
Figure 6.6 (a)
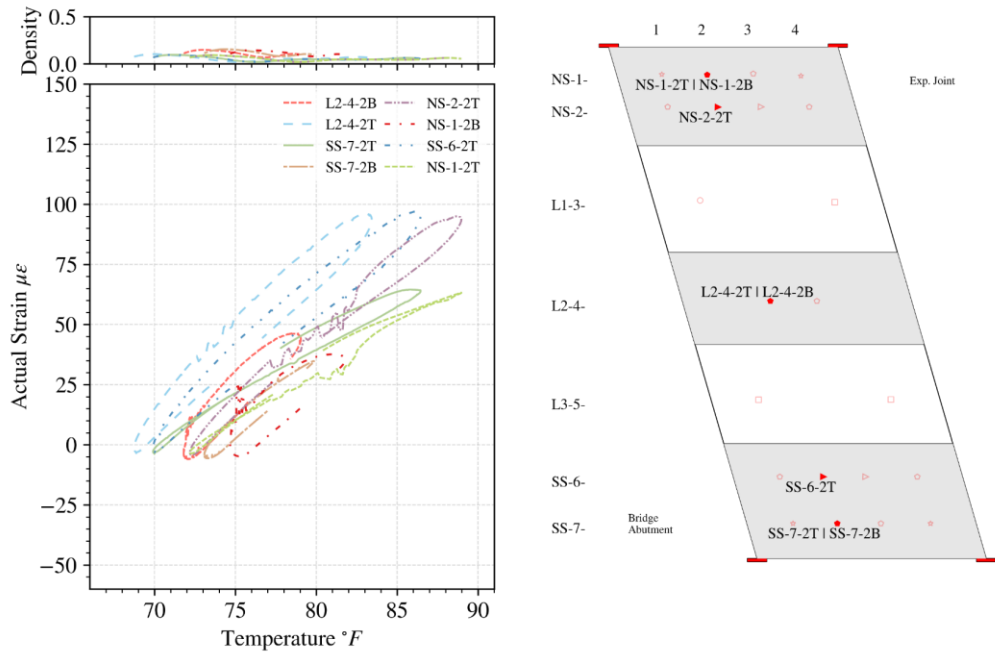
Figure 6.6 (b)
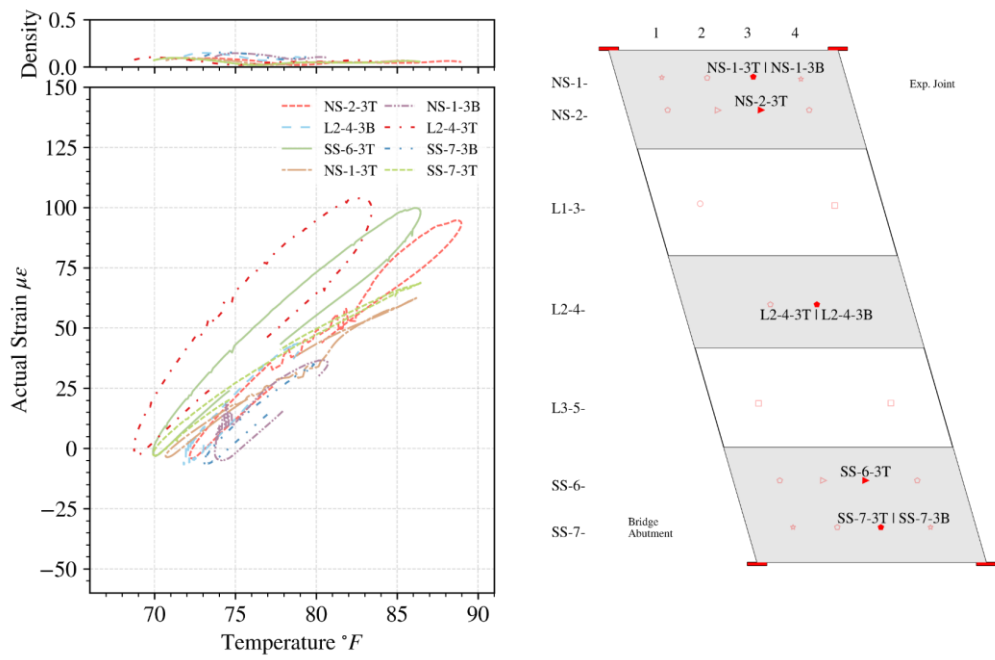
Figure 6.6 (c)
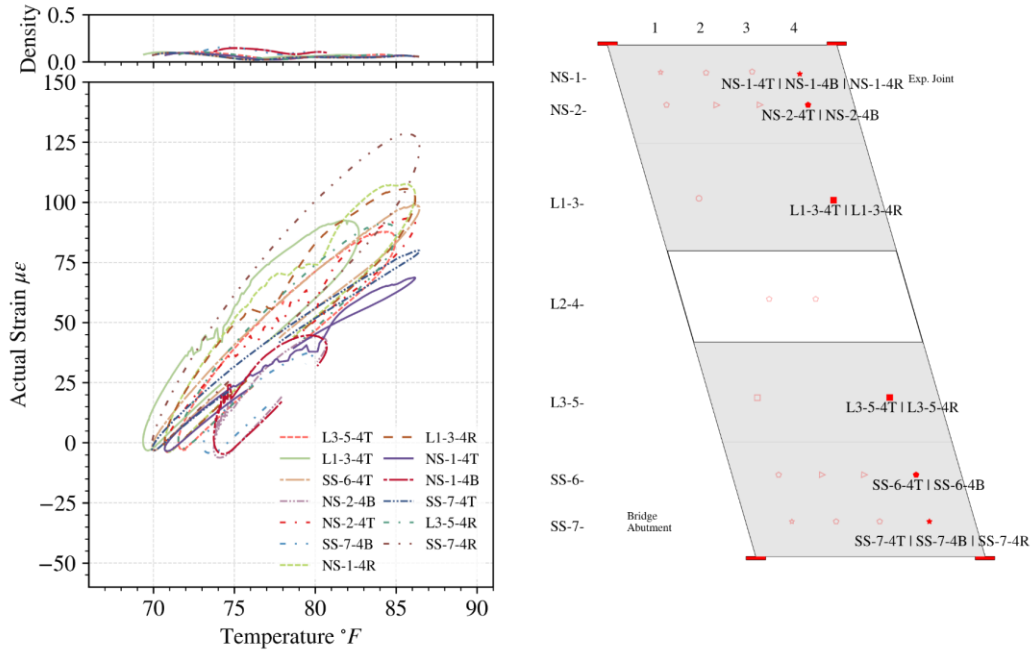
(d)

Figure 6.6 Actual strains vs. temperatures at Prospect Avenue: (a) transverse line 1, (b) transverse line 2, (c) transverse line 3, and (d) transverse line 4.
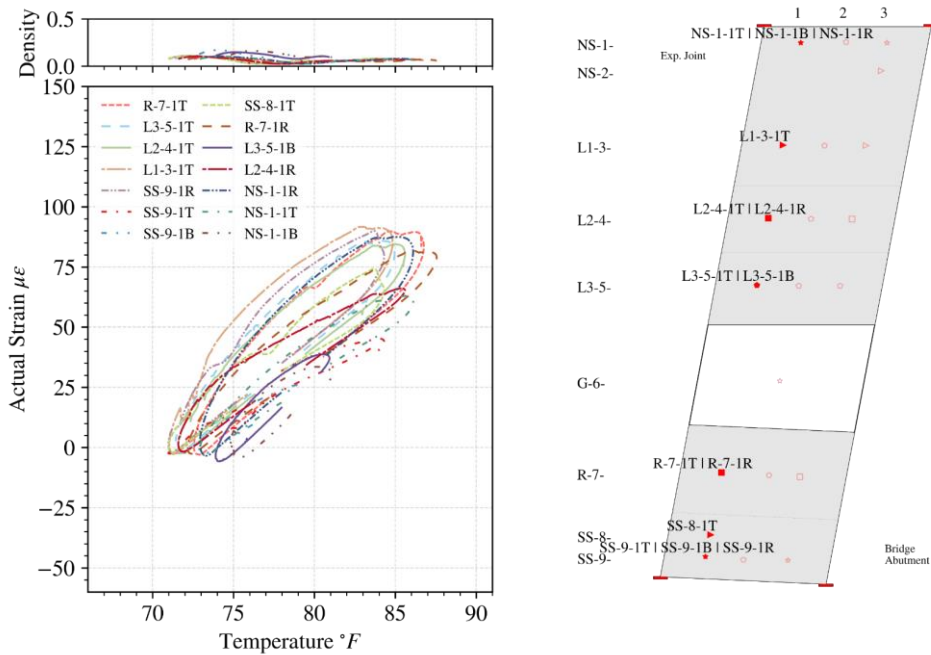
Figure 6.7 (a)
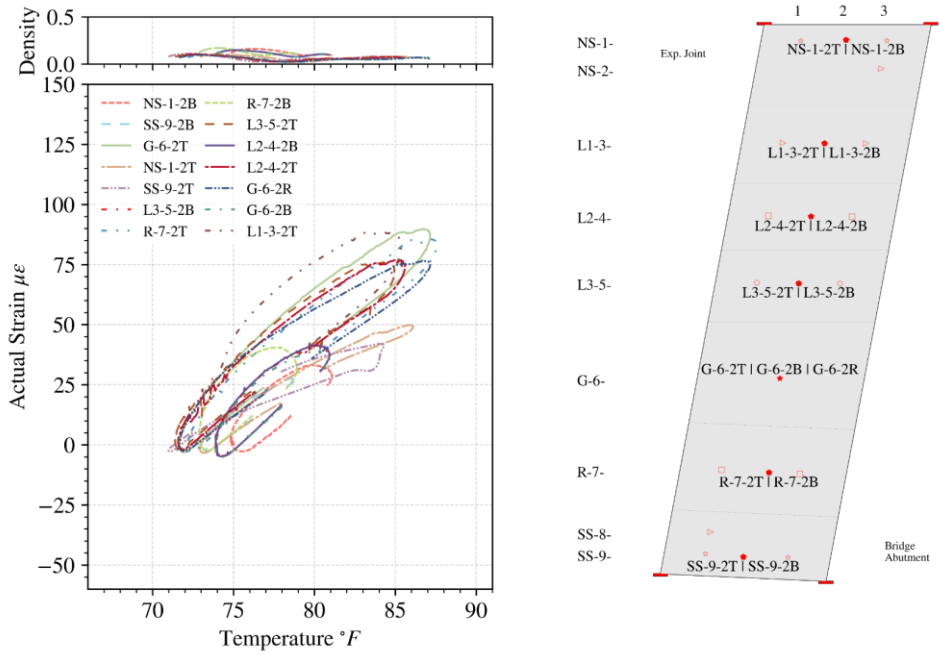
Figure 6.7 (b)
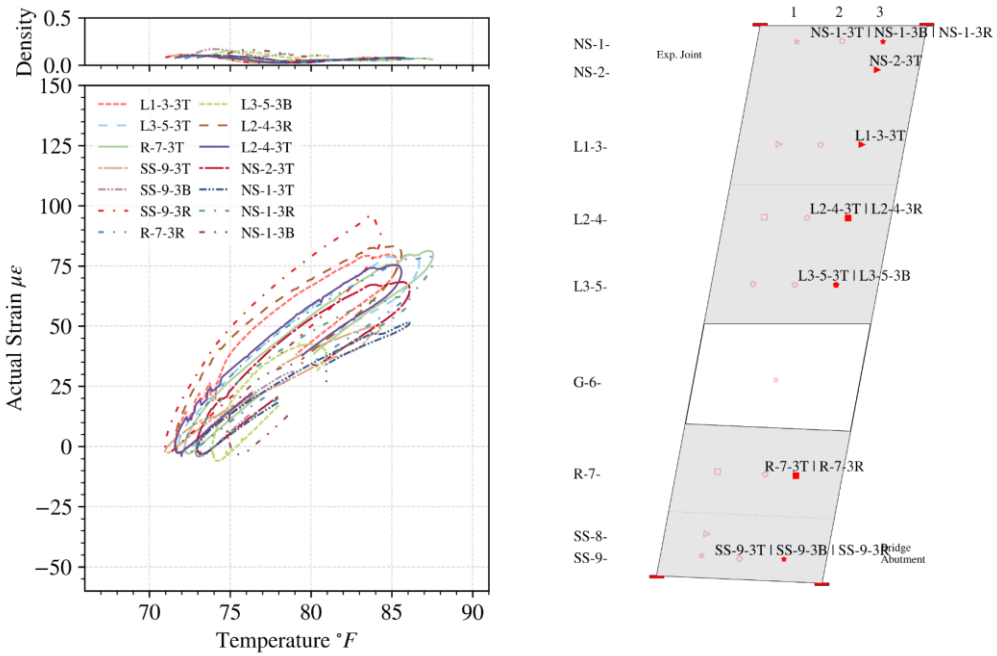
Figure 6.7 (c)

Figure 6.7 Actual strains vs. temperatures at Arlington Heights Road: (a) transverse line 1, (b) transverse line 2, and (c) transverse line 3.

On the second test day, 9/21/2018, the solar radiation was not as intense as the first test day (9/14/2018) due to the cloudy weather. Consequently, the temperature range measured from the gages on 9/21/2018 (about 6°C) was not as wide as on 9/14/2018 (about 10°C). There was a more significant temperature decrease after the sunset than before the sunrise on 9/21/2018, resulting in net contraction of the approach slabs at the end of the day, as shown in Figure 6.8 for Prospect Avenue and Figure 6.9 for Arlington Heights Road. The actual strains remained consistent along the longitudinal direction of the approach slab, which resembles the observations of the first test day. The strains at the top mat have greater changes in magnitude in both expansion and contraction than the bottom mat, as the temperature variations at the top mat are more substantial. However, there are no significant differences between the top mat strains in the transverse and longitudinal directions as found in the first test day, which can be explained by the less intense solar radiation on 9/21/2018.
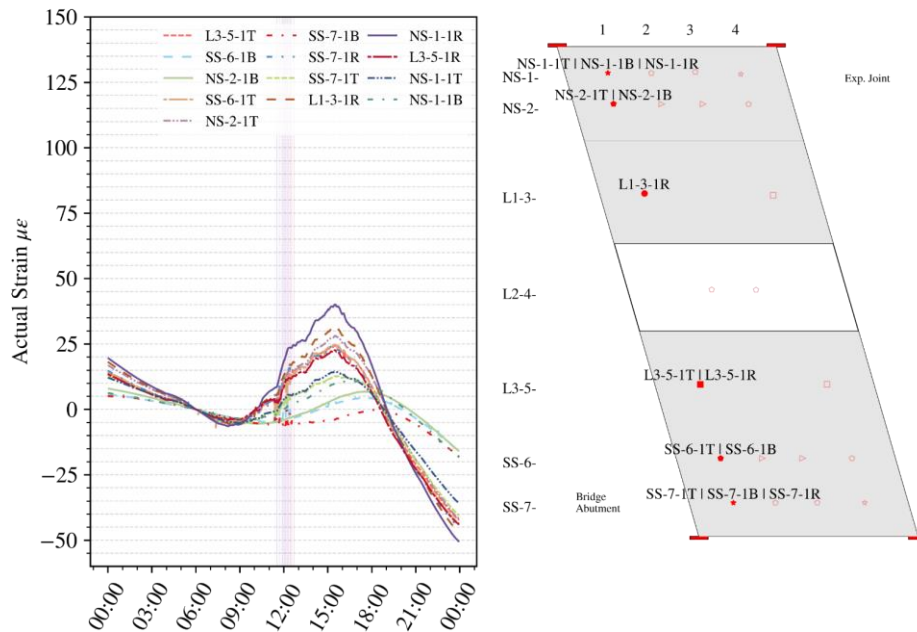
Figure 6.8 (a)
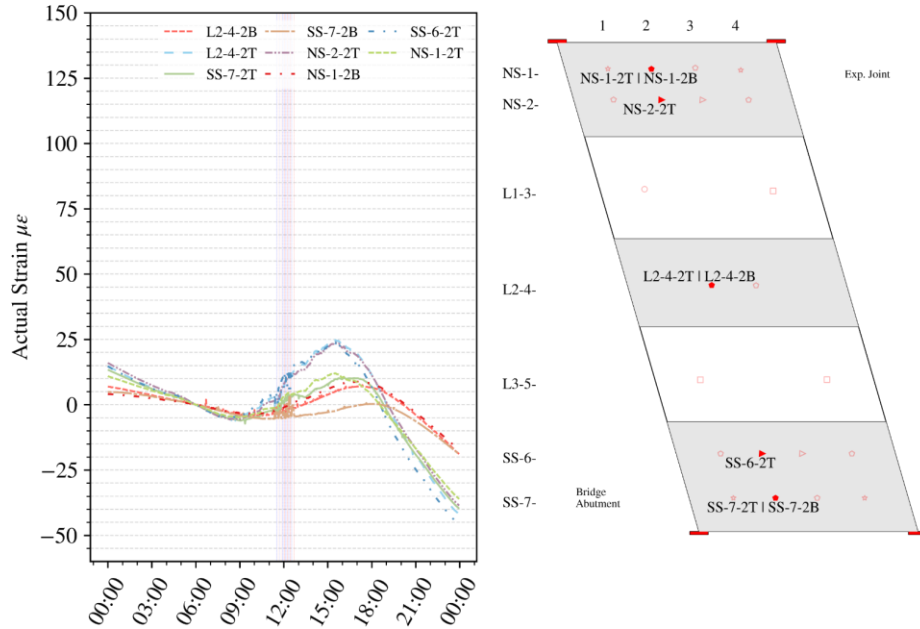
Figure 6.8 (b)
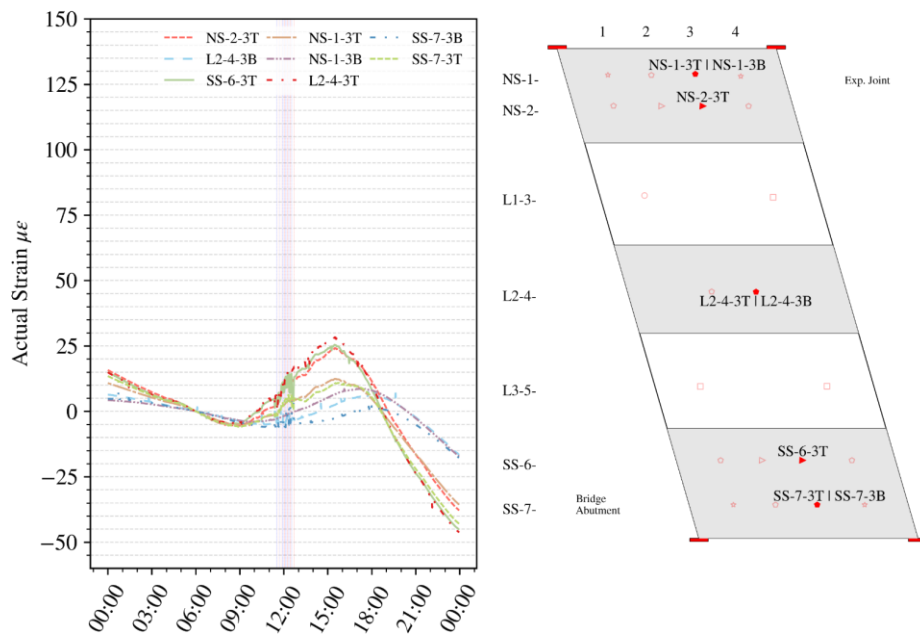
Figure 6.8 (c)
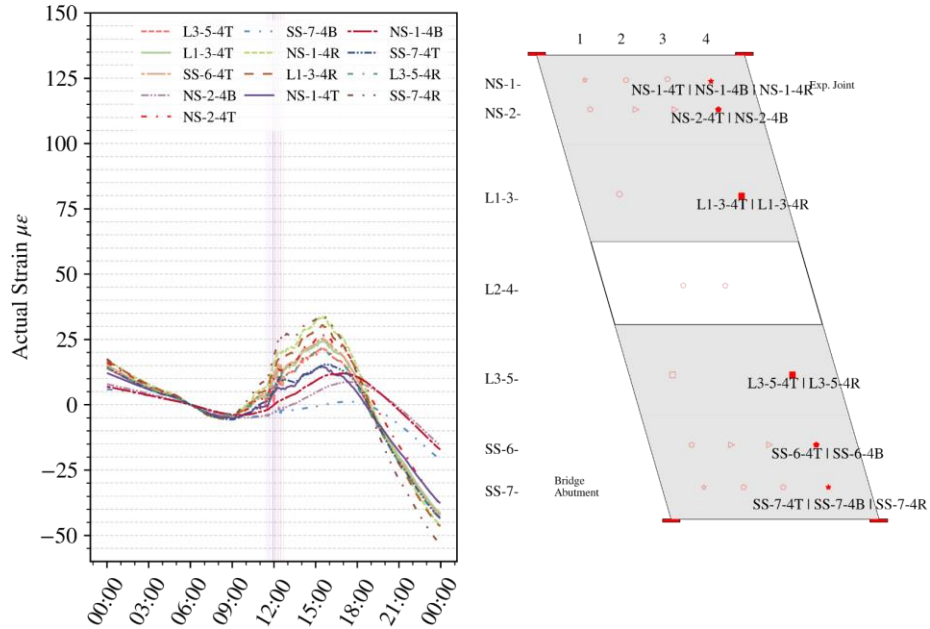
Figure 6.8 (d)

Figure 6.8 Actual strain at Prospect Avenue on 9/21/2018: (a) transverse line 1, (b) transverse line 2, (c) transverse line 3, and (d) transverse line 4.
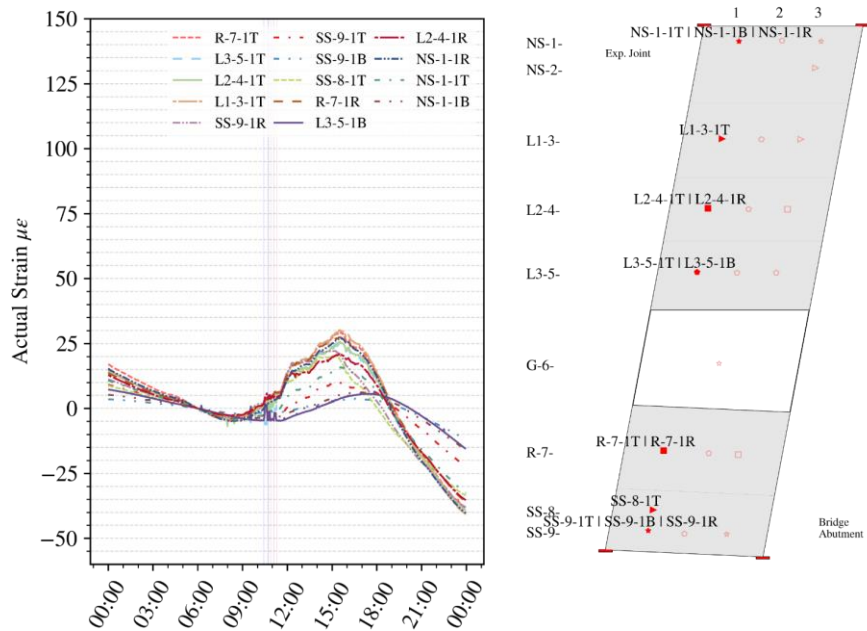
Figure 6.9 (a)
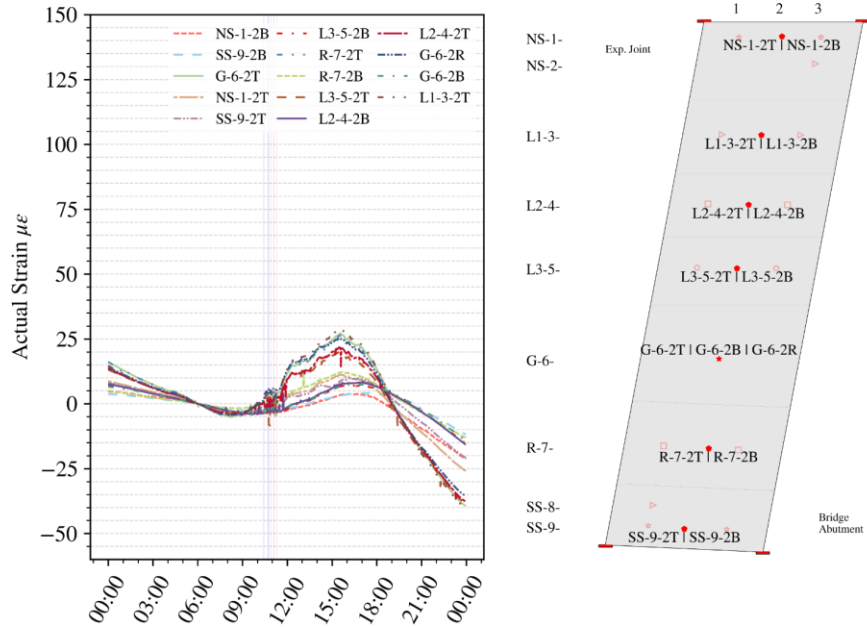
Figure 6.9 (b)
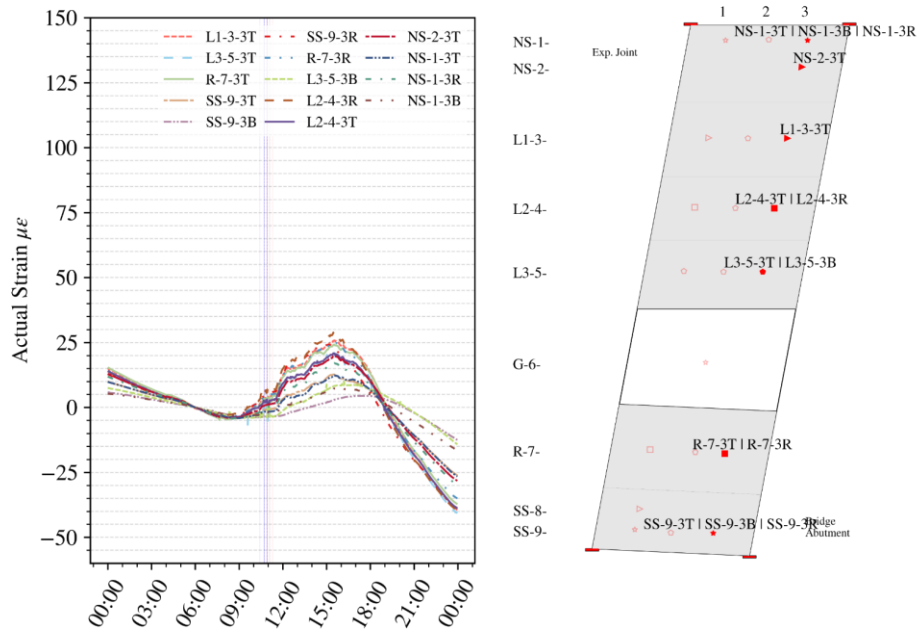
Figure 6.9 (c)

Figure 6.9 Actual strains at Arlington Heights Road on 9/21/2018: (a) transverse line 1, (b) transverse line 2, and (c) transverse line 3.

Regarding the actual strain vs. temperature relationship for 9/21/2018, an overall linear trend is observed for each embedded gage in both approach slabs. After the sunset, as temperatures

172

decreased, the actual strains accumulated compression at nearly constant rates, which is represented by the parallel straight lines in Figure 6.10 for Prospect Avenue and Figure 6.11 for Arlington Heights Road. The changes in actual strains related to live loads are moderate compared to the overall strain change range.
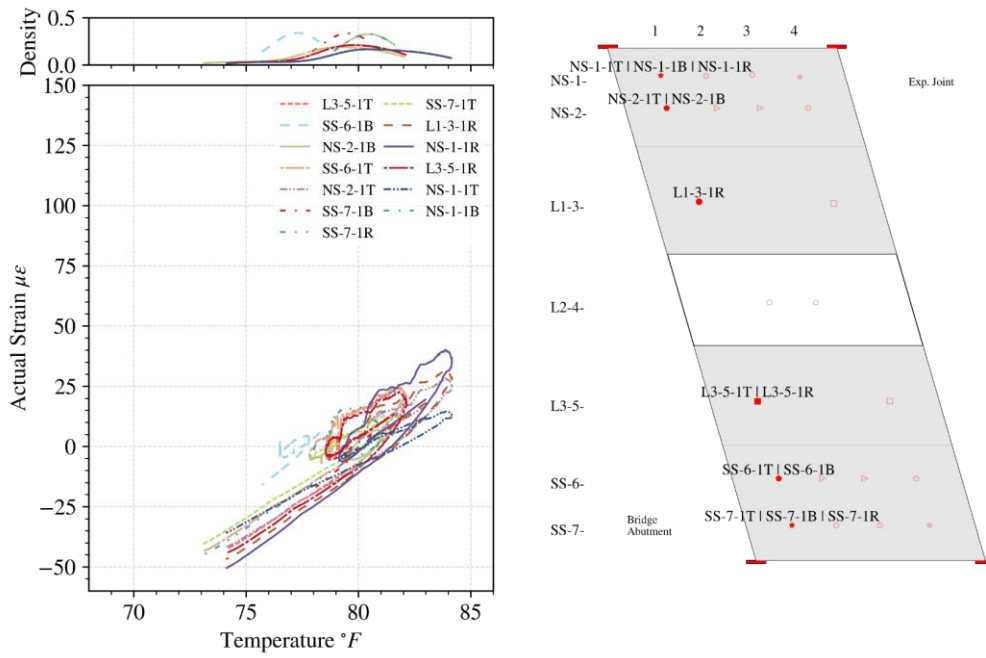
Figure 6.10 (a)
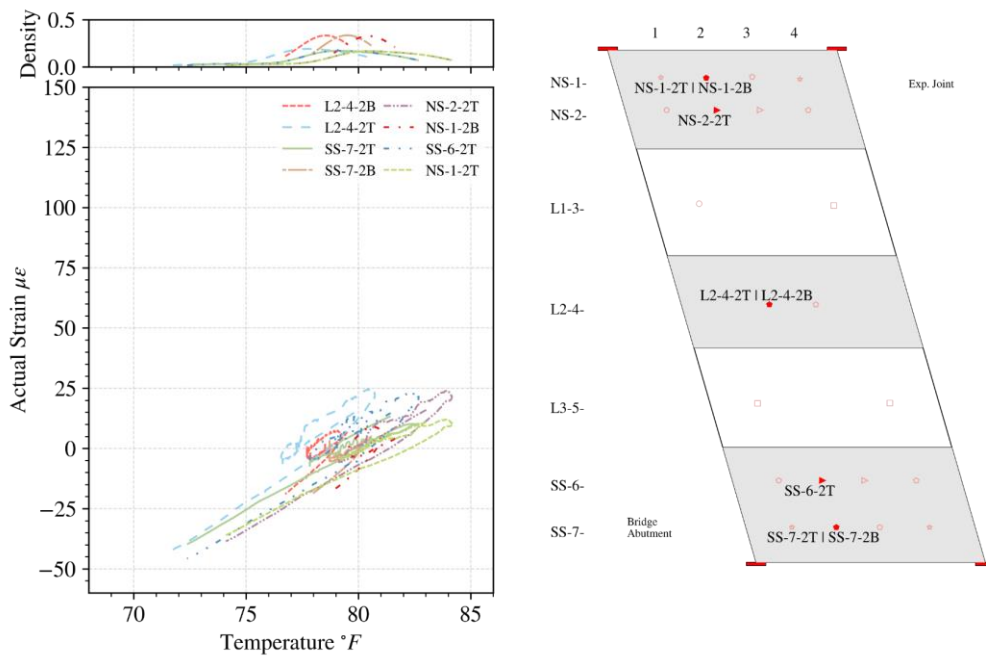
Figure 6.10 (b)
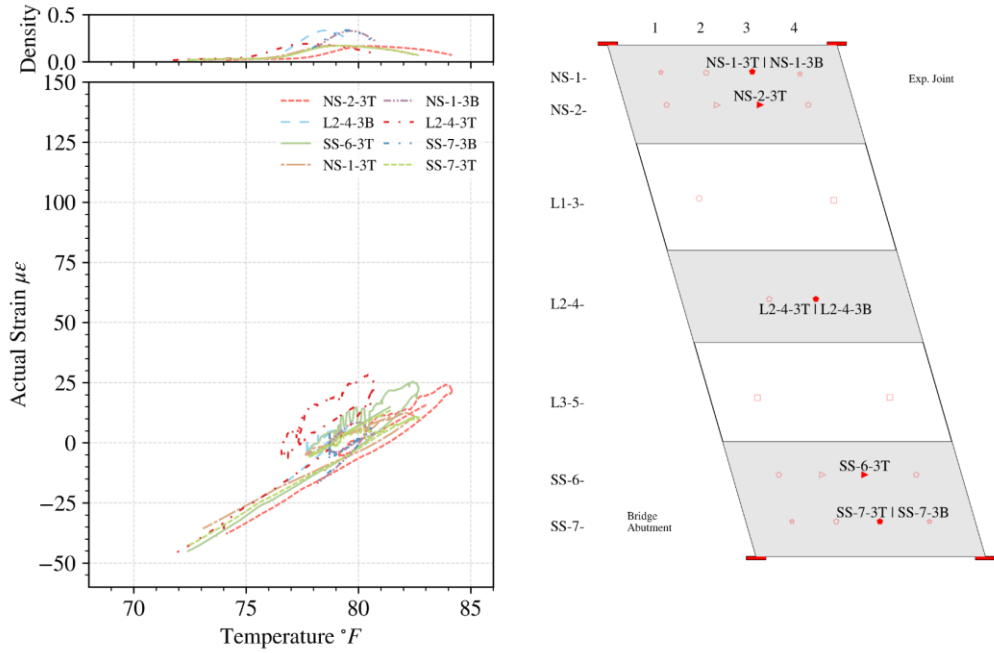
Figure 6.10 (c)
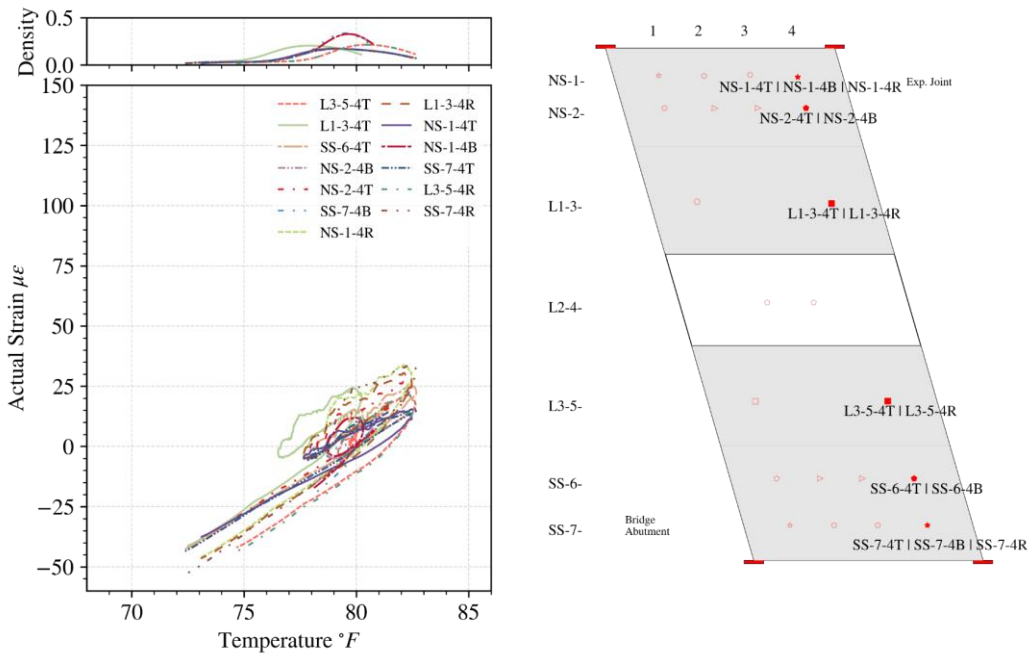
Figure 6.10 (d)

Figure 6.10 Actual strains vs. temperatures at Prospect Avenue: (a) transverse line 1, (b) transverse line 2, (c) transverse line 3, and (d) transverse line 4.
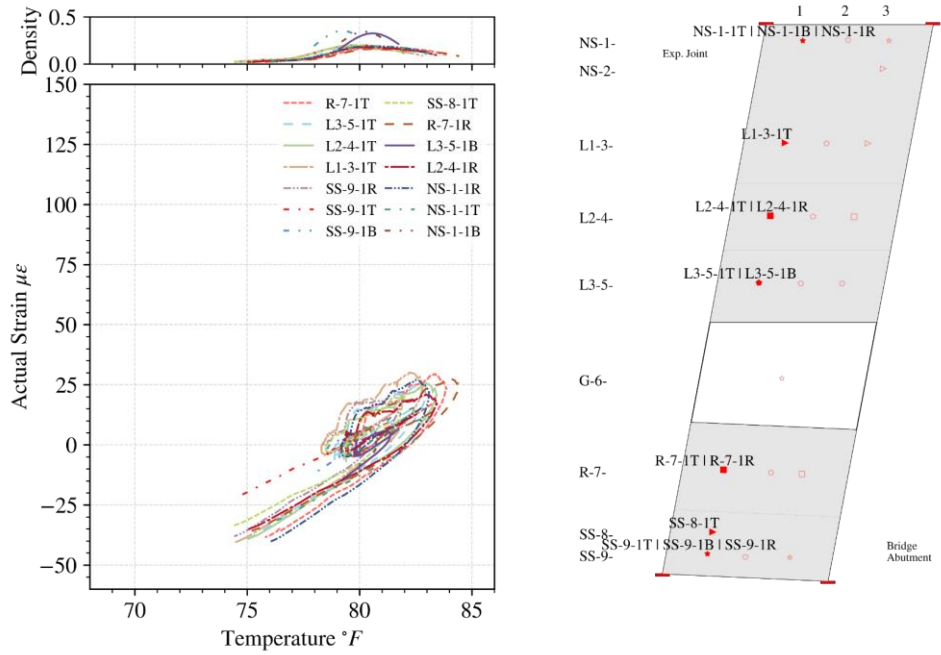
Figure 6.11 (a)
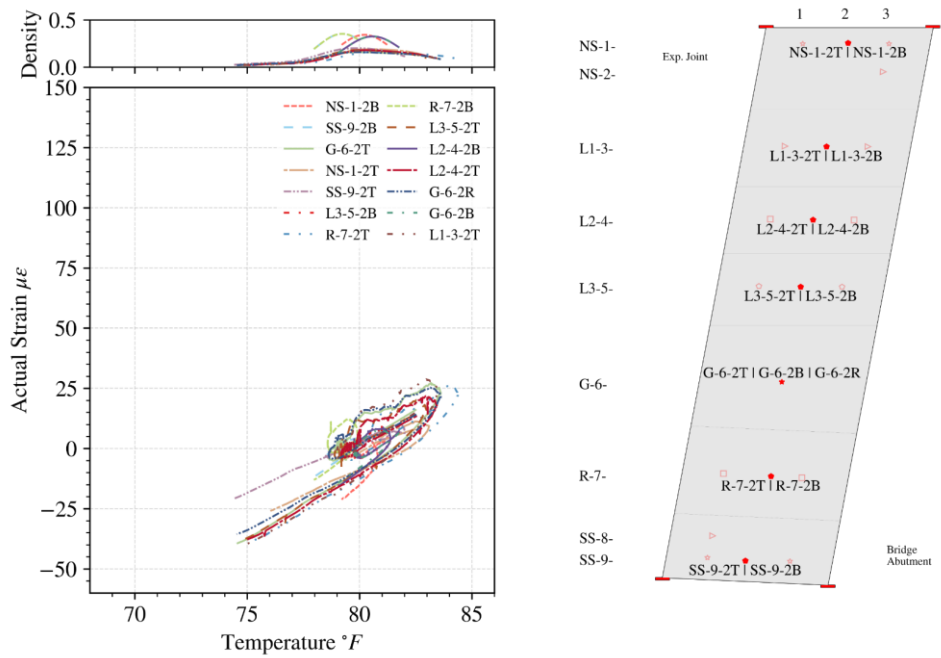
Figure 6.11 (b)
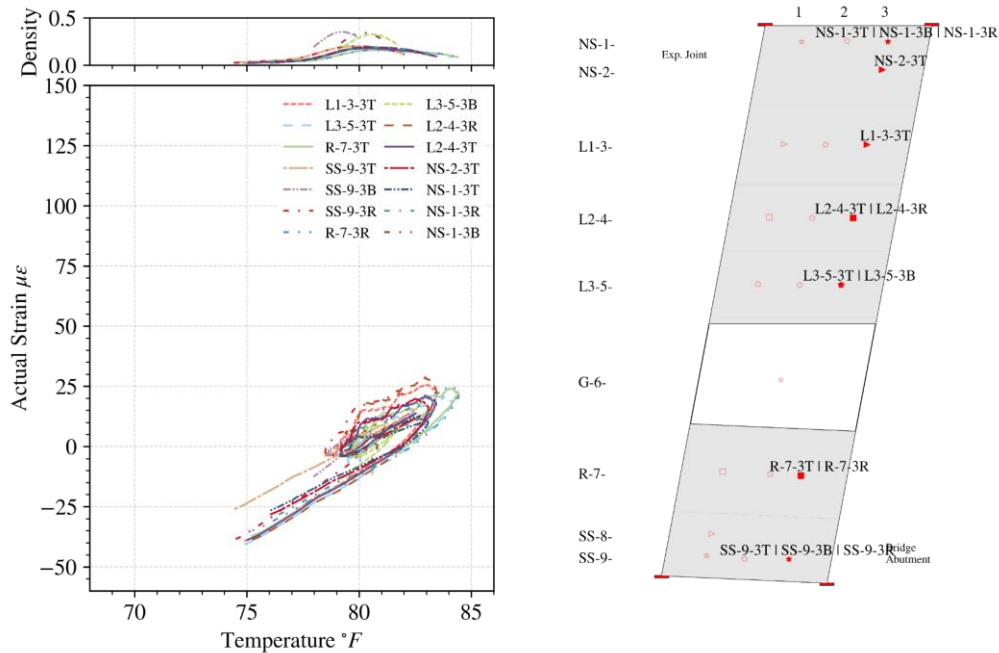
Figure 6.11 (c)

Figure 6.11 Actual strains vs. temperatures at Arlington Heights Road: (a) transverse line 1, (b) transverse line 2, and (c) transverse line 3.

6.2.2 Effects of Solar Radiation on Slab Behaviors

Ideally, for a concrete structure with constant restraints and subjected to uniform temperature changes as well as no additional external loads, the strain vs. temperature relationship should remain linear – i.e., a straight line in the strain vs. temperature plot, regardless of the type of strain. However, field data suggest loop-like behavior as shown in section 6.2.1 for the strain vs. temperature relationship of the monitored approach slabs and temperature compensation beams. Such loop-like behavior can be found more obviously in the apparent strains. Apparent strains are the raw strain readings multiplied by the batch gage factor, which are used to study the temperature related strains applied to the steel gage vibrating wires (see details in Appendix D). The slope of an apparent strain vs. temperature line accounts for both the restraint of the monitored structure and the difference in coefficient of thermal expansion (CTE) between a steel gage and concrete slab.

The loop-like strain vs. temperature behaviors in a single day can be observed from embedded strain gages in the temperature compensation beams, longitudinal gages at the top mat (T), transverse gages at the top mat (R), and longitudinal gages at the bottom mat (B), of which examples are shown in Figures 6.12, 6.13, 6.14, and 6.15, respectively. The loops are divided into two parts: **(a)** the time from sunrise to sunset, denoted by blue stars, and **(b)** the rest of the day, denoted by black dots. Two least square regression lines are created for the apparent strain of each gage: (1) the regression for all data of the day in a solid red line, and (2) the regression line only for the data in part (b) of the day, in which there was no solar radiation, in a dashed solid line.

176

It can be found that for all gages in the temperature compensation beams and top mat of the approach slabs, the red dashed regression line for the time without solar radiation roughly coincides with the apparent strain readings, indicating a strong linear trend between the apparent strains and temperatures. However, when there was solar radiation, i.e., between sunrise and sunset, additional tensile strains were developed in the steel gage vibrating wire, resulting in the loop-like behavior instead of solely linear trends. Additionally, for gages at the bottom mat, the red dashed regression lines do not match the strain readings in part (b) of the day as close as the gages at the top mat since the temperatures at the bottom portion of the approach slabs change more slowly, causing a lag in the temperature decrease after sunset.

By comparing the apparent strains during time range (a) and (b) at both top and bottom mats of the approach slabs, one can find the effects of solar radiation: approximately from the sunrise to sunset, solar radiation makes the approach slab temperature increase and the increase rate decreases from top to bottom of the approach slabs, leading to a temperature gradient though the slab thickness. Differential thermal deformations are developed due to the temperature gradient, with the top portion of the approach slab expanding more, which results in the concrete below the top surface being pulled, as proved by the additional increase in apparent strains when there is sunlight. As the solar radiation decreases gradually after sunset, the apparent strains at the top mat return to linear trends with the temperatures. The apparent strains at the bottom mat decrease without significant temperature changes because although the bottom mat temperatures are less sensitive to solar radiation, the expansion at the top portion of the slabs reduces significantly.
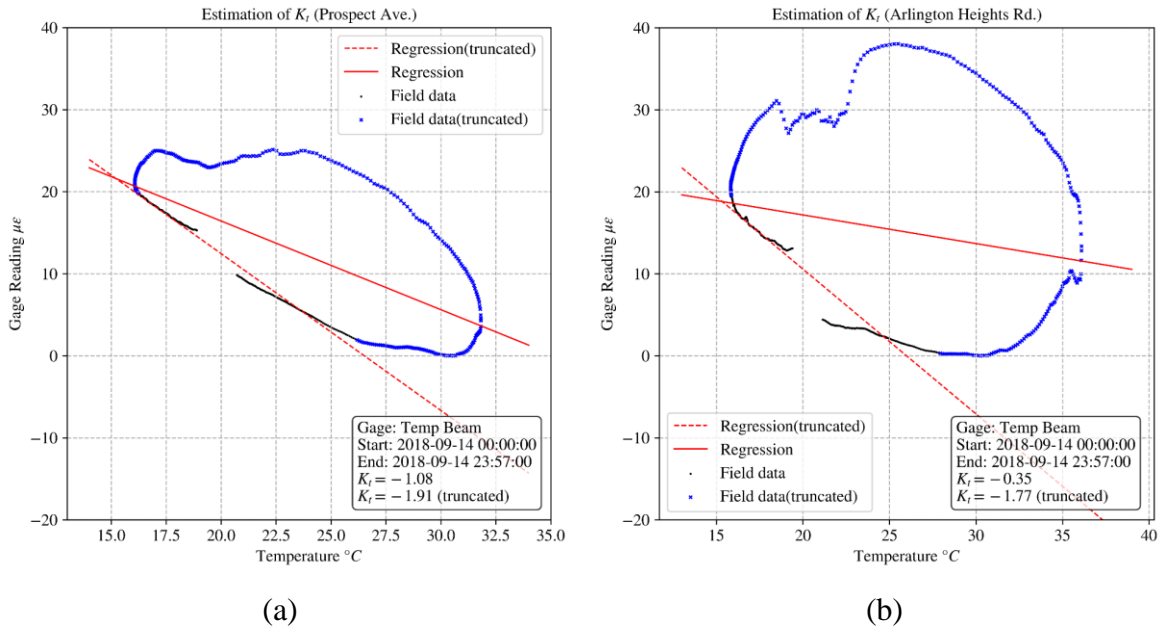
Figure 6.12 Apparent strain vs. temperature for temperature compensation beams: (a) Prospect Avenue, (b) Arlington Heights Road.

177
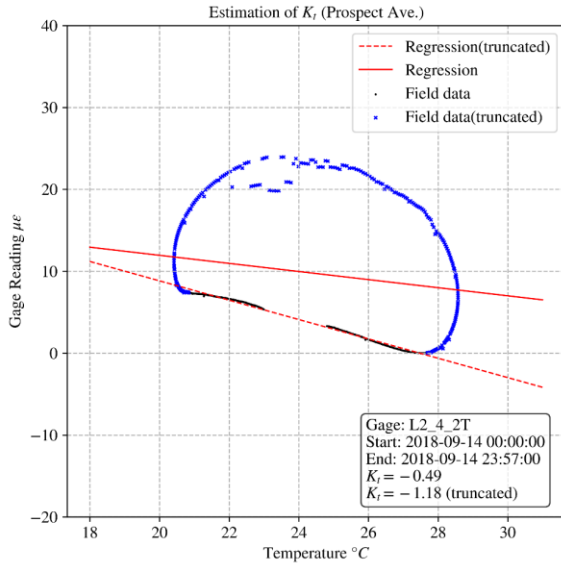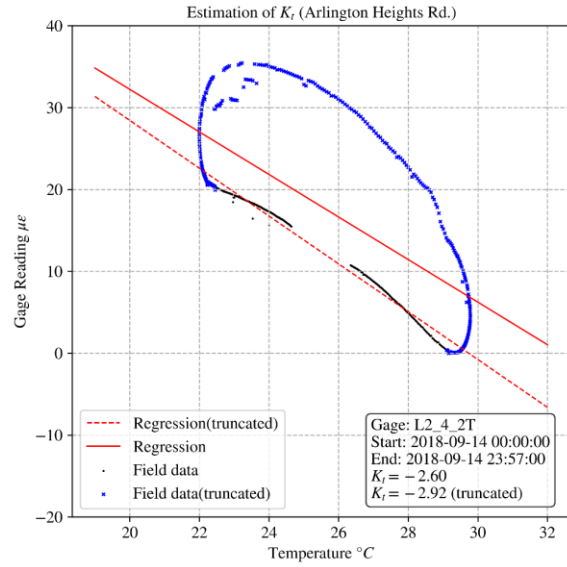
(a)   (b)

Figure 6.13 Apparent strain vs. temperature for longitudinal gages in top mat (T): (a) Prospect Avenue, (b) Arlington Heights Road.
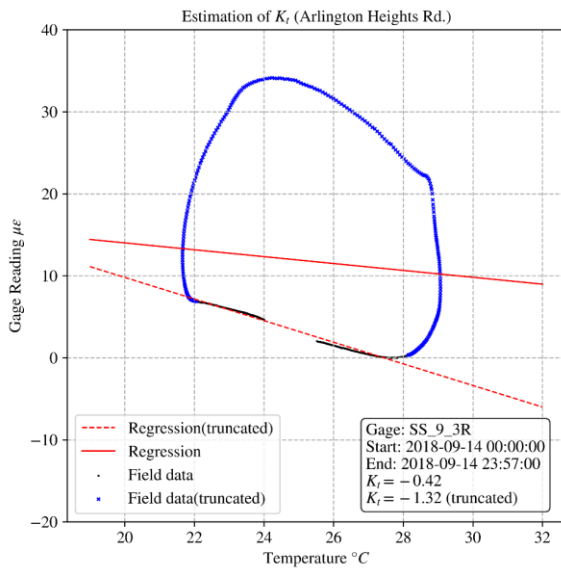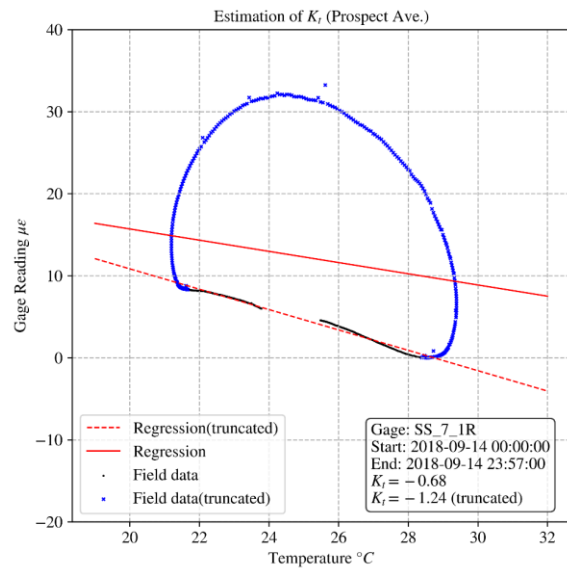
(a)   (b)

Figure 6.14 Apparent strain vs. temperature for transverse gages in top mat (R): (a) Prospect Avenue, (b) Arlington Heights Road.

178
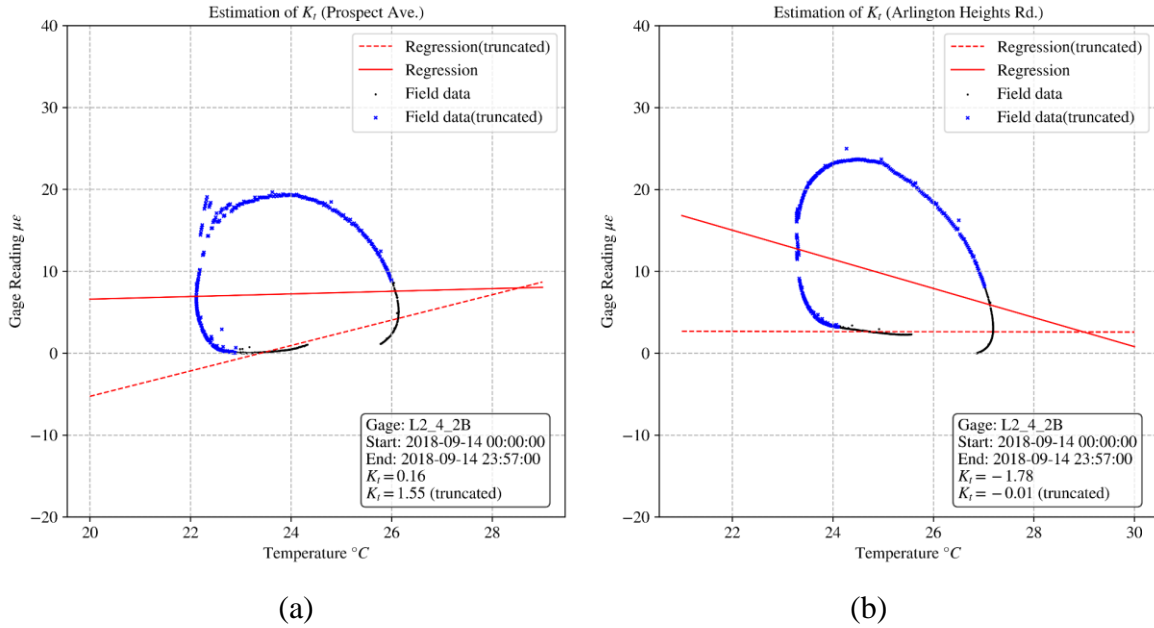
Figure 6.15 Apparent strain vs. temperature for longitudinal gages in bottom mat (R): (a) Prospect Avenue, (b) Arlington Heights Road.

6.2.3 Load Related Strains

Load related strains depict the strains that are related to stresses developed in the structure caused by combined effects of live loads and thermal loads. To understand how load related strains change on a daily basis, the time history and load related strains vs. temperature relationship are studied. Like the calculation of actual strains, the reference readings for the load related strains are set to be 6:00 AM on each test day to account for the solar radiation effects.

6.2.3.1 Test Day of 9/14/2018

The load related strain for most gages at both approach slabs became greater in tension in the morning after sunrise and started to decrease (a) at around noon for gages at the top mat in both longitudinal and transverse direction, and (b) after 3:00 PM for gages at the bottom mat. The load related strains reached their lowest values around 7:00 PM, about 30 minutes before sunset. The lowest values are around zero for most gages at Prospect Avenue, whereas the counterparts at Arlington Heights Road can be negative (compressive). The difference in the strain change for the top mat and bottom mat is attributed to the temperature gradient through thickness. Since the temperature increase for the top mat is faster than that of the bottom mat, the tensile stress/strain due to the uneven temperatures compared to the top surface reduces sooner at the top mat. In addition, the restraint of the approach slab introduces compression when the slabs expand. It is noteworthy that the longitudinal gages at the top mat on the exterior side of the approach slab shoulders exhibit significant compressive load related strains, as shown in Figure 6.16 for Prospect Avenue and Figure 6.17 for Arlington Heights Road. The load related strain vs. temperature relationships shown in Figures 6.18 and 6.19 for Prospect Avenue and Arlington Heights Road,

respectively, suggest that the restraint level, indicated by the slope of the loops, at the exterior side of the shoulders is higher than the rest of the approach slabs.
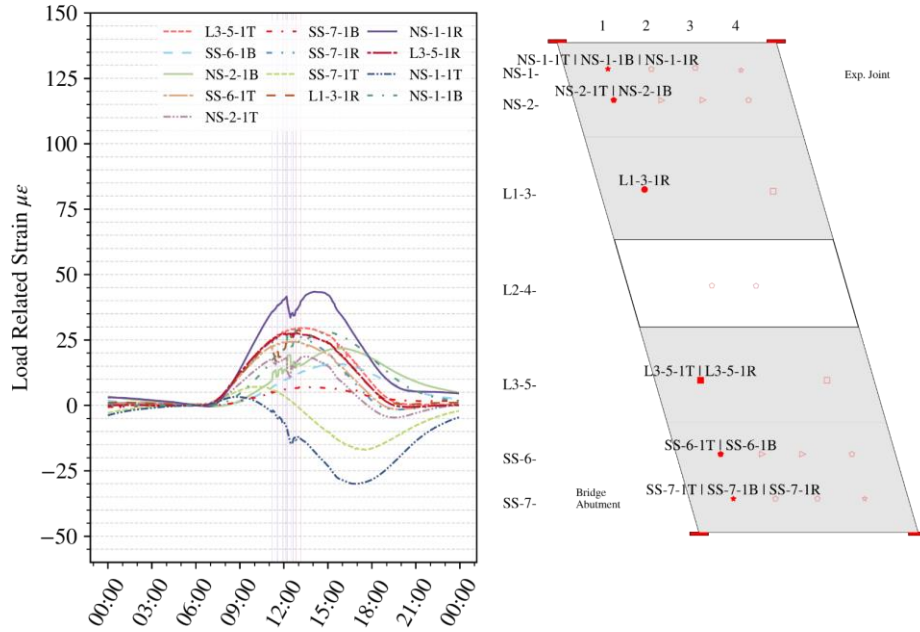
Figure 6.16 (a)
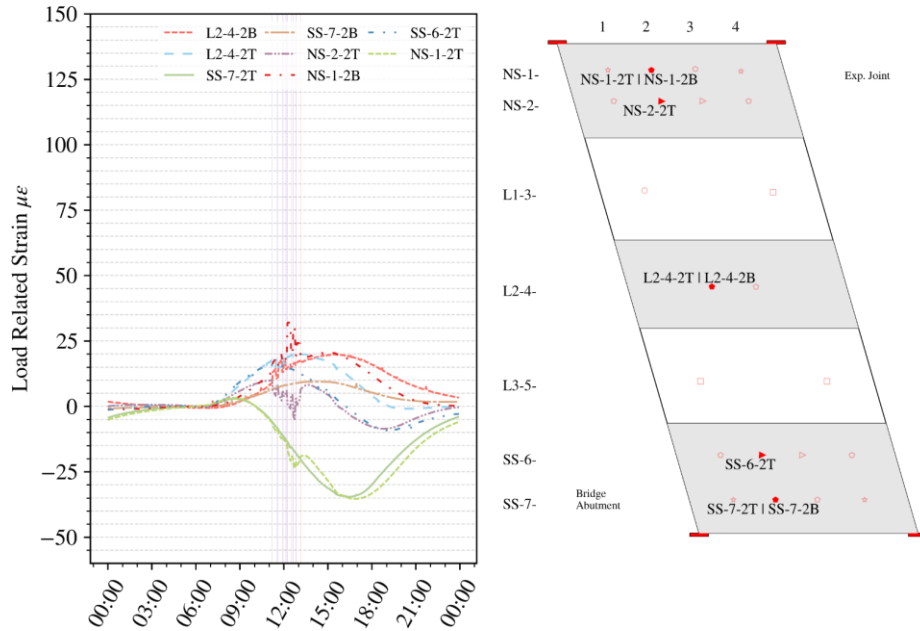
Figure 6.16 (b)
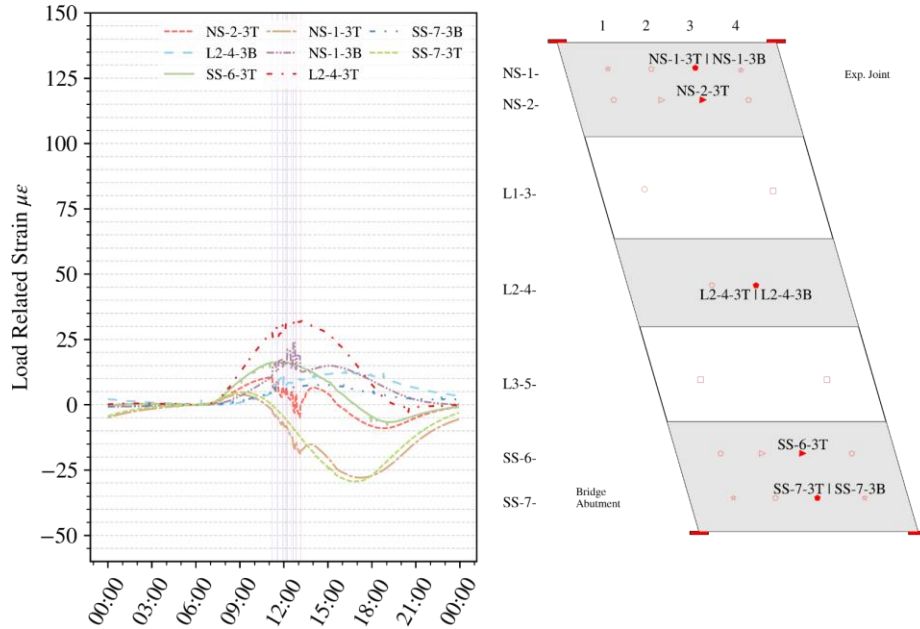
Figure 6.16 (c)
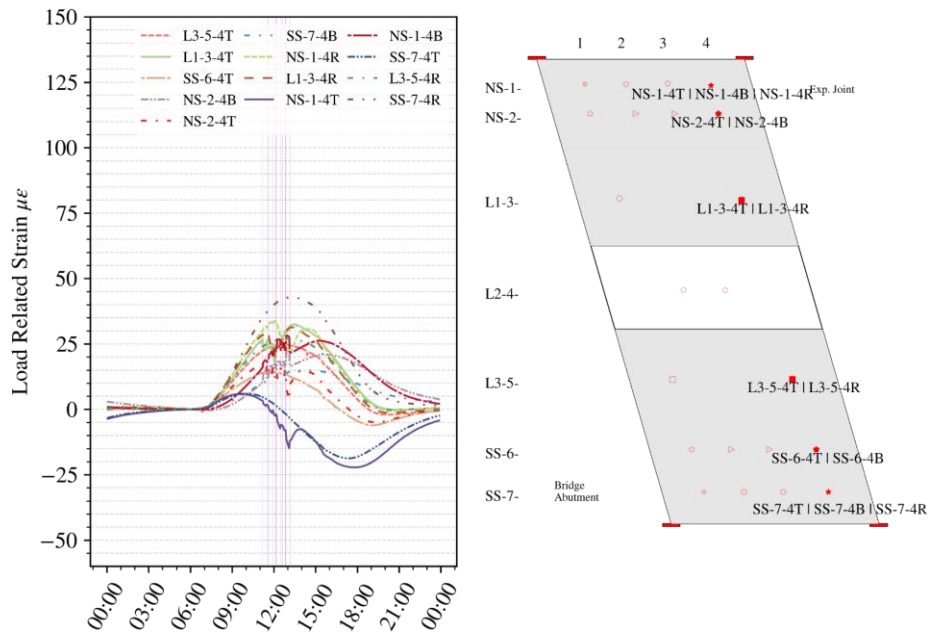
Figure 6.16 (d)

Figure 6.16 Load related strains at Prospect Avenue on 9/14/2018: (a) transverse line 1, (b) transverse line 2, (c) transverse line 3, and (d) transverse line 4.
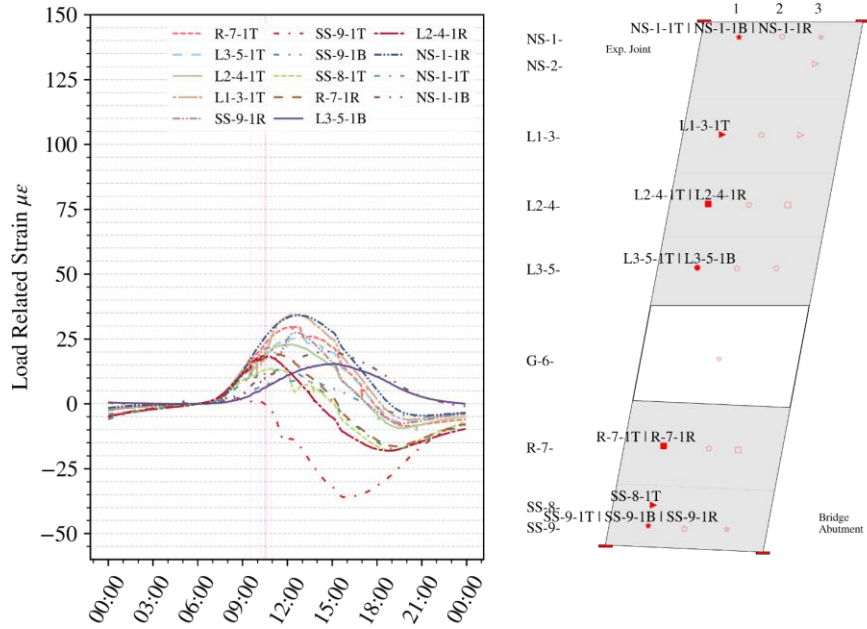
Figure 6.17 (a)
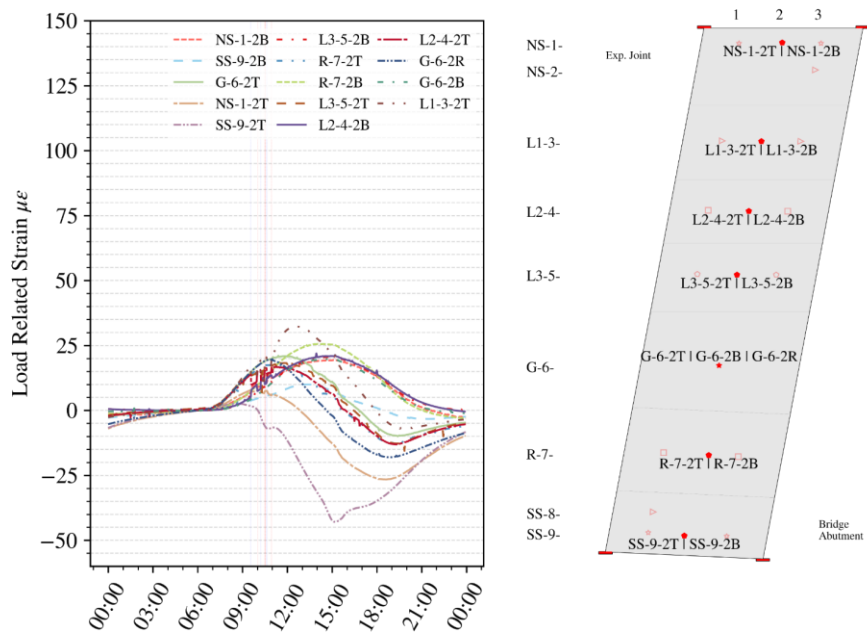
Figure 6.17 (b)
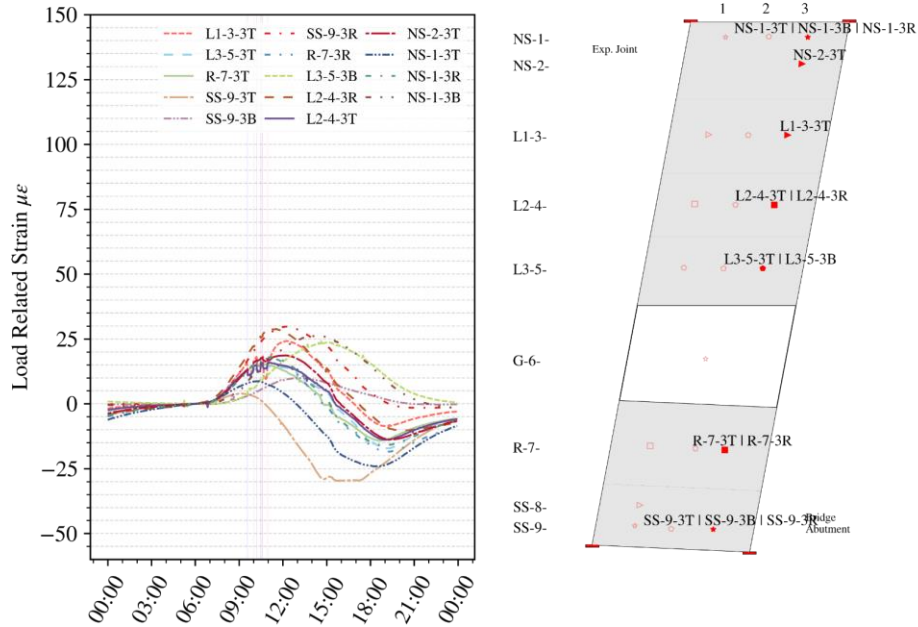
Figure 6.17 (c)

Figure 6.17 Load related strains at Arlington Heights Road on 9/14/2018: (a) transverse line 1, (b) transverse line 2, and (c) transverse line 3.
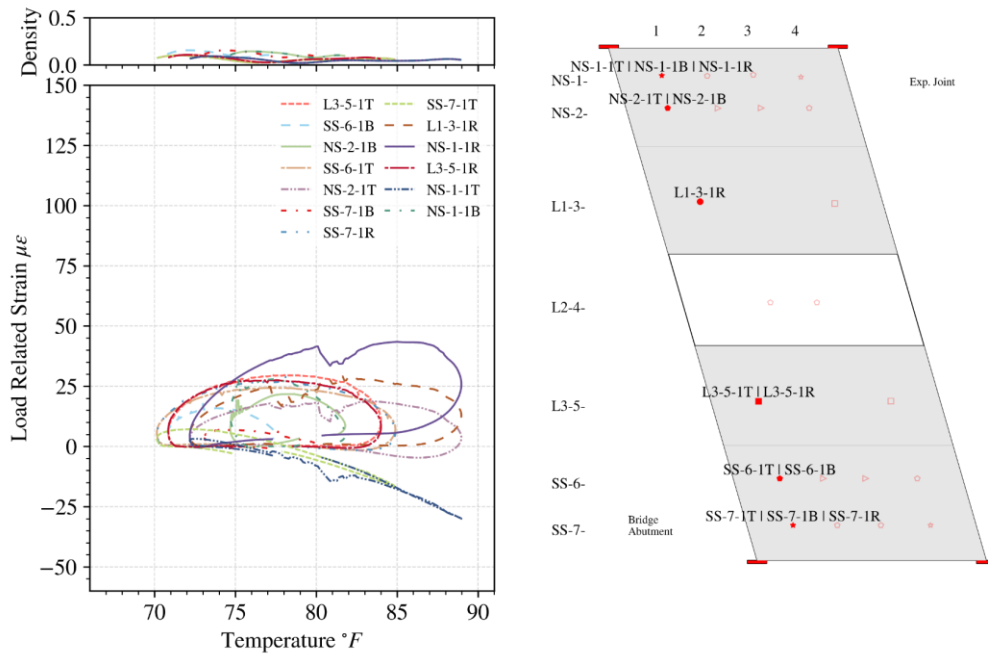
Figure 6.18 (a)
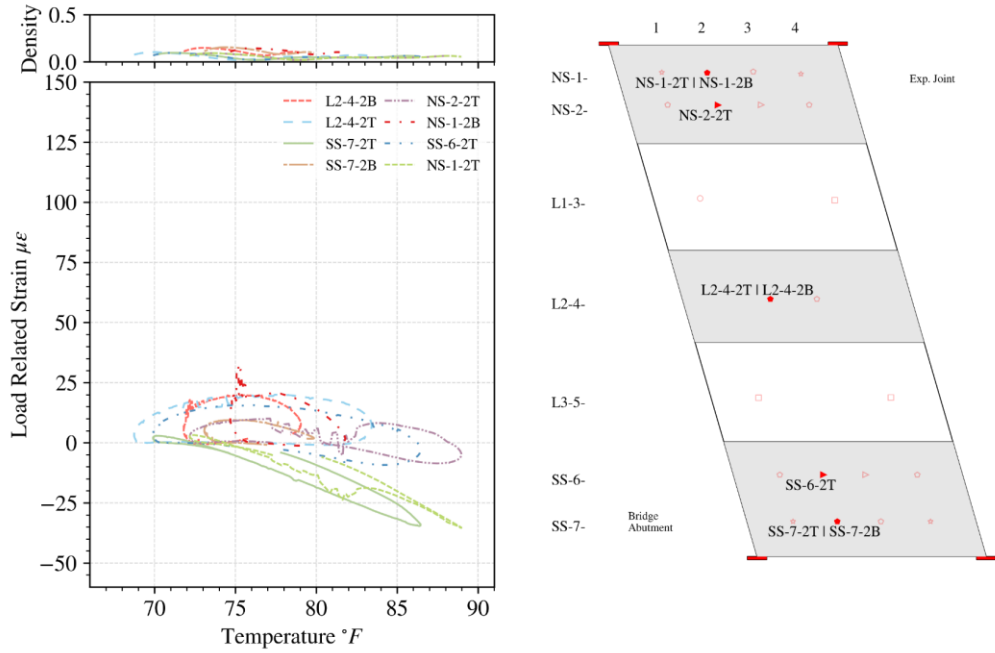
Figure 6.18 (b)
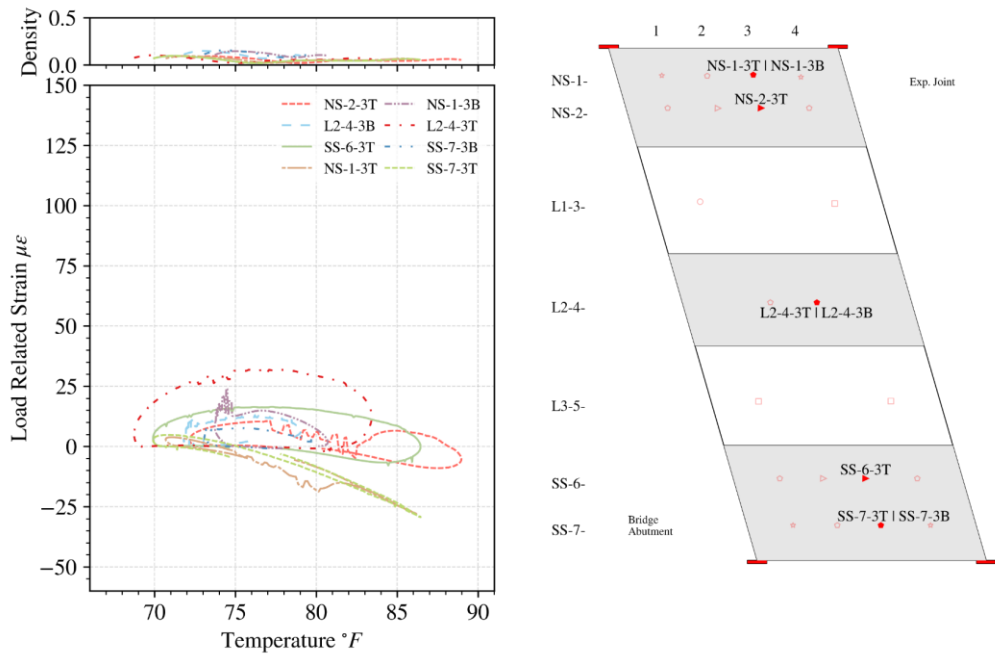
Figure 6.18 (c)
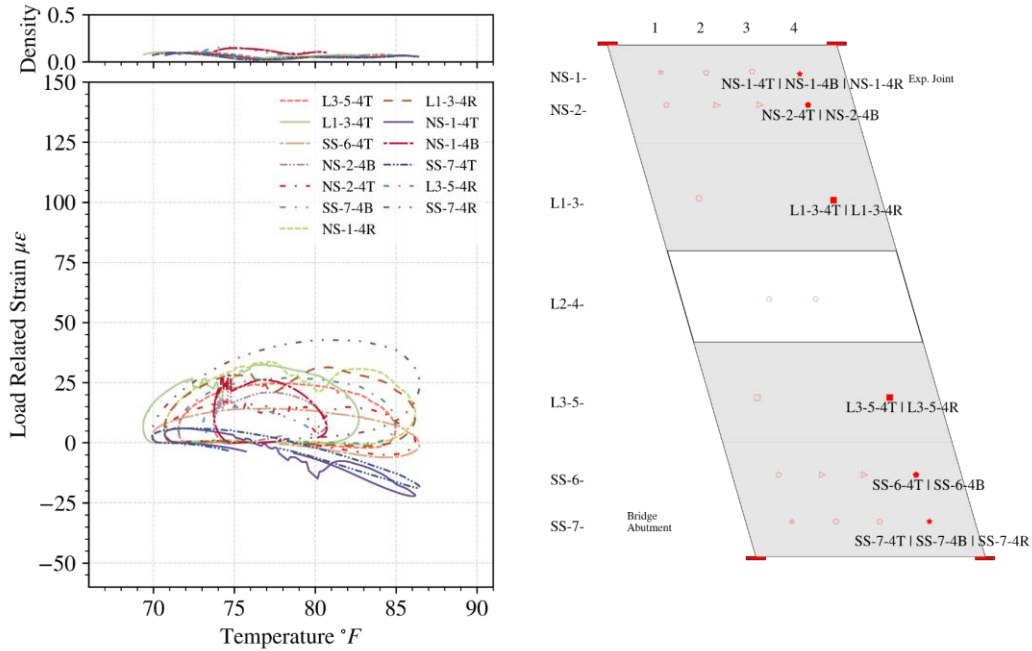
Figure 6.18 (d)

Figure 6.18 Load related strains vs. temperatures at Prospect Avenue on 9/14/2018: (a) transverse line 1, (b) transverse line 2, (c) transverse line 3, and (d) transverse line 4.
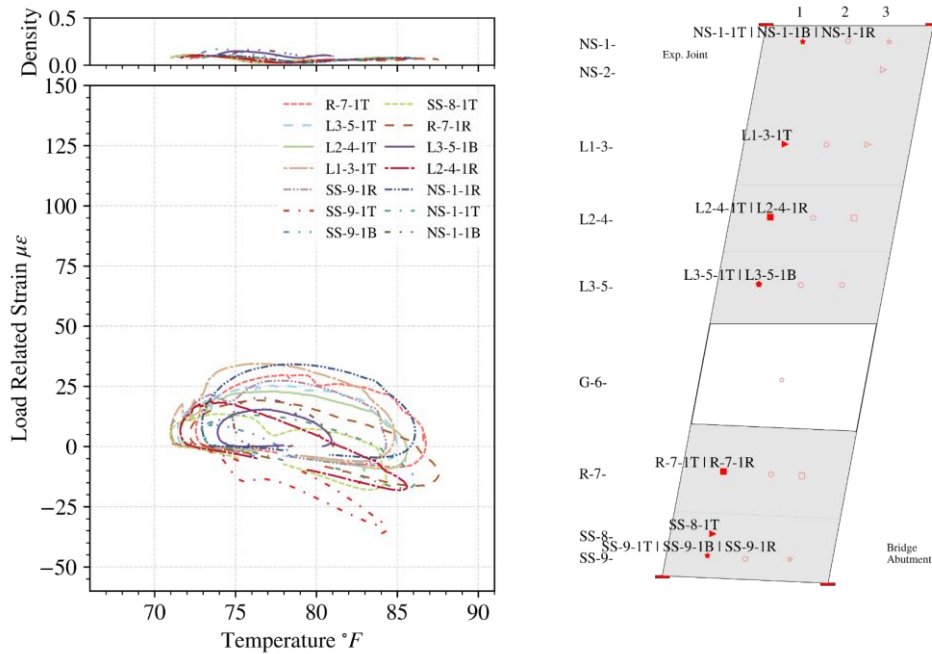
Figure 6.19 (a)
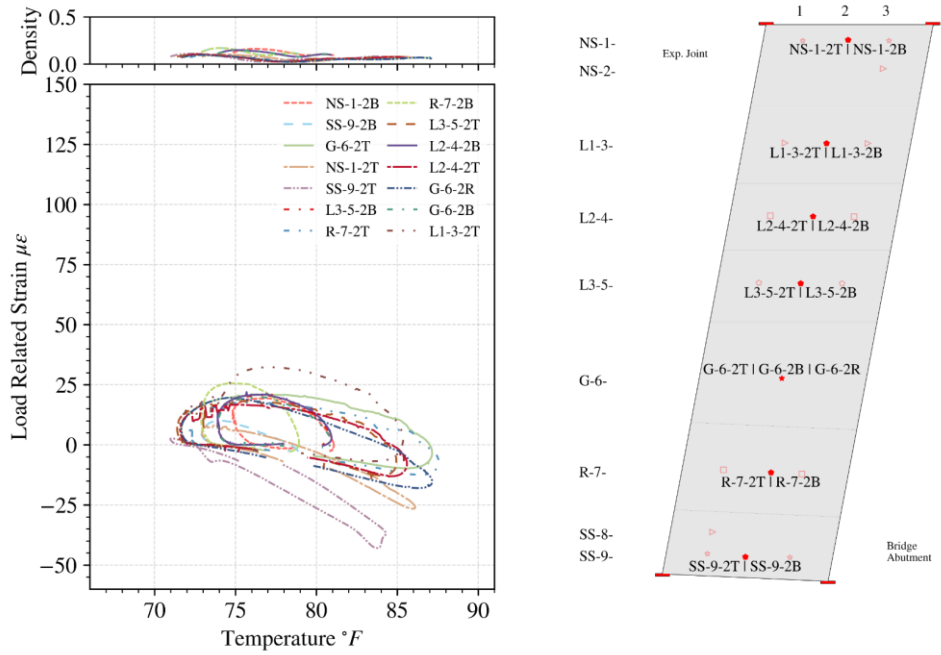
Figure 6.19 (b)
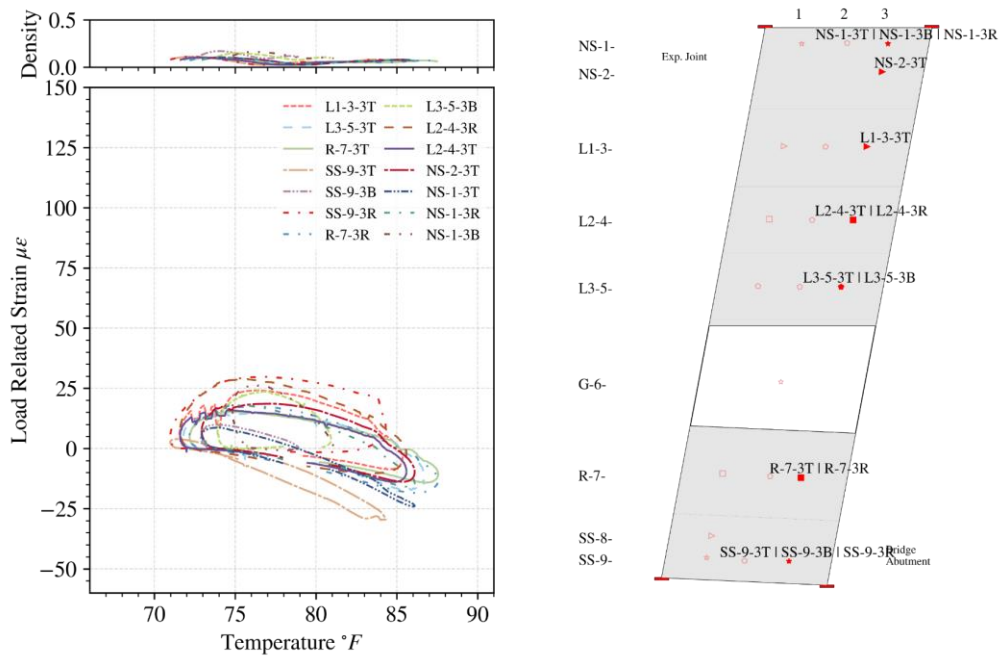
Figure 6.19 (c)

Figure 6.19 Load related strains vs. temperatures at Arlington Heights Road on 9/14/2018: (a) transverse line 1, (b) transverse line 2, and (c) transverse line 3.

6.2.3.2 Test Day of 9/21/2018

The load related strains for test day 9/21/2018 exhibit similar trends to 9/14/2018, with a smaller range since the temperature variation ranges are narrower than 9/14/2018. The response histories of the load related strains at Prospect Avenue and Arlington Heights Road are presented in Figure 6.20 and Figure 6.21, respectively. The load related strain vs. temperature relationships is shown in Figures 6.22 and Figure 6.23 for Prospect Avenue and Arlington Heights Road, respectively.
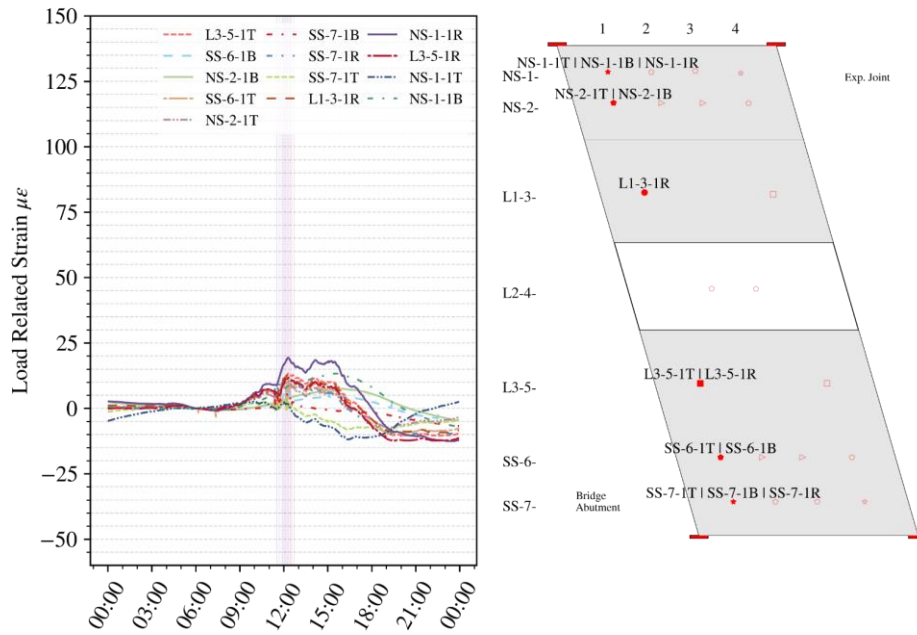
Figure 6.20 (a)
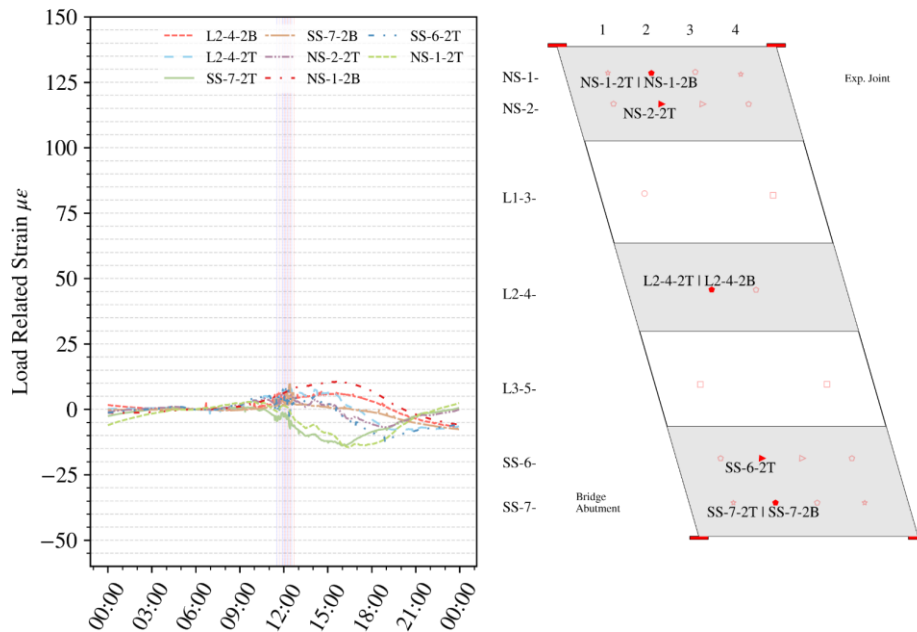
Figure 6.20 (b)
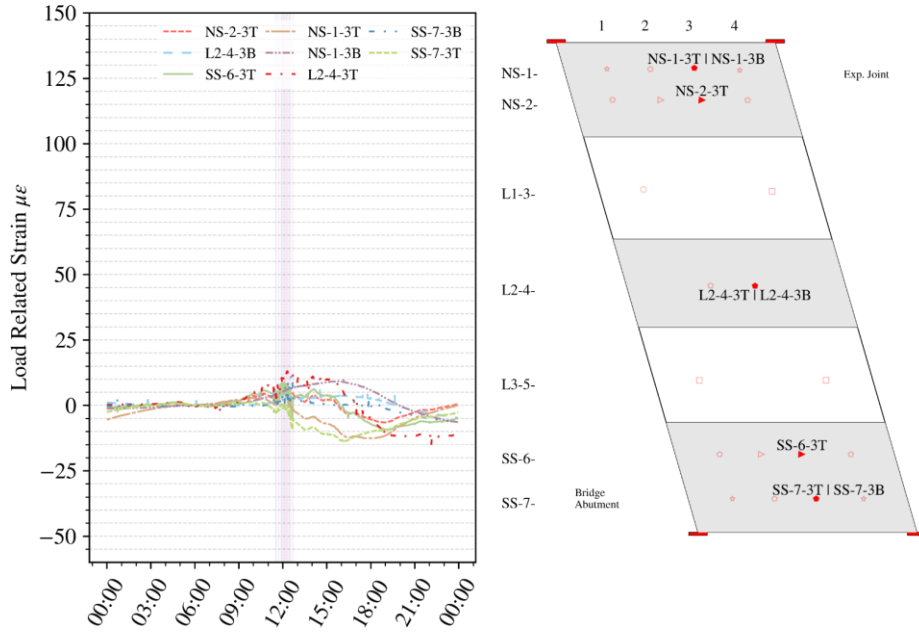
Figure 6.20 (c)
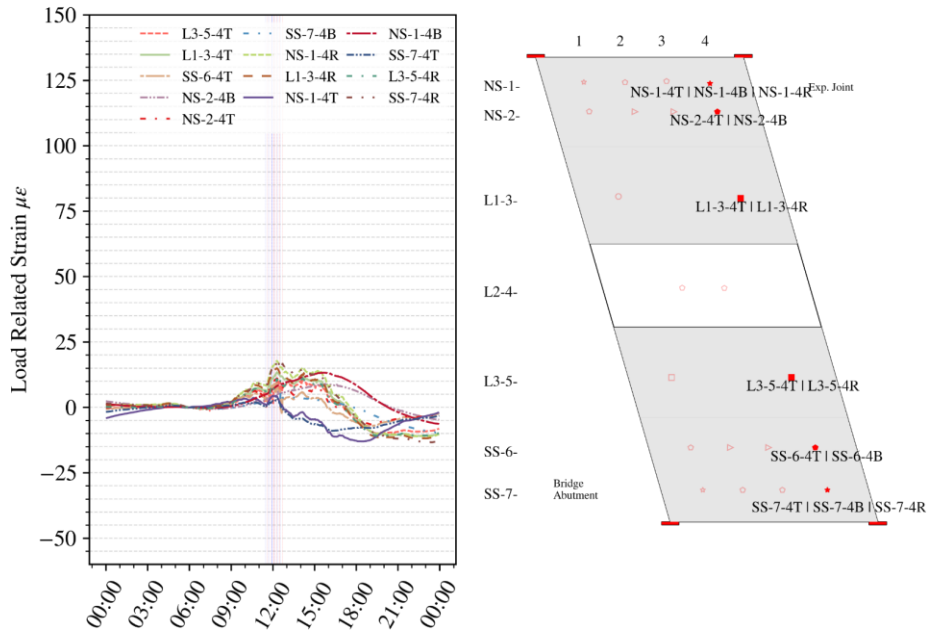
Figure 6.20 (d)

Figure 6.20 Load related strains at Prospect Avenue on 9/21/2018: (a) transverse line 1, (b) transverse line 2, (c) transverse line 3, and (d) transverse line 4.
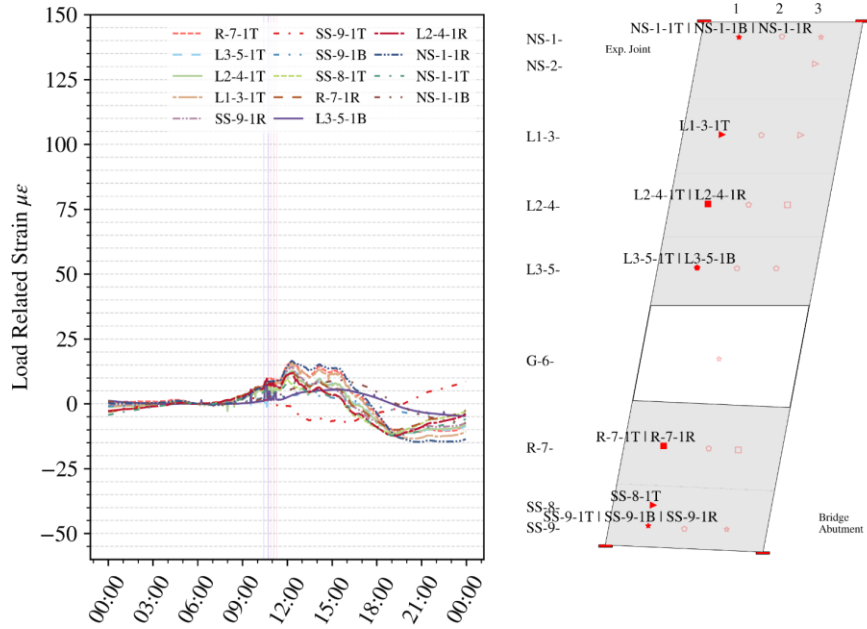
Figure 6.21 (a)
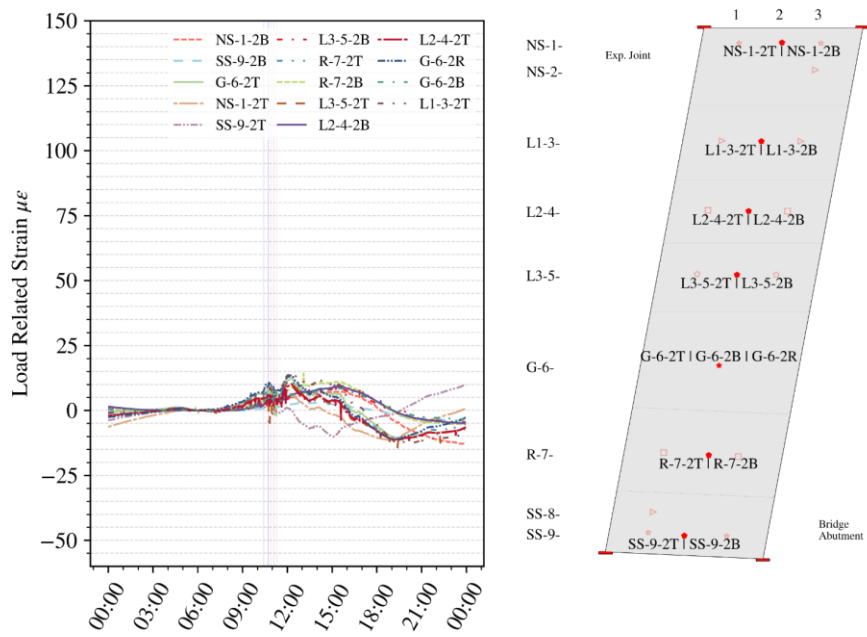
Figure 6.21 (b)
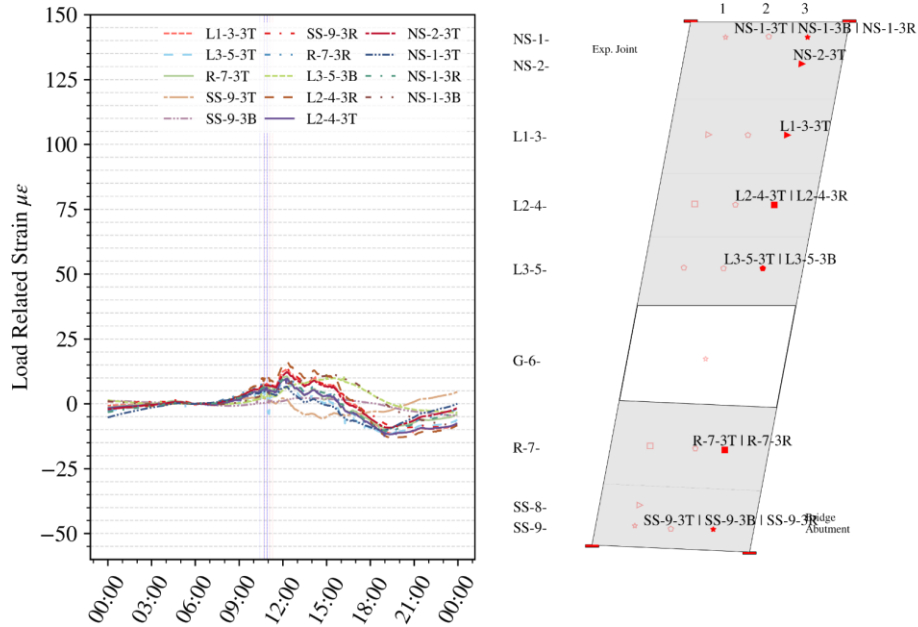
Figure 6.21 (c)

Figure 6.21 Load related strains at Arlington Heights Road on 9/21/2018: (a) transverse line 1, (b) transverse line 2, and (c) transverse line 3.
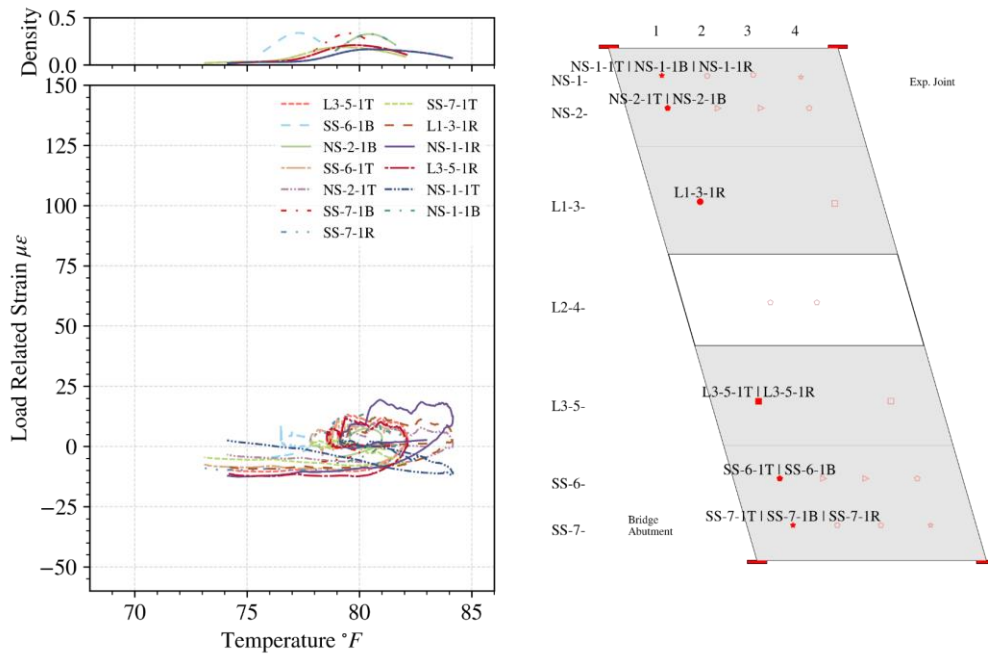
Figure 6.22 (a)
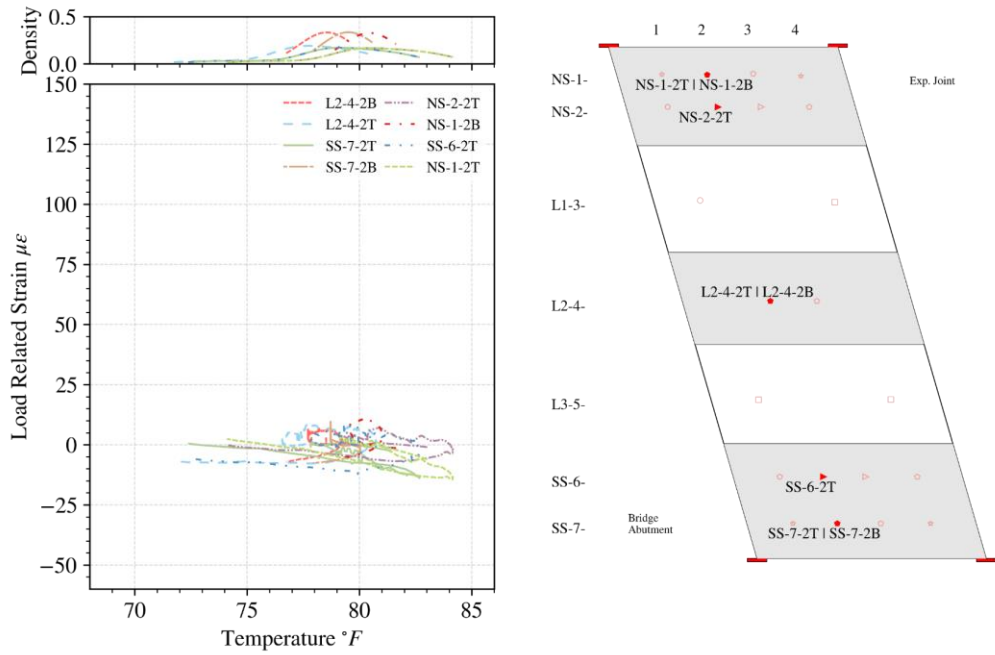
Figure 6.22 (b)
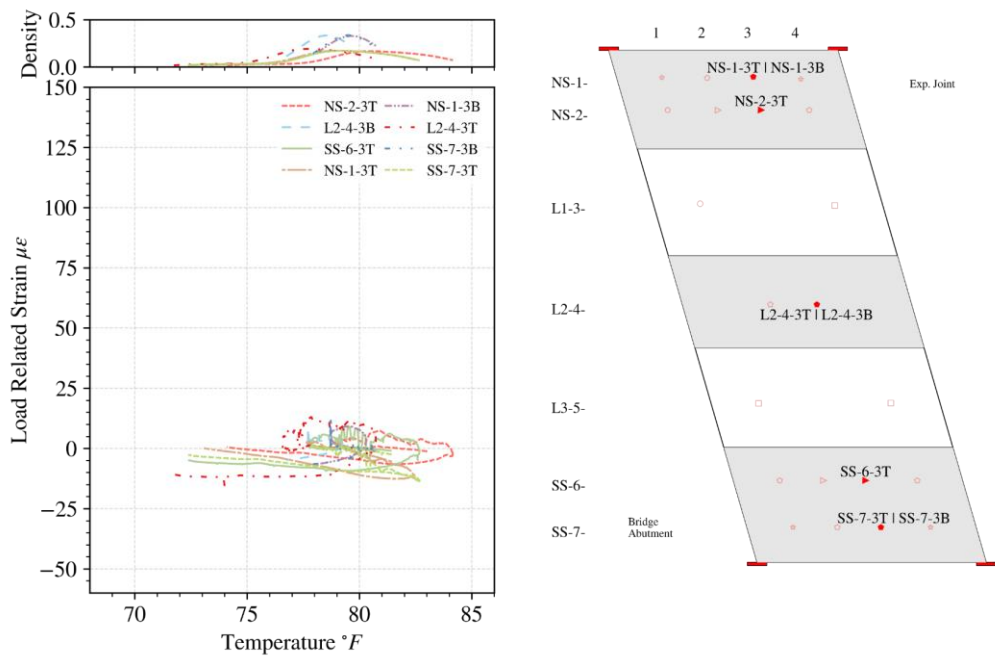
Figure 6.22 (c)
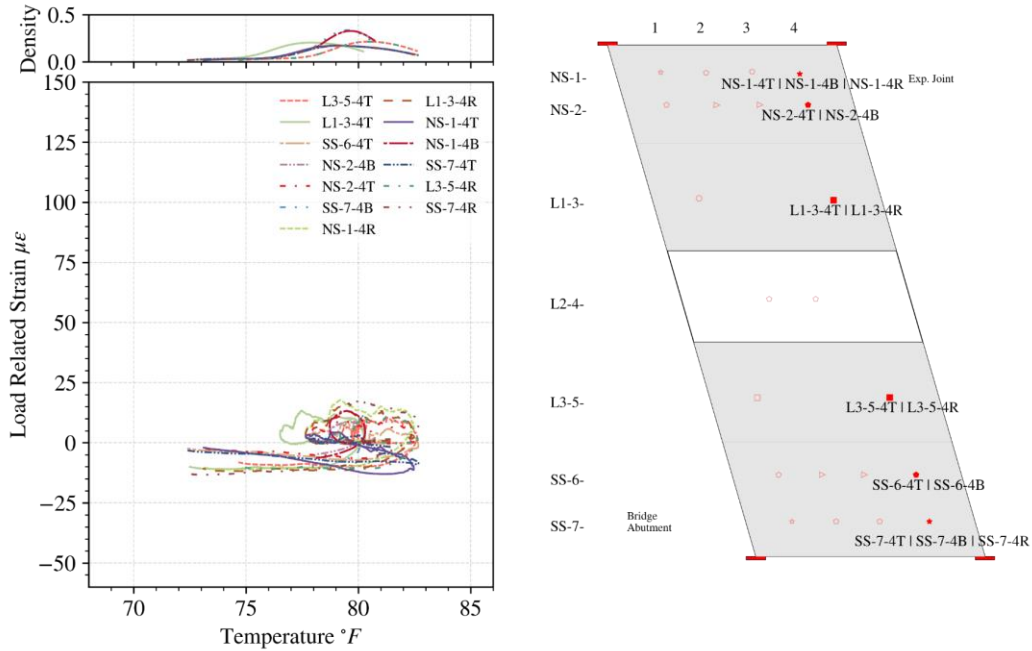
Figure 6.22 (d)

Figure 6.22 Load related strains vs. temperatures at Prospect Avenue on 9/21/2018: (a) transverse line 1, (b) transverse line 2, (c) transverse line 3, and (d) transverse line 4.

Figure 6.23 (a)

192
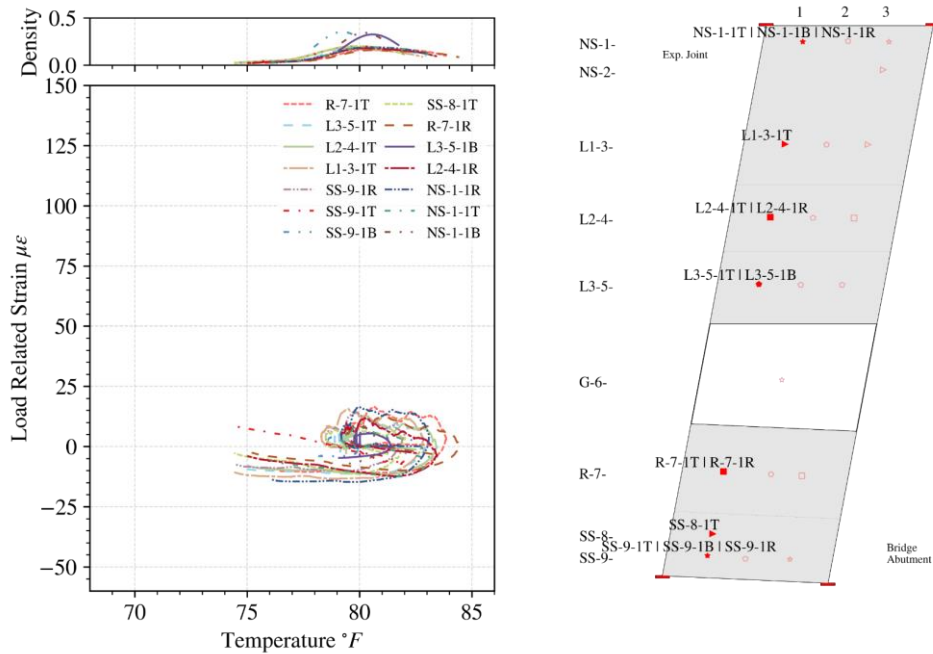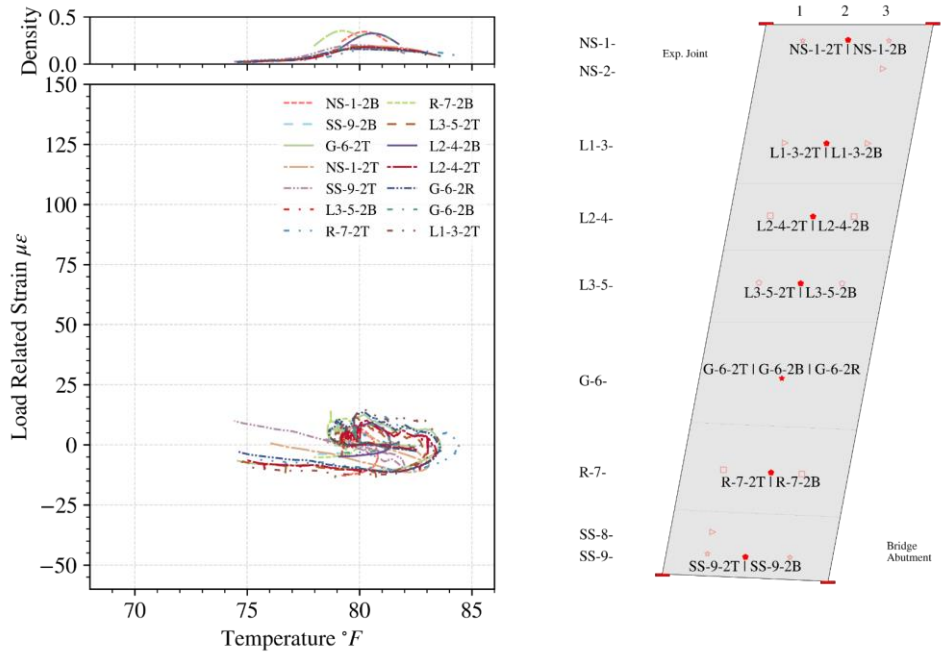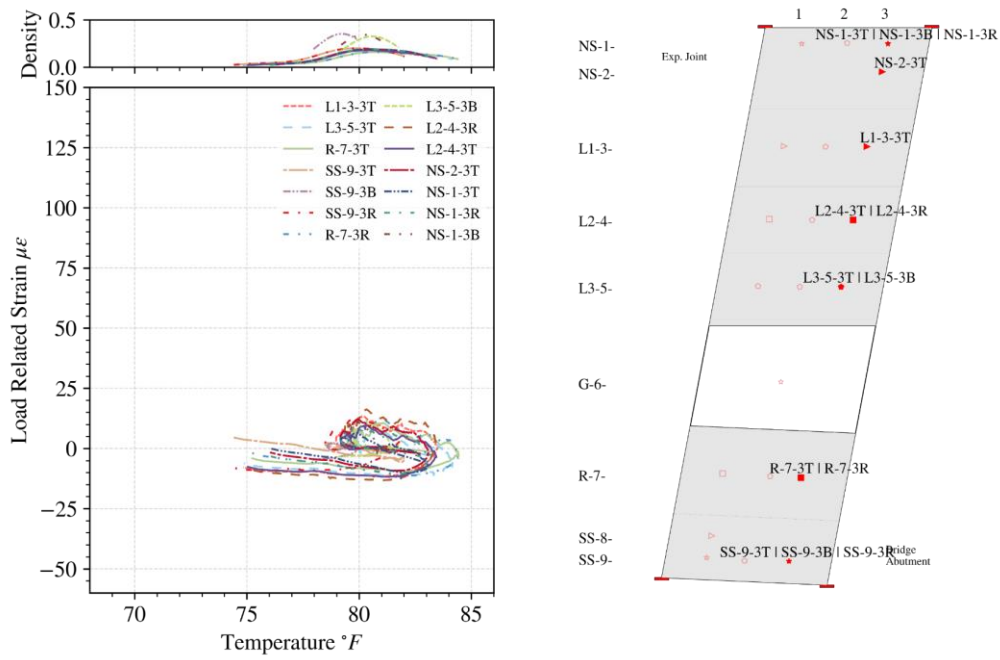
Figure 6.23 (b)

Figure 6.23 (c)

Figure 6.23 Load related strains vs. temperatures at Arlington Heights Road on 9/21/2018: (a) transverse line 1, (b) transverse line 2, and (c) transverse line 3.

6.2.4 Truck-induced Strains

Even over the course of one day (24 hours), the load related strains due to thermal effects still make significant contributions compared to the live loads. Consequently, and in order to capture the effect of live load on the slabs, the strain changes caused by only the live load were calculated. This is accomplished by subtracting the strain variations due to temperature changes from the total strains observed in the slab, of which an example is shown in Figure 6.24. The load related strain is not constant due to temperature variations in Figure 6.24 (a). The estimated truck-induced strain excluded thermal effects so that the strains roughly remain constant when there is no change of live loads.
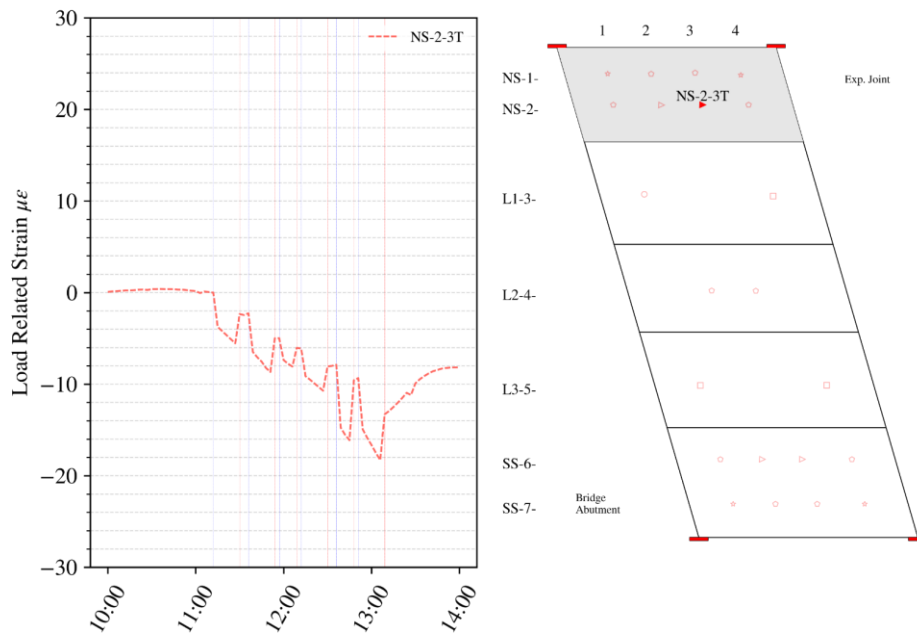
Figure 6.24 (a)
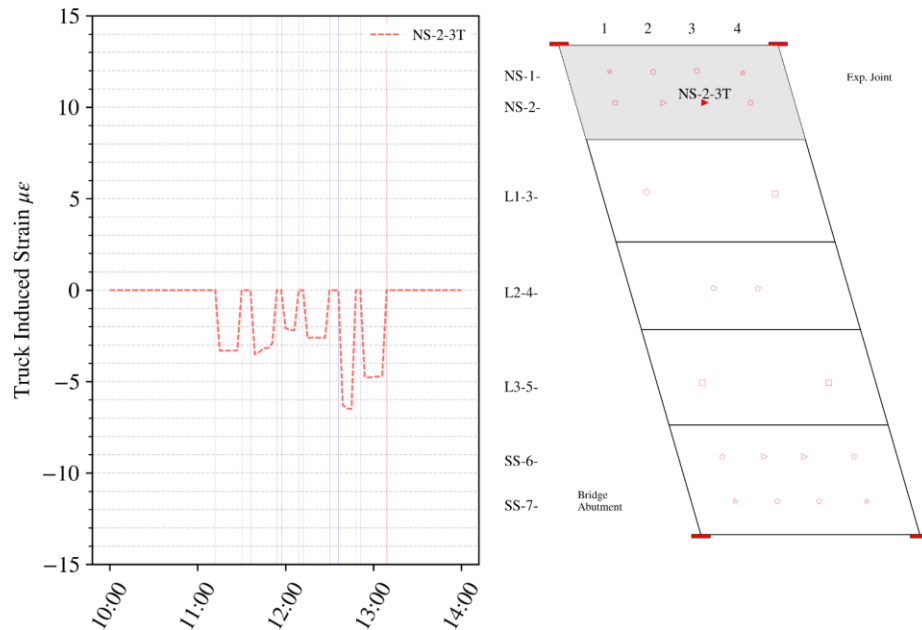
Figure 6.24 (b)

Figure 6.24 Example of truck-induced strains calculation for gage NS-2-3T at Prospect Avenue on 9/14/2018: (a) load related strains, (b) estimated truck-induced strains.

The estimated truck-induced strains are studied by comparing gages in the longitudinal and transverse direction for each truck loading test. Since the observed distribution patterns are similar among the test days, only the details of test day 9/14/2018 are explicitly presented in this section. The results for test day 9/21/2018 are included in Appendix F.

Field instrumentation and monitoring may cause some uncertainties to be introduced to the computed truck-induced strains. The main factors include: (1) gage installation and position measurements, (2) embedded vibrating wire gage resolution and error, (3) construction dimension and location errors, (4) concrete and steel material property measurements.

6.2.4.1 Distribution along Longitudinal Direction

On 9/14/2018, at Prospect Avenue, Lane 1 (L1) was loaded in tests 4, 5, and 6, and the north shoulder (NS) was loaded in tests 7, 8, and 9 (Figure 6.1 (c)). At Arlington Heights Road, Lane 1 (L1) was loaded in tests 1, 2, and 3. The corresponding truck locations are shown in Figure 6.1 (a).

In general, when the truck is on the slab, compressive strains are observed from longitudinal gages at the top mat (T), and tensile strains are found from longitudinal gages at the bottom mat (B), suggesting positive bending of the slabs due to the truck loads. Both compressive and tensile strains are obtained from transverse gages at the top mat (R). The truck-induced strains reached the greatest magnitudes (up to 14 με) at and near the section/lane that was loaded. The further a

sensor is away from the test truck, the smaller is the effect of static truck loading on the strains at the sensor locations. The truck-induced strains along the longitudinal direction for the loaded sections and the sections adjacent to them are shown in Figures 6.25 and 6.26 for Prospect Avenue and Arlington Heights Road, respectively.

An exception to the longitudinal gage at the top mat (T) exhibiting compressive strains is NS-1-1T, as shown in Figure 6.25 (a). In tests 4, 5, 6, 8, and 9, tensile strains are observed due to the truck loading. This phenomenon may be related to the boundary conditions at the northwest corner of the approach slab. It is found that the tensile strains for gages at the bottom mat (B) are significantly greater than the gages with the same location at the top mat (T), which may be attributed to the flexural stiffness provided by the parapets. When the parapet is considered to act compositely with the approach slab, the neutral axis will shift up.
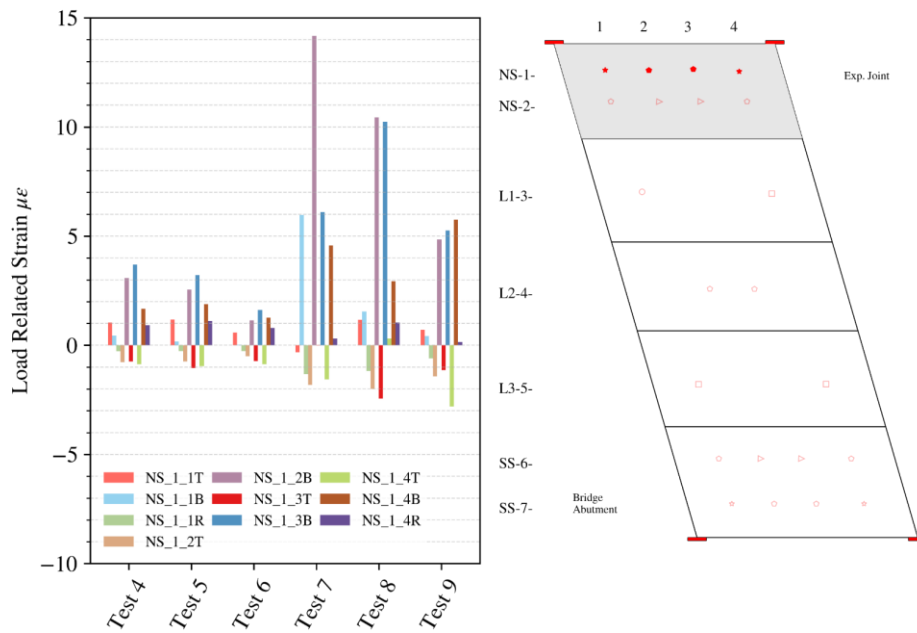
Figure 6.25 (a)
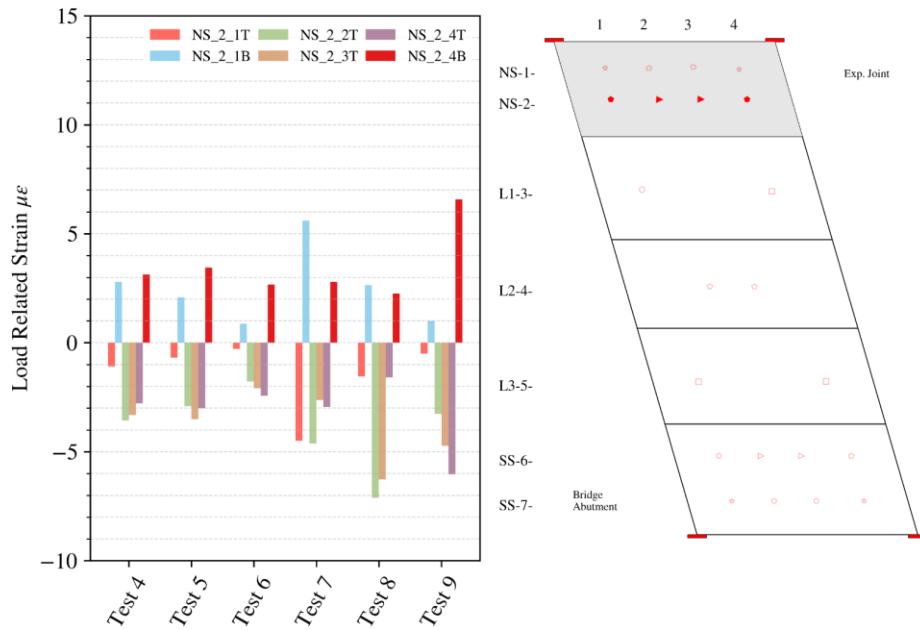
Figure 6.25 (b)
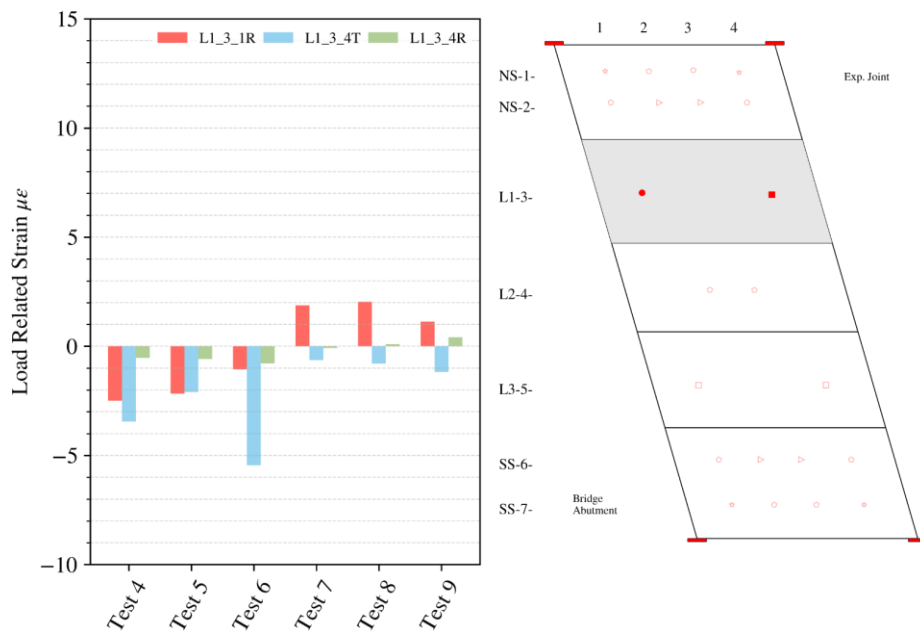
Figure 6.25 (c)
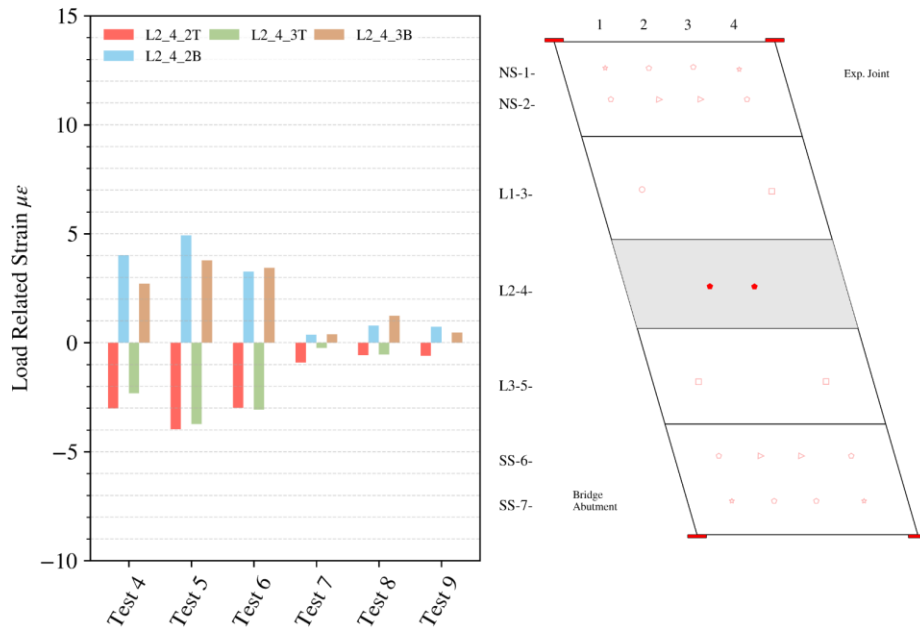
Figure 6.25 Truck-induced strains at Prospect Avenue on 9/14/2018: (a) longitudinal line NS-1, (b) longitudinal line NS-2, (c) longitudinal line L1-3, and (d) longitudinal line L2-4.
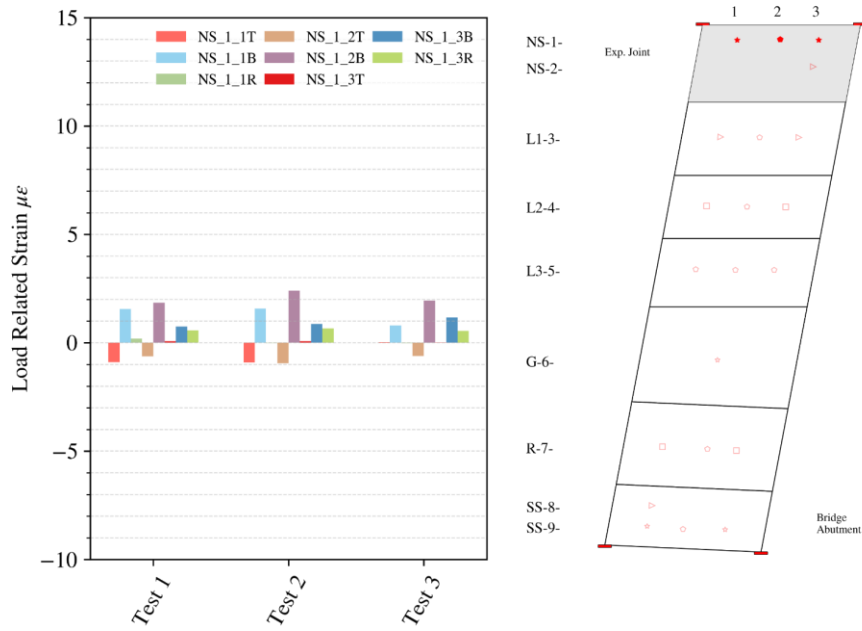
Figure 6.26 (a)
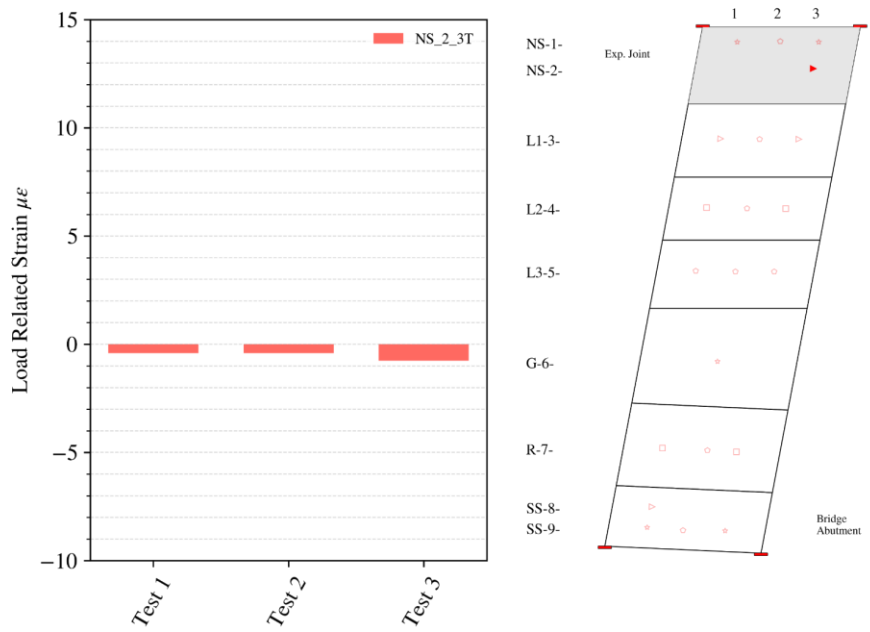
Figure 6.26 (b)
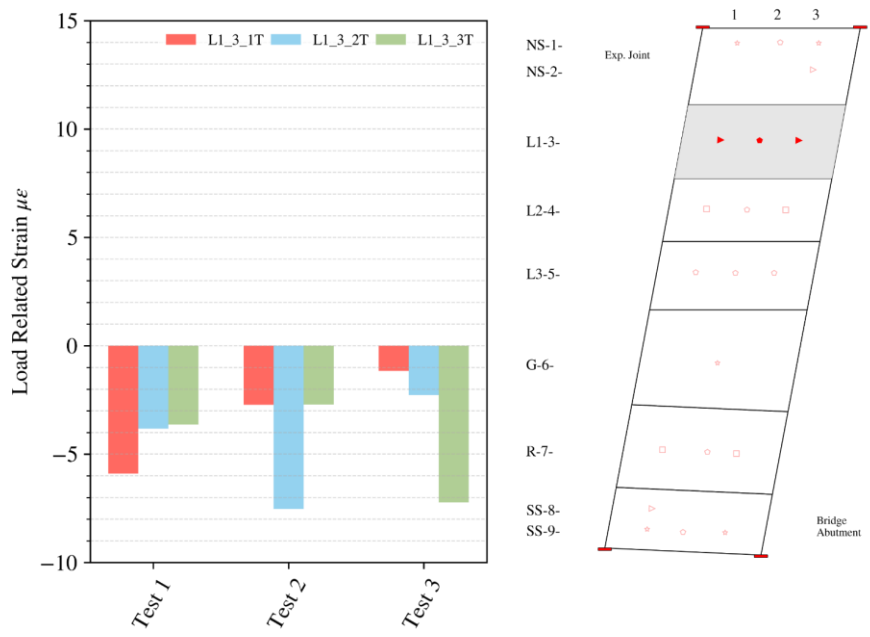
Figure 6.26 (c)
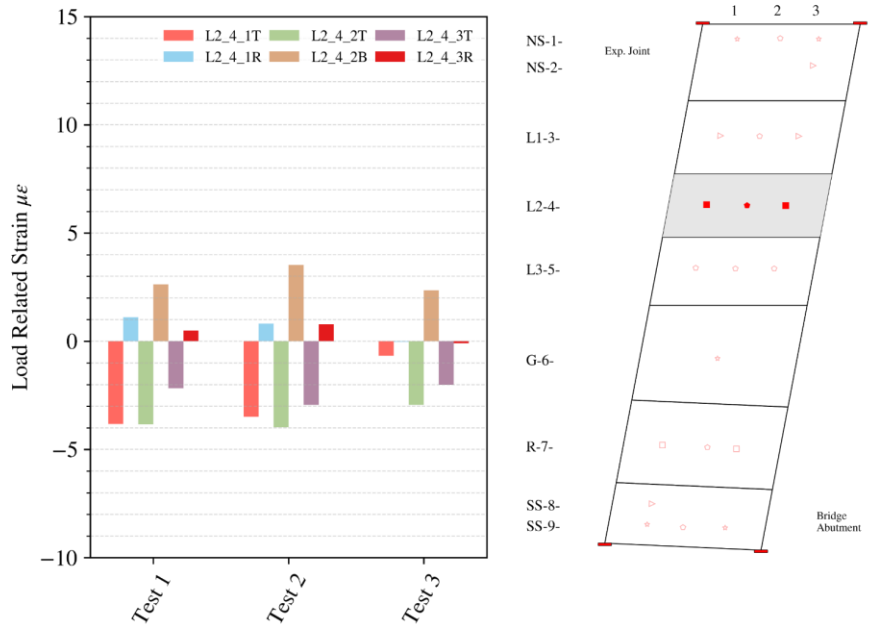
Figure 6.26 Truck-induced strains at Arlington Heights Road on 9/14/2018: (a) longitudinal line NS-1, (b) longitudinal line NS-2, (c) longitudinal line L1-3, and (d) longitudinal line L2-4.

6.2.4.2 Distribution along Transverse Direction

When comparing the truck-induced strains along the transverse direction of the approach slabs, one can find that significant strain magnitudes only appear at the loaded sections and their neighbor sections, which holds for both cast-in-place and precast approach slabs. This indicates the longitudinal joint connections between precast sections provide structural continuity to the adjacent discrete slabs. Figures 6.27 and 6.28 show the distribution of the truck-induced strains in each transverse line of the slab at Prospect Avenue and Arlington Heights Road, respectively.
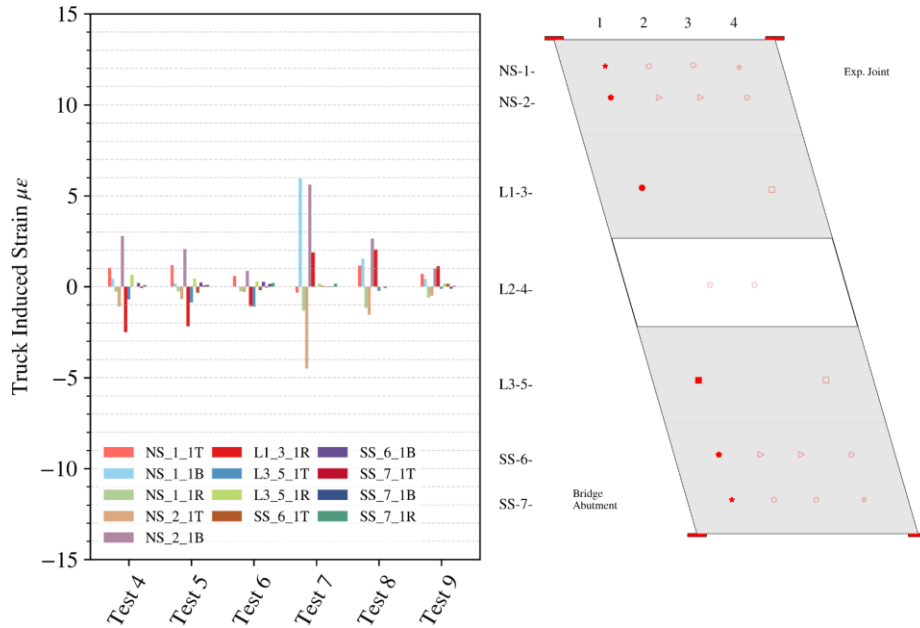
Figure 6.27 (a)
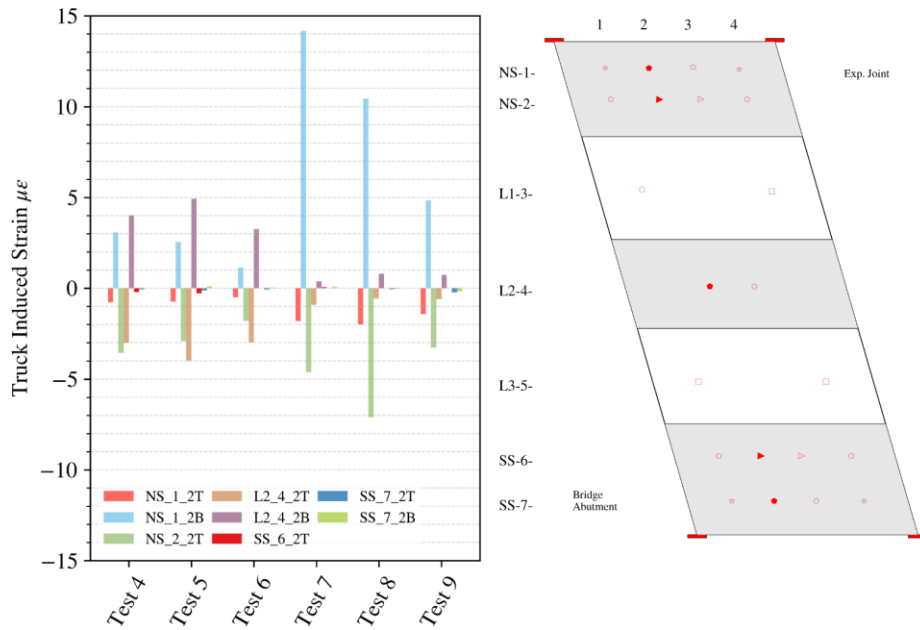
Figure 6.27 (b)
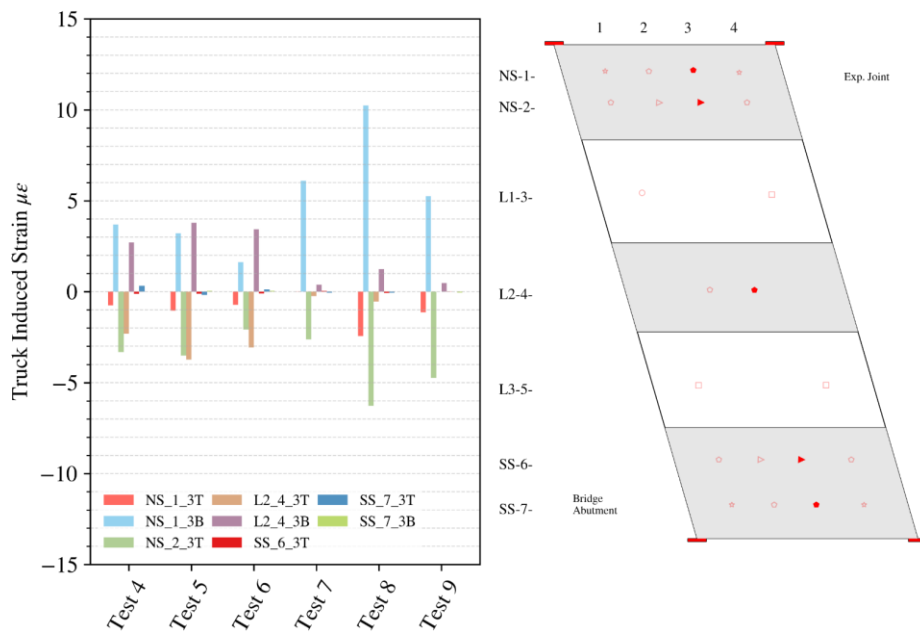
Figure 6.27 (c)
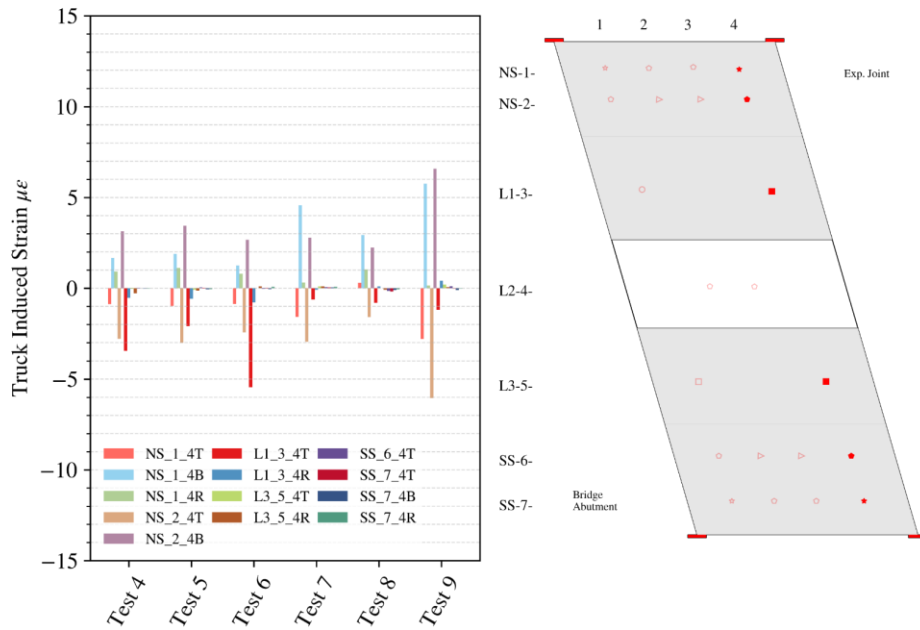
Figure 6.27 (c)

Figure 6.27 Truck-induced strains at Prospect Avenue on 9/14/2018: (a) transverse line 1, (b) transverse line 2, (c) transverse line 3, and (d) transverse line 4.
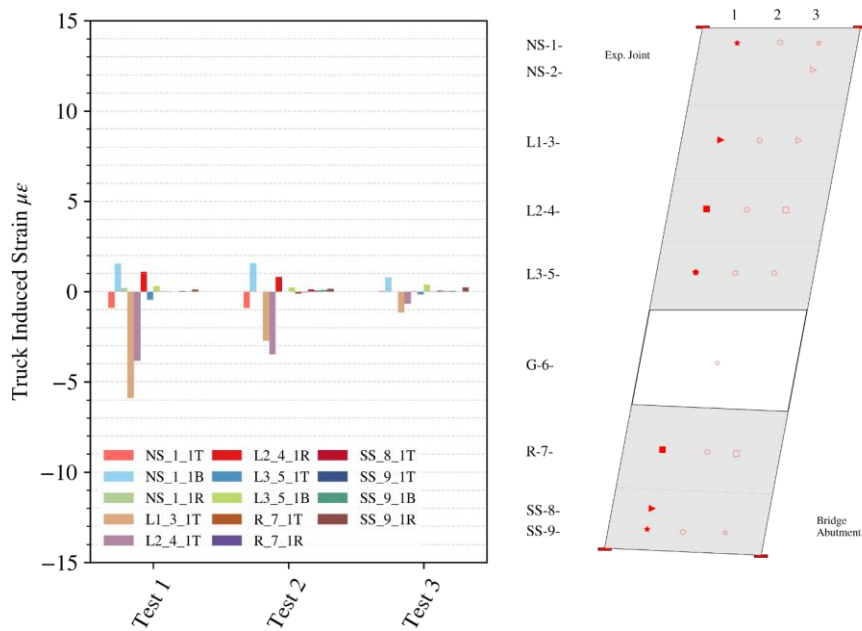
Figure 6.28 (a)
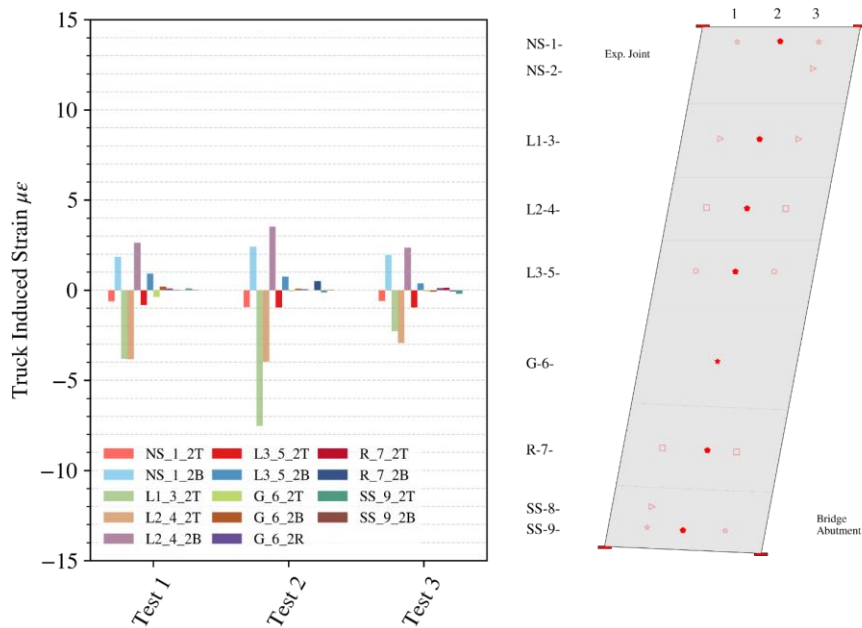
Figure 6.28 (b)
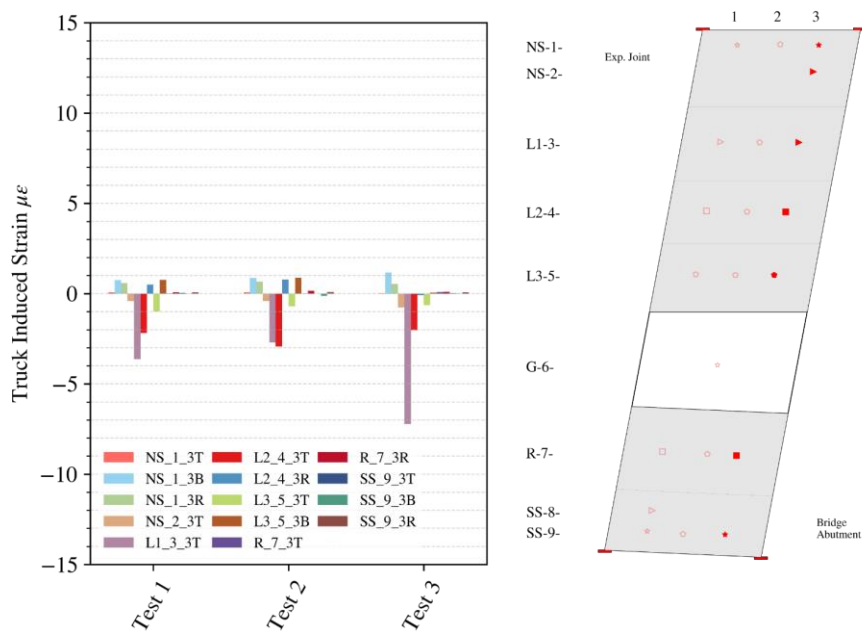
Figure 6.28 (c)

Figure 6.28 Truck-induced strains at Arlington Heights Road on 9/14/2018: (a) transverse line 1, (b) transverse line 2, and (c) transverse line 3.

The computed truck-induced strains are then used to validate and calibrate the numerical models discussed in the next section, which includes estimating the support conditions of the slabs.

6.3 Numerical Simulations and Calibrations of Loaded Slabs

To simulate the behavior of the approach slabs under the controlled static trucks, numerical models were developed in Abaqus (Dassault Systems 2017), as introduced in Chapter 5. The measured contact area of the tires resembles the defined tire areas in AASHTO (2017). As a result, the front axle tires (one on each side) were assumed to have a contact area of 10 in. x 10 in. (for one tire), while the rear axles were assumed to have a contact area of 10 inches × 20 inches (for two tires on each side). The load applied at the tire locations is assumed to be uniformly distributed.

The simulated approach slabs in the numerical modeling are supported by an abutment with dowel bars as shown in Figure 5.6 (b), and a pile bent as shown in Figure 5.7 (b). Uniformly distributed support from the subbase, modeled as an elastic foundation with a modulus of k, is applied to the numerical models. Elastic foundations of various stiffness result in different strains and stresses in the sections of the approach slab. Therefore, assessing the ground conditions is essential. The Abaqus models thus created were used to assess the subbase support conditions. The slabs were subjected to loads provided in Table 6.1 at locations of the truck indicated by the coordinates of the truck tires, which were measured during the static truck loading test, as shown in Figure 6.1. Different modulus of subbase support (k) values were used to define the stiffness of the subbase underneath the slab. It is found from the truck-induced strains at exterior portions of the shoulders that the parapets of the slab may influence the slab behaviors under live loads. Hence, numerical models that contain parapets were developed and analyzed. Specifically, the parapets were modeled by beam elements that are tied to the shell elements of the slab sections, and the centroid of the beam section coincides with the reference surface (mid-surface) of the shell (which somewhat underestimates the actual stiffness that the parapet provides).

Examples of the principal stress (ksi) distribution at the top and bottom surface of the precast slab (test 5) and cast-in-place slab (test 2) are shown in Figures 6.29 and 6.30, respectively. The modulus of the elastic foundation of the example models is 0.01 kips/in/in^2. Parapets were implemented in these example models. The same test truck is loaded in Lane 1, at the midspan, for both approach slabs. The maximum principal stress appears near the test truck tires in the loaded slab section. The principal stress gets reduced by order of magnitude within the neighbor sections of the loaded section for both the top and bottom surfaces of the slab. The maximum principal stress level is similar between the precast and cast-in-place approach slabs, although they are different in dimensions and geometry.

<center>(a)</center><center>(b)</center>
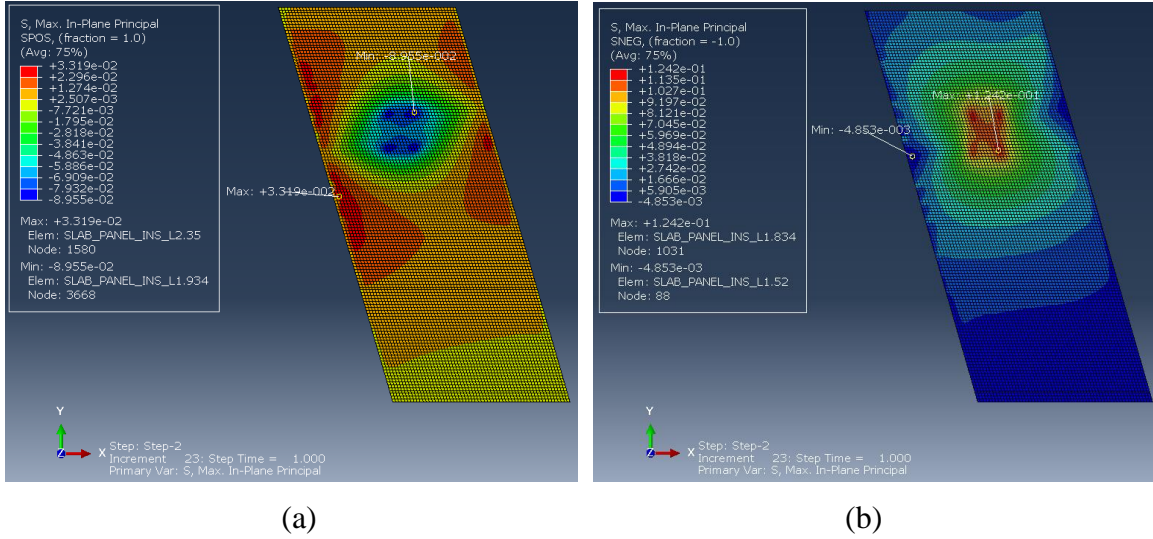
Figure 6.29 Principal stress (ksi) distribution of the precast slab (Prospect Avenue) for truck test 5 at: (a) top surface and (b) bottom surface.

<center>(a)</center><center>(b)</center>
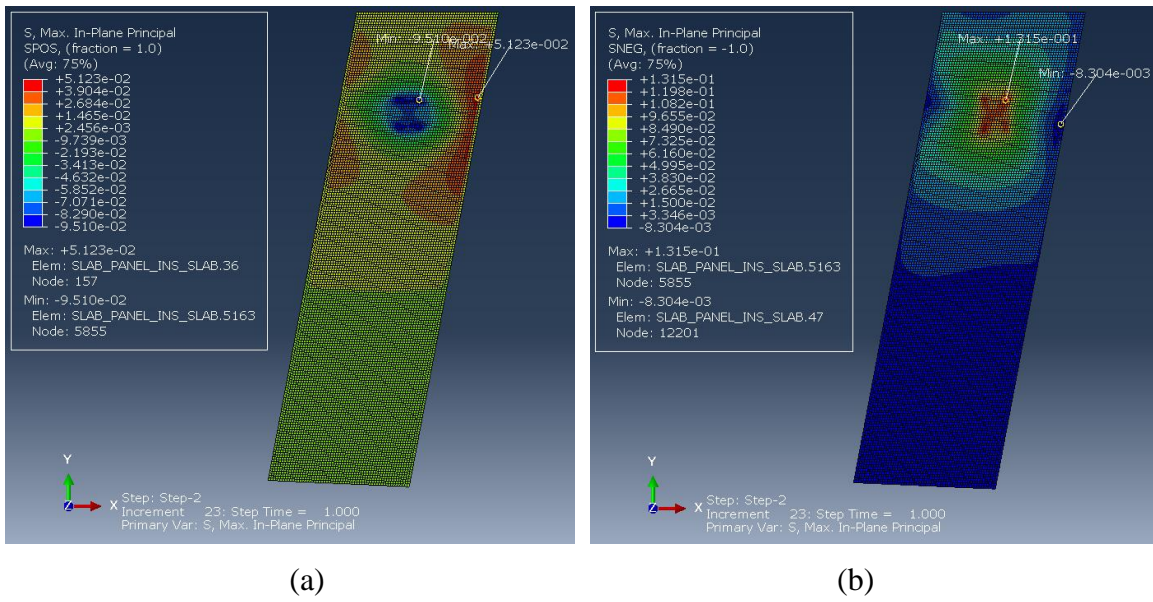
Figure 6.30 Principal stress (ksi) distribution of the cast-in-place slab (Arlington Heights Road) for truck test 2 at: (a) top surface and (b) bottom surface.

The stress and strain components at the top and bottom surfaces of the slab sections are obtained for integration points of all elements in each model. To compare the numerical analysis with the field data, the integration points closest to each sensor in the slab are selected. Linear interpolation is used to convert the stress/strain values at the top and bottom surfaces to the vertical position of the sensors, with the assumption that the curvature of the slab is constant though its thickness, i.e., the normal strains change linearly in the thickness direction. The stress/strain components in the numerical modeling results follow the global normal directions ("11" and "22" directions in Figure 6.31). However, the field-measured strains do not directly correspond. The longitudinal top and bottom (T and B) strains are in the 11 direction, but the top transverse (R) strains are rotated away

<center>206</center>

from the 22 direction by the skew angle θ. Hence, it is necessary to obtain model "R" strains by strain transformation to compare with the field "R" strains. The strain transformation equation for a two-dimensional problem is given as:

$$\epsilon_R = \frac{1}{2}(\epsilon_{11} + \epsilon_{22}) + \frac{1}{2}(\epsilon_{11} - \epsilon_{22})\cos 2(90° - \theta) + \epsilon_{12}\cos 2(90° - \theta)$$
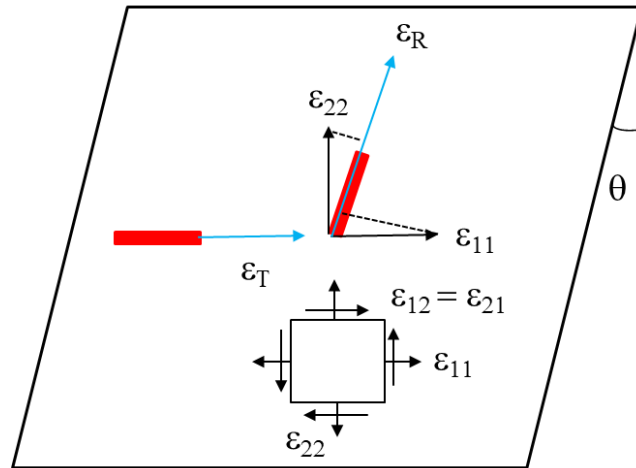
Figure 6.31 Field measured strain directions (T and R) compared to model output ("11" and "22" axes).

The transformed numerical results are then compared with the field data for each sensor and each truck test of the approach slabs. The performance of numerical models fitting the observed field data is manually evaluated into three levels: good fit, mediocre fit, and poor fit. The definition of the three level are as follows:

- Good Fit: For all the tests considered, there is no substantial difference between the two sets of results.
- Mediocre Fit: For some of the tests, the numerical simulations deliver a good fit. For the rest of the tests, the trend of the strain changes still agrees with the field observations but with a noticeable difference in magnitude.
- Poor Fit: There are test results that present a significant difference between the field results and numerical modeling results, in magnitude or trend.

Examples of good fit, mediocre fit, and poor fit are provided by bar plots in Figures 6.32 through 6.34 for sensors at the top and bottom mats of both approach slabs. For each truck test in the figures, the field data is in red and located at the very left, followed by the numerical modeling results without and with parapets. Overall, the numerical results confirm the positive bending behaviors of the approach slabs that are observed from the truck-induced strains. Typically, good fits trend well with the field data so that the best matching parameters, including the modulus of subbase support (k) and the existence of parapets (denoted by "Prpt" in the figures), fall into a narrow range of values among truck tests. Mediocre fits are prevalent in the traffic lanes (the sections at the

middle region of the slab width). The field observed strains are often greater than the maximum numerical modeling results in magnitude, as shown in Figure 6.33 (a) and (b). There are more poor fits observed at the precast slab than the cast-in-place slab, as there are significant differences between the field data and the numerical results at the exterior portion of the shoulders for the precast slab, as shown in Figure 6.33 (c), and Figure 6.34 (a) and (b). When the live loads are applied at the shoulders of the approach slab, the parapets reduce the compressive stresses/strains at the top mat. However, for sensors away from the parapets, the influence of the parapet decays, making the models with and without parapets similar. In general, the models with parapets perform at least as good if not better than the models without parapets if all the sensors are considered, so these are viewed as the most credible models from this study.
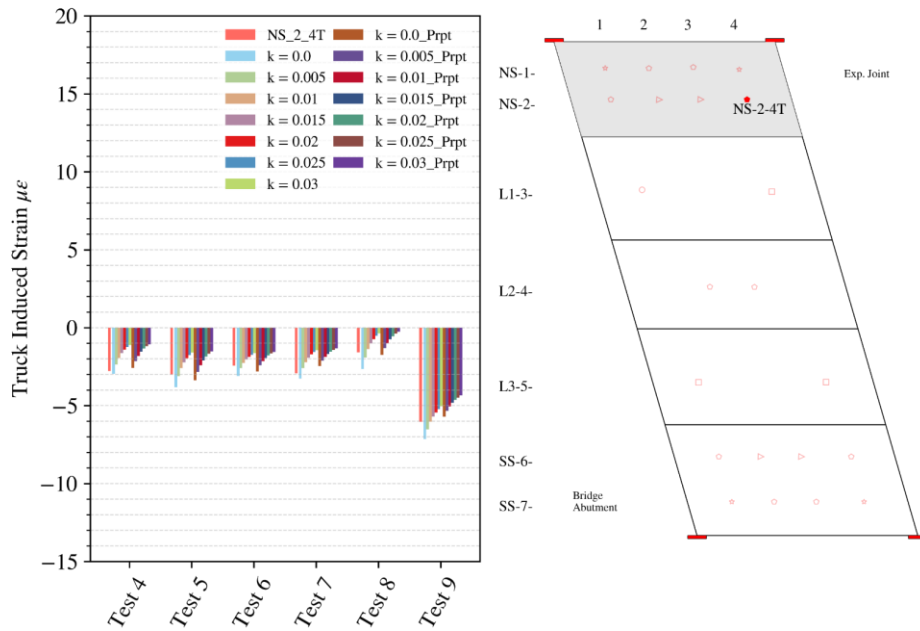
Figure 6.32 (a)
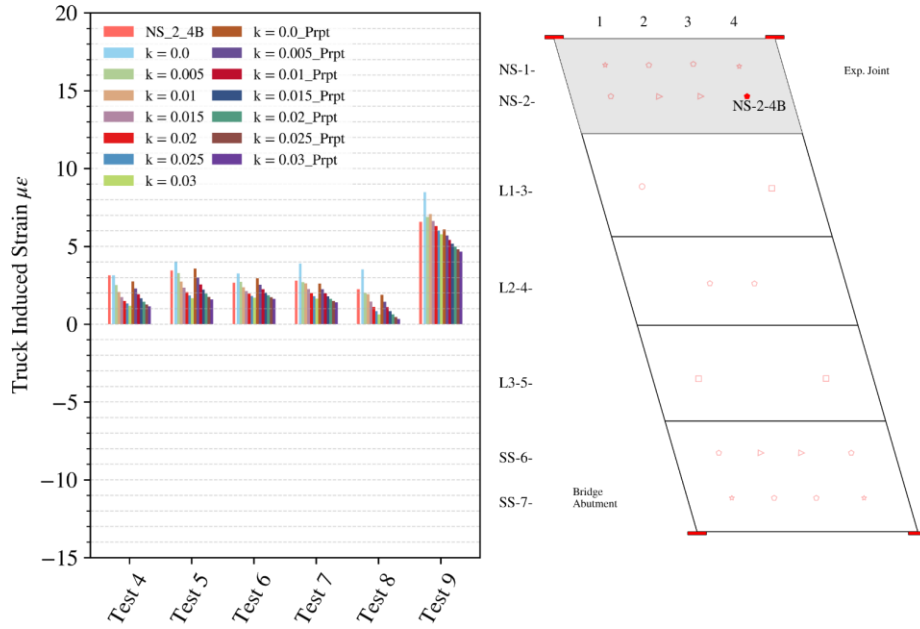
Figure 6.32 (b)
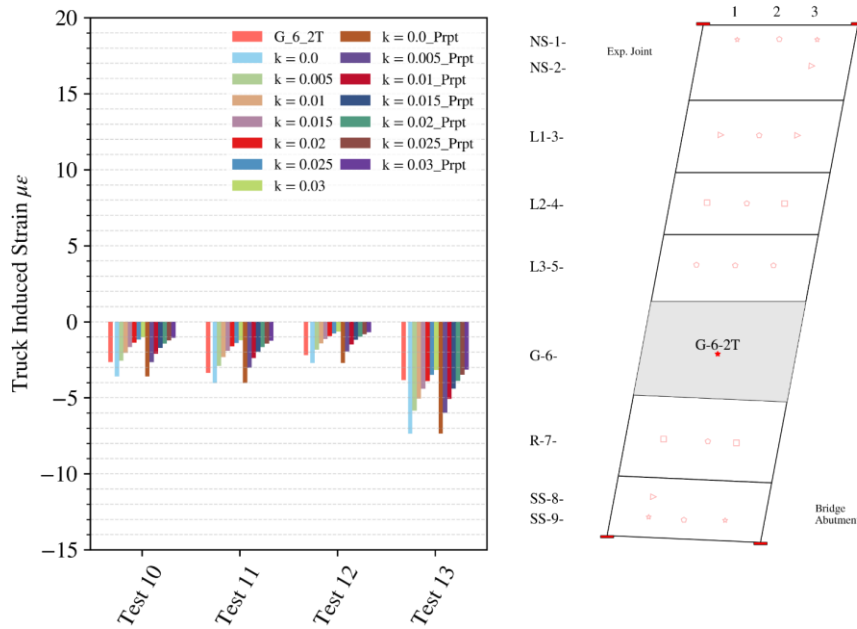
Figure 6.32 (c)
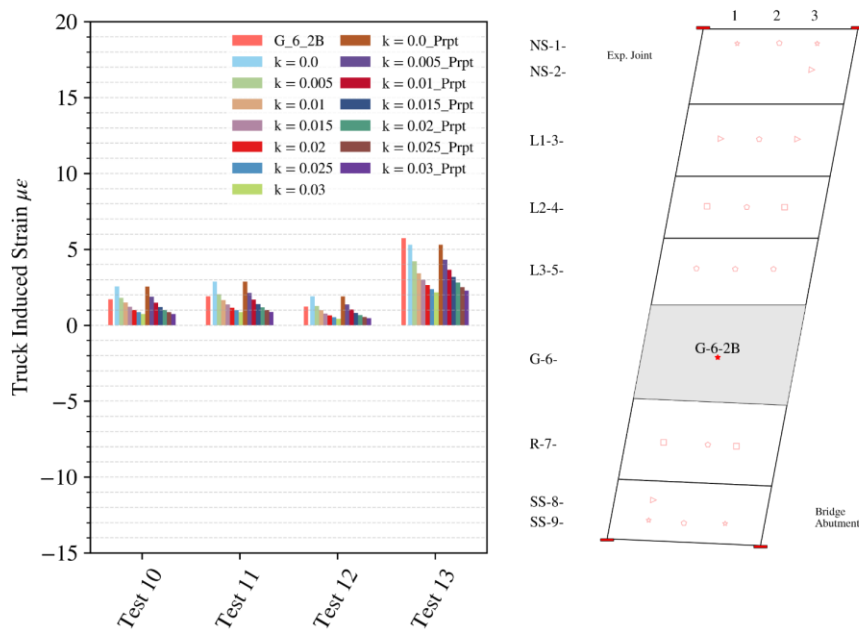
Figure 6.32 (d)

Figure 6.32 Examples of good fit of numerical modeling to field data: (a) NS-2-4T at the precast slab, (b) NS-2-4B at the precast slab, (c) G-6-2T at the cast-in-place slab, and (d) G-6-2B at the cast-in-place slab.
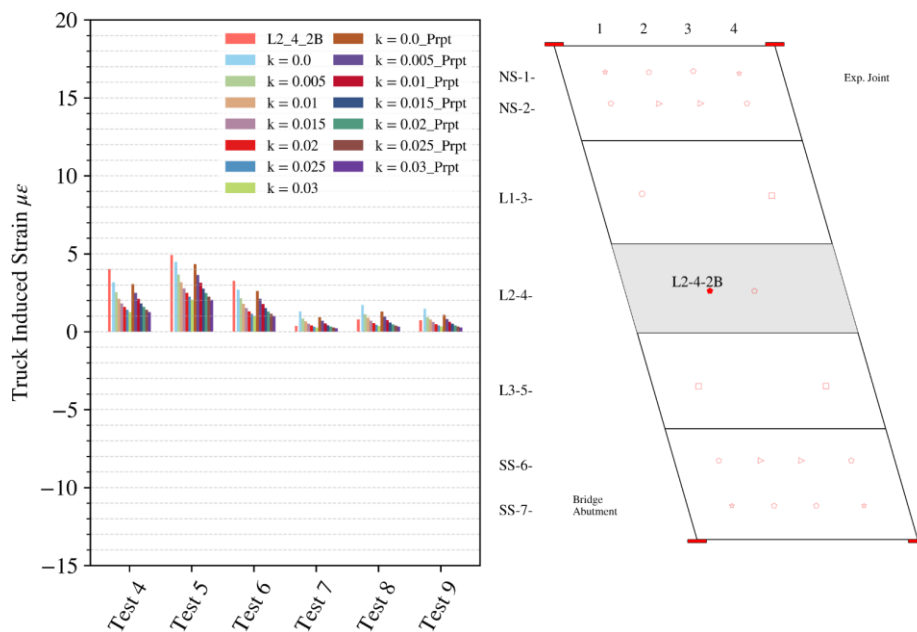
Figure 6.33 (a)
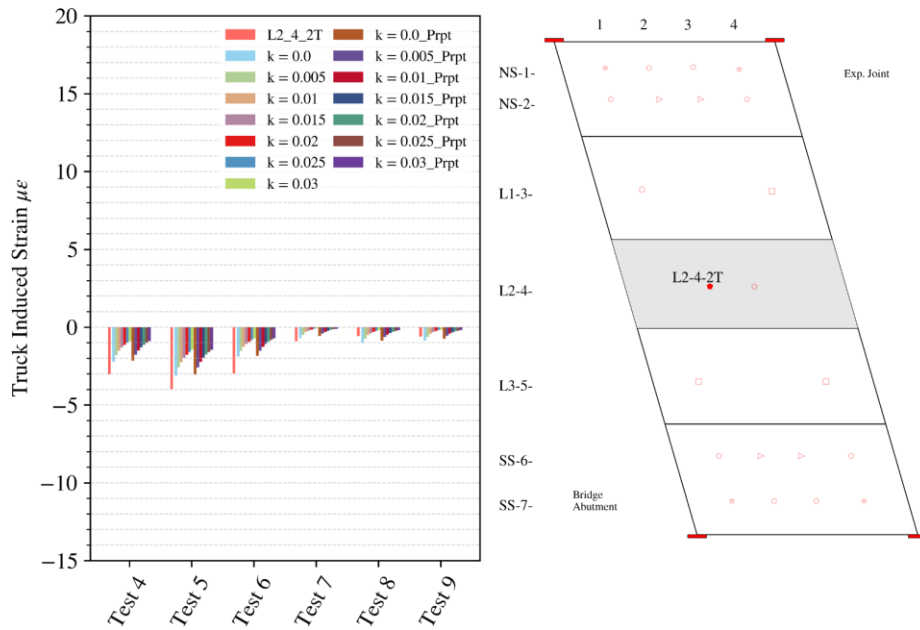
Figure 6.33 (b)
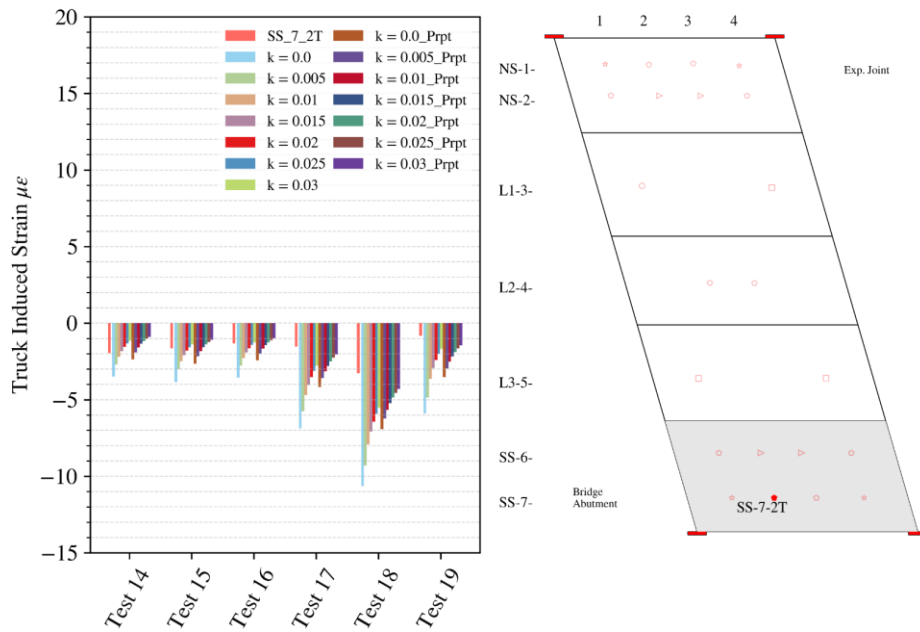
Figure 6.33 (c)
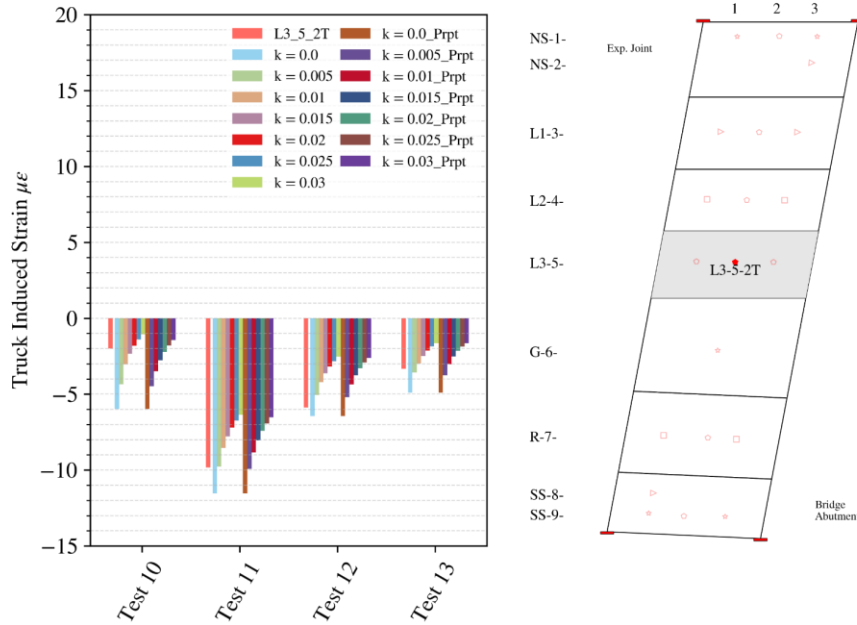
Figure 6.33 (d)
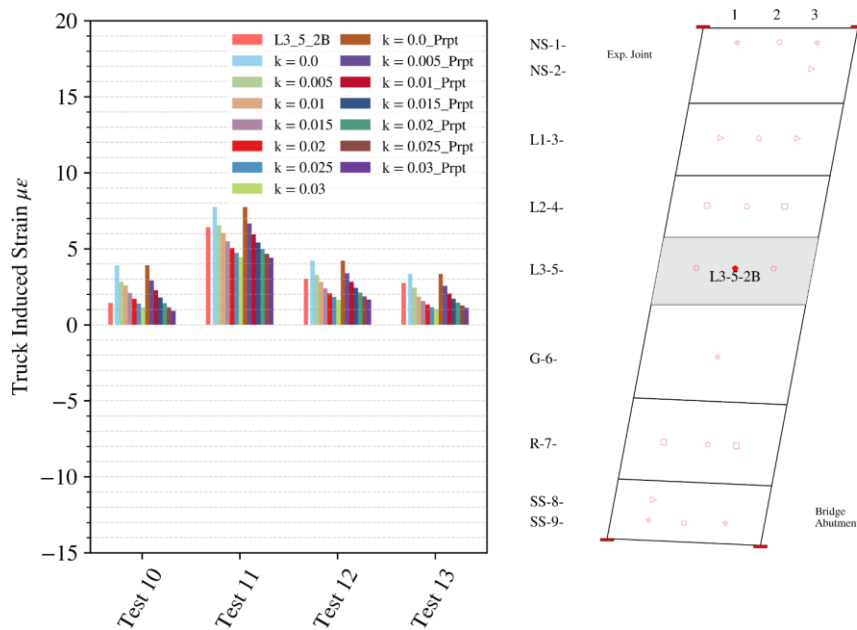
Figure 6.33 (e)

Figure 6.33 Examples of mediocre fit of numerical modeling to field data: (a) L2-4-2B at precast slab, (b) L2-42T at precast slab, (c) SS-7-2T at precast slab, (d) L3-5-2T at cast-in-place slab, and (e) L3-5-2B at cast-in-place slab.
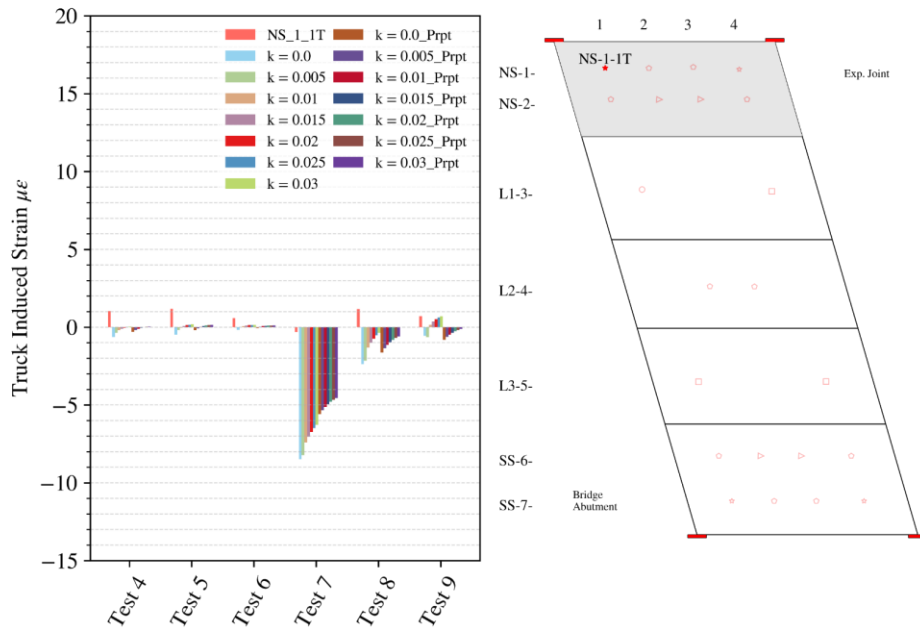
Figure 6.34 (a)
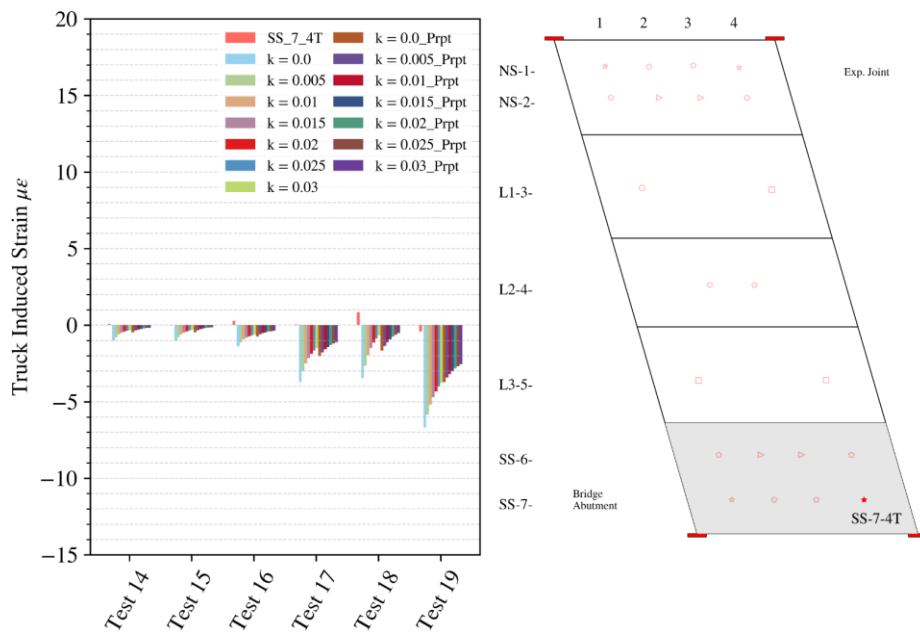
Figure 6.34 (b)
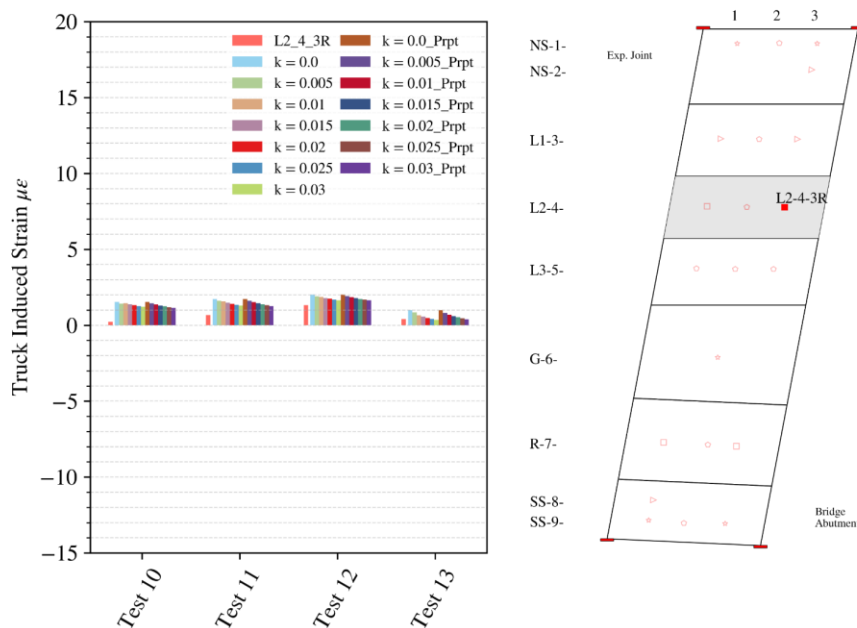
Figure 6.34 (c)

Figure 6.34 Examples of poor fit of numerical modeling to field data: (a) NS-1-1T at precast slab, (b) SS-7-4T at precast slab, and (c) L2-4-3R at cast-in-place slab.

To synthesize the best matching model parameters (including modulus of subbase support and existence of parapets) in a test-wise and sensor-wise manner, for each combination of sensor and truck test the differences between the field data and numerical modeling results are computed so the model with the minimum magnitude of the difference is selected as the estimation (represented as a colored cell of the match map in Figure 6.35). As there were sections/lanes that were open to traffic, with uncontrolled loads being applied during data collection, any data affected by the uncontrolled loads were manually identified and removed from the metric of comparing the field data and numerical results, which are represented by the yellow "nan" cells in the map. Each combination of the model parameters is represented by a distinct color in the color bar. In addition, for each approach slab an estimation of model parameters considering all truck tests is made by selecting the minimum sum of the absolute difference between field data and numerical modeling results of all truck tests, denoted as the column of "Test All" in Figure 6.35. To evaluate the overall performance of numerical models on a particular truck test, the L_2 norm of field data-numerical modeling difference for all sensors is computed, and the model with the smallest magnitude is chosen, as plotted in the row "L2_norm" in Figure 6.35. The L_2 norm is also known as the Euclidean norm, which is defined as the square root of the sum of the squared components of a vector. In other words, the L_2 norm herein first computes the difference between the field data and numerical modeling results in a vector manner, then sums the square of each difference, and finally calculates the square root of the sum.

214
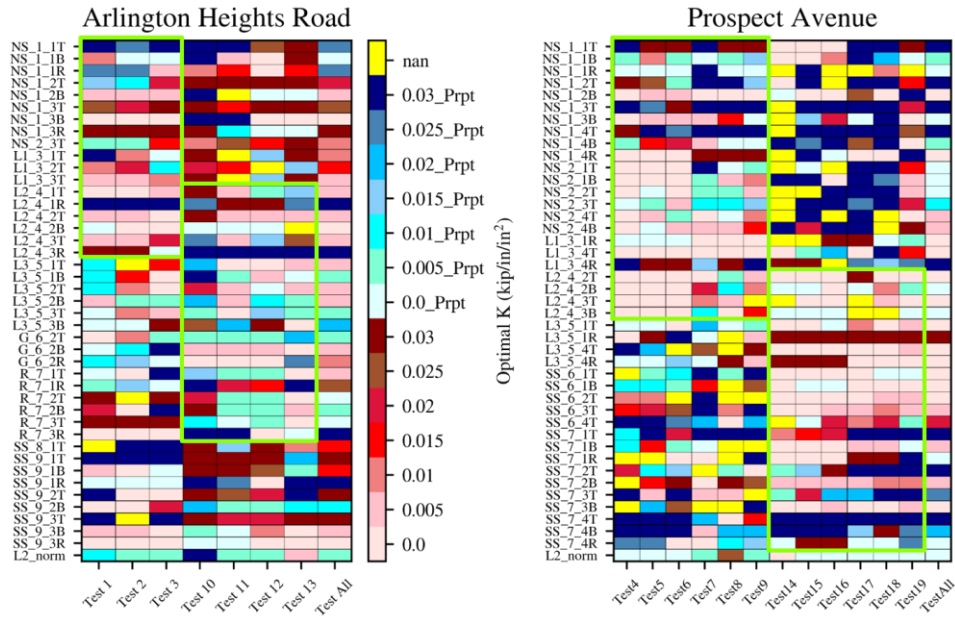
Figure 6.35 Map for best matching numerical models.

The cells within the green boxes in Figure 6.35 are the sensors located at the loaded slab section or its neighbor sections for each truck test where the truck-induced stress/strain changes are significant compared to the rest of the slab. As the sensor data in the green boxes are prone to gain greater difference from the numerical modeling results, they make more contributions to determine the best matching model parameters for a sensor given a particular truck test. Many sensors (rows) in the green boxes have consistent or close matching models among truck tests, indicating good or mediocre fits. Nevertheless, there are rows with dark colors corresponding to stiffer subbase support in the numerical models. These sensors are more located at the shoulders, confirming the observations of poor fits that can be caused by the effects of parapets and unclear boundary conditions. Emphasis is made that the darkness of the cell colors does not indicate the magnitude of difference between the field data and the selected numerical model. Although there are more variations in color at the cells outside the green boxes, it does not necessarily mean the numerical modeling provides lower accuracy at these regions since the slab response is mild in these regions and the numerical model results are close to each other, making the best match selection more sensitive. For example, for a sensor that is far away from the parapets, G-6-2T with test 13, as shown in Figure 6.32 (c), the results for a particular k value of models with and without parapets are close so that given a subtle perturbation of the field data, the best match model can change between the models with and without parapets, i.e., the color in the cell may change from blue to red.

With the simplifying assumption that the elastic foundation subbase is uniformly distributed, the estimated modulus of subgrade reaction is in the range of **0 to 0.005 kips/in/in²** for the precast slab and **0.01 to 0.015 kips/in/in²** for the cast-in-place slab. The typical modulus for loose sand is in these ranges. This field data-numerical models comparison gives a good idea about the support conditions of the slab and confirms the fidelity of the model.

215

Not all factors that affect the agreement between the simulations and the field results could be considered due to uncertainties in measurements and modeling. In terms of static truck testing, the experimental errors can be attributed to: (1) truck tire dimension and location measurements, and (2) truck axle weight measurements. Numerical modeling can be affected by: (1) the elastic foundation distribution, (2) inclusion and implementation of the parapets, and (3) restraints and boundary conditions. Potential improvements can be gained by: (1) adjusting the centroidal location for the parapet beam elements to better account for the offset of the center of gravity of the parapets from the slab, (2) introducing elastic foundations that are nonuniformly distributed.

7 Parametric Study

The two approach slabs that the research team monitored, and other ones inspected in the field, exhibit large variations in the slab geometry, loading scenarios, and possibly even their boundary conditions. All the investigated slabs are in the suburban Chicago area (in and around Itasca, IL) and experience similar overall temperature changes in addition to similar peak live load magnitude The large temperature variation in a yearly cycle is expected to have a significant effect on demands in the approach slabs. As a result, a numerical study using the developed finite element modeling framework was conducted to comprehensively investigate the effects that various parameters have on the approach slab behavior. This chapter includes the organization of the parametric study and discussion of the results.

7.1 Organization of Parameters

In this section, all major parameters – including constant parameters and variable parameters – are described and discussed.

7.1.1 Constant Parameters

Although there are certain parameters with a large range of variations, such as skew and number of lanes, some parameters have commonly shared values among most of the approach slabs in typical design practice. To save computational cost, the values of these parameters are fixed based upon current design practice, as well as suggestions from the Tollway and the project's Technical Review Panel. Table 7.1 lists all the parameters with unchanged values among the models in the parametric study space. Note that end settlement is not considered in the parametric study, as IABs in Illinois have pile-supported abutments and pile bents, respectively, at the two ends of approach slabs. The indicated concrete and steel material properties are simply the design values taken from the structural drawings.

Table 7.1 Approach slab parameters with a fixed value in the parametric study.

	Parameters	Selected Values / Cases
Geometry	Approach Slab Span (ft)	30
	Approach Slab Thickness (in)	15
	Lane or Shoulder Width (ft)	12
Material	Concrete Compressive Strength, f_c' (psi)	5000
	Rebar Steel Yield Stress, f_y (psi)	60,000
	Concrete Modulus of Elasticity (ksi)	4069.6
	Steel Modulus of Elasticity (ksi)	29,000
	Concrete Coefficient of Thermal Expansion ($\times 10^{-6}/°F$)	6.5
	Steel Coefficient of Thermal Expansion ($\times 10^{-6}/°F$)	5.5
Approach Slab Reinforcement	Top Longitudinal Mat	#5 @ 12"
	Top Transverse Mat	#5 @ 6"
	Bottom Transverse Mat	#8 @ 6"
	Bottom Longitudinal Mat	#9 @ 5"
	Top Concrete Cover (in)	2.25
	Bottom Concrete Cover (in)	2
Boundary Conditions	Abutment Settlement	No settlement
	Pile Bent Settlement	No settlement

7.1.2 Variable Parameters

7.1.2.1 Approach Slab Geometry

Although IDOT (2012) states that the skew of IABs in Illinois is generally less than or equal to 30°, approach slabs with a skew larger than 40° were still observed in the field. Hence, to consider all possibilities of the skewed approach slabs, the skew is selected as 0°, 5°, 10°, 15°, 20°, 25°, 30°, 35°, 40°, and 45° in the parametric study.

The orientation of the skew is also a geometric factor. The skew orientation is defined to be positive if the transverse edges of the approach slab are rotated clockwise in plan view, as shown in Figure 7.1 (a), and negative if rotated counterclockwise. It is assumed that the north direction is upward in the plan view of the approach slab. When the skew direction is considered, the location of the abutment/expansion joint doubles the number of possible cases. For example, approach slabs at two ends of a -15° skew eastbound bridge have the supporting abutment located at their east and west end, respectively.
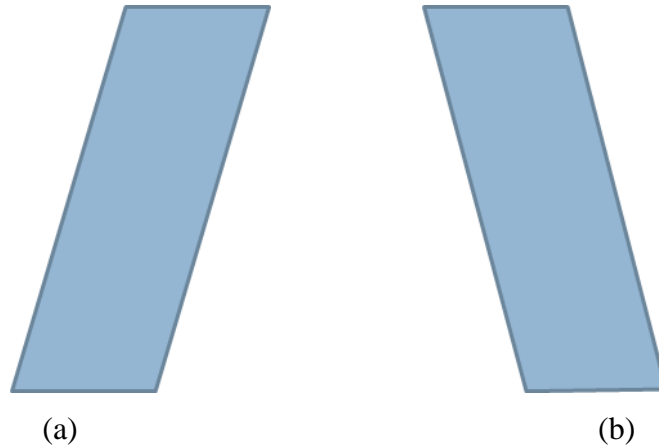
Figure 7.1 Skew orientation of the approach slab: (a) positive, (b) negative.

The total width of the bridge or approach slab varies due to the number of traffic lanes, where 2, 3, and 4 are the possible number of traffic lanes in an approach slab (as well as two shoulders at the sides in the transverse direction). In general, section/lane width varies in a particular approach slab from 12 feet to 15 feet. In addition, the lane load applied to each section/lane has a fixed width of 10 feet (AASHTO 2017), which makes sections with smaller width prone to greater stresses. Hence, although the total width of the approach slab is also affected by the difference in section (lane or shoulder) width, for simplicity of the parameter space the section width in the parametric study is set to be 12 feet, as indicated in Table 7.1.

7.1.2.2 Reinforcement Orientation

It was observed that for the monitored cast-in-place approach slab at Arlington Heights Road, the transverse reinforcement is parallel to the skewed edge of the slab, as shown in Figure 7.2 (a), in contrast to the case of the instrumented precast approach slab at Prospect Avenue where the transverse reinforcement is 90° to the longitudinal reinforcement regardless of the skew, as shown in Figure 7.2 (b). Consequently, both configurations are considered in the parametric study.
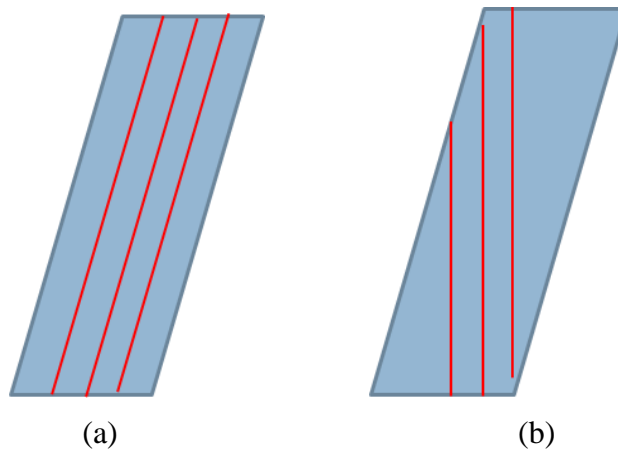
Figure 7.2 Orientation of the transverse reinforcement: (a) parallel to the skew, (b) perpendicular to the longitudinal reinforcement.

7.1.2.3 Boundary Conditions

The numerical modeling for the static truck loading test, which adopts JOIN connector elements, delivers reasonable agreements with the field results. Therefore, at the abutment-approach slab interface, the boundary conditions are modeled with JOIN connector elements for both live load analysis and thermal analysis (see Figure 5.7 (b)).

At the approach slab-pile bent interface, the interaction in the contact region is explicitly considered in the parametric study. Since there is a little longitudinal movement of the approach slab when subjected to live load, the friction between the bottom of the approach slab and the pile bent is ignored. However, such frictional interaction becomes more significant when there is longitudinal deformation/movement of the approach slab due to temperature changes. Thus, a coefficient of friction of 0.5 (Maitra et al. 2009, Jeong et al. 2014,) is used for the friction between the approach slab and the elastomeric or polyethylene sheet (see Figure 5.5).

As studied in Chapter 6, the subgrade under the slab can affect the behavior of the approach slab. Based on the numerical model calibration (with help from the static truck loading tests), the modulus of the elastic foundation is varied with values of 0.05, 0.02, 0.01, 0.005, 0.002, and 0.001 $kip/in/in^2$.

7.1.2.4 Live Load

The HL-93 tandem and IL-120 design trucks introduced in section 5.1.4, together with the design lane load, are adopted in the parametric study. It is assumed that the truck loads are always eastbound. With different combinations of skew orientation and abutment side of approach slab support, all possible loading cases for the westbound bridges are also equivalently considered.

The spatial distribution of the design truck load could vary for a non-zero skew case, as shown in Figure 7.3. If more than one traffic lane is loaded, these trucks can enter the skewed slab at the same time, as indicated in Figure 7.3 (a). The other representative case is that there is zero relative longitudinal distance among these trucks in the traffic direction, as shown in Figure 7.3 (b).

(a)   (b)
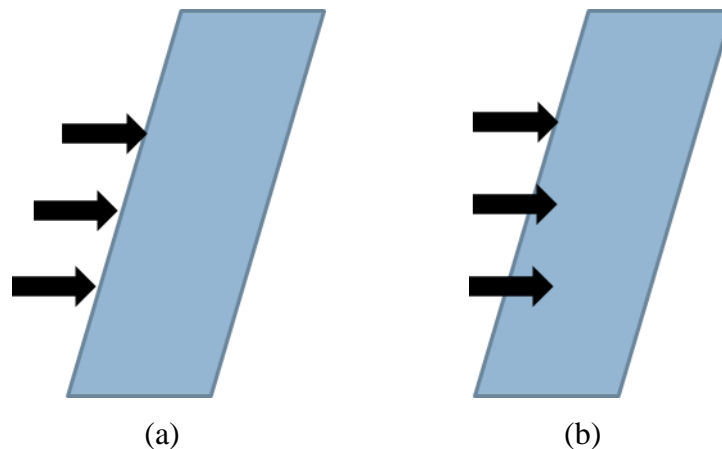
Figure 7.3 Spatial distribution of the trucks: (a) parallel to the skew. (b) aligned side-by-side.

7.1.2.5 Temperature Field

Based on the 2.5 years of field monitoring data, the approach slabs experienced approximately 108°F (60°C) of total temperature change. Considering the temperature of the approach slab during construction was around 68°F (20°C) and the maximum temperature was about 104°F (40°C), a range of -72°F (-40°C) to 36°F (+20°C) temperature change was chosen as the temperature changes in the numerical models. In a prior study, LaFave et al. (2021) considered a pure positive temperature change of 80°F and a pure negative temperature change of -80°F as the extreme cases for analysis of bridge structures in Illinois, which is more severe than the proposed temperature change range in this study. As will be discussed, numerical modeling results suggest that even with the smaller proposed temperature range, potential cracking can appear in the approach slabs.

Since temperature variations through the thickness of the approach slab were observed in the field data, a range of temperature gradient from -0.72°F/inch (-0.4°C/inch) to 1.26°F/inch (+0.7°C/inch) is considered in the parametric study. The positive and negative boundary of the temperature gradient is shown in Figure 7.4, where the width of the triangles at a certain height represents the temperature increase compared to the minimum temperature in the section.
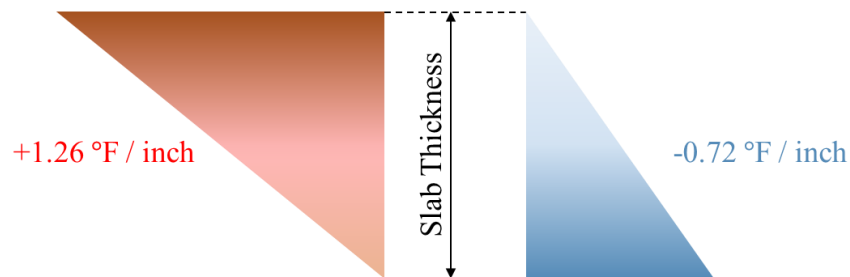
Figure 7.4 Temperature gradients through approach slab thickness.

7.2 Results and Discussions

7.2.1 Live Load Analysis

For each numerical model used in the live load analysis, either HL-93 or IL-120 is selected, always entering the approach slab from its west side, passing through the slab, and exiting from the slab on its east side. Figure 7.5 shows a typical principal stress distribution at the bottom of the approach slab. The maximum principal stress appears when the trucks are located approximately at the midspan of the approach slab. For instance, in Figure 7.5 there are four traffic lanes and two shoulders, with all traffic lanes loaded by the IL-120 design truck. As indicated in Figure 7.5, positive bending is caused by the test truck in most of the slab area. Due to the dowel bar restraint at the abutment-approach slab interface, some modest negative moment is developed at the region near the abutment, as indicated by the tensile principal stresses on the top surface at that location.

(a)   (b)
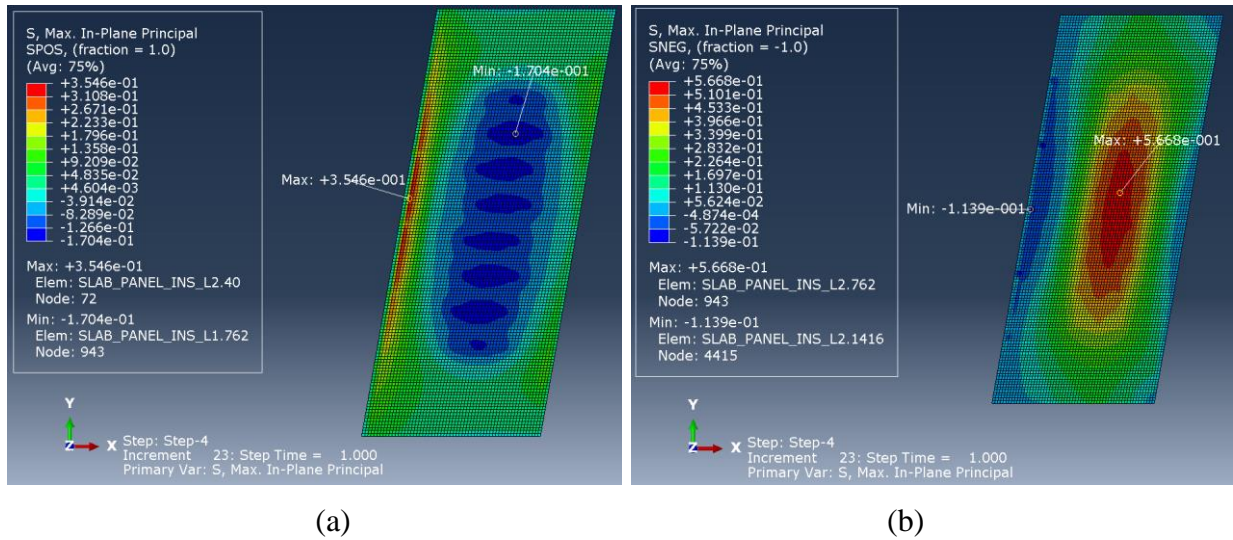
Figure 7.5 Typical principal stress distribution of a 15° skew approach slab with 4 traffic lanes under IL-120 design truck at all traffic lanes, aligned parallel to the skew at: (a) top surface and (b) bottom surface.

To study how the variables affect the approach slab performance, a baseline reference group is selected. In the reference group, each model has transverse reinforcement parallel to the transverse edges of the slab; has the abutment on its west side; is loaded by the IL-120 design truck; has three traffic lanes, and has trucks entering the slab at the same time.

Figure 7.6 examines how skew magnitude, truck type, transverse rebar orientation, and spatial truck alignment affect the critical tensile principal stress in the approach slab. It is observed that the critical principal stress decreases as the skew increases, when the skew is greater than 10°, and as the skew decreases from 10° to 0°. The general trend of decreasing stress with increasing skew can be explained by the fact that the maximum principal stress is approximately perpendicular to the skewed transverse edge of the approach slab, leading to a decreasing length of the load path between the supports of the slab when the skew increases. For all selected skews, the IL-120 design truck results in higher critical principal stresses than the HL-93 tandem. Trucks entering the slab at the same time induce greater principal stresses than the case of trucks aligned side-by-side when the skew is greater than 10°, but the maximum critical principal stress is caused by the IL-120 design truck load aligned side-by-side with a skew of 5°. The orientation of transverse reinforcement does not significantly affect the critical principal stresses. Figure 7.7 shows contour plots for the principal stress distribution at the critical truck locations for the reference group.
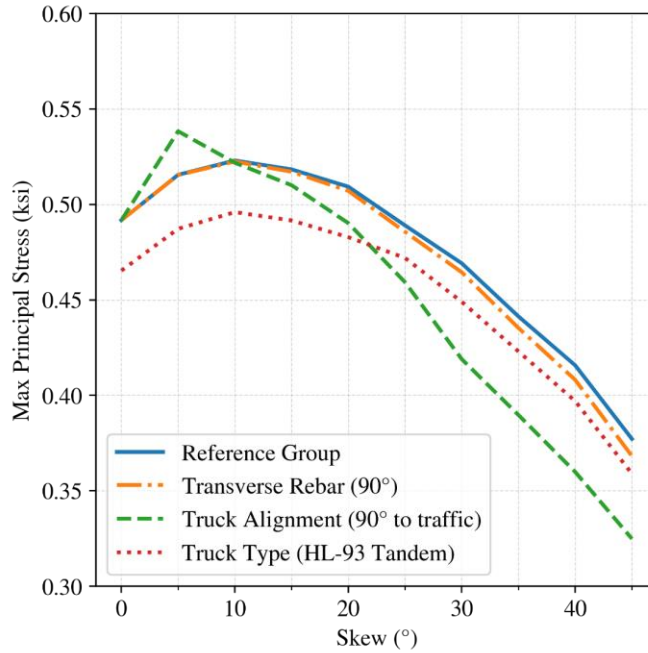
Figure 7.6 Critical principal stresses under live load considering truck type, truck alignment, and transverse rebar direction.

| (a) | (b) |

(c)

(d)

(e)

(f)

(g)

(h)

$$(i) \qquad\qquad\qquad\qquad (j)$$
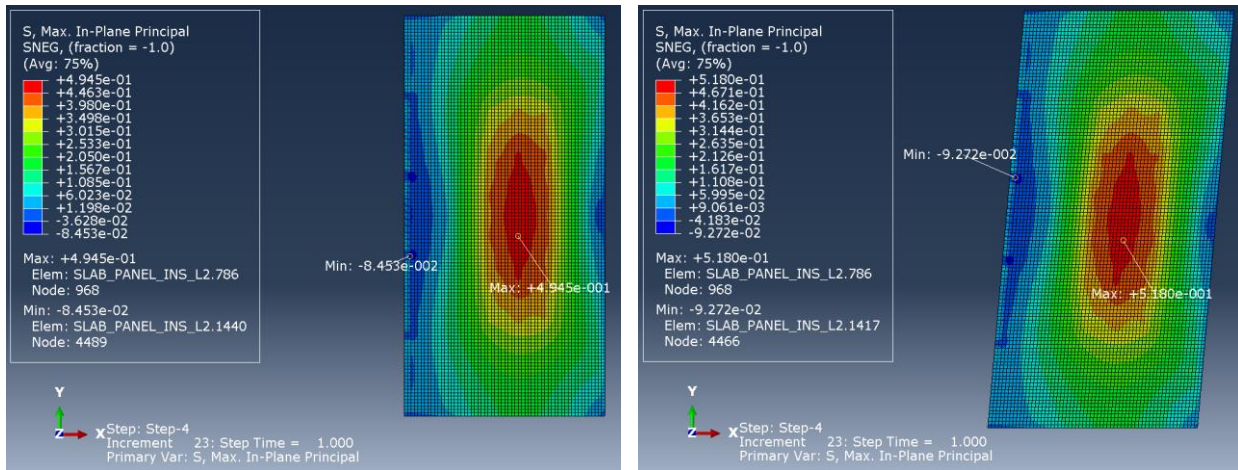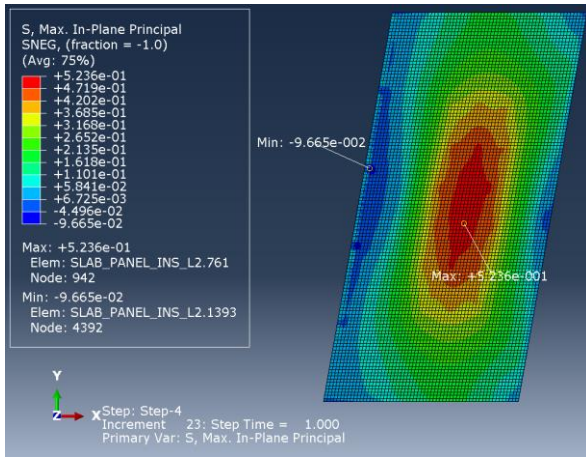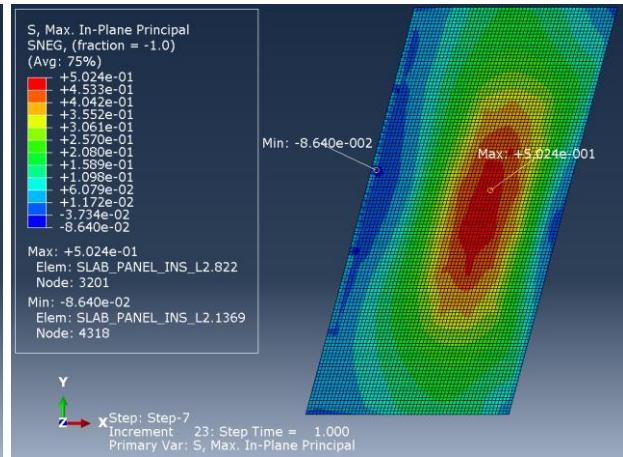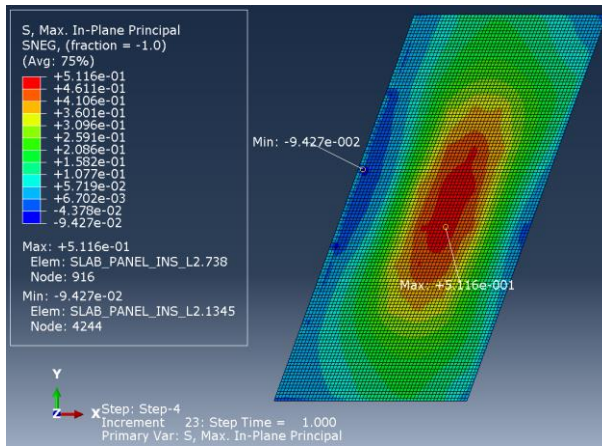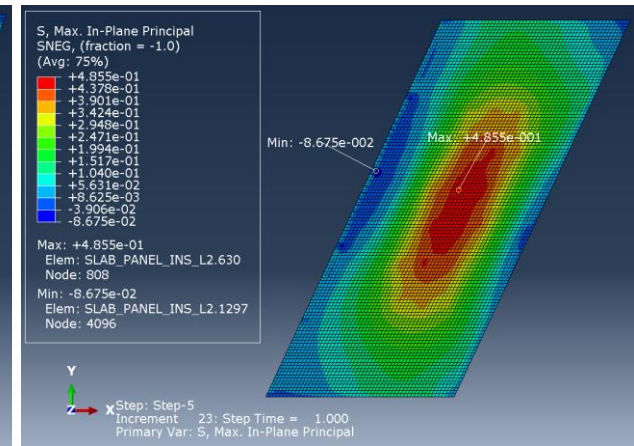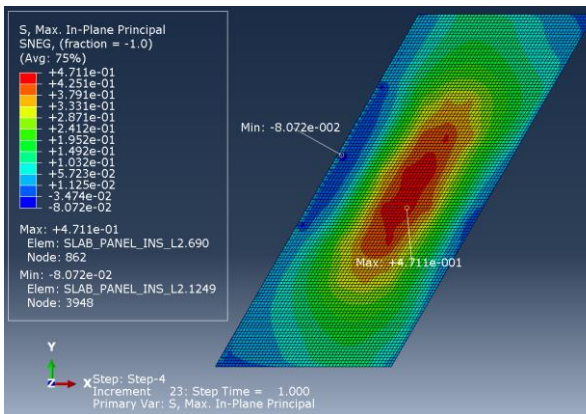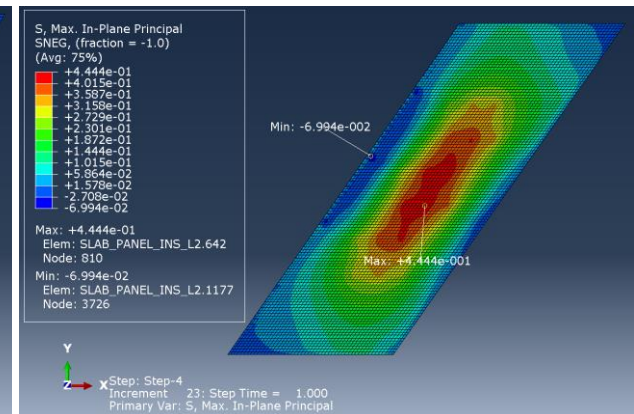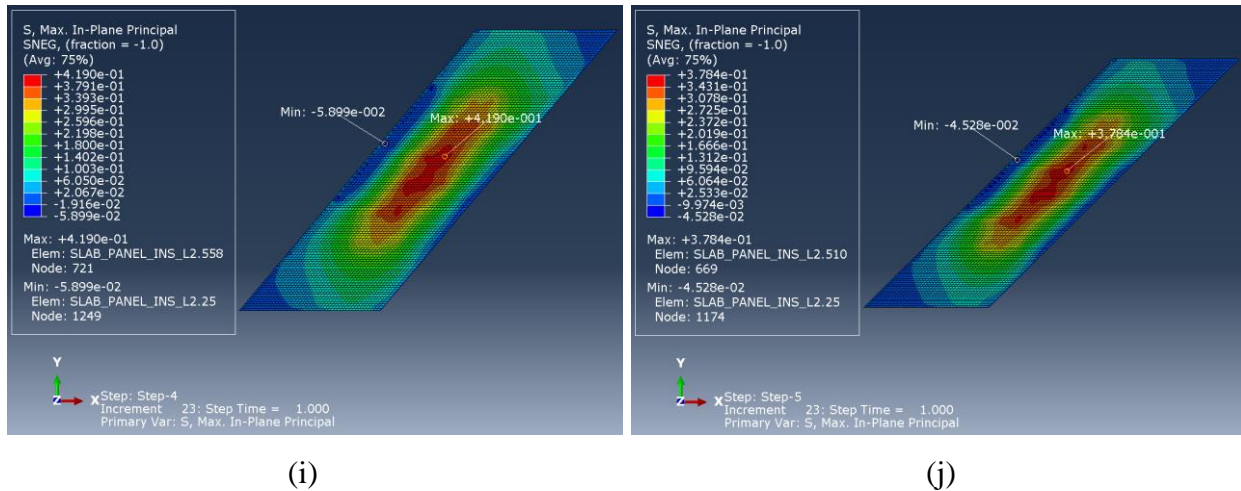
Figure 7.7 Critical principal stress distribution of models in the reference group with skew of (a) 0°, (b) 5°, (c) 10°, (d) 15°, (e) 20°, (f) 25°, (g) 30°, (h) 35°, (i) 40°, and (j) 45°.

For the other geometric considerations – including the direction of skew, the abutment location with respect to the approach slab, and the combination of the two – the critical principal stresses do not exhibit significant variations, as shown in Figure 7.8, indicating that these geometric variables are not as important as the skew of the slab or the type of truck load.

The total width of the approach slab significantly affects the critical principal stress, as indicated in Figure 7.9. The more traffic lanes there are in the slab, the higher is the critical principal stress. For the case of four traffic lanes, with a skew of 10°, the critical principal stress reaches 567 psi. It is also observed that the maximum critical principal stress is achieved when all the traffic lanes are loaded, as shown in Figure 7.10. This is explained by two-way slab bending behavior – as the total width of the approach slab increases, the span in the transverse direction gets greater, and when the middle region is loaded, the resultant stress becomes more critical.
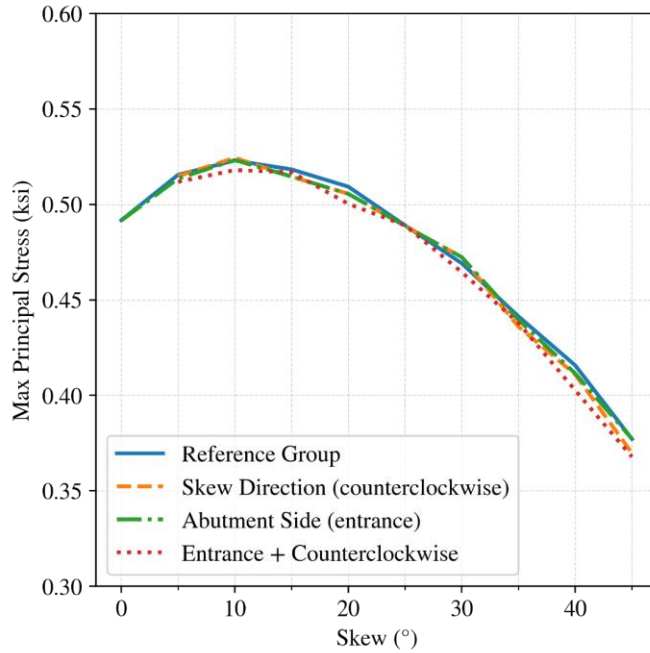
Figure 7.8 Critical principal stresses of the approach slab under IL-120 design truck with respect to geometric variables.
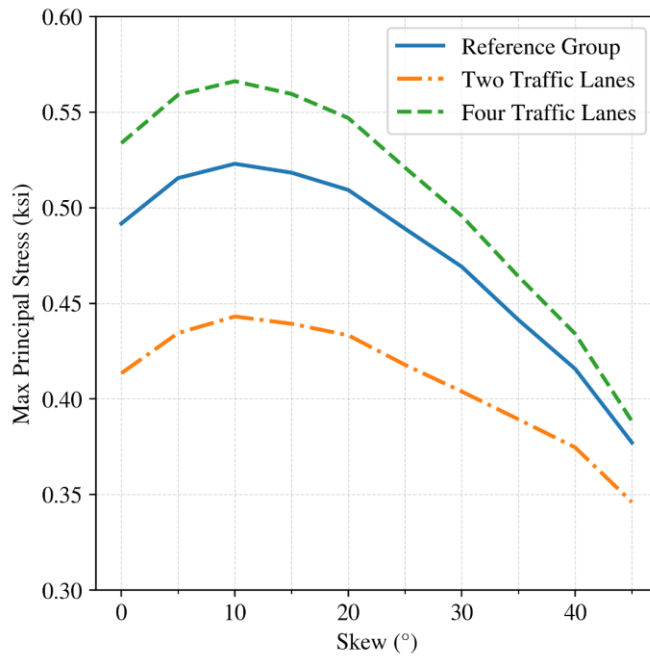
Figure 7.9 Critical principal stress variation with number of traffic lanes.
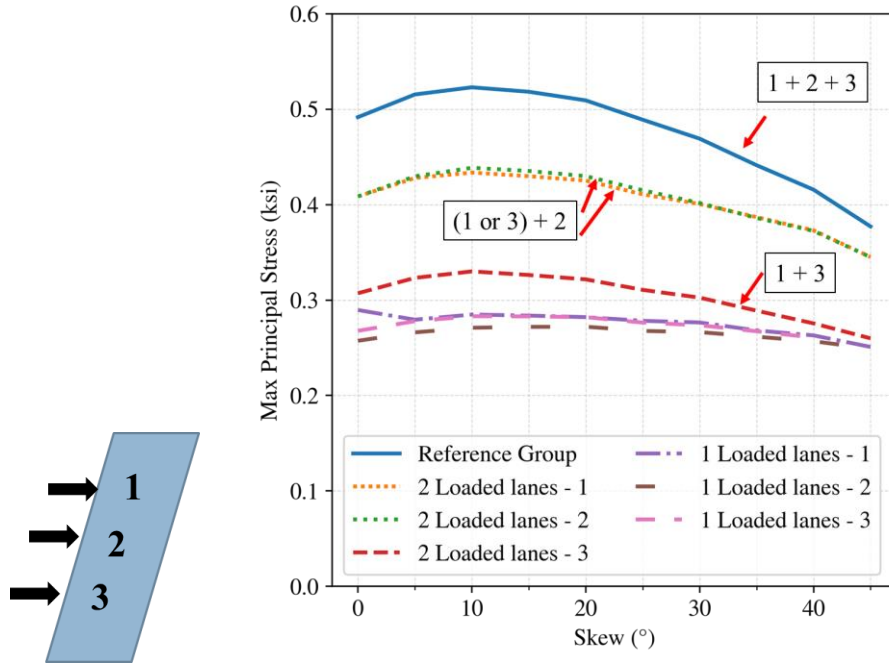
Figure 7.10 Critical principal stress with respect to loaded lanes.

When there is support from the subbase, i.e., the subbase stiffness is not zero, the critical stress decreases compared to the simple support scenario. Typically, for approach slab models with a field-estimated modulus of subbase reaction that is uniformly distributed, the critical stresses remain lower than 0.5 ksi (sometimes by as much as 30%), as shown in the boxed region of Figure 7.11 (a). As movement of the integral abutment needs to be accommodated by a wedge of granular soil behind the abutment, a well-compacted granular subbase under the approach slab may not be feasible for approximately half of its width. This leads to differential support conditions of the subbase, with strong support under the half of the approach slab near the expansion joint and weak support near the abutment. Figure 7.11 (b) shows the critical stresses when there is uniformly distributed subbase support on only the half of the approach slab near the expansion joint. As expected, the approach slabs with full uniform subbase support exhibit critical stresses of smaller magnitude than those with partial uniform subbase support; the difference increases as the modulus of subbase reaction increases. For the partial uniform subbase support when the modulus of subbase reaction is 0.05 kip/in/in^2, the critical stress is 58% larger compared to the full uniform support case. Though critical stresses are larger, their magnitude is still below the modulus of rupture of the concrete material of the approach slabs, which indicates that the potential risk of cracking in the approach slabs is still relatively low. Table 7.3 shows that, compared to no subbase support, partial uniform subbase support can provide reduction in stress in the range of 30 to 45% when the modulus of subbase reaction is 0.05 kip/in/in^2.

227
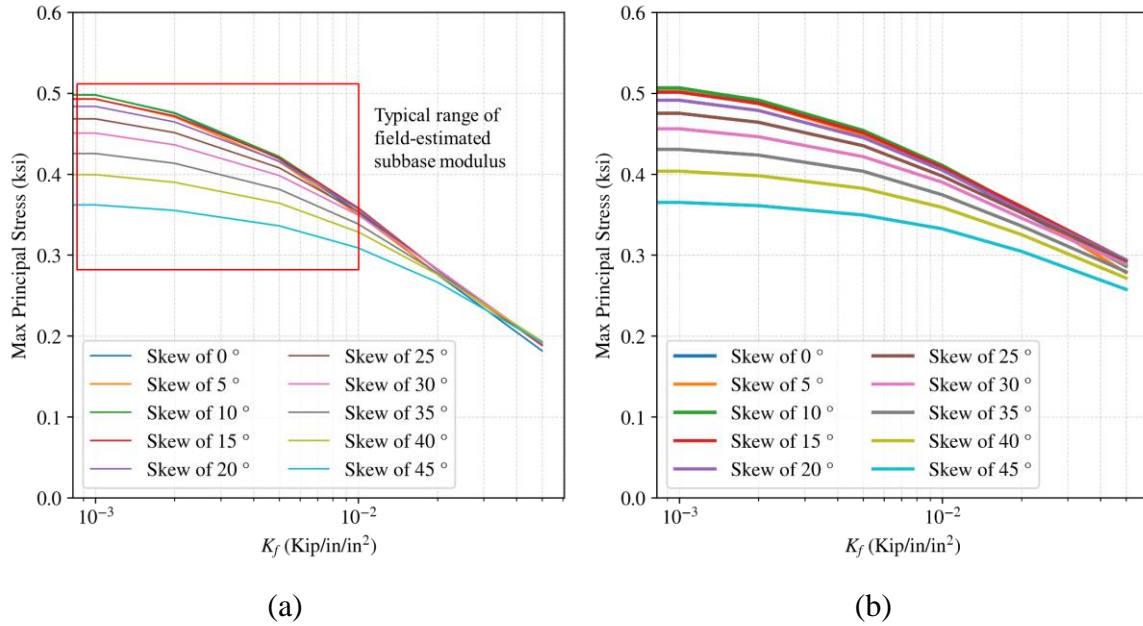
Figure 7.11 Critical principal stress with respect to subgrade stiffness (a) full uniformly distributed subbase support, (b) partial uniformly distributed subbase support.

Table 7.2 Difference (%) in critical stress between full and partial uniform subbase support of approach slabs

Skew	K_f (kip/in/in^2)						
	0	0.001	0.002	0.005	0.01	0.02	0.05
0	0	1.7	3.3	7.9	15.3	27.7	57.6
5	0	1.8	3.5	8.0	16.1	28.5	47.3
10	0	1.7	3.3	7.6	14.9	27.5	51.6
15	0	1.7	3.3	7.4	14.0	27.8	56.1
20	0	1.6	3.0	7.0	13.5	26.3	54.4
25	0	1.5	2.8	6.7	12.4	24.6	53.4
30	0	1.2	2.3	5.8	11.6	22.2	51.3
35	0	1.2	2.4	5.8	10.7	20.8	45.6
40	0	1.1	2.1	5.0	9.2	17.8	40.4
45	0	0.8	1.7	4.0	7.6	14.3	34.0

Table 7.3 Difference (%) in critical stress between no and partial uniform subbase support of approach slabs

Skew	K_f (kip/in/in^2)						
	0	0.001	0.002	0.005	0.01	0.02	0.05
0	0	-3.3	-6.3	-13.7	-22.2	-32.7	-45.3
5	0	-3.1	-6.0	-13.5	-21.6	-31.2	-46.3
10	0	-3.0	-5.9	-13.1	-21.3	-31.3	-45.2
15	0	-2.8	-5.5	-12.6	-20.8	-30.2	-43.0
20	0	-2.7	-5.2	-11.8	-19.8	-29.6	-41.7
25	0	-2.4	-4.7	-10.6	-18.3	-27.6	-40.0
30	0	-2.2	-4.3	-9.6	-16.4	-25.8	-38.1
35	0	-1.8	-3.4	-7.9	-14.6	-23.3	-36.3
40	0	-1.4	-2.8	-6.6	-12.3	-20.5	-33.6
45	0	-1.1	-2.2	-5.3	-10.0	-17.5	-30.2

In summary, the approach slab skew, type of truck load, and the total number of traffic lanes affect the approach slab bending behavior more significantly than other parameters. Especially for mildly skewed approach slabs with more traffic lanes and all lanes loaded by IL-120 trucks, the critical principal stress can be higher and is reached when all trucks are aligned parallel to the skew and located at roughly the mid-span of the approach slab.

7.2.2 Thermal Analysis

Thermal stresses can be introduced if there is thermal deformation of the approach slab and some level of restraint is applied to the slab such that it cannot deform as much as free expansion or contraction would dictate. In a yearly cycle, the approach slab experiences both increases and decreases in temperature compared to the construction temperature, which is incorporated as the overall temperature change in the approach slab. The approach slab also experiences daily temperature cycles where there are differences between the temperatures at the top and bottom surfaces of the slab due to solar radiation. Such temperature variation through the thickness is implemented by defining a linear temperature gradient in the numerical models. Table 7.2 shows all the combination cases of overall temperature change and temperature gradient in the parametric study.

Table 7.4 Thermal load cases in the parametric study.

Case	Overall Temperature Change	Temperature Gradient
1	0 °F (0 °C)	0 °F/inch (0 °C/inch)
2	0 °F (0 °C)	-0.72°F/inch (-0.4°C/inch)
3	0 °F (0 °C)	+1.26°F/inch (+0.7°C/inch)
4	-72°F (-40°C)	0 °F/inch (0 °C/inch)
5	-72°F (-40°C)	-0.72°F/inch (-0.4°C/inch)
6	-72°F (-40°C)	+1.26°F/inch (+0.7°C/inch)
7	+36°F (+20°C)	0 °F/inch (0 °C/inch)
8	+36°F (+20°C)	-0.72°F/inch (-0.4°C/inch)
9	+36°F (+20°C)	+1.26°F/inch (+0.7°C/inch)

The other primary aspect that affects the thermal stresses in the approach slab is the restraint applied to it. At the abutment-approach slab interface, the restraint that the abutment provides to the approach slab is due to the incompatible movement / difference in movement between the abutment and the approach slab, which is caused by the dowel bars, as well as the potential friction between the abutment and the approach slab. The incompatible movement / difference in movement can be attributed to two factors: 1) the difference in the thermal deformation between the abutment and the approach slab due to different temperature distributions in these structural components and different material properties, such as coefficient of thermal expansion (CTE); and 2) the additional restraints applied to the abutment due to the piles and embankment backfill near the abutment backwall. At the approach slab-pile bent interface, the restraint is mainly caused by the contact friction between the approach slab and the pile bent. Since there are no sensors dedicated to collect the field data related to the abutment and pile bent, hypothetical scenarios are made in the parametric study to account for different extreme levels of restraint: 1) there is no temperature change in the abutment and pile bent, and the bottom of both supports are restrained in three orthogonal (U1, U2, and U3) degrees of freedom, providing the strongest restraint to the approach slab; 2) the abutment and pile bent have exactly the same overall temperature changes as the approach slab, and they are free to move in the transverse direction about the centerline (mid-width of whole the approach slab). Figure 7.12 (a) shows the case of high restraint from the support, where the displacement of U2 is small in the abutment compared to the approach slab, whereas the other extreme scenario that captures a small difference in movement between the abutment and the pile bent is illustrated in Figure 7.12 (b).
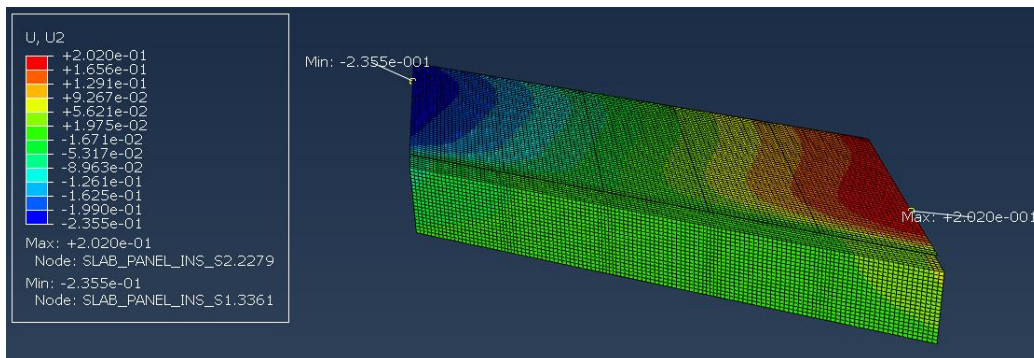
(a)
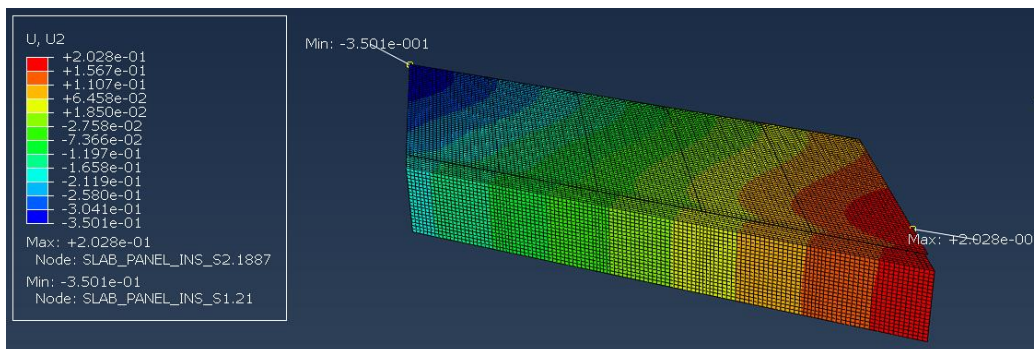
(b)

Figure 7.12 Displacement of U2 (inch) in the approach slab and abutment with (a) strong restraint and (b) weak restraint.

230

Cracking of concrete is one of the primary interests when analyzing the structures. Consequently, the critical tensile principal stresses are evaluated and if not otherwise stated, the critical principal stresses refer to the tensile critical principal stresses. Table 7.3 and Table 7.4 show the critical principal stresses, among all the cases defined in Table 7.2 for approach slabs with 3 traffic lanes and skews of 0°, 15°, and 30°, at their top and bottom surface, respectively. The temperature fraction indicates how much the temperature of the support (including abutment and pile bent) changes compared to the approach slab. The critical principal stress at the bottom surface is slightly greater than at the top surface, with the values for both surfaces exceeding 1 ksi. The critical principal stresses on both the top and bottom surfaces appear when there is a -72°F (-40°C) temperature change in the approach slab as the slab contracts and is restrained by the support, especially the abutment. If the temperature changes in a greater range as suggested by LaFave et al. (2021), the critical stresses will increase from the values in Table 7.3 and 7.4. In addition, a negative temperature gradient induces tensile stresses for the top portion of the slab and a positive temperature gradient does the same for the bottom portion of the slab. In summary, the critical principal stresses are observed in case 5 of Table 7.2 for the top surface and case 6 of Table 7.2 for the bottom surface. When the bottom restraint of the supports (abutment and pile bent) is released in U2, the critical stresses decrease. When the temperature variation of the supports more closely resembles that of the approach slab, the critical principal stresses decrease significantly, which conveys that the differential temperature field of the IAB structural components can substantially affect the approach slab stress. Generally, as the skew of the approach slab increases, the critical thermal induced stresses increase as well.

Figure 7.13 presents the principal stress distribution of case 6 in Table 7.2 at the bottom surface of the approach slab with 15° skew and the supports fully restrained at the bottom. The critical stress appears near the abutment-approach slab interface, indicating the most restrained region of the approach slab. The principal stress distribution remains similar among temperature fractions in Table 7.4. The principal stress distribution of the corresponding top surface is shown in Figure 7.14, which is similar to the observations made in Figure 7.13.

Table 7.5 Critical tensile thermal stresses due to thermal effects at the top surface.

Skew	Temperature Fraction	Critical Principal Stress (ksi) (Strong Support Restraint)	Critical Principal Stress (ksi) (Weak Support Restraint)
0	1	1.488	0.375
0	0.5	1.647	1.022
0	0	**1.944**	1.751
15	1	1.520	0.365
15	0.5	1.705	1.038
15	0	**1.984**	1.775
30	1	1.600	0.350
30	0.5	1.788	1.035
30	0	**2.016**	1.768

Table 7.6 Critical tensile thermal stresses due to thermal effects at the bottom surface.

Skew	Temperature Fraction	Critical Principal Stress (ksi) (Strong Support Restraint)	Critical Principal Stress (ksi) (Weak Support Restraint)
0	1	1.583	0.412
0	0.5	1.800	1.118
0	0	**2.071**	1.867
15	1	1.614	0.401
15	0.5	1.836	1.127
15	0	**2.091**	1.876
30	1	1.693	0.391
30	0.5	1.900	1.125
30	0	**2.107**	1.857

S, Max. In-Plane Principal
SNEG, (fraction = -1.0)
(Avg: 100%)
+1.614e+00
+1.473e+00
+1.332e+00
+1.191e+00
+1.050e+00
+9.096e-01
+7.688e-01
+6.280e-01
+4.872e-01
+3.463e-01
+2.055e-01
+6.467e-02
-7.616e-02

Max: +1.614e+00
 Elem: SLAB_PANEL_INS_L3.2
 Node: 1482
Min: -7.616e-02
 Elem: SLAB_PANEL_INS_L3.1345
 Node: 21

Max: +1.614e+000

Min: -7.616e-002

Y
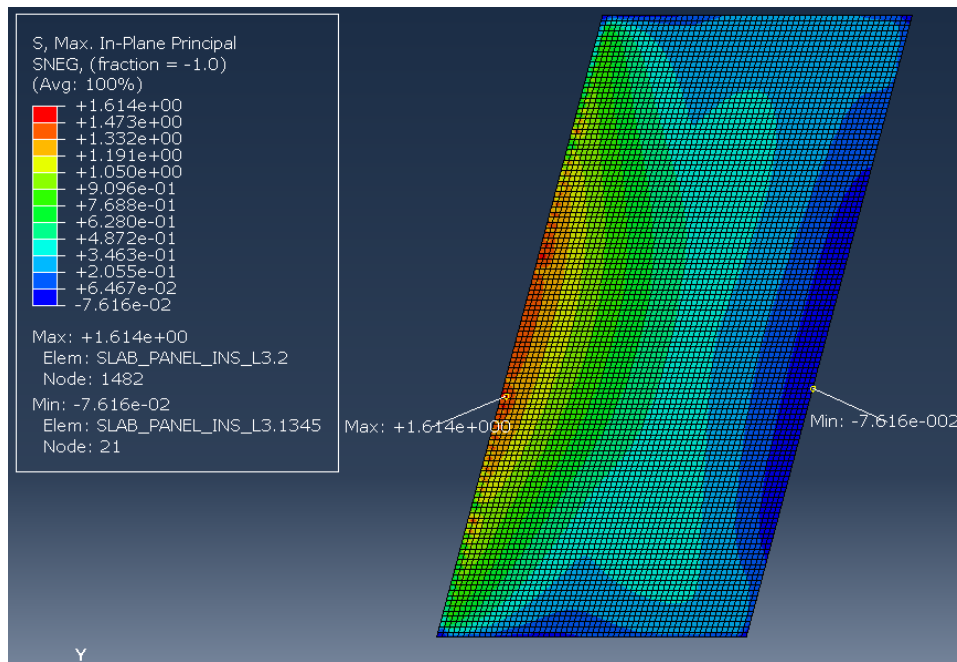
(a)
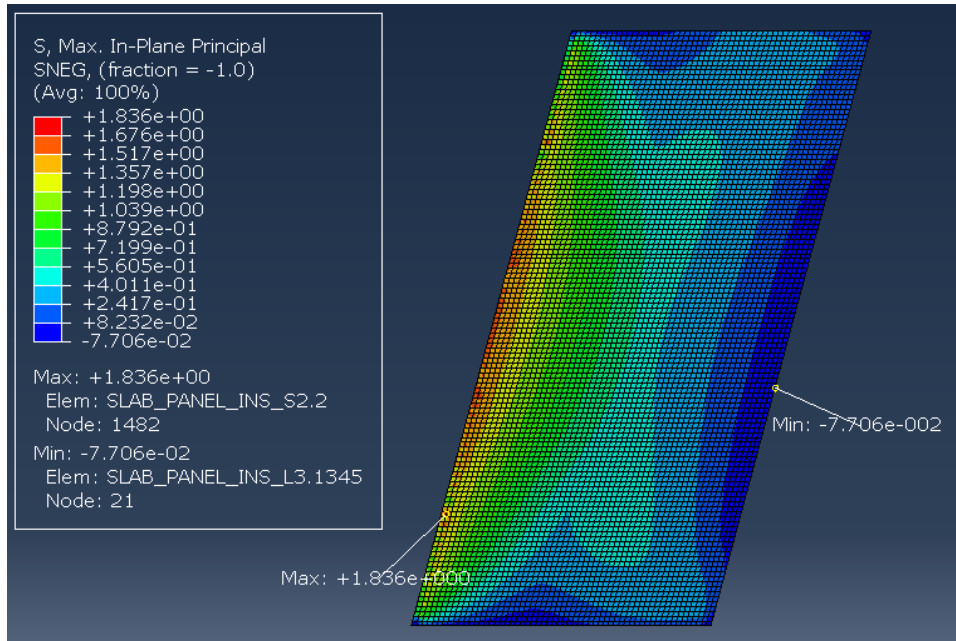
(b)
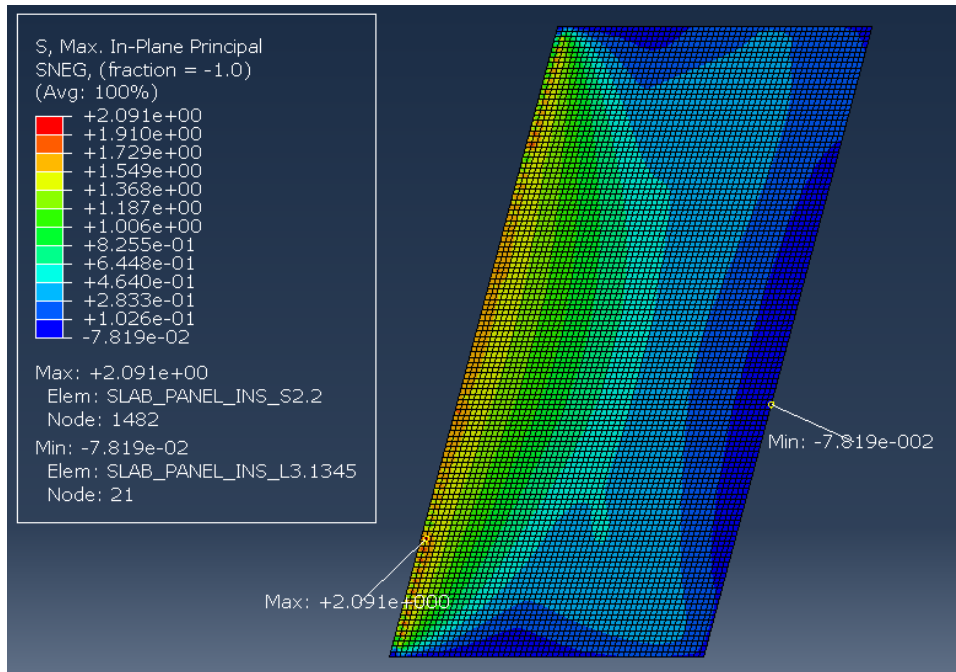
(c)

Figure 7.13 Principal stress (ksi) distribution at bottom surface of the approach slab with a temperature fraction of (a) 1, (b) 0.5, and (c) 0.

(a)

(b)

234

S, Max. In-Plane Principal
SPOS, (fraction = 1.0)
(Avg: 100%)
+1.984e+00
+1.808e+00
+1.631e+00
+1.455e+00
+1.278e+00
+1.102e+00
+9.256e-01
+7.492e-01
+5.728e-01
+3.964e-01
+2.200e-01
+4.358e-02
-1.328e-01

Max: +1.984e+00
 Elem: SLAB_PANEL_INS_S2.2
 Node: 1482
Min: -1.328e-01
 Elem: SLAB_PANEL_INS_L2.1141
 Node: 3852

Min: -1.328e-001

Max: +1.984e+000
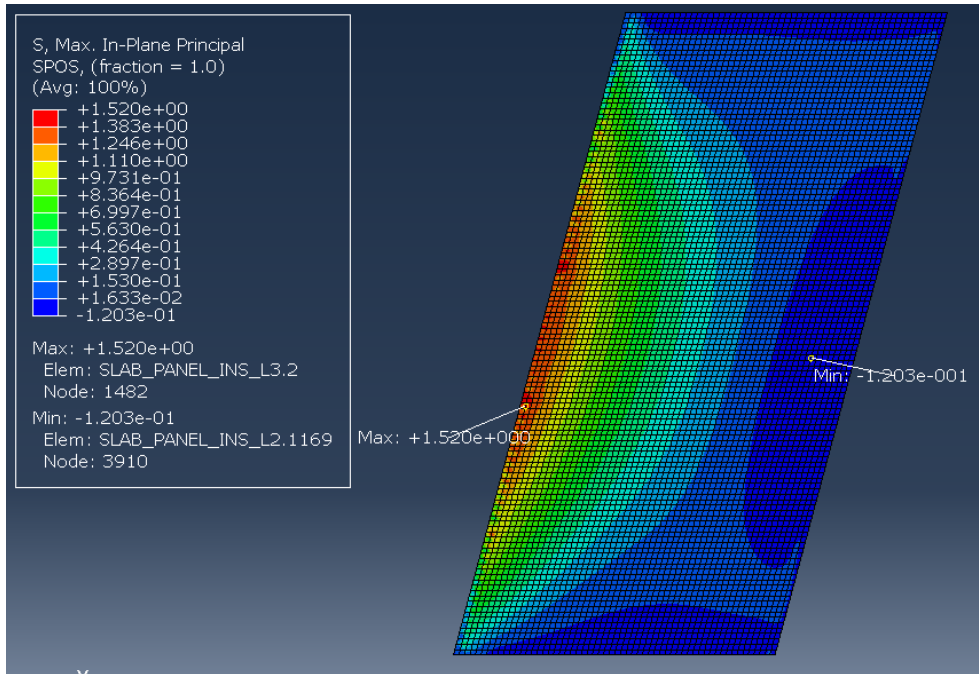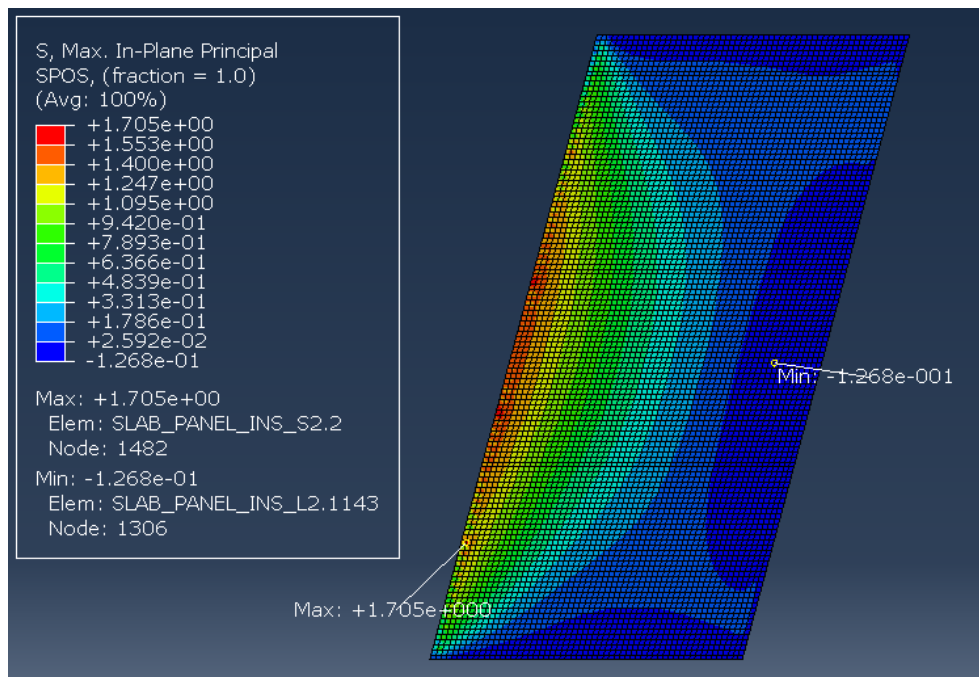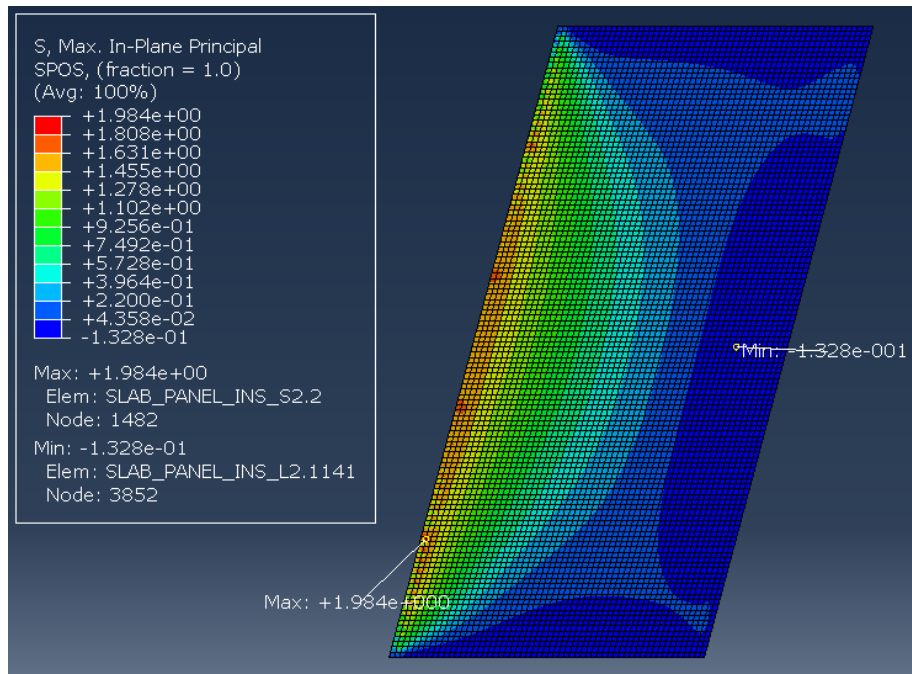
(c)

Figure 7.14 Principal stress (ksi) distribution at top surface of the approach slab with a temperature fraction of (a) 1, (b) 0.5, and (c) 0.

Thermal gradient through the slab thickness induces stresses in the slab. As the thermal gradient adopted in the numerical models is linear, which differs from the actual temperature profile of a slab-on-grade in the sense that the temperature near the top surface varies more significantly, the numerical modeling does not fully capture the exact stress distribution of the slab in the field. However, the numerical results can still provide interpretations to the field observed crack patterns. In the case of temperature variation due solely to positive thermal gradient, tensile principal stresses are developed at the bottom portion of the slab, of which the maximum component is shown in Figure 7.15 (a). The magnitude (color) and direction (arrow) of maximum component for the tensile principal stresses in Figure 7.15 (b) suggest a similar crack pattern as observed from the field – namely, cracks appearing near the corners of the approach slab and approximately perpendicular to the transverse edge. The similar principal stress distribution is observed at the top surface given a negative thermal gradient, as shown in Figure 7.16. Note that the magnitude range of the maximum component of principal stresses differs between Figure 7.15 (a) and Figure 7.15 (b), as well as between Figure 7.16 (a) and Figure 7.16 (b). This is attributed to the way that Abaqus (Dassault Systems 2017) creates the contour plot and the stress trajectory plot. The most accurate results that the Abaqus solver delivers are those at the integration points of every element. When preparing for the contour, nodal results are needed so linear extrapolating from integration points and averaging the nodal values over all elements sharing the node are carried out. On the other hand, for the trajectory plot, only the results at integration points are used. As a result, essentially, Figure 7.15 (a) and (b) are showing the same variables but in slightly different ways. Although the numerical accuracy of contour plots is sacrificed due to linear extrapolation and averaging, it estimates the stress magnitude distribution in the whole domain of the approach slabs and conveys the trend of stress changes.

|(a)|(b)|
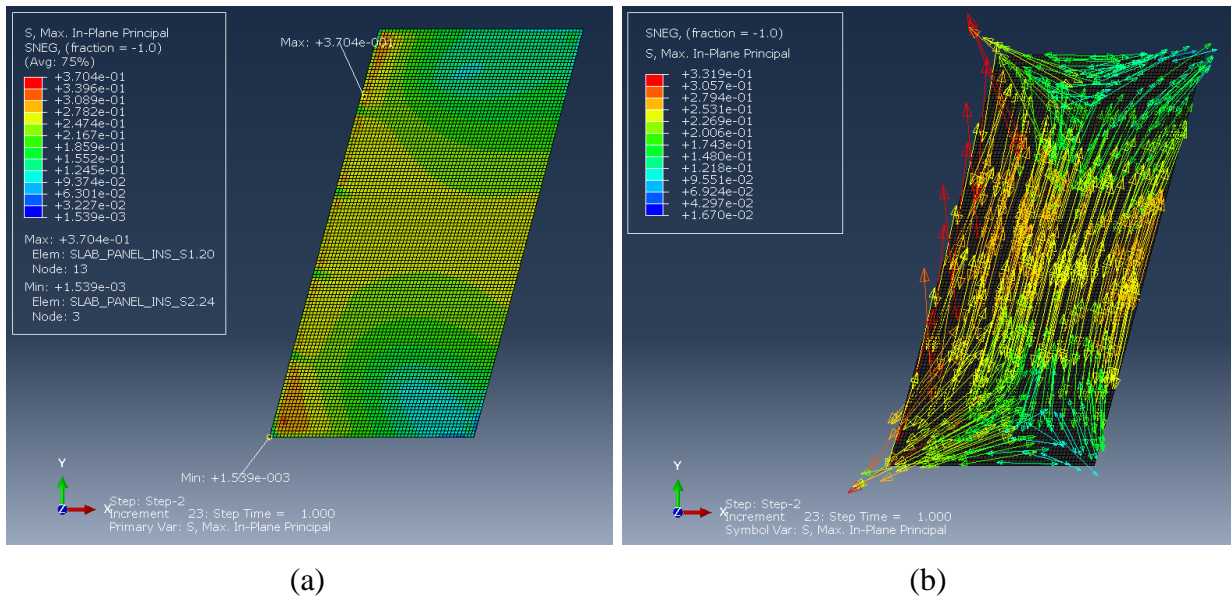
Figure 7.15 Principal stress (ksi) at bottom surface of approach slab with a positive thermal gradient of +1.26°F/inch (+0.7°C/inch): (a) stress magnitude and (b) stress trajectory.

|(a)|(b)|
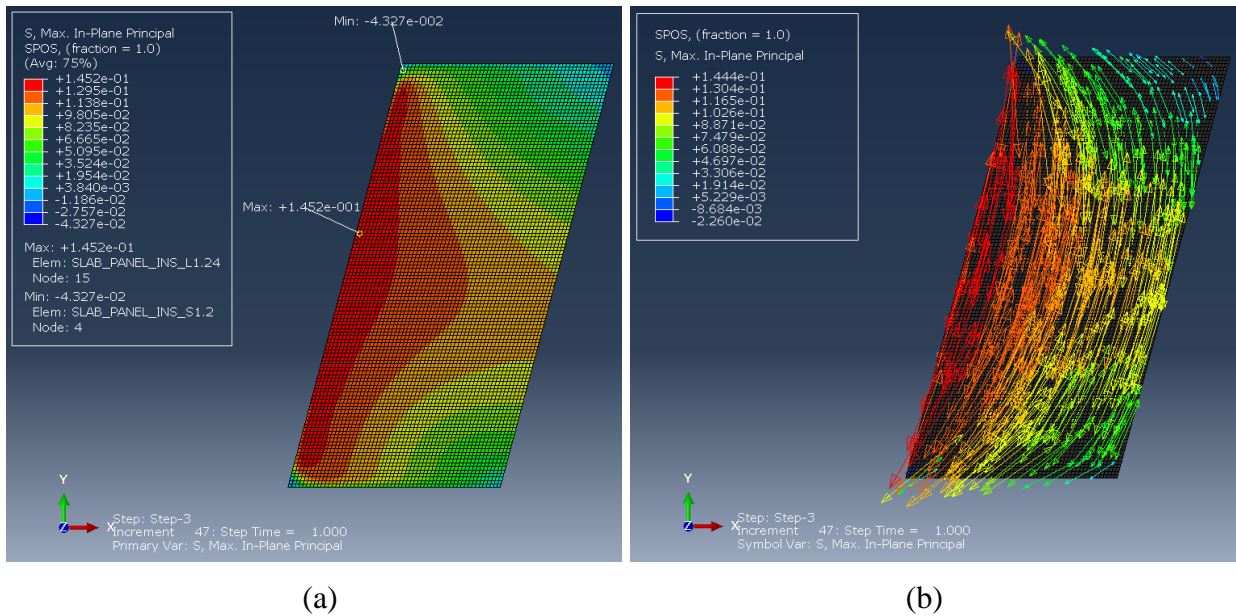
Figure 7.16 Principal stress (ksi) at the top surface of approach slab with a negative thermal gradient of -0.72°F/inch (-0.4°C/inch): (a) stress magnitude, and (b) stress trajectory.

The details of the abutment-approach slab connection affect the critical stress in the slab due to thermal loading effects. Abaqus JOIN and SLOT connector elements are compared in the parametric study to represent two possible physical conditions. For a JOIN connector element, the translation in all three directions is restrained between the abutment and the approach slab, whereas for a SLOT connector element the relative displacement in the direction of the transverse edge of

236

the slab is released, which reduces the stresses caused by incompatible deformation between the abutment and approach slab. Table 7.5 details the significant reduction in critical principal stresses attributed to the released restraint. Hypothetical scenarios suggest that releasing the restraint along the transverse edge of the approach slab can effectively reduce the critical stress and potential for cracking.

Table 7.7 Comparison of critical stresses for JOIN and SLOT.

Skew	Fraction	Max Principal (ksi) (JOIN)	Max Principal (ksi) (SLOT)
	1	1.207	0.340
0	0.5	1.330	0.364
	0	1.629	0.389
	1	1.240	0.243
15	0.5	1.386	0.242
	0	1.668	0.251
	1	1.314	0.245
30	0.5	1.473	0.192
	0	1.702	0.194
	1	1.422	0.291
45	0.5	1.570	0.329
	0	1.719	0.326

8 Summary and Recommendations

8.1 Summary

This research project was funded by the Illinois Tollway to investigate cracking that has been observed in bridge approach slabs, particularly at integral abutment bridges, with the goals of improving performance and reducing maintenance at bridge approach slabs on the Tollway. The primary tasks undertaken by the research team from the University of Illinois were:

- Literature review,
- Agency survey,
- Review and synthesis of prior approach slab field inspections (crack surveys),
- New approach slab field inspections (crack surveys),
- Field instrumentation of two Tollway approach slabs,
- Long-term data collection and evaluation of traffic and thermal effects,
- Short-term static truck loading tests and evaluation of thermal effects,
- Numerical simulations of approach slab behavior under traffic and thermal effects.

Although approach slab design practice in the U.S. varies significantly between states – such as in approach slab length, thickness, reinforcement, end support at the pavement end, and connection to the abutment – there are commonalities in bridge approach system problems. For example, states report problems related to differential settlement, approach slab cracking, excessive deflection of the approach slab, and water intrusion into the backfill under the approach slab. Mitigation methods for approach slab distress include: structural improvements such as increasing slab thickness, reinforcement, using anchor bar connections at the abutment end as well as introducing an expansion joint; and geotechnical improvements such as using sleeper slabs or pile-supported beams to control the settlement of the slab.

A comprehensive agency survey was conducted by the research team to learn the current design practice adopted by other state transportation agencies for IABs and approach slabs, to identify the primary problems associated with approach slabs and to explore possible solutions to approach slabs cracking. The agency survey found that approach slabs with skews larger than 30° tend to have diagonal cracks that extend out of the obtuse corners and across the acute corners. Longitudinal cracks are common among approach slabs that have little or no skew. Increasing reinforcement is the most common method among states to minimize cracks in approach slabs.

Structural drawings and photos of approach slab cracking for 46 Illinois Tollway bridges were studied to identify cracking patterns and bridge design and construction parameters that may influence approach slab cracking. The generally observed patterns include:

- For skew less than 30°, mainline highway bridge approach slabs have cracks near the corners and shoulders, whereas crossroad bridge approach slabs have cracks in the travel lanes that propagate in the direction of traffic.
- For skew of 30° and greater, many diagonal cracks extend out of the obtuse corners and across the acute corners of travel lanes and shoulders of approach slabs, and other cracks originate from both the expansion and construction joints and are roughly perpendicular to those joints.

The severity of cracking for the inspected bridge approach slabs can be categorized as follows:

- Severe: there are on average are 3 or more cracks per approach slab;
- Moderate: there are on average 1 or 2 cracks per approach slab;
- Uncracked: there are no cracks.

By evaluating design and construction parameters and relating them to occurrence of cracking, it is found that skew over 30°, staged construction, and presence of wingwalls may be primary causes of severe cracking in approach slabs at mainline bridges. For crossroad bridges, severe cracking was observed more frequently in approach slabs at IABs and approach slabs with wingwalls.

Two Tollway IAB approach slabs, one cast-in-place and one precast, along Illinois Route 390 were instrumented and monitored. Embedded strain gages were installed at the top and bottom reinforcement mats to measure the change in strain of the concrete and the temperature at the gage locations. Displacement transducers were installed at the corners of the approach slabs to measure the relative movement between the approach slab and abutment or transition slab.
The major observations and findings from the analysis of field data are:

- The two monitored approach slabs experience very similar weather conditions.
- Field data suggest that top gage temperatures tend to fluctuate more than the bottom gage temperatures as gages at the top reinforcement mat are more sensitive to the ambient environmental changes. In general, top gage temperatures are higher than the bottom ones during the afternoon time.
- Actual strain is defined as the strain observed due to all effects, including slab dead load, live load, thermal load, bridge abutment displacement, and restraints imposed on the slab. Load-related strain is defined as the stress-causing strain observed due to live load, thermal load, abutment displacement, and restraints. Load-related strain is calculated by subtracting the theoretical strain caused by the thermal expansion of concrete from the measured actual strain.
- The actual strain at the embedded gage locations for the cast-in-place slab at Arlington Heights Road ranged from about 400 $\mu\varepsilon$ in compression to 400 $\mu\varepsilon$ in tension. The actual strain for the precast slab at Prospect Avenue was in a similar range, from about 400 $\mu\varepsilon$ in compression to 350 $\mu\varepsilon$ in tension.
- The load-related strains for the cast-in-place slab at Arlington Heights Road ranged from about 200 $\mu\varepsilon$ in compression to 200 $\mu\varepsilon$ in tension, while for the precast slab, the range was 200 $\mu\varepsilon$ in compression to 240 $\mu\varepsilon$ in tension.
- The actual strain change tends to be tensile during periods with temperatures higher than reference temperature (summer season) and compressive during the period with temperature lower than the reference temperature. However, tensile load-related strains are observed during the time when the temperature is lower than the reference and compressive load-related strain are observed during the time when temperature is higher than the reference at most of the gages in the cast-in-place slab and some gages in the precast slab.
- The load-related strain at twenty-one of forty-three gages at the cast-in-place slab as well as ten out of forty-two gages at the precast slab exhibits generally linear trends versus

temperature and strong consistency among year 1, 2, and 3. These gages are scattered through the slabs with no clear pattern.

- Eleven gages at the cast-in-place slab and fifteen gages at the precast slab maintain a linear relation to the temperature for each year, and there are gradual accumulations in compression for the cast-in-place slab gages while both compression and tension accumulate at different gages in the precast slab gages. For the cast-in-place slab, it is found that top longitudinal gages at the midspan tend to accumulate compressive load-related strains whereas bottom longitudinal gages at the midspan are more likely to gain accumulation in tensile load-related strains, indicating there was an increase in positive bending at the cast-in-place slab.

- Eleven gages at the cast-in-place slab and seventeen gages at the precast slab experience significant change in load-related strain magnitude (large changes in strain within a small range of temperature) at some time but otherwise are approximately linear with respect to the temperature. For the cast-in-place slab, only a significant increase in compression is observed, and it appears more frequently at the gages close to the abutment side. For the precast slab, a noticeable increase in compression is widely found in the two sections on the north side (North Shoulder and Lane 1), and a large increase in tension occurred at the remaining three sections, suggesting the possibility of clockwise global rotation of the whole approach slab.

- The behavior of the slab under the highest and lowest temperature during the first two years appears to be similar, with a higher magnitude (tensile) load-related strain observed during the lowest temperature.

- Load-related strain changes were used to calculate the estimated stress changes by assuming the slabs to be linear elastic. The stresses thus calculated were extrapolated to the surface to obtain an approximate extreme layer stress for the slab. By comparing these approximate stresses to the estimated modulus of rupture, several bottom gage locations at both instrumented slabs are found to have a potential risk of cracking.

- The variation of extreme layer stress with time shows that the stress is generally uniform in each lane of the slab since start of service (October 2017) to March 2018, but the stress diverges as the slab experiences more temperature variation cycles.

- At the transition slab ends of the approach slabs, the relative movements observed were approximately 1 inch (due to the expansion joint). At the abutment ends of the approach slabs, the relative movements were approximately 0.1 inch (due to the dowel bars). The opening between the abutment and the approach slab as well as the opening between the approach slab and the transition slab are always smaller on the north side than on the south side at the precast slab, indicating that there may be moderate clockwise in-plane rotations at the precast slab.

Static truck loading tests were conducted to study the behavior of the approach slabs under known live load. Distinct changes in strain due to the applied truck load at different gage locations were measured and post-processed to estimate the subgrade stiffness under the slab and calibrate the numerical models. Based on the results, the modulus of subgrade reaction (k) is 0.005 kip/in/in^2 or smaller for the precast approach slab and 0.01 to 0.015 kip/in/in^2 for the cast-in-place approach

slab. The estimated field values for k correspond to typical values representative of loose sand. Short term behavior of the approach slabs was studied based on the test days' data. A strong linear trend of slab actual strains vs. temperatures during the nighttime (no solar radiation) was found. In a typical day with stable and normal sunlight, solar radiation from sunrise to sunset of a day has significant impact on the slab temperature gradient through the thickness, leading to load related strains/stresses associated with thermal effects comparable or greater than load related strains/stresses associated with the live loads.

Numerical models were developed using the computational platform Abaqus (Dassault Systems 2017) to analyze the approach slab behavior and performance under live load and thermal load. A parametric study was conducted considering various approach slab geometric variables, live load conditions, thermal load conditions, and boundary restraint conditions. For live load, the principal stress generally follows a decreasing trend when the bridge skew increases due to the two-way slab bending behavior and a more direct load path to the support for larger skew. The IL-120 truck loading, mild skew, more loaded traffic lanes, and reduced support from the subbase all contribute to larger tensile principal stress in the approach slab (>550 psi). Thermal analysis suggests that overall temperature change in the slab, temperature gradient through the slab thickness, the difference in temperature distribution between the approach slab and supports (abutment and pile bent), and the restraint of the supports can significantly affect the critical stresses in the approach slab. Hypothetical cases in the parametric study suggest that the critical stresses can be greater than 2 ksi with an overall change of -72°F in slab temperature, a +1.26°F/inch temperature gradient, and no temperature changes in the supports of which the translations at the bottom are fully restrained. If the restraint at the abutment-approach slab connection is released along the length of abutment, the critical thermal induced stress can decrease to less than 0.4 ksi.

The instrumented approach slabs provide acceptable performance during the term of field monitoring from November 2017 to April 2020. No significant cracks were observed in either approach slab. Considering the similarity between the design of the monitored approach slabs and the slabs where severe cracking was observed, potential causes of approach slab cracking for IABs that were not considered in this study may be related to unique geotechnical conditions, construction quality of the approach slab, and material quality of the approach slabs.

8.2 Recommendations

Based on this research project, the following recommendations are made related to approach slab design, detailing and performance:

- For the two monitored approach slabs, the current Tollway approach slab details (both cast-in-place and precast) appear to be performing well with almost no evidence of cracking.
- Although live load effects in the approach slabs are not deemed to be problematic, the longitudinal reinforcement for the bottom mat at the middle lanes could be increased for long-term robustness against high truck load demands, especially for wide approach slabs.
- A well-compacted subbase can help reduce the stress demand due to the truck loads for both cast-in-place and precast approach slabs. Practically, compaction of the subbase can only be achieved for a portion of the approach slab span due to the typical backfill procedures for IABs. Simulations demonstrate that when uniform subbase support, with modulus of subbase reaction equal to 0.05 kip/in/in^2, is provided under the half of the

approach slab away from the abutment, the critical stress is reduced in the range of 30 to 45% compared to no subbase support.

- The lateral restraint from the abutment can be partially released by introducing new details that allow the approach slab to expand and contract with less restriction. This increased flexibility in the transverse direction is expected to reduce the potential risk of cracking due to thermal loads. For the dowel bars between the abutment and the cast-in-place approach slabs, employing oversized precast holes with durable and flexible filler material around the dowel bars into the abutment instead of casting the dowel bars into the abutment may release restraint due to the thermal loading at the abutment-approach slab interface.

- New details that reduce friction between the abutment and the approach slab in the support region will also allow the approach slab to expand and contract with less restriction, and this reduction in constraint is expected to reduce the potential risk of cracking due to thermal loads.

References

AASHTO. 2002. *LRFD Bridge Design Manual*. Washington, D.C.

AASHTO. 2017. *LRFD bridge design specifications*. 8th ed. Washington, DC: AASHTO

Abendroth, R. E., L.F. Greimann, and M. D. LaViolette. 2007. *An Integral Abutment Bridge With Precast Concrete Piles, Final Rep.* IHRB Project TR-438, CTRE Project No. 99-48, Ames, Iowa: IOWA Department of Transportation, Center for Transportation Research and Education Report.

Allen, D.L. 1985. *A Survey of the States on Problems Related to Bridge Approaches*. Research Report UKTRP-85-25, Kentucky Transportation Research Program 188 pp.

Arsoy, S., R. M. Barker, and J. M. Duncan. 1999. *The Behavior of Integral Abutment Bridges*. Rep. No. VTRC 00-CR3, Charlottesville, VA: Virginia Transportation Research Council.

Arsoy, S., J. M. Duncan, and R. M. Barker. 2004. "Behavior of a semi-integral bridge abutment under static and temperature-induced cyclic loading." Journal of Bridge Engineering, March, Vol. 9, No. 2, pp. 193–199.

Bakeer, R. M., N. J. Mattei, B. K. Almalik, S. P. Carr, and D. Homes. 2005a. *Evaluation of DOTD semi-integral bridge and abutment system.* (No. FHWA/LA. 05/397). Tulane University. Dept. of Civil and Environmental Engineering.

Bakeer, R. M., M. A. Shutt, J. Zhong, S. C. Das, and M. Morvant. 2005b. "Performance of pile-supported bridge approach slabs." Journal of Bridge Engineering, 10(2), 228-237.

Bowders, J. J., J. E. Loehr, R. Luna, and T. M. Petry. 2003. *Determination and prioritization of MoDOT geotechnical related problems with emphasis on effectiveness of design for bridge approach slabs and pavement edge drains.* (No. RI99-026; RDT 03-001). Missouri. Dept. of Transportation.

Breña, S. F., C. H. Bonczar, S. A. Civjan, J. T. DeJong, and D. S. Crovo. 2007. "Evaluation of seasonal and yearly behavior of an integral abutment bridge." *Journal of Bridge Engineering*, 12(3), 296-305.

Briaud, J. L., S. F. Maher, and R. W. James, 1997. "Bump at the end of the bridge." *Civil Engineering*, 67(5), 68-69.

Burdette, E. G., E. E. Ingram, J. B. Tidwell, D. W. Goodpasture, J. H. Deatherage, and S. C. Howard. 2004. "Behavior of Integral Abutments Supported by Steel H-Piles." *Transportation Research Record*, 1892(1), 24–28.

Burke, M.P. 1993. "The design of integral concrete bridges." Concrete International, Vol. 15, June, pp. 37-42.

Cai, C. S., X. M. Shi, G. Z. Voyiadjis, and Z. J. Zhang. 2005. "Structural performance of bridge approach slabs under given embankment settlement." Journal of Bridge Engineering, 10(4), 482–489.

Cross, H. 1932. "Analysis of continuous frames by distributing fixed-end moments." Proceedings of the American Society of Civil Engineers.

Dassault Systems. 2017. Abaqus. https://www.3ds.com/products-services/simulia/products/abaqus/

Emerson, M. 1977. *Temperature differences in bridges: basis of design requirements*. TRRL Lab Report 765, Crowthorne, Berkshire: Transport and Road Research Laboratory.

Farris A. 2009. *An integral precast approach slab to bridge connection*. University of Iowa, MS dissertation.

Greimann, L. F., R. E. Abendroth, D. E. Johnson, and P. B. Ebner. 1987. *Pile design and tests for integral abutment bridges. Final Report*, No. Iowa DOT Proj HR-273, Ames, IA: Iowa Department of Transportation.

Greimann, L., B. Phares, A. Faris, and J. Bigelow. 2008. *Integral bridge abutment-to-approach slab connection.* Report No. IHRB Project TR-530 & TR-539. Iowa State University. Center for Transportation Research and Education.

Hoffman, P. C., R. M. McClure, and H. H. West. 1983. "Temperature study of an experimental segmental concrete bridge." PCI Journal, Precast/Prestressed Concrete Institute, 28(2), 78-97.

Hopkins, T.C. 1969. *Settlement of Highway Bridge Approaches and Embankment Foundations*. Rep. No. KYHPR-64-17; HPR-1(4), Kentucky Transportation Center, Lexington, Kentucky.

Hoppe, E. J. 1999. *Guidelines for the use, design, and construction of bridge approach slabs*.

Hoppe, E. J., and J. Gomez. 1996. *Field study of an integral backwall bridge*. No. VTRC 97-R7, Charlottesville, VA: Virginia Transportation Research Council.

Horvath, J. S. 2000. *Integral-abutment bridges: problems and innovative solutions using EPS geofoam and other geosynthetics*. Res. Rpt. No. CE/GE-00, 2, Bronx, NY: Manhattan College.

Hu, Y., T. Wa, C. E. Lee, and R. Machemehl. 1979. *Roughness at the Pavement-Bridge Interface*. Report No. 213- IF, Austin, Texas: Texas State Department of Highways and Public Transportation.

IDOT (Illinois Department of Transportation). 2012. *Bridge Manual*. Bureau of Bridges and Structures, Springfield, IL.

IDOT (Illinois Department of Transportation). 2019. "Integral and Semi-Integral Abutment Bridge Policies and Details". https://idot.illinois.gov/Assets/uploads/files/Doing-Business/Memorandums-&-Letters/Highways/Bridges/ABD-Memos/ABD198.pdf

Illinois Tollway (Illinois State Toll Highway Authority). 2015. *Contract I-13-4629*; *Contract I-14-4642*. Downers Grove, IL.

Illinois Tollway (Illinois State Toll Highway Authority). 2015. *Structure Design Manual.* Downers Grove, IL. https://www.illinoistollway.com/documents/20184/238200/Structure+Design+Manual_Mar2019.pdf/e1cae7d5-947d-4d02-8b98-2c29e88463bb?version=1.6

Imbsen, R. A., D. E. Vandershaf, R. A. Schamber, and R. V. Nutt. 1985. *Thermal effects in concrete bridge superstructures*. NCHRP Report 276, Washington, D.C.: Transportation Research Board.

James, R.W., H. Zhang, and D.G. Zollinger. 1991. *Observations of severe abutment backwall Damage*. Transportation Research Record 1319, Transportation Research Board, No. 1319, pp. 55-61.

Jeong, J. H., J. Y. Park, J. S. Lim, and S. H. Kim. 2014. "Testing and modelling of friction characteristics between concrete slab and subbase layers." Road Materials and Pavement Design, 15(1), 114-130.

Kim, W., J. A. Laman. 2014. "Seven-Year Field Monitoring of Four Integral Abutment Bridges." *J. Perform. Constr. Facil.* 26(1): 54-64.

Kong, B., C. S. Cai, and X. Kong. 2015. "Field monitoring study of an integral abutment bridge supported by prestressed precast concrete piles on soft soils." *Engineering Structures*, *104*, 18-31.

Kramer, S. L. and P. Sajer. 1991. *Bridge Approach Slab Effectiveness, Final Report*. Olympia, Washington: Washington State Department of Transportation.

Kunin, J., and S. Alampalli. 2000. "Integral abutment bridges: Current practice in United States and Canada." *J. Perform. Constr. Facil*, 14(3), 104-111.

LaFave, J. M., L. A. Fahnestock, B. A. Wright, J. K. Riddle, M. W. Jarrett, J. S. Svatora, H. An, and G. Brambila. 2016. *Integral abutment bridges under thermal loading: Numerical simulations and parametric study*. Illinois Center for Transportation Series No. 16-015. Research Rep. No. FHWA-ICT-16-014. Rantoul, IL: Illinois Center for Transportation.

LaFave, J., L. Fahnestock, G. Brambila, J. Riddle, M. Jarrett, J. Svatora, B. Wright, and H. An. 2017. *Integral abutment bridges under thermal loading: Field monitoring and analysis*. Illinois Center for Transportation/Illinois Department of Transportation. Research Rep. No. FHWA-R27-115. Rantoul, IL: Illinois Center for Transporation.

LaFave, J. M., G. Brambila, U. Kode, G. Liu, and L. A. Fahnestock. 2021. "Field Behavior of Integral Abutment Bridges under Thermal Loading." *Journal of Bridge Engineering*, *26*(4).

Laguros, J. G., M. M. Zaman, and I. U. Mahmood. 1990. *Evaluation of Causes of Excessive Settlements of Pavements Behind Bridge Abutments and their Remedies; Phase II. (Executive Summary)*. Rep. No. FHWA/OK 89 (07), Oklahoma Department of Transportation.

Lawver, A., C. French, and C. K. Shield. 2000. "Field performance of integral abutment bridge." *Transportation Research Record*, 1740(1), 108-117.

Lenke, L. R. 2006. *Settlement Issues--Bridge Approach Slabs.* (No. NM04MNT-02).

Long, J. H., S. M. Olson, T. D. Stark, and E. A. Samara. 1998. *Differential movement at embankment-bridge structure interface in Illinois*. Transportation Research Record, 1633(1), 53-60.

Ma, S. 2011. "Bridge Approach Slab Analysis and Design Incorporating Elastic Soil Support." M.S. thesis, Dept. of Civil and Environmental Engineering, Univ. of Missouri-Columbia.

Maitra, S. R., K. S. Reddy, and L. S. Ramachandra. 2009. "Experimental evaluation of interface friction and study of its influence on concrete pavement response." *Journal of transportation engineering*, *135*(8), 563-571.

Martin, R. D. and T. H. K. Kang. 2013. "Structural design and construction issues of approach slabs." *Practice Periodical on Structural Design and Construction*, 18(1), 12-20.

Maruri, R. F., and S. H. Petro. 2005. *Integral abutments and jointless bridges (IAJB) 2004 survey summary*. In Integral Abutment and Jointless Bridges (IAJB 2005) Federal Highway Administration West Virginia Department of Transportation.

McBride, K. C. 2005. "Thermal stresses in the superstructure of integral abutment bridges." M.S. thesis, Morgantown, WV: West Virginia University.

Nadermann, A. and L. Greimann. 2010. *Instrumentation and Monitoring of Precast Bridge Approach Tied to an Integral Abutment Bridge in Bremer County*. Report No. 08-335. Iowa State University.

Nassif, H. 2002. *Finite Element Modeling of Bridge Approach and Transition Slabs*. Rep. No. FHWA-NJ-2002-007, Rutgers, New Jersey: Department of Civil and Environmental Engineering, Center for Advanced Infrastructure & Transportation (CAIT).

Nassif, H., N. Suksawang, N. Shah, and T. Abu-Amra. 2007. *Field Implementation and Monitoring of Bridge Approach Slabs*. Report No. FHWA-NJ-2007-012. Rutgers, The State University; Florida International University; University of Alabama at Birmingham. Federal Highway Administration U.S. Department of Transportation, Washington, D. C.

Oesterle, R. G., H. Tabatabai, T. J. Lawson, T. M. Refai, J. S. Volz, and A. Scanlon, 1999. *Jointless and integral abutment bridges summary report*. Final Report to Federal Highway Administration, Washington DC.

Potgieter, I. C., and W. L. Gamble. 1989. "Nonlinear temperature distributions in bridges at different locations in the United States." PCI Journal, Precast/Prestressed Concrete Institute, 34(4), 80-103.

Puppala, A. J., S. Saride, E. Archeewa, L. R. Hoyos, and S. Nazarian. 2009. *Recommendations for design, construction, and maintenance of bridge approach slabs: synthesis report*. Report No. FHWA/TX-09/0-6022-1, The University of Texas at Arlington; The University of Texas at El Paso. Texas Department of Transportation, Austin, Texas.

Roy, S., and G. Thiagarajan. 2007. "Nonlinear finite-element analysis of reinforced concrete bridge approach slab." Journal of Bridge Engineering, 12(6), 801-806.

Seo, J., H. Ha, and J. L. Briaud. 2002. *Investigation of settlement at bridge approach slab expansion joint: Numerical simulations and model tests*. Report No. FHWA/TX-03/0-4147-2, Texas Transportation Institute; The Texas A&M University System. Texas Department of Transportation Research and Technology Implementation Office, Austin, Texas.

Smith, J. 1985. *Bridge Approach Settlement and Proposed Repairs, Natchez Trace*. Internal Report, Federal Highway Administration, Washington, DC.

Soltani, A. A., and A. R. Kukreti. 1992. "Performance evaluation of integral abutment bridges." Transportation research record, 1371, Bridge, Culvert, and Tunnel Research.

Thiagarajan, G., V. Gopalaratnam, C. Halmen, S. Ajgaonkar, S. Ma, B. Gudimetla, and R. Chamarthi. 2010. *Bridge Approach Slabs for Missouri DOT: Looking at Alternative and Cost-Efficient Approaches*. Report No. OR 11.009. University of Missouri Kansas City; University of Missouri.

Thippeswamy, H. K., H. V. S. GangaRao, and J. M. Franco. 2002. "Performance evaluation of jointless bridges." J. Bridge Eng., 7(5), 276–289.

Wahls, H. E. 1990. *NCHRP Synthesis of Highway Practice No. 159: Design and Construction*

of Bridge Approaches. Transportation Research Board, National Research Council, Washington, D.C.

Wasserman, E. P., and J. H. Walker, 1996. "Integral abutments for steel bridges." In Highway Structures Design Handbook, No. H009, Nashville, TN: Tennessee Department of Transportation.

White, D., S. Sritharan, M. T. Suleiman, and S. Chetlur. 2005. *Identification of the best practices for design, construction, and repair of bridge approaches*. Report No. CTRE Project 02-118). Iowa. Dept. of Transportation.

White, D. J., M. M. Mekkawy, S. Sritharan, and M. T. Suleiman. 2007. "Underlying causes for settlement of bridge approach pavement systems." *J. Perform. Constr. Facil*, 21(4), 273-282.

Wolde-Tinsea, A. M. and Klinger, J. E. 1987. *Integral abutment bridge design and construction, Final Report*, FHWA/MD-87/04, Baltimore, MD: Maryland DOT.

Xanthakos, P. P. 1994. *Theory and design of bridges*. Hoboken, NJ: John Wiley & Sons.

Appendix A Agency Survey Summary Report

*This appendix was previously submitted as the *Agency Survey Task Report* and is included here for completeness.

A.1 Introduction

There are over 9,000 integral abutment bridges (IABs) and over 4,000 semi-integral abutment bridges in the United States. The expansion joints between the bridge deck and the approach slabs are eliminated in an IAB so the superstructure and substructure move together to accommodate thermal movement (White 2007). The lack of joints in bridge decks of IABs reduces the potential for water and salt damage to the bridge superstructure and substructure, and therefore maintenance costs are decreased. Although IABs cost less to build and have a longer life span than conventional bridges, undesirable behaviors – such as cracking – have been observed in some approach slabs adjacent to IABs.

A.1.1 Project Background and Objectives

The problem of approach slab cracking has become evident for many Illinois State Toll Highway Authority (hereafter referred to as "the Tollway") IABs that were built in the past ten years. According to the Tollway, approach slab cracking has been observed in cast-in-place approach slabs at abutments with mechanically stabilized earth (MSE) walls and there is interest in using precast modular approach slabs instead. The Tollway applied the Illinois Department of Transportation (IDOT) precast approach slab design to crossroad bridges (typically single structures consisting of two travel lanes and two shoulders) and noticed cracking on the wearing surface of the approach slabs. The Tollway has also observed cracks in approach slabs that were constructed based on the IDOT detail for cast-in-place approach slabs.

Currently, the University of Illinois at Urbana-Champaign has partnered with the Tollway to study approach slab cracking in IABs. The main objectives of the project are to:

1. Identify the fundamental causes of approach slab cracking in IABs built by the Tollway.
2. Develop improved design criteria, construction details, and other procedures for preventing or mitigating future approach slab cracking.
3. Evaluate efficient full-depth precast modular approach slab designs that could replace cast-in-place and IDOT precast details.

As one facet of developing a comprehensive understanding of IAB approach slab behavior, approach slabs have been instrumented at two Tollway bridges on the Illinois Route 390 Elgin O'Hare West Access expansion project. One bridge has a precast approach slab while the other bridge has a cast-in-place approach slab. The field data will be used along with numerical simulations of the instrumented approach slabs and a parametric study of a broader range of scenarios to obtain a comprehensive understanding of approach slab behavior and performance.

A.1.2 Agency Survey Creation Process

In addition to a literature review, a nation-wide agency survey was conducted. A set of questions regarding approach slab design and performance was created. This set of questions was then formatted into an online survey and sent to fifty states across the United States. The survey was aimed to elicit responses from states of interest with similar climates and environmental conditions as Illinois: for example, Wisconsin, Iowa, Missouri, Tennessee, Kentucky, and Indiana. Oklahoma, Iowa, South Dakota, Louisiana, Minnesota, North Dakota, Wisconsin, and New Jersey are known to have designed non-planar approach slab elements. In addition, details of approach slab-to-abutment or approach slab-to-deck connections from Illinois, Kansas, Michigan, Minnesota, Missouri, Nebraska, North Dakota, South Dakota, Wisconsin are available (Greimann et al. 2008).

Several online survey platforms were considered, and SurveyGizmo was ultimately chosen based on its quality interface and flexible structure. The survey questions were divided into four sections: Agency Information, Conventional and IAB Approach Slab Performance, Approach Slab Analysis / Design / Construction, and General Integral Abutment Bridge (IAB) Questions. In addition to the survey questions, supplemental documents with drawings or details of typical IABs for each state were requested to provide better comparisons with Illinois IAB practices. The survey link was shared with each state's Department of Transportation (DOT) or similar agency through Dan Brydl, the Illinois Division Bridge Engineer for the Federal Highway Administration (FHWA). The twenty-three states that responded to the survey are indicated in Figure A.1.1. The majority of these states are in the Midwest surrounding Illinois. With the exception of Kansas, all primary states of interest responded to the survey.
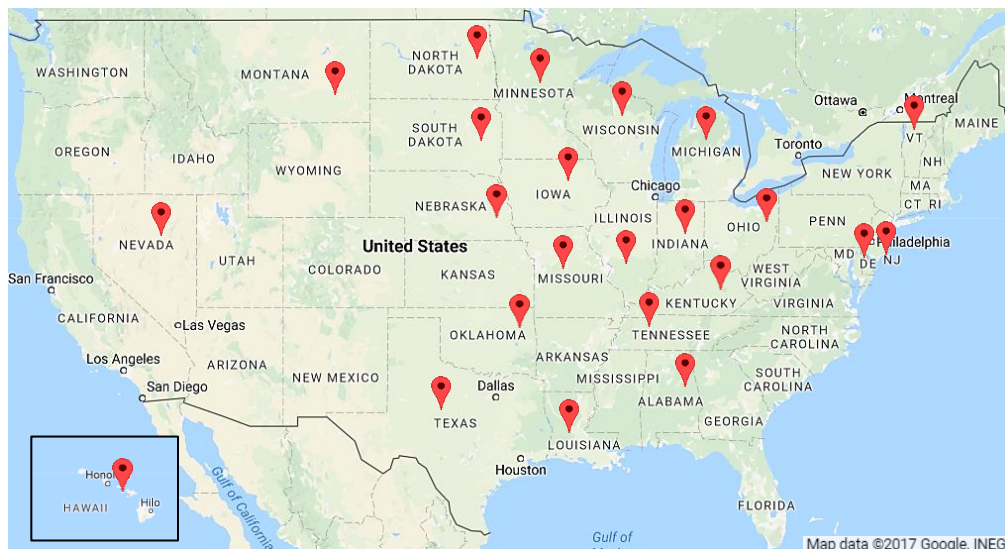
Figure A.1 States that have responded to the approach slab survey.

A.2   Agency Information

The respondents' title and represented agency for each state are listed in Table A.1. The majority of the respondents were either a Bridge Engineer or Manager. In addition to IDOT, the Tollway was asked to complete the survey to have a better comparison of the design and construction

practices between the two agencies. With the exception of Illinois, the agencies that have responded to the survey will be referred to by the state name instead of the name of the agency.

A.3   Approach Slab Performance
A.3.1   Primary Problems with Approach Slabs

The primary problems that have been observed with approach slabs are shown in Table A.2 for each state that responded to the survey. Out of the twenty-three states that responded to the survey, approach slab cracking is a primary problem in twelve states. Alabama did not respond to this question and Hawaii did not have any primary problems with their approach slabs. The survey results show that approach slab settlement is also a common problem across many states, so this issue should be considered with respect to potential influence on approach slab cracking.

Vermont did not list approach slab cracking as a primary problem, but pavement cracking at the end of the approach slab is a primary problem in this state. In addition to settlement as a primary problem with approach slabs, Ohio noted that the end of the approach slabs pulls away from the roadway allowing drainage to wash out the fines supporting the slab. Embankment settlement coupled with the consolidation of soil under the approach slab is a major problem for Louisiana's approach slabs, leading to a slab that is not supported by soil for its full length. Wisconsin noted that the main problems with approach slabs are maintenance for settled approach slabs, detailing complexities, and addressing construction questions or issues.

A.3.2   Approach Slab Cracking Percentage

Ohio, Louisiana, and Wisconsin did not list cracking as a primary problem for approach slabs, but mentioned that approach slab cracking has been an issue in their state. The percentage of approach slabs that exhibit cracking is shown in Table A.3 for states that indicated approach slab cracking as an issue. Illinois, Missouri, and New Jersey have the highest percentage of approach slabs that exhibit cracking at 50% or higher. The percentage of approach slabs that exhibit cracking in Michigan, Delaware, and Minnesota is 20% or lower. The percentage of approach slabs that exhibit cracking in the remaining states are unknown.

A.3.3   Approach Slab Cracking Direction and Location

The direction and location of approach slab cracking for the states that indicated approach slab cracking as an issue in their state are shown in Table A.4. Longitudinal and transverse cracks in approach slabs are both commonly observed. Illinois, North Dakota, Texas, and Minnesota have approach slabs with diagonal cracks. Only North Dakota and Illinois have approach slabs with transverse and diagonal cracks. Missouri and Nebraska have approach slabs that longitudinally exhibit a random cracking pattern. Approach slab cracks near the abutment are common among several states. Missouri, Oklahoma, Ohio, New Jersey, and Indiana did not specify a location where approach slab cracks occur. Nevada did not respond to this question.

A.3.4   Performance of Approach Slabs in Conventional Bridges and IABs

Oklahoma, Nebraska, Michigan, Ohio, North Dakota, Minnesota, Iowa, and Indiana are the states that indicated observed differences between the performance of approach slabs in conventional bridges compared to IABs. The observed differences are shown in Table A.5. Four out of these eight states indicated that approach slabs in IABs have more issues than approach slabs in conventional bridges.

A.3.5   Instrumented or Studied Approach Slabs

Illinois, Missouri, North Dakota, Louisiana, Wisconsin, Iowa, and New Jersey have instrumented or studied approach slabs.

- In addition to the current approach slab project, the University of Illinois at Urbana-Champaign has analyzed the behavior of IABs with composite steel girders under thermal loading and conducted field monitoring on two bridges. Numerical simulations of the instrumented bridges and a broader parametric study were compared with field data (LaFave et al. 2016). At one bridge, one approach slab was instrumented.
- The University of Missouri conducted a nonlinear finite element analysis on reinforced concrete bridge approach slabs. One of the main findings from this study is that the probability of approach slab cracking decreases as soil stiffness increases (Roy and Thiagarajan 2007).
- North Dakota has studied or instrumented approach slabs, but indicated that the data is unknown.
- The Louisiana Transportation Research Center has developed a new design for bridge approach slabs with an increased flexural rigidity, and it uses a reinforced soil foundation to minimize the bump at the end of the bridge (Abu-Farsakh and Chen 2014).
- The University of Wisconsin-Madison has instrumented an approach slab with strain gages and deflection gages in a traffic lane (Oliva and Rajek 2011).
- Iowa and New Jersey responded "No" to this question, but reports from Iowa State University and Rutgers University are publicly available. Iowa State University has studied the IAB abutment-to-approach slab connection and instrumented a precast approach slab tied to an IAB (Greimann et al. 2008). Rutgers University has conducted a finite element analysis on bridge approach and transition slabs in addition to monitoring a bridge approach slab in New Jersey (Nassif et al. 2002) and (Nassif et al. 2007).

A.4   Approach Slab Analysis, Design and Construction
A.4.1   Analysis and Design of Approach Slabs in Conventional Abutment Bridges and IABs

Nebraska, South Dakota, Alabama, and New Jersey are the only states that used different criteria to analyze or design approach slabs in conventional bridges and IABs. Nebraska indicated that the approach slabs in conventional bridges and IABs have different connections. South Dakota uses movable approach slabs to accommodate structure movement at the far end of the approach slab. Alabama accounts for negative movement in the analysis of approach slabs in conventional bridges. New Jersey designs approach slabs that are shorter in length for IABs. Texas is investigating and

evaluating different approach slab designs and detailing practices. Similarly, Indiana is considering designs that are intended to eliminate problems for slabs with large skews.

A.4.2 Approach Slab Design Guidelines

Illinois, Kentucky, Missouri, Ohio, North Dakota, Louisiana, and Texas use additional criteria in addition to the American Association of State Highway and Transportation Officials (AASHTO) guidelines in designing approach slabs. IDOT has recently increased approach slab reinforcement in the transverse direction. The Tollway uses an additional IL-120 live load in addition to the AASHTO HL-93 live load. Kentucky uses a standard 25' length approach slab that is analyzed to be supported only at the ends. Missouri uses additional requirements in the design of approach slabs based on their own research. Ohio designs the approach slabs to be 75% of the bridge span length. North Dakota assumes that there are voids beneath the approach slab and designs the approach slab as a slab bridge. Louisiana has developed a truck / lane model that is heavier than the AASHTO HL-93 model. The Louisiana model was based on extensive Weigh-in-Motion (WIM) data in the state. Texas indicated that the state does not have its own guidelines and the design of approach slabs is based on the AASHTO guidelines and assumes the approach slab is a one-way simple span from the abutment backwall to the back end of the approach slab. The Texas DOT is using cement-stabilized sand behind the abutment and this type of backfill has shown good results in several districts.

A.4.3 Methods to Minimize Approach Slab Cracking

States have used a variety of methods in the effort to minimize approach slab cracking as shown in Table A.6. Using top and bottom reinforcement is the most common method among several states to mitigate approach slab cracking.

A.4.4 Standard Type of Approach Slab Used in Construction

Illinois, Nebraska, and Vermont use both cast-in-place and precast approach slabs in both conventional bridges and in IABs. Texas uses both cast-in-place and precast approach slabs in conventional bridges as it does not have many IABs. According to IDOT, if the expansion length is 130 feet or longer, precast approach slabs are used. If the length from the end of the abutment to the centroid of stiffness is larger than 130 feet, the Tollway uses precast approach slabs. In Nebraska and Vermont, precast approach slabs are used with Accelerated Bridge Construction (ABC).

A.4.5 Standard or Limit to Approach Slab Length and Thickness

Montana, Texas, and Minnesota do not have a standard or limit to approach slab length and thickness. Limits for the approach slab length and thickness are shown in Table A.7 for the states that responded to the survey. Common approach slab lengths are 20' to 30' and common thicknesses are 12" to 16" although there is also variation above and below these ranges. Ohio has several standard approach slab lengths (15'-30') and thicknesses (12"-17"), where each thickness corresponds to a length as shown in Table A.7.

A.4.6 Standard Approach Slab-to-Abutment Connection

The types of connections used at the approach slab-to-abutment interface are shown in Table A.8. Several states use dowels for this connection.

A.4.7 Type of Support Used for the Transition / Pavement End of the Approach Slab

Sleeper slabs are commonly used for support at the transition / pavement end of the approach slab as shown in Table A.9. IDOT uses a sleeper slab, while the Tollway uses a pile bent as the type of support at the transition / pavement end of the approach slab. Nebraska, Hawaii, and Iowa use a different type of support other than a pile bent or sleeper slab. In Nebraska, a 2'-6" concrete beam on deep pile foundation is used. In Hawaii, a thickened edge is used. In Iowa, a 12" by 12" cast-in-place pavement lug is used.

A.4.8 Material Used Beneath the Approach Slab to Reduce Friction with the Soil

Almost half of the states that responded to the survey have used something beneath the approach slab to reduce friction with the soil. Table A.10 shows the material that each state uses beneath the approach slab.

Illinois, South Dakota, Vermont, Louisiana, Wisconsin, Delaware, Minnesota, and New Jersey use polyethylene sheeting beneath the approach slabs. The number of layers and thickness of the sheets vary between states. Nebraska and Texas use another (unspecified) material beneath the approach slab. Nebraska uses granular backfill underneath the approach slab to reduce friction with the soil and Texas uses a 1" Aluminum Composite Panel (ACP) stress relieving pad between the approach slab and subgrade. The other states indicated that nothing is used beneath the approach slab to reduce friction with the soil.

A.5 General IAB Information
A.5.1 Existing and Planned Bridges that are IABs

The percentage of existing bridges that are IABs and the percentage of new and planned bridges that are IABs for each state are shown in Table A.11. Nebraska, Ohio, and North Dakota did not specify a percentage, but indicated that a large portion of their existing bridges are IABs. Ohio indicated that the state has been building IABs for more than thirty years. Louisiana has built a total of two IABs. More than half of the states that responded to the survey are planning to build new bridges in which 50% or more will be IABs.

A.5.2 Length and Skew Limits for IABs

The length and skew limits for IABs for each state are shown in Table A.12. The majority of the states that responded to the survey have a maximum skew of 30 degrees for IABs. The maximum lengths corresponding to this 30-degree skew are longer than or equal to 300 feet. IABs with concrete girders are approximately double the length of steel girder IABs.

A.5.3 Basis for Length and Skew Limits on IABs

IAB length and skew limits are commonly based on experience and the consensus of other state practices as shown in Table A.13. In addition, a variety of reasons behind the IAB length and skew limits are also shown in Table A.13. The length and skew limits for IABs in Missouri, Oklahoma, Michigan, South Dakota Montana, Ohio, and Iowa are based on experience. The IAB length and skew limits in Michigan and North Dakota are based on other state guidelines in addition to experience and performance history. The length and skew limits for IABs in Delaware are based on the research of other states' practices. The basis for IAB length and skew limits in Louisiana are not available. Nevada and Hawaii did not respond to this question.

A.5.4 Type of Foundation Used at the Abutments in IABs

Many states use HP piles in the weak axis orientation as the foundation type at the abutments in IABs as shown in Table A.14. Nebraska, Alabama, North Dakota, Wisconsin, and Tennessee use HP piles in the strong axis orientation. Several states also use shell piles or drilled shafts at the abutments in IABs.

A.6   Comparison of Cracking Trends

Previously, several approach slab cracking trends have been identified for bridges in Illinois. The cracking trends observed in Illinois bridges are:

1. Cracks in approach slabs tend to develop diagonally from obtuse corner to obtuse corner for skewed bridges. The cracks run both from the expansion joint to the construction joint or vice versa.
2. Bridges with zero skew have few cracks in the approach slabs. The cracks appear mainly in the shoulders or corners of the approach slab.
3. Bridges with 30° skew and above exhibit approach slab cracks in the travel lanes and shoulders.
4. For bridges with one or two lanes, and zero or low skew, cracks usually run in the travel lanes and are parallel to traffic (longitudinal cracks).

Many states that indicated approach slab cracking as an issue in their state described approach slab cracks occurring near the abutment or abutment joints. Similar to the trend observed in Illinois, approach slabs in North Dakota, Texas, and Minnesota also have cracks that run diagonally towards the obtuse corners in skewed bridges. Wisconsin noted that approach slabs exhibit cracks that run parallel to traffic, which are common in the approach slabs of smaller bridges in Illinois.

A.7   Summary

Only Illinois, Nebraska, and Vermont have used precast and cast-in-place approach slabs in both conventional bridges and IABs. Texas has used cast-in-place and precast approach slabs in conventional bridges and did not comment on the type of approach slab used in the 1% of bridges that are IABs in Texas. Out of these four states that have used precast approach slabs, only

Vermont did not have issues with approach slab cracking. However, pavement cracking at the end of the approach slab is present in Vermont.

Illinois, Missouri, North Dakota, New Jersey, and Iowa indicated that approach slab cracking is an issue in their state and have instrumented or studied approach slabs. 50% or more bridges in Illinois, Missouri, and New Jersey exhibit approach slab cracking. Oklahoma, Nebraska, Michigan, Nevada, Delaware, Texas, Minnesota, and Indiana have indicated cracking as a primary issue, but have not instrumented or studied approach slabs. Ohio, Louisiana, and Wisconsin did not indicate approach slab cracking as a primary problem, but approach slab cracking is present.

There are no clear trends across various states relating bridge parameters to approach slab cracking. Designs for bridges in one state may be prone to cracks, whereas cracking may not be present in another state using a similar design. For example, aside from South Dakota, Alabama, and Montana, all of the other states that have used sleeper slabs as the support type for the transition / pavement end of the approach slab have had problems with approach slab cracking. However, the one clear general pattern across states with approach slabs that are at least 30 feet in length is that approach slab cracking occurs and the states consider it an issue of concern. An increase in reinforcement is the most common method among states to minimize cracks in approach slabs. Bridge drawings for bridges that exhibit cracking in each state along with the number of cracks per bridge may provide more insight into bridge parameters that would most likely lead to approach slabs with cracks.

A.8   References

Abu-Farsakh, M. and Chen, Q. (2014). *Field Demonstration of New Bridge Approach Slab Designs and Performance*. Report No. FHWA/LA. 13/520. Louisiana Transportation Research Center. Baton Rouge, Louisiana.

Greimann, L., Phares, B., Faris, A. and Bigelow, J. (2008). *Integral Bridge Abutment-to-Approach Slab Connection*. Report No. IHRB Project TR-530 & TR-539 ; CTRE Project05-197 & 05-219. Iowa State University. Iowa Department of Transportation, Ames, Iowa.

LaFave, J. M., Fahnestock, L. A., Wright, B. A., Riddle, J. K., Jarrett, M. W., Svatora, J. S., An, H., and Brambila G. (2016). *Integral Abutment Bridges Under Thermal Loading: Numerical Simulations and Parametric Study*. Report No. FHWA-ICT-16-014. University of Illinois at Urbana-Champaign. Illinois Center for Transportation. Illinois Department of Transportation, Springfield, Illinois.

Nassif, H., Abu-Amra, T. and Shah, N. (2002). *Finite Element Modeling of Bridge Approach and Transition Slabs*. Report No. FHWA-NJ-2002-007. New Jersey Department of Transportation. Federal Highway Administration U.S. Department of Transportation, Washington, D.C.

Nassif, H., Suksawang, N., Shah, N. and Abu-Amra, T. (2007). *Field Implementation and Monitoring of Bridge Approach Slabs*. Report No. FHWA-NJ-2007-012. Rutgers, The State University; Florida International University; University of Alabama at Birmingham. Federal Highway Administration United States Department of Transportation, Washington, D.C.

Oliva, M. and Rajek, G. (2011). *Toward Improving the Performance of Highway Bridge Approach Slabs*. Report No. CFIRE 03-10. University of Wisconsin-Madison. Research and

Innovative Technology Administration United States Department of Transportation, Washington, D.C.

Roy, S., and Thiagarajan, G. (2007). "Nonlinear Finite-Element Analysis of Reinforced Concrete Bridge Approach Slab." *Journal of Bridge Engineering*, 12(6), 801–806.

White, H. (2007). *Integral Abutment Bridges: Comparison of Current Practice Between European Countries and the United States of America*. Special Report No. 152. Transportation Research and Development Bureau. New York State Department of Transportation, Albany, New York.

A.9 Tables

Table A.1 Respondent title and represented agency.

State	Agency	Title
Alabama	ALDOT	Assistant State Bridge Engineer
Delaware	DOT	Bridge Design Engineer
Hawaii	Dept. of Transportation, Highways Division, Design Branch	Bridge Engineer
Illinois	Illinois Department of Transportation	Estimates and Review Engineer
Illinois	Illinois Tollway	Engineer
Indiana	INDOT	Bridge Design Manager
Iowa	Department of Transportation	Bridge Maintenance and Inspection Engineer
Kentucky	KYTC	TEBM Structural Design
Louisiana	Louisiana DOTD	Engineer 6 DCL
Michigan	Michigan Department of Transportation	Bridge Standards Specialist
Minnesota	Minnesota Department of Transportation	Bridge Construction and Maintenance Engineer
Missouri	Missouri DOT	State Bridge Engineer
Montana	DOT	Bridge Engineer
Nebraska	Nebraska department of Roads	assistant State Bridge Engineer
Nevada	Department of Transportation	State Bridge Engineer
New Jersey	NJDOT	Exec Manager Structural Engineer
North Dakota	NDDOT	Assistant Bridge Engineer
Ohio	ODOT	Administrator
Oklahoma	ODOT	Assistant Bridge Engineer - Maintenance
South Dakota	SDDOT	Chief Bridge Engineer
Tennessee	TDOT	Civil Engineering Manager 2
Texas	Texas DOT	Bridge Design Director
Vermont	Vermont Agency of Transportation	VAOT Structures Design Engineer
Wisconsin	WisDOT	Structures Development Engineer

*Note: in all of the following tables, states highlighted in gray did not report major concerns or significant observed problems with approach slabs.

Table A.2 Primary problems with approach slabs experienced by states.

State	Cracking	Settlement	Bump	Other
Alabama				
Delaware	X	X		
Hawaii				
Illinois	X			
Indiana	X	X		
Iowa		X	X	
Kentucky			X	
Louisiana		X		X
Michigan	X	X		
Minnesota	X	X		
Missouri	X	X		
Montana		X		
Nebraska	X			
Nevada	X			
New Jersey	X	X		
North Dakota	X	X		
Ohio		X		X
Oklahoma	X	X	X	
South Dakota		X		
Tennessee		X	X	
Texas	X	X		
Vermont				X
Wisconsin		X		X

Table A.3 Percentage of approach slabs that exhibit cracking.

State	Percentage
Delaware	5-10
Illinois	50-70
Indiana	Unknown
Iowa	Unknown
Louisiana	Unknown
Michigan	< 5
Minnesota	20
Missouri	50
Nebraska	Unknown
Nevada	Unknown
New Jersey	50
North Dakota	Unknown
Ohio	Unknown
Oklahoma	Unknown
Texas	Unknown
Wisconsin	Unknown

Table A.4 Direction and location of cracking in approach slabs.

State	Longitudinal	Transverse	Diagonal	Random	Location
Delaware		X			Midspan.
Illinois	X	X	X		At the tops parallel to abutment near the abutment.
Indiana	X				
Iowa		X			Cracks present across entire lane, located about 10-12 ft. from the end of the bridge and are usually full depth cracks.
Louisiana	X	X			Transverse cracking on the bottom / tension side and failure across width of slab.
Michigan		X			5-7' from reference line and run parallel to reference line.
Minnesota		X	X		Cracks present in obtuse corners of skewed bridges. Cracking present around the support points for settled panels. The crack will follow the joint for complicated pourable joint layouts.
Missouri				X	
Nebraska	X			X	Abutment joints.
Nevada					
New Jersey		X			
North Dakota	X	X	X		Midpanel transverse cracking, longitudinal cracking at the ends of the approach slab where they are tied to the end walls, and diagonal cracking on skewed approach slab ends.
Ohio	X	X			
Oklahoma	X				
Texas	X		X		Initiate at the abutment backwall and extend towards the departure end. On skewed bridges with a skewed approach slab, cracking is diagonal – typically normal to backwall.
Wisconsin	X				The 1/2 and/or 1/3 points along slab width, and typically run parallel to traffic, terminating at the bridge deck.

Table A.5 Differences between the performance of approach slabs in conventional bridges and IABs.

State	Observed Differences
Indiana	Different pavement ledge details have been used over the years with mixed results. Approach slabs are detailed as trapezoidal in Indiana leading to issues for wide bridges on large skews.
Iowa	The IAB approach slabs are not tied to the abutment. In terms of cracking, there are no major differences.
Michigan	There have been less issues with approach slabs in conventional bridges compared to approach slabs in IABs.
Minnesota	The joint between the approach slab and pavement deteriorates faster and is harder to seal.
Nebraska	Approach slabs did not have to be connected with backwall abutments for conventional bridges.
North Dakota	Approach slabs in IABs are more prone to settlement issues.
Ohio	Approach slabs in IABs move with the bridge and open up a gap.
Oklahoma	IABs tend to have more bumps and settlement than conventional bridges.

Table A.6 Methods taken to minimize approach slab cracking.

State	Method
Alabama	
Delaware	Approach slabs restricted to have a maximum length of 30'.
Hawaii	Not aware of any.
Illinois	In addition to increasing the transverse reinforcement, the Illinois DOT plans to sawcut along lane lines to allow cracking to form there in order to minimize cracking in approach slabs. The Tollway is looking into a concrete mix design that will help minimize approach slab cracking.
Indiana	Top and bottom reinforcing, control joints, compaction requirements, and uniform length approaches are being considered.
Iowa	First 20 feet of the panel designed as a doubly reinforced section and have also increased the support width to allow more movement on an IAB. Also, they have a better process for placing the fill behind the abutment footing to minimize the settlement.
Kentucky	Buried approach slabs.
Louisiana	The approach slab design considers the slab as a simply supported slab (full loss of contact with the underlying soil) and is designed for full moment capacity under the heaviest truck loads.
Michigan	Top and bottom reinforcement are used in approach slabs to minimize cracking.
Minnesota	A 3-day wet cure, low slump wearing coarse is placed on approach slabs when applied to bridge deck. The approach barrier is on the approach panel and not on the wingwall. A stainless-steel dowel bar from abutment to approach slab is used. Two layers of reinforcement are used. Polypropylene fibers are used to prevent settlement cracks. Plastic is placed below the approach slab to help with IABs. After wet cure, alpha-methylstyrene (AMS) curing compound is applied.
Missouri	Heavily reinforced slabs (top and bottom, laterally and longitudinally) to decrease cracking in approach slabs.
Montana	Design approach slabs in the same manner as bridge spans to minimize cracking.
Nebraska	Piles are used under sleeper slabs to prevent settlement.
Nevada	
New Jersey	Old conventional approach slabs were cast in one pour. New conventional approach slabs are cast in several individual sections separated by longitudinal controlled joints and transverse expansion joints to accommodate movements, thus minimizing cracking.
North Dakota	The thickness and reinforcement were increased for the approach slabs and the skew on the approach slabs was limited to 45 degrees.
Ohio	A sealed joint added between the end of the approach slab and the pavement.
Oklahoma	Reinforcing steel in the top and bottom of their approach slabs.
South Dakota	A short bar added in the top mat immediately adjacent to the joint between the bridge and the approach slab.
Tennessee	None.
Texas	Approach slabs are treated similar to the bridge decks in regard to wet curing in order to minimize approach slab cracking.
Vermont	Vermont uses 7-day wet cure cast-in-place approach slabs.
Wisconsin	Slabs are reinforced on all faces and in each direction with #5's at 1'-0" on center in addition to flexural reinforcement (#8's at 7 ½") and concrete is placed based on bridge specifications.

Table A.7 Limits for approach slab length and thickness.

State	None	Length	Thickness
Alabama		As needed	As needed
Delaware		30'	16"
Hawaii		20'	
Illinois		30'	15"
Indiana		20.5' (short end of skew)	
Iowa		20'	12"
Kentucky		25'	17"
Louisiana		25'	24" along centerline; 18" at shoulders
Michigan		20'	12"
Minnesota	X		
Missouri		20'	12"
Montana	X		
Nebraska		20'	14"
Nevada		24'	12"
New Jersey		25' (conventional); 10' (IAB)	
North Dakota		20'; 40' (pile supported slabs at middle & end)	14"
Ohio		15'; 20'; 25'; 30'	12"; 13"; 15"; 17"
Oklahoma		30'	13"
South Dakota		20' (no skew); 15' (short end of skew)	9"
Tennessee		24'	12"
Texas	X		
Vermont		20' (skew < 35°); 25' (skew > 35°)	
Wisconsin		20'	16"

Table A.8 Typical approach slab-to-abutment connection.

State	Approach Slab-to-Abutment Connection
Alabama	A positive connection.
Delaware	A hook bar is used as the standard approach slab-abutment connection type. The approach slab rests on end diaphragm.
Hawaii	Dowels.
Illinois	A vertical #5 reinforcement at 12" spacing is the standard approach slab-abutment connection used in Illinois DOT bridges. Grout in place is the standard approach slab-abutment connection used for the Tollway bridges.
Indiana	A longitudinal reinforcing through cold joint.
Iowa	A corbel support that is 15" wide with no physical connection between the abutment and slab.
Kentucky	Dowels.
Louisiana	The slab and end bent are bonded with an adhesive and tied together using #6 bars at 7" on center.
Michigan	A bottom mat of steel extending from the deck into the approach slab and lapped with approach slab steel.
Minnesota	An 8" wide corbel on back side abutment with single mat of stainless dowel bar from abutment to AP. AP thicker at abutment location.
Missouri	A single row of #5's at 12" spacing.
Montana	Pinned connection.
Nebraska	Simple span pinned connections
Nevada	Nevada did not respond to this question.
New Jersey	Pinned connection.
North Dakota	Approach slabs are tied to the abutment endwall. The approach slab sits on a 10" corbel.
Ohio	Reinforcing steel #8 hooked bars at 18" on center.
Oklahoma	Rebar in the bottom of the deck extending into the bottom of the approach slab.
South Dakota	No. 7 dowels at 18" spacing.
Tennessee	A rebar connection from the backwall into the approach slab through roadway bracket.
Texas	No standard approach slab-abutment connection type for IABs.
Vermont	No. 8 dowels at 12" spacing are fixed to the abutment.
Wisconsin	The slab is tied to the abutment with 'z' shaped stainless-steel bars (#9 at 1'-0" o.c.) and supported by a 1'-0" wide paving notch. The paving notch is coated a protective surface treatment prior to the approach pour to act as bond breaker and for added protection.

Table A.9 Type of support used for the transition / pavement end of the approach slab.

State	Pile Bent	Sleeper Slab	None	Other
Alabama		X		
Delaware		X		
Hawaii				X
Illinois	X	X		
Indiana		X		
Iowa				X
Kentucky			X	
Louisiana		X		
Michigan		X		
Minnesota		X		
Missouri	X			
Montana		X		
Nebraska				X
Nevada				
New Jersey		X		
North Dakota	X			
Ohio		X		
Oklahoma			X	
South Dakota		X		
Tennessee		X		
Texas		X		
Vermont			X	
Wisconsin		X		

Table A.10 Material used beneath the approach slab to reduce friction with the soil.

State	None	Polyethylene Sheeting	Other
Alabama	X		
Delaware		X	
Hawaii	X		
Illinois		X	
Indiana	X		
Iowa	X		
Kentucky	X		
Louisiana		X	
Michigan	X		
Minnesota		X	
Missouri	X		
Montana	X		
Nebraska			X
Nevada			
New Jersey		X	
North Dakota	X		
Ohio	X		
Oklahoma	X		
South Dakota		X	
Tennessee	X		
Texas			X
Vermont		X	
Wisconsin		X	

Table A.11 Percentage of existing and new bridges that are IABs.

State	Percentage of existing bridges that are IABs	Percentage of new and planned bridges that are IABs
Alabama	10	75
Delaware	< 5	> 75
Hawaii	Unsure	98
Illinois	50	90
Indiana	Unsure	100
Iowa	39	Anything < 600'
Kentucky	40	85
Louisiana	2 bridges	Unsure / minimal
Michigan	30	70
Minnesota	10	80
Missouri	50	95
Montana	1	1
Nebraska	Most	All
Nevada		
New Jersey	0.24	Unsure
North Dakota	Majority	As much as possible
Ohio	Big percentage	All
Oklahoma	7	5-10
South Dakota	70	90
Tennessee	50	90
Texas	< 1	0
Vermont	5	50
Wisconsin	50	90

Table A.12 Limits for length and skew for IABs.

State	Length	Skew
Alabama		60°
Delaware	400'	30°
Hawaii	Not aware of any	Not aware of any
Illinois	610' (IDOT); 550' (Tollway)	45°
Indiana	1000' (h-piles up to 30° skew & then 800' linear reduction at 60°); 500' (shell piles up to 30° & then 300' linear reduction at 60°)	30°
Iowa	575' (prestressed girders & 0 skew); 425' (for 45° skew); 400' (steel girder & 0 skew); 300' (for 45° skew)	45°
Kentucky	500'	None
Louisiana	N/A	N/A
Michigan	300' (steel); 400' (concrete)	30°
Minnesota	Linear limit	Linear limit
Missouri	600' (prestressed concrete); 400' (steel)	N/A
Montana	300'	30°
Nebraska	None	None
Nevada		
New Jersey	450'	30°
North Dakota	400'	30°
Ohio	400'	30°
Oklahoma	300'	None
South Dakota	350' (steel girder); 700' (concrete girder)	30°
Tennessee	400' (steel girder); 800' (concrete)	None
Texas	None	None
Vermont	395' (steel); 695' (concrete)	20°
Wisconsin	150' (steel girders and 40° skew); 300' (concrete girders and 40° skew); 300' (concrete slabs and 30° skew)	30°

Table A.13 Basis for IAB length and skew limits.

State	Experience	Other States	Other
Alabama			Guardrail attachment.
Delaware		X	
Hawaii			
Illinois			IDOT indicates that limit on the length of IABs is dictated by the 2" pavement joint at the end of the approach slab. The skew is determined using various models and checking pile stresses. The Tollway use expansion limitations as the basis for the limit of IAB lengths.
Indiana			Research from Purdue University.
Iowa	X		
Kentucky			Had problems with the basis for length limits for IABs.
Louisiana			N/A.
Michigan	X	X	
Minnesota			Cracking of the approach panel between wingwalls, movement capacity of the pavement AP joint.
Missouri	X		
Montana	X		
Nebraska			Prevent or minimize torsion and cracking at the support and prevent or minimize lateral movement.
Nevada			
New Jersey			The understanding that longer length and greater skew will require more in-depth analysis to evaluate effect of thermal movement on pile and stresses acting on the structure.
North Dakota		X	Performance history.
Ohio	X		
Oklahoma	X		
South Dakota	X		
Tennessee			Amount of thermal movement.
Texas			A lowered risk for initial trial projects.
Vermont			Simplified design procedures that make assumptions that would not be valid for longer spans or greater skews. Bridges that have a refined analysis are up to 45 degrees and have span lengths shorter than 100'.
Wisconsin	X		Economics.

Table A.14 Type of foundation used at the abutments in IABs.

State	HP Piles Weak Axis	HP Piles Strong Axis	Other
Alabama		X	
Delaware	X		
Hawaii			Drilled shafts.
Illinois	X		Metal shell piles.
Indiana	X		Concrete filled steel shells.
Iowa	X		
Kentucky			Depends on height of IAB.
Louisiana	X		
Michigan	X		
Minnesota	X		CIP shell piles.
Missouri	X		
Montana			Varies.
Nebraska	X	X	
Nevada			
New Jersey	X		
North Dakota		X	
Ohio	X		
Oklahoma	X		
South Dakota	X		
Tennessee		X	Steel pipe lines.
Texas			Drilled shafts, prestressed concrete piling, steel H-piles less commonly used.
Vermont	X		
Wisconsin		X	Spread footings bearing on soil or rock.

Appendix B   Preliminary Synthesis of Approach Slab Cracking in Tollway Bridges and Recommendations for Near-Term Re-Inspection

*This appendix was previously submitted as the report on *Preliminary Synthesis of Approach Slab Cracking in Tollway Bridges and Recommendations for Near-Term Re-Inspection* and is included here for completeness.

B.1   Introduction

In the investigation of current integral abutment bridge (IAB) approach slab cracking, the Tollway provided photos and a spreadsheet in 2016 detailing approach slab cracking for bridges that were constructed between 2013 and 2015. These photos may not represent the current condition of the approach slabs. Moreover, there were some contradictions between the spreadsheet and photos, such as cracks were recorded in the spreadsheet but could not be found in photos. A re-inspection is essential to improve the accuracy of crack trend investigations.

The key tasks of the future field survey will include taking pictures and recording the locations of the cracks, measuring the lengths of cracks, checking for settlement of the approach slabs and the evaluating the condition of expansion joints. If time permits, the condition of adjacent structural components (wing walls, MSE walls and abutments) will be observed. Cracks are assumed to be full-depth cracks unless accurate depths of the cracks can be measured.

Several bridges, some of which are non-integral abutment bridges, are to be selected for supplemental field inspection. The first step in selecting bridges to visit, consisted of reviewing photos of approach slab cracking on I-90 Mainline, I-90 Cross Road, Illinois Route 390 Mainline, and I-88 bridges (consisting of Mainline and Cross Road bridges) and creating maps of the cracks for each approach slab (I-90 Mainline and I-90 Cross Road). Bridge information corresponding to each approach slab was then tabulated. The bridge information and the crack maps were then analyzed to identify trends between bridge parameters and approach slabs that exhibit cracking.

This summary will outline the procedure for creating the crack maps and bridge information data sheet, followed by synthesis of approach slab cracking trends that were present. This information guided the selection of four bridges that are proposed for re-inspection. These re-inspections, which will be coordinated with S.T.A.T.E. Testing, should take place in the near future (mid-October to early-November).

B.2   Crack Maps

From the provided photos, schematic crack maps of the location and direction of the cracks were developed for each approach slab, as shown in Figure B.2.1. The skew of the bridges and approach slabs are not taken into consideration in the creation of the crack maps. As a result, the geometry of the approach slabs in the crack maps may not realistically represent the actual slabs. The relative locations of the cracks are not precise and are only based on the photos that were provided in the fall of 2016, but they do provide a general understanding of the approach slab cracking. Cracks

may have developed or elongated since the photos were taken. The crack maps were then compared with a provided spreadsheet (Tollway Bridge Cracking Information.xlsx) that notes the number of cracks for each approach slab of the I-90 Mainline and I-90 Cross Road bridges.
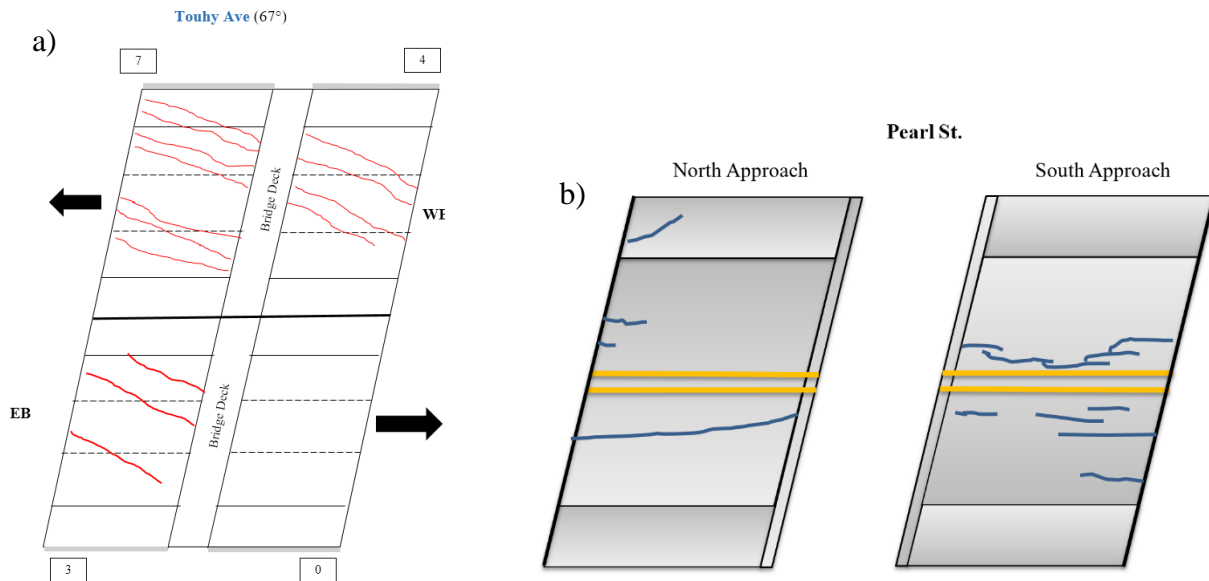
Figure B.1 Crack map of approach slabs from: a) an I-90 Mainline bridge over Touhy Avenue; b) an I-90 Cross Road bridge over Pearl St.

B.3   Bridge Information

Bridge contracts or drawings of (24) I-90 Mainline, (21) I-90 Cross Road, (7) Illinois Route 390 Mainline, and (6) I-88 bridges were provided by the Tollway. Several parameters were extracted from each bridge contract and compiled into a spreadsheet detailing pertinent bridge information. The parameters included basic bridge information (contract number, structure number, and year constructed), bridge geometry (total length, span lengths, width, and skew), the presence of an MSE wall or wing wall (and its location), the type of abutment (integral abutment, semi-integral abutment, or non-integral abutment), whether staged construction took place, whether the bridge was one single structure or two separate structures, approach slab and transition slab geometry (length and thickness), and approach slab support type (approach – abutment connection, approach – transition support, expansion joint, and pressure relief joint).

Among the **I-90 Mainline** bridges investigated, all the approach slabs are cast-in-place, 30 ft. long, 15 in. thick, and adjacent to a 70 ft. long transition slab (minimum length of the transition slab, where the maximum length may vary along the transverse direction due to the skew). A pile bent is used as the only support type under the approach-transition joint and the common length of the approach slab resting on the bent is 15 in. There is a 3 in. wide expansion joint at the approach-transition joint in most IABs, whereas there is no expansion joint at the approach-abutment side or approach-transition side in non-IABs. A 2 in. wide pressure relief joint can be found between the transition slab and the adjacent pavement in all of the bridges. Vertical or diagonal anchor rods can be found at the abutment-approach joint for all bridges. There is always a 4 in. granular subbase layer under the approach, which may be coupled with porous granular embankment at the

abutment end. Most of the transition slabs are supported by a 3 in. thick asphalt base course and 12 in. of subgrade aggregate below the asphalt.

Each **I-90 Cross Road** bridge consists of one structure that carries both directions of traffic. The approach slabs are all 30 ft. long and 15 in. (cast-in-place) or 16 in. (precast) thick. The 16-inch precast approach slab include 5 inches to 8 inches of concrete wearing surface on the top. There is no transition slab between the approach slab and pavement. The connection between the cast-in-place approach slabs and abutments is vertical anchor rods, whereas dowel rods are used as the connection between precast approach slabs and abutments. Most of the approach slabs are supported by an approach footing with various lengths at the approach-pavement joint. There is an expansion joint, of which the opening varies from 1.5 to 2 in. at the approach-pavement end. Most of the bridges have wing walls, of which the lengths vary from 10 ft. to 15.5 ft. measured from the abutment end.

All the **Illinois Route 390 Mainline** bridges considered are either 1-span or 2-span structures. The approach slabs are 30 ft. long and 15 in. (cast-in-place) or at least 18 in. (precast) thick. The precast approach slabs consist of a 9 to11 inches HPC (High Performance Concrete) slab on the top and an at least 9 inches of a precast slab on the bottom. Most of the approach slabs are supported by pile bents on the approach slab-transition slab (pavement) end.

The **I-88** bridges consist of two sets of eastbound/westbound Mainline bridges (four structures) and two Cross Road bridges (two structures). All structures in the Mainline are semi-integral abutment bridges with 70 ft. transition slabs and 3 in. expansion joints at the approach transition end, whereas both Cross Road bridges are integral abutment bridges with no transition slab or expansion joint at the approach-pavement end. Approach footings are utilized in both IABs and pile bents are selected as the support of the approach and transition slabs among all semi-IABs. All the approach slabs on I-88 are 30 ft. long and 15 in. thick (cast-in-place).

B.4   Cracking Trends

The crack maps were linked with the bridge information to determine which parameters were common in approach slabs with cracks, as shown in Tables B.1 to B.4. (The cracking trends spreadsheet that is the source for these tables is being submitted with this report.) The bridges with approach slabs that have five or more cracks are highlighted in red. Bridges with approach slabs that have one to four cracks are highlighted in orange. Approach slabs that show no cracking are highlighted in green.

Regarding the **I-90 Mainline** Bridges, bridges with approach slabs that have five or more cracks tend to have a wingwall that runs the entire length of the approach slab. Non-IABs generally exhibit more cracking than IABs. Another trend is that bridges with skews greater than 30° are more likely to have approach slab cracking.

For **I-90 Cross Road** Bridges, approach slab cracking trends are more difficult to determine because the relationship between a certain parameter and the number of cracks is not as clear as in the I-90 Mainline Bridges. There is a general trend that older approach slabs (built in 2013 or 2014) are more likely to have cracks. As the length of the slab resting on the approach footing

decreases, cracking appears to be more severe. All the precast approach slabs are in the red or orange category, whereas cast-in-place approach slabs are not necessarily in the red or orange category.

There is no strong connection between the parameters and the number of cracks among bridges in Illinois Route 390. The only two bridges in the red category have skews larger than 15 degrees.

There are two Cross Road bridges and one Mainline bridge (EB and WB) in orange. An interesting phenomenon is that the **I-88 Cross Road** bridges, which are IABs, do not have an expansion joint on either side of the approach slab, being the potential cause for cracking. The approach slabs in these Cross Road bridges are supported by approach footings.

B.5   Bridges for Re-inspection

An initial set of four bridges has been selected for re-inspection, which is targeted to occur in mid-October to early-November of this year with assistance from S.T.A.T.E. Testing. If possible, a more comprehensive re-inspection program conducted by S.T.A.T.E testing in conjunction with the research team may be beneficial for the other I-90 Mainline and Cross Road bridges that were built between 2013 and 2015.

The four bridges that have been selected for initial re-inspection are:

1. I-90 Mainline over **US-20**
2. I-90 Mainline over **Kishwaukee River**
3. I-90 Cross Road on **Brier Hill Road**
4. I-90 Cross Road on **Irene Road**

The Kishwaukee River bridge was selected because a number of embedded strain gages have been installed in the approach slabs for a prior project. The US-20 bridge was chosen because three out of four approach slabs have five or more cracks. Irene Road was chosen because both North and South approach slabs have seven or more cracks. Lastly, Brier Hill Road was selected because it has the most cracks (two on the North approach slab and five on the South approach slab) for a bridge with precast approach slabs. US-20, Kishwaukee, and Irene Road bridges have cast-in-place approach slab panels.

Table B.1 I-90 Mainline bridge approach slab cracking trends.

Bridge	Total Length	# of Spans	Skew	IAB	Approach Slab Length	Approach Slab Thickness	Approach Slab Support Type	EXP joint opening at 50°F (Approach - transition)	Wingwall	Wingwall Location	EB-East	EB-West	WB-East	WB-West
Wisconsin Central RR	301'-2"	3	46°27'00"	N	30'	15"	Pile bent, Metal shell	No clear EXP joint	Y - entire length; slab on the wall	EB-W-S; EB-E-S	0	0	3	11
Higgins Rd	309'-11 1/2"	3	57°17'00"	N	30'	15"	Pile bent; HP10x42	No clear EXP joint	Y - entire length; slab on the wall	EB-N-W; EB-S-W	2	0	11	6
US 20	124'-2"	1	36°48'00"	Y	30'	15"	Pile bent; Metal shell 14" dia	3"	Y - entire length; 7 piles; slab on the wall	EB-W-S (SW); EB-E-S (SE); WB-W-N (NW); WB-E-N (NE)	5	7	10	3
Touhy Ave	340'-8 3/4"	2	67°39'00"	N	30'	15"	Pile bent; HP10x42	No clear EXP joint	Y - entire length; 4 piles; slab on the wall	EB-W-S; WB-W-N; WB-E-N; EB-E-S	0	3	4	7
UPRR (concrete)	122'6 1/4"	1	21°21'00"	Y	30'	15"	Pile bent, HP 10x42	3"	N	N/A	6	2	2	1
Golf Rd	249'-6"	2	56°47'00"	N	30'	15"	Pile bent; 12"x .179"	3"	N	N/A	3	3	4	3
Busse Rd	209'	2	45°52'00"	N	30'	15"	Pile bent, HP12x5	No clear EXP joint	N	N/A	0	2	1	0
Mannheim Rd	128'-5 3/8"	1	31°41'00"	Y	30'	15"	Pile bent, Metal shell	3"	N	N/A	0	0	2	3
Higgins Creek	88'-9 1/8"	1	13°00'00"	Y	30'	15"	Pile bent, Metal shell	3"	N	N/A	1	1	0	0
Oakton/Rt. 83	254'-6 1/4"	3	43°45'00"	Y	30'	15"	Pile bent, Metal shell	3"	N	N/A	0	0	3	1
Kishwaukee	553'-7 1/2"	4	35°00'00"	Y	30'	15"	Pile bent; Metal Shell 12" x .25"	2.25"	Y - 15'; 2 piles; slab on the wall	EB-W-S; EB-E-S	N/A	1	N/A	N/A
Sleepy Hollow	83'-3/4"	1	20°45'20"	Y	30'	15"	Pile bent; HP 12x53	3"	Y - 18'-9"; 3 piles; slab on the wall	EB-E-S; EB-W-S; WB-E-N; WB-W-N	1	3	1	N/A
Mosquito Creek	111'-2 1/4"	1	15°00'00"	Y	30'	15"	Pile bent; HP1x42	3"	Y - 20'-2"; 5 piles; slab on the wall	EB-W-S (SW); EB-E-S (SE); WB-W-N (NW); WB-E-N (NE)	N/A	2	1	N/A
Coon Creek	143'-4"	1	0°00'00"	Y	30'	15"	Pile bent; HP10x43	3"	Y - 15'-6"; 2 piles; slab on the wall	EB-W-S; WB-W-N; WB-E-N; EB-E-S	0	N/A	2	1
Arlington Heights Rd	189'-11"	2	23°51'08"	N	30'	15"	Pile bent, HP 10x42	3"	N (Lays on 1' curtain walls)	N/A	0	0	0	0
UPRR (Steel)	189'-1/4"	1	42°30'00"	Y	30'	15"	Pile bent; Metal shell	3"	N	N/A	0	0	0	0
Mt. Prospect Rd	103'-1 7/8"	1	20°12'00"	Y	30'	15"	Pile bent, Metal shell	3"	N	N/A	0	0	0	0
UPRR Spur	126'-9 3/4"	1	19°50'00"	Y	30'	15"	Pile bent, Metal shell	3"	N	N/A	0	0	0	0
Wolf Rd	118'10 3/4"	1	20°00'00"	Y	30'	15"	Pile bent, Metal shell	3"	N	N/A	0	0	0	0
Salt Creek	92'-8"	1	8°00'00"	Y	30'	15"	Pile bent, Metal shell	3"	N	N/A	0	0	0	0
Fox River	1315'-9"	8	0°00'00"	N	30'	15"	Pile bent; HP12x53	No clear EXP joint	N	N/A	0	0	0	0
WCL RR	91'-8 7/8"	1	10°56'00"	Y	30'	15"	Pile bent; Metal shell	3"	Y - entire length; slab NOT on the wall	EB-E-S; EB-W-S; WB-E-N; WB-W-N	0	0	0	0
Dryland Bridge	235"-8"	3	0°00'00"	Y	30'	15"	Pile bent	3"	N	N/A	N/A	N/A	0	0
IL Rt. 31	129'-2 3/8"	1	7°00'30"	Y	30'	15"	Pile bent; HP 14x73	3"	Y - entire length; slab on the wall	WB-W-N; WB-E-N	N/A	N/A	0	0

Table B.2 I-90 Cross Road bridge approach slab cracking trends.

Bridge	Year Constructed	Total Length	Span Lengths	Skew	IAB	Stage Construction	MSE Wall	Approach Slab Type	Approach Slab Support Type	Approach slab length on the support	EXP joint location (opening)	Wingwall	Wingwall Location	North Approach	South Approach
Irene Rd.	2013	236'-2"	113'-11";118'-11"	2°45'48"	Y	N	N	Cast-in-place	Approach footing	7'-0 1/8"	1 3/4" at 50° F between slab and rigid pavement	Y - 13'-10"; 2 piles; slab on the wall	SABTMNT-E; SABTMNT-W	7	8
Pearl St.	2014	234'-8"	114'-0";117'-0"	00°43'0"	Y	N	N	Cast-in-place	Approach footing	7'	1 3/4" at 50° F between slab and rigid pavement	Y - 14'; 2 piles; slab on the wall	NABTMNT-E; NABTMNT-W; SABTMNT-E; SABTMNT-W	4	10
Stone Quarry Rd.	2013	231'-4 1/16"	114'-0";114'-0"	00°33'0"	Y	N	N	Cast-in-place	Approach footing	7'	1 3/4" at 50° F between slab and rigid pavement	Y - 14'; 2 piles; slab on the wall	NABTMNT-E; NABTMNT-W; SABTMNT-E; SABTMNT-W	2	5
Brier Hill Rd.	2014	241'-6 1/4"	119'; 119'	18°47'00"	Y	N	N	Precast	Approach footing	7'	1 1/2" strip seal joint at 50° F	Y - from 11'-8 1/8" to 12'-4 1/4"; 3 piles; slab on the wall	NABTMNT-E; NABTMNT-W; SABTMNT-E; SABTMNT-W	2	5
Genoa Rd.	2014	264'-7"	135'-9 1/2"; 128'-9 1/2"	21°15'52"	Y	N	N	Cast-in-place	Approach footing	7'	1 1/2" expansion joint at 50° F	Y - 14'-9 1/8"; 2 piles; slab on the wall	NABTMNT-E; NABTMNT-W; SABTMNT-E; SABTMNT-W	4	3
Harmony Rd.	2014	249'-11 1/2"	123'; 123'	22°18'35"	Y	N	N	Cast-in-place	Approach footing	7'-6 3/4"	No gap between slab and flexible pavement. 1 3/4" at 50° F between slab and rigid pavement.	Y - 11'; 2 piles; slab on the wall	NABTMNT-E; NABTMNT-W; SABTMNT-E; SABTMNT-W	4	3
Mill Rd.	2013	238'-0"	113'-0";125'-0"	7°14'00"	Y	N	N	Precast	Approach footing	7'	1 1/2" strip seal joint at 50° F	Y - 14'; 2 piles; slab on the wall	NABTMNT-E; NABTMNT-W; SABTMNT-E; SABTMNT-W	4	2
Harmony - Riley Rd	2014	317'-7 1/2"	156'; 156'	43°53'50"	Y	N	N	Cast-in-place	Approach footing	7'	2" strip seal joint at 50° F	Y - 15'-6"; 2 piles; slab on the wall	EABTMNT-N; EABTMNT-S; WABTMNT-N; WABTMNT-S	4	2
Johnson Rd.	2014	239'-8"	120'-10";118'-10"	2°38'36"	Y	N	N	Cast-in-place	Approach footing	7'-0 1/16"	1 3/4" at 50° F between slab and rigid pavement	Y - 10'; 2 piles; slab on the wall	NABTMNT-E; NABTMNT-W; SABTMNT-E; SABTMNT-W	4	1
Hennig Rd.	2014	231'-8 5/8"	116'; 112'	9°57'30"	Y	N	N	Cast-in-place	Approach footing	7'-1 1/4"	1 3/4" at 50° F between slab and rigid pavement	Y - from 11'-5" to 11'-10"; 3 piles; slab on the wall	NABTMNT-E; NABTMNT-W; SABTMNT-E; SABTMNT-W	3	2
Getty Rd.	2013	263'-2"	135'-4"; 127'-10"	25°43'15"	Y	N	N	Precast	Approach footing	7'	2" strip seal joint at 50° F	Y - from 9'-1 1/2" to 11'-4 1/2"; 2 piles; slab on the wall	NABTMNT-E; NABTMNT-W; SABTMNT-E; SABTMNT-W	2	3
Town Hall Rd.	2014	234'-8"	119'-0";112'-0"	00°38'0"	Y	N	N	Cast-in-place	Approach footing	7'	1 3/4" at 50° F between slab and rigid pavement	Y - 14'; 2 piles; slab on the wall	NABTMNT-E; NABTMNT-W; SABTMNT-E; SABTMNT-W	2	2
Sandwald Rd.	2013	249'-7 5/8"	127'; 119'	23°33'00"	Y	N	N	Precast	Approach footing	7'	1 1/2" strip seal joint at 50° F	Y - from 11'-8 1/4" to 12'-6 5/8"; 3 piles; slab on the wall	NABTMNT-E; NABTMNT-W; SABTMNT-E; SABTMNT-W	2	2
Shattuck Rd.	2014	231'-4"	113'-6";114'-6"	00°39'37"	Y	N	N	Cast-in-place	Approach footing	7'	1 3/4" at 50° F between slab and rigid pavement	Y - 11'; 2 piles; slab on the wall	NABTMNT-E; NABTMNT-W; SABTMNT-E; SABTMNT-W	2	2
Bartlett Rd.	2014	246'-6 5/8"	113'; 129'	8°49'00"	Semi-IAB	N	Y	Cast-in-place	Approach footing	7'-1"	1 1/2" strip seal joint at 50° F	N	N/A	1	2
Powers Rd.	2013	281'-2"	138'-6"; 138'-6"	36°48'09"	Y	N	N	Cast-in-place	Approach footing	8'-8 3/4"	1/2" strip seal joint at 50° F	Y - 10'; slab on the wall	NABTMNT-E; NABTMNT-W; SABTMNT-E; SABTMNT-W	1	1
Tyrell Rd	2015	245'-9"	106'-6"; 135"	30°15'00"	Y	Y	Y-SABTMNT	Cast-in-place	Approach footing	8'-1 1/4"	1 3/4" at 50° F between slab and rigid pavement.	Y - from 12'-10 1/2" to 14'-9 3/4"; 2 piles; slab on the wall	NABTMNT-E; NABTMNT-W	2	0
County Line Rd.	2014	248'-11 1/4"	124'-11 5/8";123'-11 5/8"	21°21'39"	Y	N	N	Cast-in-place	Approach footing	7'-6 1/4"	1 3/4" at 50° F between slab and rigid pavement	Y - 12'-0";2 piles; slab on the wall	NABTMNT-E; NABTMNT-W; SABTMNT-E; SABTMNT-W	0	2
Anthony Rd	2015	325'-2 1/4"	160'; 160'	45°	Y	N	N	Cast-in-place	Approach footing	9'-10 3/4"	No gap between slab and flexible pavement. 1 3/4" at 50° F between slab and rigid pavement.	Y - 15'-6"; 2 piles; slab on the wall	EABTMNT-N; EABTMNT-S; WABTMNT-N; WABTMNT-S	0	0
Garden Prairie Rd	2015	231'-8"	114'-10";114'-10"	00°0'0"	Y	N	N	Cast-in-place	Approach footing	7'	1 3/4" at 50° F between slab and rigid pavement	Y - 14'; slab not on the wall	NABTMNT-E; NABTMNT-W; SABTMNT-E; SABTMNT-W	0	0
IL Rt. 25 Interchange Ramp	2014/2015	267'	126'; 137'	00°0'0"	Semi-IAB	Y	N	Cast-in-place	Pile bent; HP 12x63	1'-3"	1 1/2" expansion joint at 50° F	N	N/A	0	0

Table B.3 Illinois Route 390 Mainline bridge approach slab cracking trends.

Contract #	Bridge Name	Total Length	Span Lengths	Skew	IAB	MSE Wall	Wingwall	Wingwall Location	Abutment-Approach Connection	Approach Slab Type	Approach Slab Thickness	Transition Slab Dimension (L, T)	Approach Slab Support Type	Approach Slab length on the	EXP joint opening at 50°F (Approach - transition)	Pressure relief joint (Transition-pavement)	Longitudinal joint	Approach Slab Soil	Transition Slab (Pavement) Soil	EB-E	EB-W	WB-E	WB-W
I-13-4607	WB IL 390 over I-290	303'-6 1/4"	155'-0", 145'-0"	18°57'04"	Y	N	Y - 16'-9"; 3 piles; slab on the wall	WB-W-S, WB-W-N, WB-E-S, WB-E-	Anchor rod (V)	Precast	18" (2 layers)	70'; 10.5"	Pile bent; HP 10x42	1'-3"	3"	Y - 2"	B	No requirtemen	3" Asphalt Base course & 12" subgrade aggregate	N/A	N/A	9	5
I-13-4607	WB IL 390 to Rt 53	132'-3 11/16"	119'-5 15/16"	53°48'06"	N	Retaining wall -	N	N/A	Anchor rod (D)	Cast-in-place	15"	70'; 10"	Pile bent; HP 12x53	1'-3"	No clear EXP joint	Y - 2"	C	4" Granular Subbase	3" Asphalt Base course & 9" subgrade aggregate	N/A	N/A	5	6
I-13-4631	Mittel Blvd	153'-4"	142'-3"	0°00'00"		Y - Both two	N	N/A	Anchor rod (V)	Cast-in-place	15"	Y - Not shown	Pile bent; HP 10x42	1'-3"	Y - Not shown	Not shown	D	4" Granular Subbase	N/A	0	1	0	0
I-13-4607	EB IL 390 to WB I-290	306'-6 1/4"	155'-0", 148'-0"	18°57'04"	Y	N	Y - 16'-9"; 3 piles; slab on the wall	EB-W-S, EB-W-N, EB-E-S, EB-E-N	Anchor rod (V)	Precast	18" (2 layers)	79'-82'; 10.5"	Pile bent; HP 10x42	1'-3"	3"	Y - 2"	A	No requirtemen	3" Asphalt Base course & 12" subgrade aggregate	0	0	N/A	N/A
I-13-4602	Rodenburg Rd	178'-7"	129'-6"	3°19'50"	N	N	N	N/A	Anchor rod (V)	Cast-in-place	15"	70'; 10.5"	Apprch footing (Shoulder)	10'	No clear EXP joint	N	C	4" Granular Subbase	4" Granular Subbase & 12" subgrade aggregate	N/A	N/A	0	0
I-13-4630	Lively Blvd	167'-4"	156'-0"	0°00'00"		Y - Both two	N	N/A	Anchor rod (V)	Cast-in-place	15"	N/A	Pile bent; HP 10x42	1'-3"	3"	N	D	4" Granular Subbase	N/A	0	0	0	0
I-13-4631	Salt Creek	227'-2"	119'-6", 104'-0"	0°00'00"	Y	N	Y - 14'; 3 piles; slab on the wall	All eight (EB & WB)	Anchor rod (V)	Cast-in-place	15"	N/A	Pile bent; HP 10x42	1'-3"	3"	N	D	4" Granular Subbase	N/A	0	0	0	0

Table B.4 I-88 bridge approach slab cracking trends.

Structure #	Bridge Name	Total Length	Span Lengths	Skew	Skew direction	Stage Construction	IAB	Wingwall	Wingwall Location	Transition Slab Dimension (L, T)	Approach Slab Support Type	Approach Slab length on the bent	EXP joint opening at 50°F (Approach - transition)	Longitudinal joint	Approach Slab Soil	Transition Slab (Pavement) Soil	EB-E /North	EB-W /South	WB-E	WB-W
813(SB&NB)	Mitchell Rd	258'-0"	129'-0" each	2°47'00"	CCW	N	Y	Y - 22'; Slab on the wall	All four	N	Approach footing	7'-1/8"	No clear Exp. Joint	N	Granular backfill for structures (abutment side), subbase granular mat'l type B, 4" (btwn abutment & pavement)	N/A	0	3	N/A	N/A
815(SB&NB)	Church Rd	270'-6"	133'-3 3/4" each	18°08'20"	CCW	N	Y	Y - 21'-7"; Slab on the wall	All four	N	Approach footing	6'-7 7/8"	No clear Exp. Joint	N	Granular backfill for structures (abutment side), subbase granular mat'l type B, 4" (btwn abutment & pavement)	N/A	1	1	N/A	N/A
1201(EB)&1202(WB)	Steward Creek	94'-7 1/2"	89'-0"	18°30'00"	CCW	Y	Semi	Y - 12'-5" to 13'-5"; Slab on the wall	All eight (EB & WB)	70'; 11"	Pile bent; Metal shell	1'-3"	3"	A	4" Granular Subbase	3" Asphalt Base course & 9" subgrade aggregate	1	0	0	0
1205(EB)&1206(WB)	Beach Creek	85'-7"	80'-0"	17°00'00"	CW	Y	Semi	Y - 12'-5" to 13'-5"; Slab on the wall	All eight (EB & WB)	70'; 11"	Pile bent; Metal shell	1'-3"	3"	A	4" Granular Subbase	3" Asphalt Base course & 9" subgrade aggregate	0	0	0	0
1213(SB&NB)	Aston Rd	219'-0"	29'-10"; 78'; 78'; 26'-10"	0°00'00"	N/A	N	Semi	Y - spec. not shown	All four	Not shown	Not shown	Not shown	Not shown	Not shown	Not shown	Not shown	0	0	N/A	N/A
1227(NB&SB)	Nachusa Rd	219'-6"	33'-3"; 78'; 78'; 30'-3"	0°00'00"	N/A	N	Not shown	Not shown	Not shown	Not shown	Not shown	Not shown	Not shown	Not shown	Not shown	Not shown	0	0	N/A	N/A

Appendix C   Updated Crack Maps

As proposed in Appendix B, approach slabs at four bridges are reinspected in November 2017. The crack maps were updated based on the actual geometry of the approach slabs and the observed cracks in the field. The detailed crack maps are as follows.

C.1   I-90 Mainline over US-20
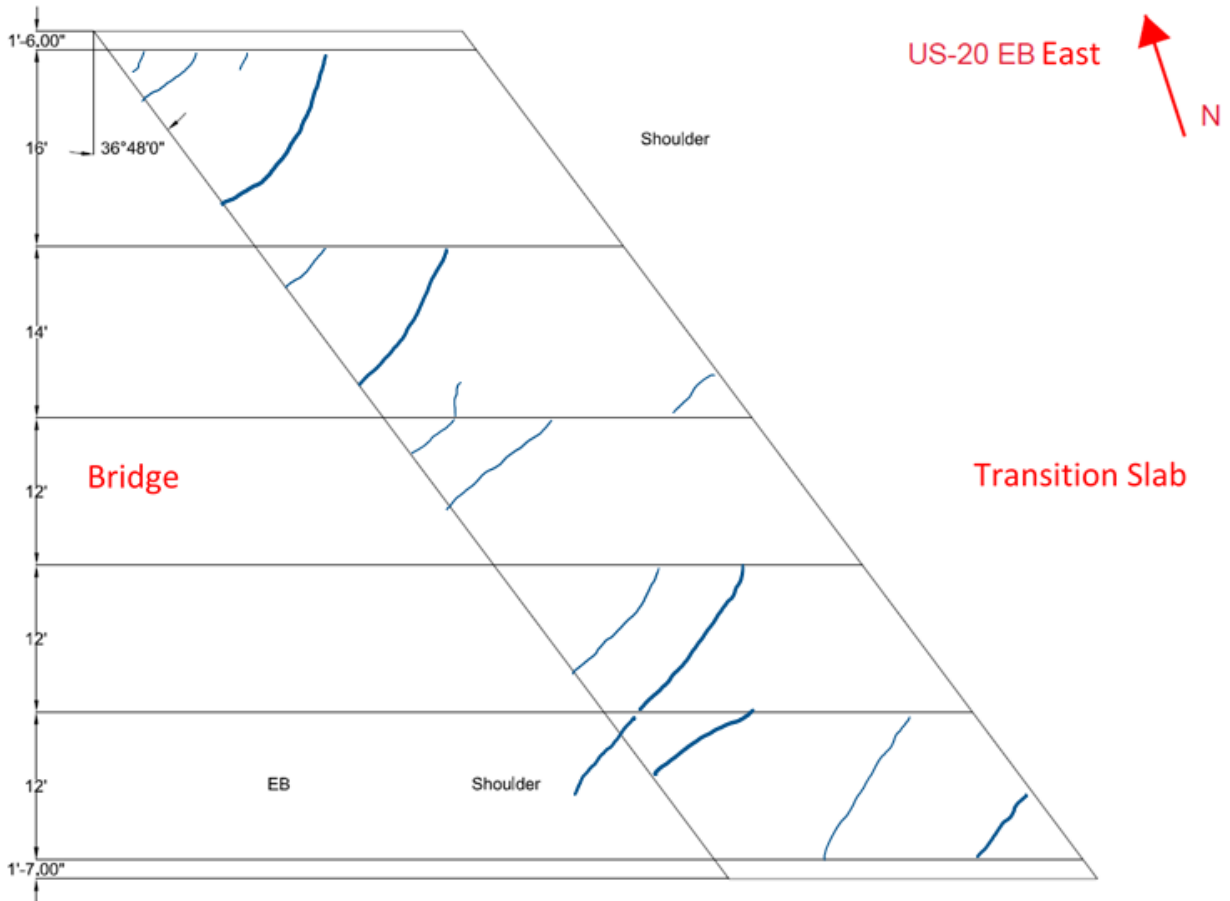
Figure C.1 US-20 Eastbound East.
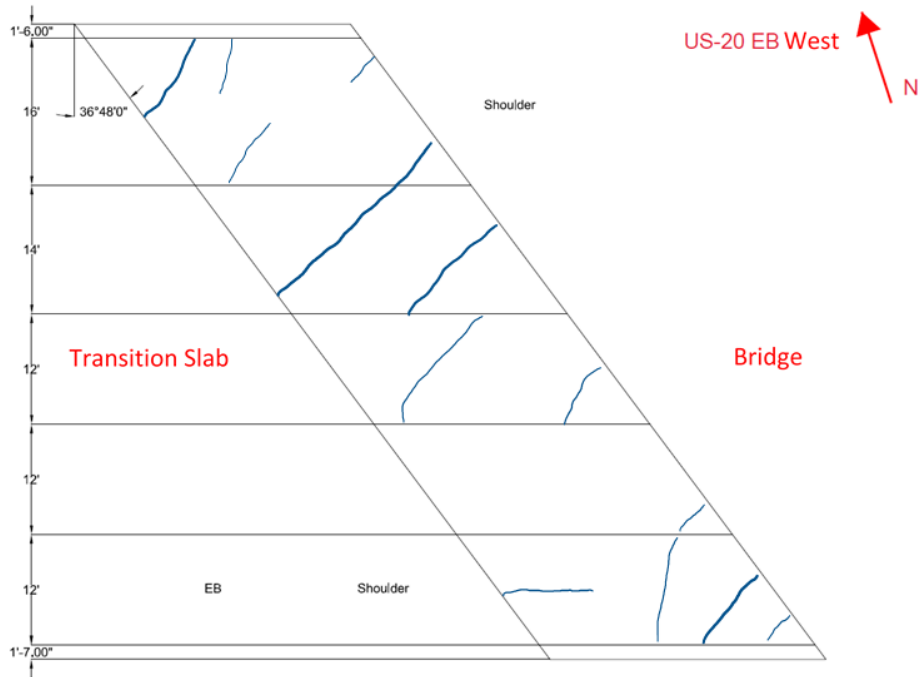
Figure C.2 US-20 Eastbound West.
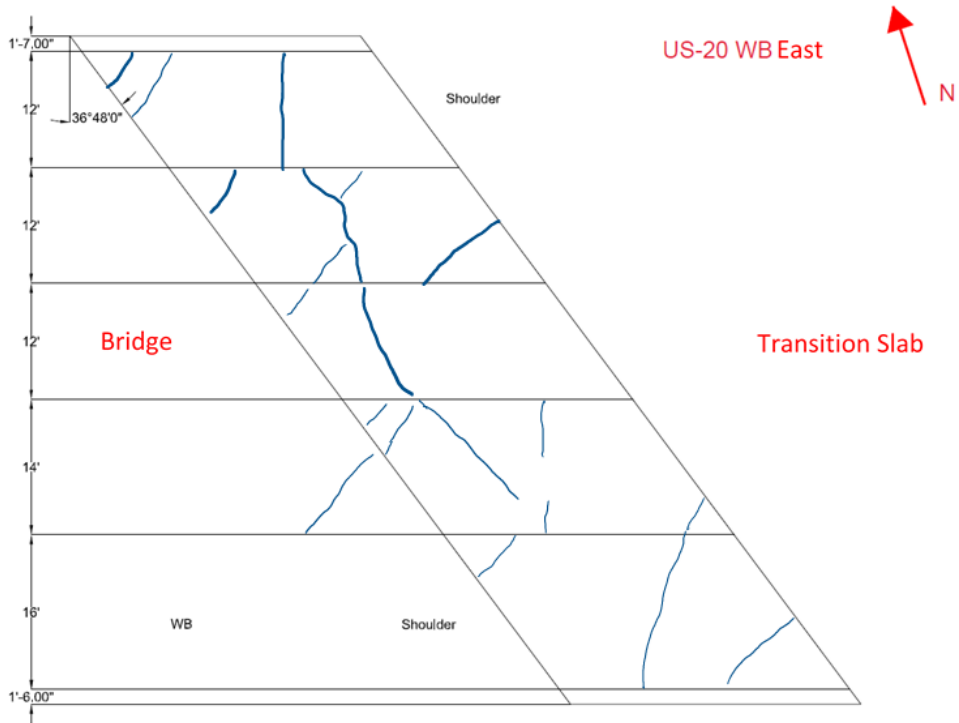
Figure C.3 US-20 Westbound East.

278
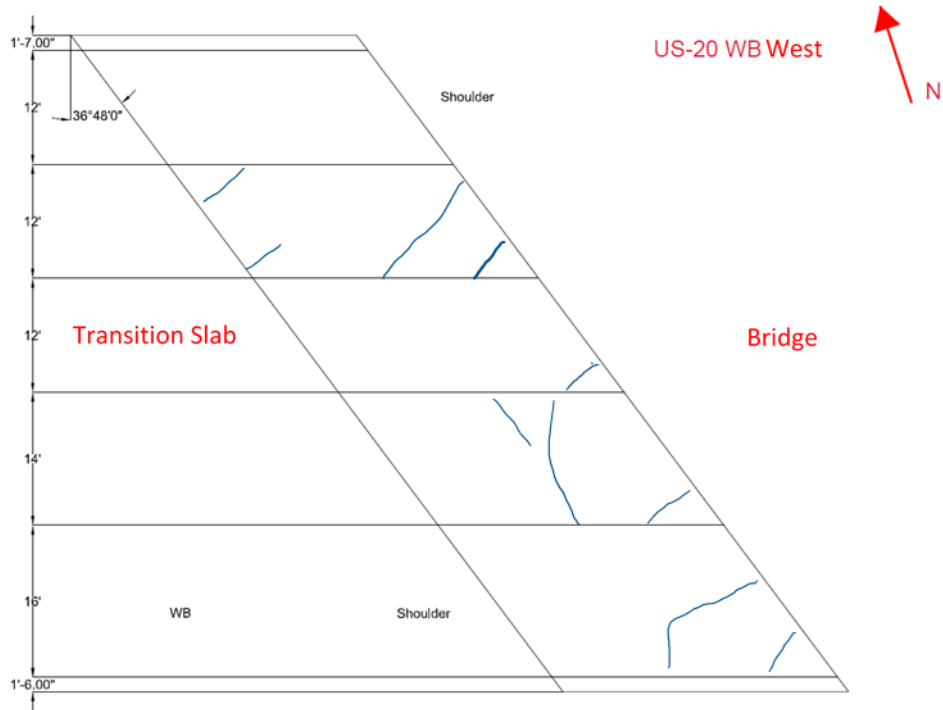
Figure C.4 US-20 Westbound West.

## C.2   I-90 Mainline over Kishwaukee River
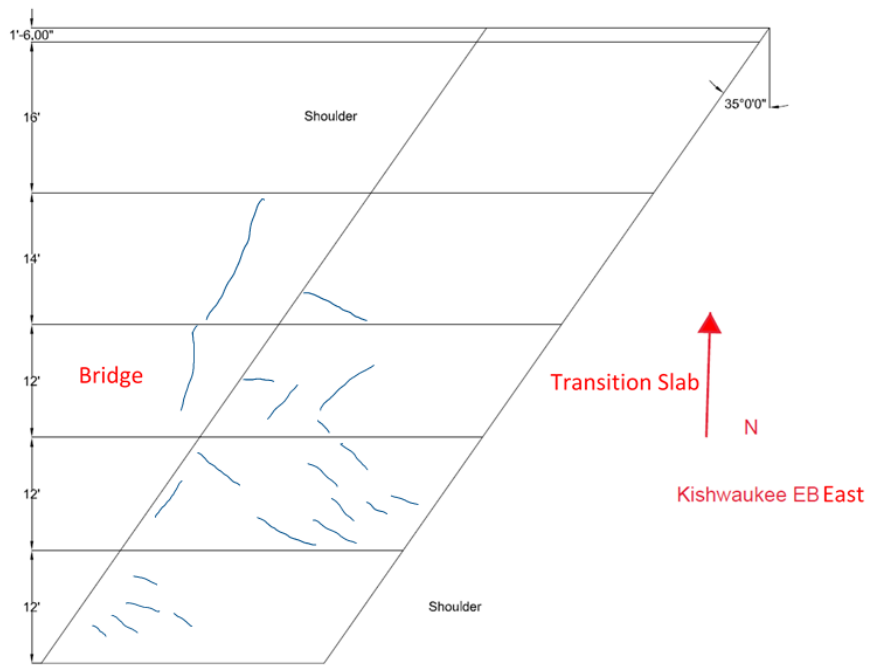
Figure C.5 Kishwaukee River Eastbound East.
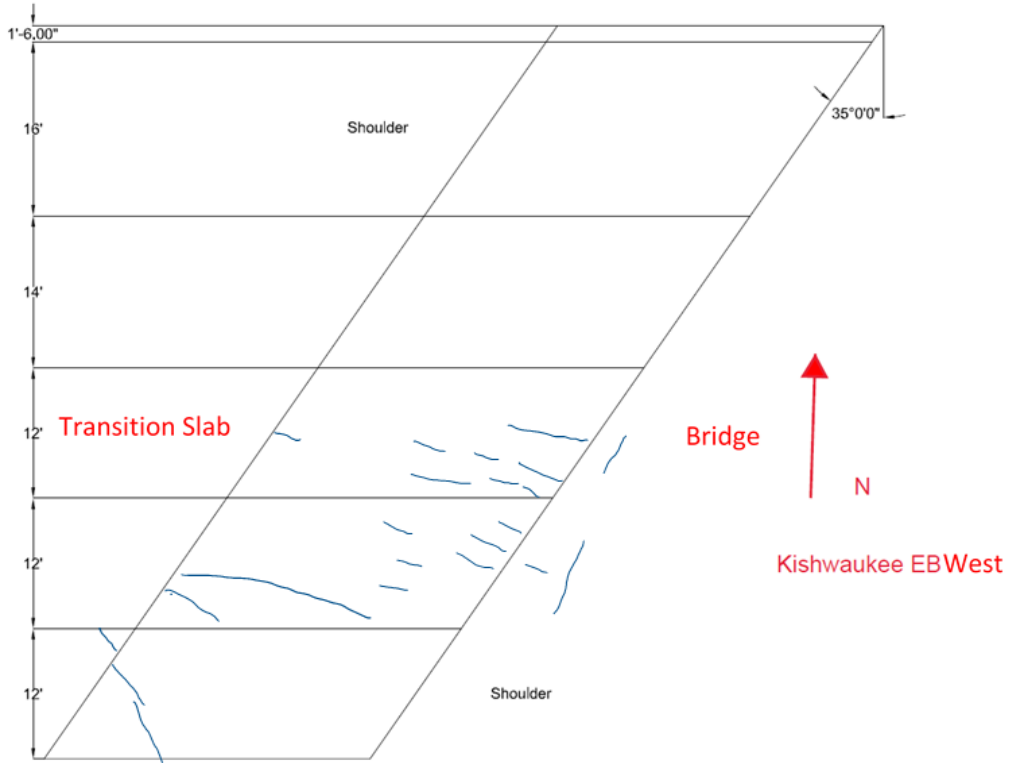
Figure C.6 Kishwaukee River Eastbound West.
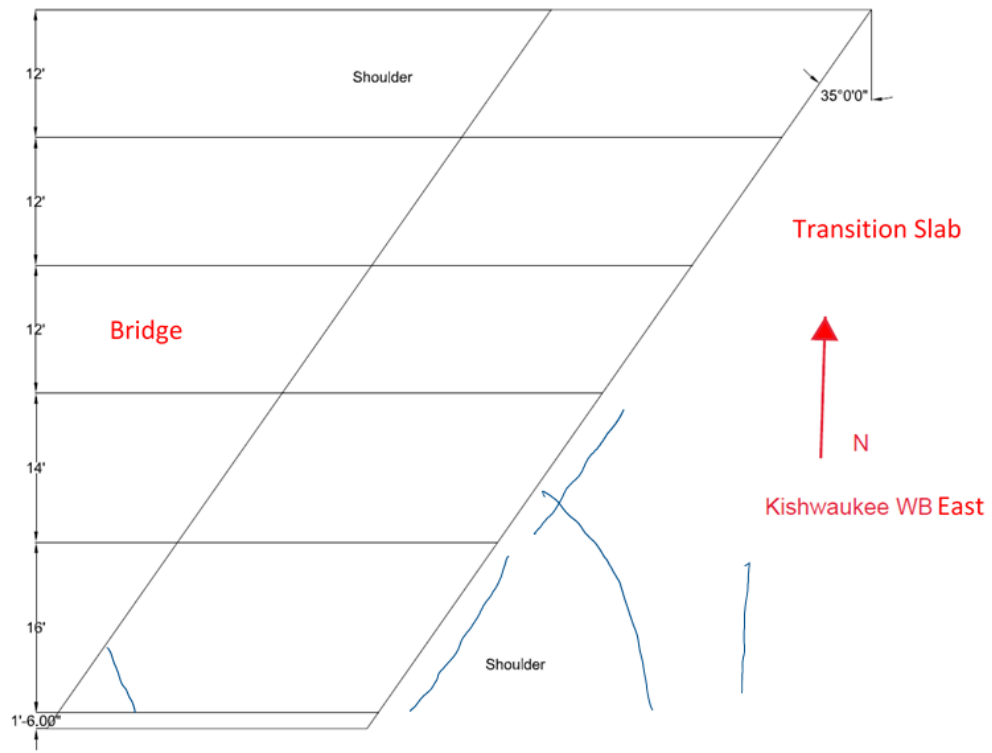

Figure C.7 Kishwaukee River Westbound East.
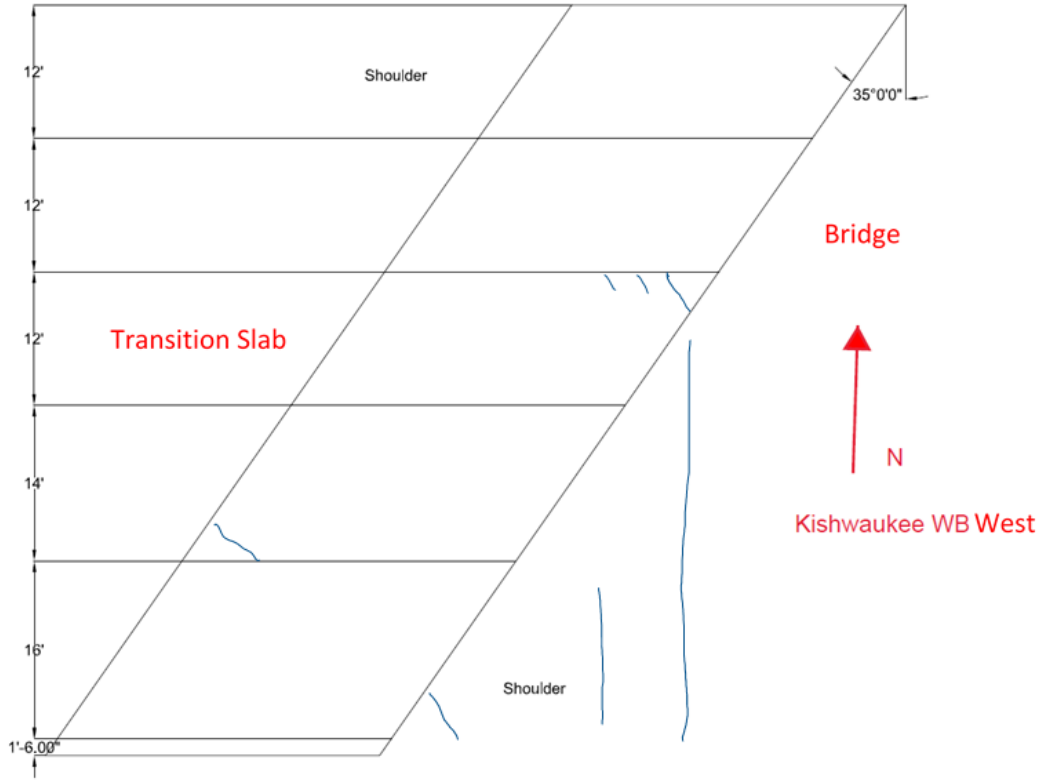
Figure C.8 Kishwaukee River Westbound West.

C.3   I-90 Cross Road on Brier Hill Road
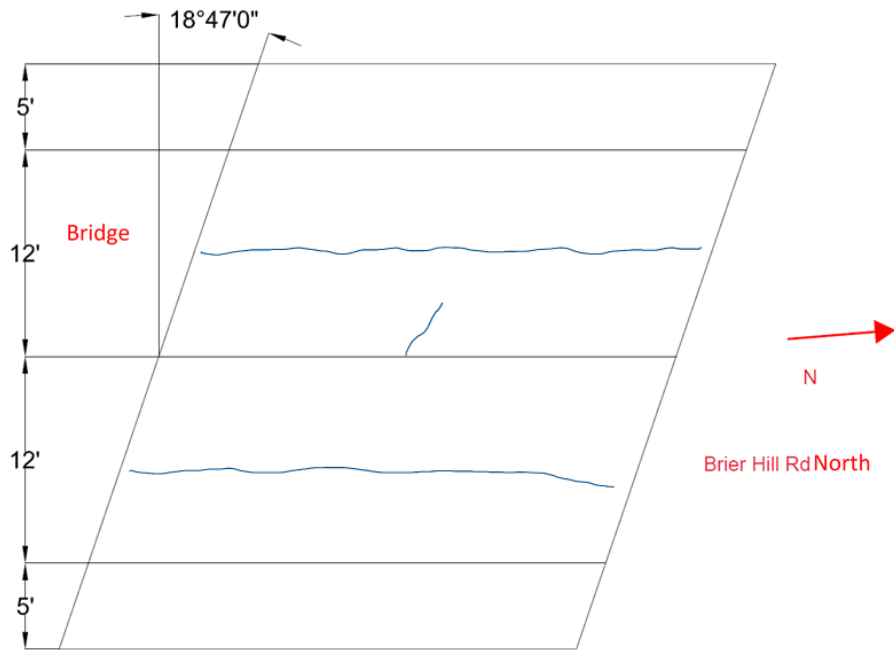

Figure C.9 Brier Hill Road North.
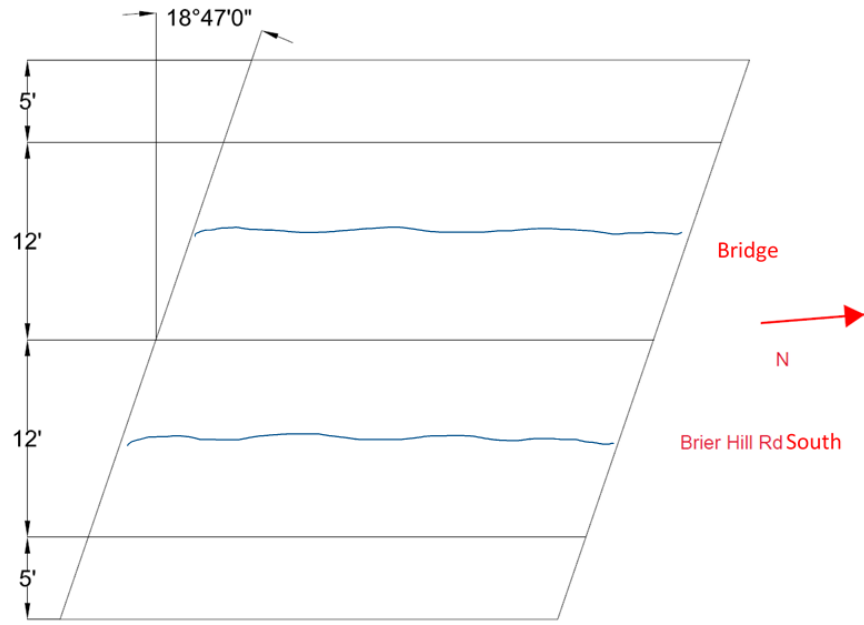
Figure C.10 Brier Hill Road South.

## C.4 I-90 Cross Road on Irene Road
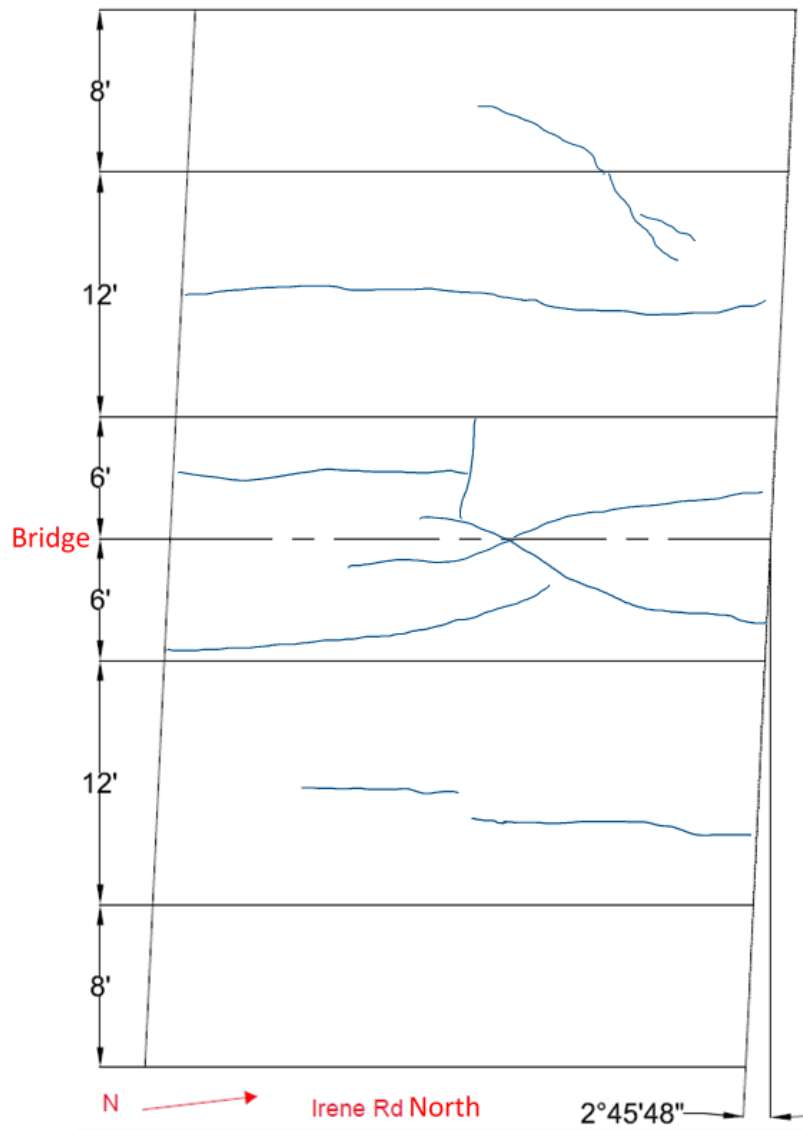
Figure C.11 Irene Road North.
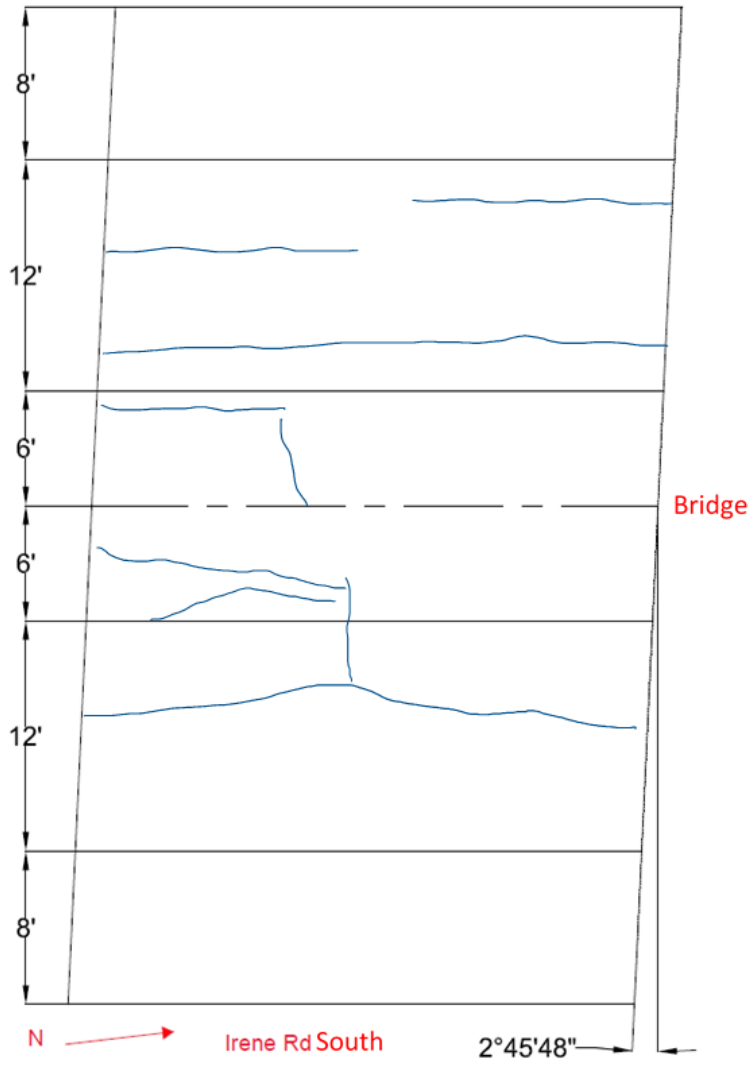
Figure C.12 Irene Road South.

Appendix D Gage Reading Calculations and Estimation of Coefficient of Thermal Expansion of Concrete

D.1 Explanation of Gage Reading Calculations

When the concrete structure is subjected to temperature changes, restraints of the structure cause thermal stresses in concrete, which may result in cracking. Such thermal stress and deformation are related to the coefficient of thermal expansion of the concrete. Hence, it is important to estimate the coefficient of thermal expansion (CTE) of concrete in the structures.

Vibrating wire embedment strain gages were installed in the integral abutment bridge (IAB) approach slabs to monitor the structural behavior and temperature changes at various locations of the slabs. There is a steel wire in the strain gage that deforms with the two end blocks of the gage, which are firmly anchored into the surrounding concrete. The gage readings, measured as change in the resonant frequency of the steel wire vibration, indicate the change in axial force that the steel wire in the gage experiences. If the change in strain reading is positive, namely $+\Delta R$, there is tension developed in the steel wire and vice versa.

The difference in the free thermal expansion/contraction for steel and concrete, i.e., the difference in CTE of the two materials, affects the embedment strain gage readings, which emphasizes the need to estimate the CTE of the concrete. For instance, if the concrete component around the strain gage has the same CTE as the steel wire, in the case of free expansion/contraction with temperature change $+/-\Delta T$, there is no change in strain reading as there is no force developed in the steel wire. Another example that helps explain the importance of the concrete CTE is that provided a positive temperature change $+\Delta T$ and change in gage reading $-\Delta T(C_1 - C_2)$, there is no thermal stress in the concrete as the concrete can expand freely. C_1 and C_2 are the CTE of steel wire and concrete, respectively. In general, such gage readings (y axis) vs. temperature readings (x axis) for a free expansion/contraction case can be plotted as a straight line with negative slope, $-(C_1 - C_2)$.

With the understanding of the strain gage readings, several types of strains and stresses can be derived: apparent strain $\epsilon_{apparent}$, actual strain ϵ_{actual}, and load related strain ϵ_{load}.

The **apparent strain** $\epsilon_{apparent}$ measures the apparent change in strain read from the readout device. Since the steel wire is shortened by wire clamping, a batch gage factor is applied to compensate such effect. The apparent strain is written as:

$$\epsilon_{apparent} = (R_1 - R_0)B$$

Where R_1 is the current gage reading; R_0 is the initial/reference gage reading measurement; and B is the batch gage factor.

The **actual strain** ϵ_{actual} represents the change of unit length that would be measured by a dial gage attached to the surface, if there is any, of the concrete. It is defined as:

$$\epsilon_{\text{actual}} = (R_1 - R_0)B + (T_1 - T_0)C_1$$

Where T_1 is the current temperature reading; T_0 is the initial temperature reading; and $C_1 = +6.78\ \mu\epsilon/°F\ (+12.2\ \mu\epsilon/°C)$ is the CTE of steel wire.

The **load related strain** ϵ_{load} accounts for the strain related to the combination of both the external load and restraint of thermal expansion/contraction, and is given by:

$$\epsilon_{\text{load}} = (R_1 - R_0)B + (T_1 - T_0)(C_1 - C_2)$$

Where C_2 is the CTE of concrete. The term $(T_1 - T_0)(C_1 - C_2)$ accounts for the difference in thermal deformation of steel and concrete material given a temperature change.

D.2   Coefficient of Thermal Expansion of Concrete

If the CTE of concrete is to be determined based on the embedment strain gage readings in the temperature compensation beams, the case where the beams have constant restraint in a short period of time and no external loadings is considered. The stress developed in the concrete beam, if there is any, is in proportion to the change in temperature. Thus, the load related strain is equivalent to the strain induced by the restraint of thermal expansion/contraction. A coefficient K is used to represent the slope of the line for the load related strain vs. temperature relationship, as shown below:

$$K = [(R_1 - R_0)B + (T_1 - T_0)(C_1 - C_2)]/(T_1 - T_0)$$

$$K_T = \frac{(R_1 - R_0)B}{(T_1 - T_0)} = K - (C_1 - C_2)$$

Here K_T is the slope obtained from the apparent strain vs. temperature relationship. In the ideal case where there is no restraint to the concrete beam, i.e., no friction, $K = 0$, the CTE of concrete can be estimated by:

$$C_2 = C_1 + K_T$$

However, in practice, there is always some level of restraint applied to the concrete beam. Hence, an estimation of K_T must be made. The K_T value is computed on monthly, weekly, and daily basis. After removing the samples with apparent anomalies, it was found that a K_T of value -1 $\mu\varepsilon/°C$ is around or less than the magnitude of 80% samples of K_T, thus K_T=-1 corresponds to a condition where the temperature compensation beams are subject to low restraint level, so the CTE of concrete is estimated to be around 11 $\mu\epsilon/°C$. Figure D.1 provides examples of the temperature compensation beam apparent strain reading vs. temperature relationships. The daily cyclic behavior approximately resembles the monthly regression. Figure D.2 shows the estimated K_T values in monthly and weekly manner.
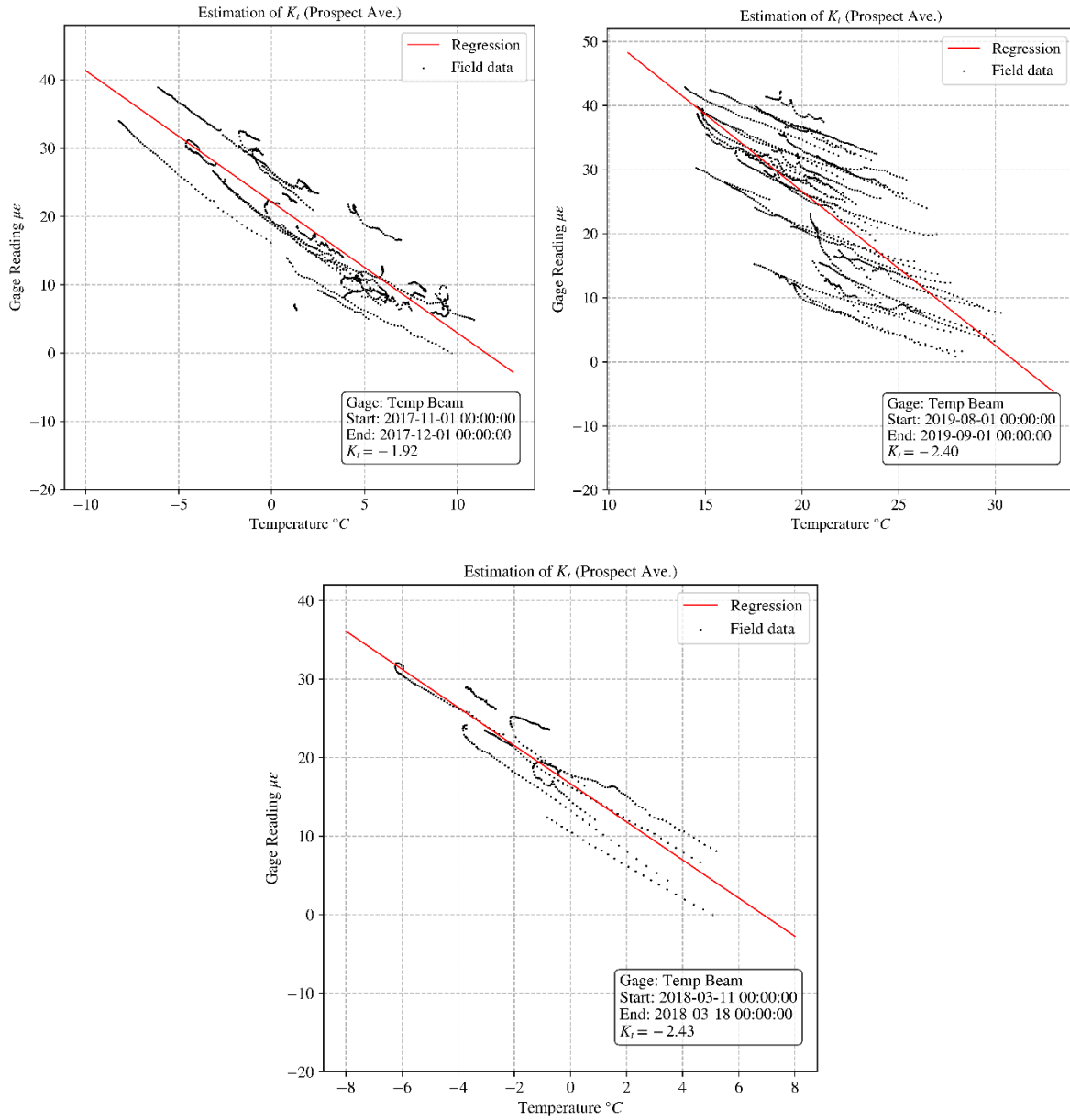
Figure D.1 Examples of monthly data for temperature compensation beam.
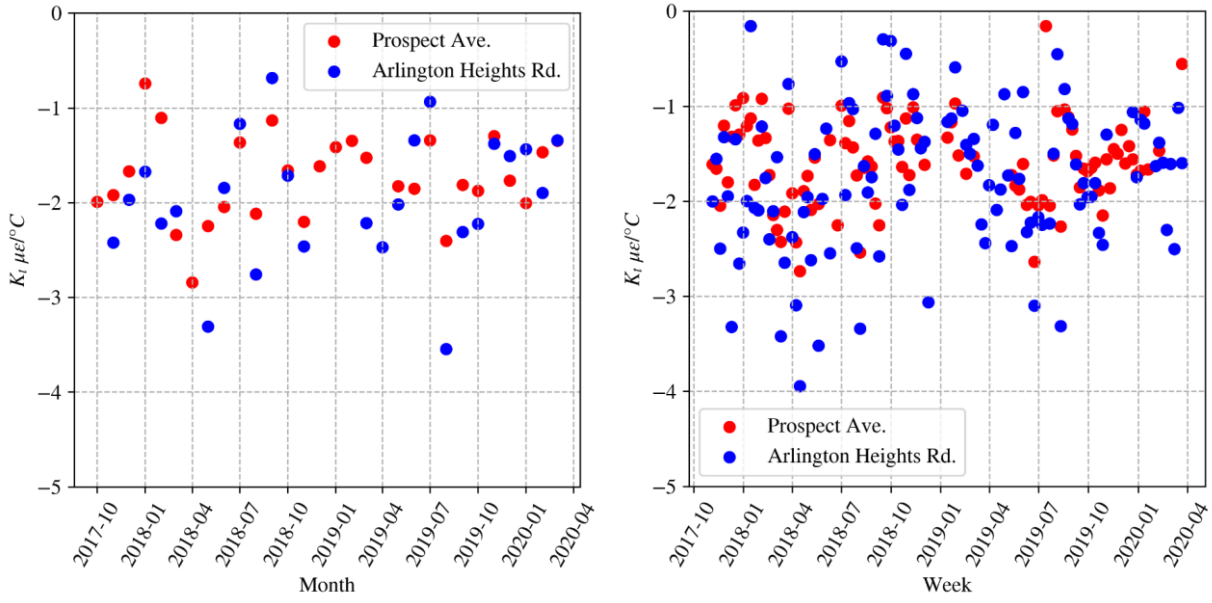
Figure D.2 Estimation of K_T on: (a) monthly basis and (b) weekly basis.